HYDROAROMATIC EQUILIBRATION DURING SHIKIMIC ACID AND QUINIC ACID BIOSYNTHESIS

By

David R. Knop

A DISSERTATION

Submitted to
Michigan State University
in partial fulfillment of the requirements
for the degree of

DOCTOR OF PHILOSOPHY

Department of Chemical Engineering and Materials Science

2002

ABSTRACT

HYDROAROMATIC EQUILIBRATION DURING SHIKIMIC ACID AND QUINIC ACID BIOSYNTHESIS

By

David R. Knop

The expense and limited availability of shikimic acid and quinic acid isolated from plants has impeded utilization of these hydroaromatics as synthetic starting materials. The microbial biocatalyses reported in this account could supplant the tedious, multi-step natural product isolation of shikimic acid and quinic acid. Recombinant *Escherichia coli* biocatalysts genetically engineered to biosynthesize shikimic acid from glucose accumulated not only shikimic acid, but sizable concentrations of quinic acid and 3-dehydroshikimic acid byproducts. 3-Dehydroshikimic acid accumulation results from the feedback inhibition of shikimate dehydrogenase by shikimic acid. The source of quinic acid formation is less clear however. Kinetic experiments revealed shikimate dehydrogenase was capable of accepting both 3-dehydroshikimic acid and 3-dehydroquinic acid as substrates for reduction. Fed-batch fermentor conditions which employed unlimited glucose availability shifted the typical 48 h glucose-limited *E. coli* SP1.1/pKD12.138A equilibrium from 28 g/L shikimic acid in 13% yield (mol/mol) from glucose as a 1.6:1.0:0.65 (mol/mol/mol) shikimate:quinate:3-dehydroshikimate mixture to 58 g/L shikimic acid in 23% yield (mol/mol) from glucose as a 18:1.0:4.9 (mol/mol/mol) mixture in 60 h.

Homologous quinic acid biosynthesis was investigated by evaluating *E. coli* QP1.1/pKD12.138A under glucose-limited fed-batch fermentor conditions.

QP1.1/pKD12.138A synthesized 49 g/L of quinic acid from glucose in 20% (mol/mol) yield as a 15:1.0 (mol/mol) quinate:3-dehydroquinate mixture and established a high-titer, homologous route for quinic acid biosynthesis. Fed-batch fermentor conditions unlimited in glucose decreased the quinate:3-dehydroquinate ratio of QP1.1/pKD12.138A to 0.74 however.

Physiological State (PS) variable monitoring and control was applied to QP1.1/pKD12.138A within the framework of a Knowledge-Based (KB), intelligent control system. The KB control system consisted of four phases. The novel attributes of the KB control system included phase three manipulation of the specific oxygen uptake rate (SOUR) to approximate the oxygen transfer rate (OTR) increases observed during unlimited glucose availability, and phase four control of the carbon dioxide evolution rate (CER) by manipulating the glucose feed rate to the reactor. Reactor studies revealed that perturbations in the pseudo-steady-state glucose concentration of less than 1 mM could shift the quinate:3-dehydroquinate equilibrium ten-fold.

An online stoichiometric model (SM) was constructed using reactor mass balances and pseudo-online artificial neural network predictions as inputs. The SM predicted phosphoenolpyruvate (PEP) limitations occurred under high glucose uptake rate fermentation conditions during peak growth rates. The predicted PEP limitations were consistent with literature precedent and suggest that *pps*-encoded PEP synthase overexpression might alleviate QP1.1/pKD12.138A intracellular PEP limitations.

To my wife Kristin, for her love and support.

ACKNOWLEDGEMENTS

The following dissertation is the product of myself and numerous people that I am indebted to for their help. First and foremost I would like to thank my advisors Dr. John W. Frost and Dr. R. Mark Worden, for their insight and guidance during my dissertation research. I would like to thank Dr. Bruce Dale and Dr. Daina Briedis for their input and support. I would also like to thank members of both groups, past and present, for their help and friendship: Dr. John Arthur, Dr. Jessica Barker, Dr. Sunil Chandran, Dr. Kai Li, Dr. Amy Dean, Dr. Feng Tian, Dr. Spiros Kambourakis, Dr. Mark Widman, Dr. Tyler Ames, Dr. Marshall Bredwell, Dr. Prashant Srivastava, Dr. Chad Hansen, Mr. Mark Mikola, Mr. Padmesh Venkitasubramanian, Mr. Jian Yi, Ms. Wei Niu, Mr. Ningqing Ran, Mr. Jianto Guo, and Mr. Casey Preston. I would especially like to thank Kai, Chad, Jessica, Sunil, and Padmesh for their help and camaraderie during my graduate education. I would also like to thank my parents, Ralph J. Knop, M.S. and Janice K. Knop, M.S., for their strong emphasis on academic pursuits, it has truly paid me dividends. Thank you to my brother Robert "Sideshow" Knop and sister Dr. Kristine Spence, D.O., for everything they have done for me, especially in the past five years.

My projects have been highly collaborative throughout my graduate career, and I would like to acknowledge my collaborators. Mr. Kun Xu has been both a mentor in regard to electrical engineering and control prowess, but also an exemplary friend. I thank him for his key contributions to this work, insight into computer systems, and for going above and beyond what was required of him to assist me in my academic pursuits. Dr. Karen Draths began working with me on my shikimic acid fermentation endeavors in

the Frost laboratory. Since that time Dr. Draths has proven to be an indispensable asset in my understanding of biological systems, and in my graduate studies in general. Dr. Draths has been a candid mentor, a friend, and a sympathetic confidant. I owe her more than I could ever hope to expound upon in this brief text. For this and more, Dr. Draths has my enduring gratitude and friendship, and I thank her. I would also like to acknowledge the hard work and dedication of Mr. Michael Hines and Mr. William R. Sillers. Their assistance was instrumental in completing this work, and I am in their debt.

My most heart-felt gratitude belongs to my wife Kristin. Kristin has been with me since the inception of my graduate career, providing continuous support, love, and encouragement, even when it was very difficult for her to do so. Kristin has been the one constant in my life, my singular source of inspiration. She has been strong during the tough times and jubilant during the good ones. She has my admiration, respect, and love, and I dedicate this work to her.

This work was graciously funded by the National Science Foundation, the Center for Plant Products and Technologies at Michigan State University, the Crop and Food Bioprocessing Center at Michigan State University, the Environmental Protection Agency, the United States Department of Agriculture, and the National Institutes of Health.

TABLE OF CONTENTS

LIST OF TABLES

LIST OF FIGURES

NOMENCLATURE AND ABBREVIATIONS

a	specific interfacial area (m^2/m^3)
AcCoA	acetyl-coenzyme A
ACE	acetate
ADP	adenosine diphosphate
Ap	ampicillin
ATP	adenosine triphosphate
b	glucose feed liquid fraction
CER	carbon dioxide evolution rate (g/h)
CIAP	calf intestinal alkaline phosphatase
C_L^*	saturation liquid phase oxygen concentration (g/L)
Cm	chloramphenicol
C_o	liquid phase oxygen concentration (g/L)
COMT	catechol-*O*-methyltransferase
DAH	3-deoxy-D-*arabino*-heptulosonic acid
DAHP	3-deoxy-D-*arabino*-heptulosonic acid 7-phosphate
DCU	digital control unit
DHQ	3-dehydroquinic acid
DHS	3-dehydroshikimic acid
D_i	impeller diameter
D_t	fermentor vessel diameter
D.O.	dissolved oxygen

DTT	dithiothreitol
E4P	D-erythrose-4-phosphate
EDTA	ethylenediaminetetraacetate
EPSP	5-enolpyruvyl-shikimate-3-phosphate
ESDT	expert system development tool
F_G	glucose feed rate (g/h)
FSA	(6S)-6-fluoro-shikimic acid
F6P	D-fructose-6-phosphate
$FADH_2$	flavin adenine dinucleotide (reduced form)
g	gram
g	acceleration due to gravity
GLU	D-glucose
G6P	D-glucose-6-phosphate
GAP	D-glyceraldehyde-3-phosphate
GFR	glucose feed rate (g/h)
GUR	glucose uptake rate (g/h)
h	hour
H	Henry's Law constant
ICT	isocitrate
Kan	kanamycin
KB	knowledge-based
K_c	PID control loop proportional term
KG	α-ketoglutarate

k_g	gas-film resistance mass transfer coefficient
K_L	overall gas-liquid mass transfer coefficient
k_L	liquid-film resistance mass transfer coefficient
K_m	Michaelis constant
L	liter
LB	luria broth
mL	milliliter
mM	millimolar
min	minute
M	molar
MAB	*N*-2-(6-methyl-pyridyl)-aminomethylene bisphosphonic acid
MIC	minimal inhibitory concentration
N/A	not applicable
NADH	nicotinamide adenine dinucleotide (reduced form)
NADPH	nicotinamide adenine dinucleotide phosphate (reduced form)
OAA	oxaloacetate
OTR	volumetric oxygen transfer rate ($g \cdot L^{-1} \cdot h^{-1}$)
OUR	volumetric oxygen uptake rate ($g \cdot L^{-1} \cdot h^{-1}$)
PCA	protocatechuic acid
PCR	polymerase chain reaction
PEP	phosphoenolpyruvic acid
PS	physiological state
PTS	phosphoenolpyruvate:carbohydrate phosphotransferase

PYR	pyruvic acid
QA	quinic acid
QA:DHQ	quinic acid to 3-dehydroquinic acid molar ratio (mol/mol)
rpm	revolutions per minute
R5P	ribose-5-phosphate
Ru5P	ribulose-5-phosphate
S3P	shikimate-3-phosphate
S7P	sedoheptulose-7-phosphate
S	glucose concentration (g/L)
SA	shikimic acid
SA:DHS	shikimic acid to DHS molar ratio (mol/mol)
SA:QA	shikimic acid to quinic acid molar ratio (mol/mol)
SA:QA:DHS	shikimic acid to quinic acid to 3-dehydroshikimic acid molar ratio (mol/mol/mol)
SAER	specific acetate excretion rate (g acetate·g biomass^{-1}·h^{-1})
SCER	specific carbon dioxide evolution rate (g CO2·g biomass^{-1}·h^{-1})
SGR	specific growth rate (h^{-1})
SGUR	specific glucose uptake rate (g glucose·g biomass^{-1}·h^{-1})
SOUR	specific oxygen uptake rate (g O_2·g biomass^{-1}·h^{-1})
Sp	spectinomycin
SUC	succinate
Tc	tetracycline
τ_D	PID controller derivative time (s)

TE	Tris-EDTA
TSP	3-(trimethylsilyl)propionic-2,2,3,3-d_4 sodium salt
τ_I	PID controller integral time (s)
X	biomass concentration (g/L)
X5P	D-xylulose-5-phosphate

CHAPTER 1

Biocatalysis, the Shikimate Pathway, and Biochemical Engineering

The petroleum price spikes of 1973 and 1979 jolted the world, and served notice that crude oil supplies would remain neither an inexpensive nor a limitless commodity. Today the grip of petroleum consortia may be strongest on organic chemical manufacture, where reliance on petroleum has continued unabated despite predictions that conventional petroleum supplies could be outstripped by demand within the next decade.[1] Examining the chemical industry reveals a disturbing dependence upon petroleum for a feedstock, with approximately 95% of organic chemicals derived from oil and natural gas.[2] Benzene isolation serves as a useful paradigm for organic chemical dependence upon fossil fuels since 98% of all benzene is obtained from these non-renewable resources.[3]

The continued utilization of oil and natural gas will become increasingly problematic as conventional oil fields become depleted. Conventional supplies of oil have been projected to last until about 2039, while supplies of natural gas are expected to be depleted around 2050.[4] It is unclear if these predictions account for the potentially volatile growth rate in petroleum consumption of about 2% per year, or the suspicious increase in proven reserves reported by OPEC from about 400 billion barrels to about 700 billion barrels between 1987 and 1990, which corresponded to no major discovery of new fields.[1] The utilization of renewable feedstocks and development of new processes for

the manufacture of organic chemicals will therefore become increasingly critical to meeting the world's demand for cost effective fuels, plastics, synthetic rubber and fibers, as well as pharmaceuticals. Ironically perhaps, the near doubling of the cost of petroleum in 1979 may be prophetic in heralding the next technological explosion for organic chemical manufacture from renewable feedstocks such as corn via biocatalysis. Corn has garnered significant attention recently as a renewable resource, especially in the production of fuel ethanol. In 1990, 179 million metric tons of corn (6.2 billion bushels) where produced in the United States alone,[5] and that figure has increased substantially in the last 10 years to about 250 million metric tons,[6] with the glucose-laden starch component accounting for 143 x 10^9 kg.[6b] Additionally, corn fiber comprises about 10% of corn dry weight wet milled,[7] and represents a vast untapped source of carbon in the form of pentoses and hexoses.

The following dissertation details research primarily dedicated to elucidating and optimizing environmentally benign bioprocesses for production of hydroaromatic metabolite intermediates in the aromatic amino acid biosynthesis pathway. Chapter 1 reviews select biocatalytic processes and/or industrially important molecules derived from aromatic amino acid biosynthesis pathway metabolites and address hurdles associated with utilizing the aromatic amino acid biosynthesis pathway for small molecule production. Chapter 2 will address several challenges attendant with biocatalytic conversion of glucose to shikimic acid and elaborate the resolutions. Chapter 3 will detail biocatalytic production of quinic acid from glucose, and address the problematic equilibrium observed in this system. Finally, Chapter 4 illustrates the

application of advanced control methodologies targeted at quinic acid production enhancement and process scale up.

Biosynthesis of Value-Added Chemicals.

In the quest for supplanting reliance on petroleum as the world's primary chemical feedstock, one must question feedstock availability, the robustness, and the scalability of emerging technologies for the conversion of new feedstocks. Supplanting petroleum-based technologies is a two-fold problem. First, manufacturing technologies capable of producing the quantities of petroleum-derived end products required to meet consumer demands and/or compete with the cost-effectiveness of petroleum-based technologies must be developed. Second, new feedstock sources must be developed which can supply a carbon stream on par with that of petroleum production at its current level. One potential feedstock that is in abundant supply in both the United States and throughout the world is corn, with hexoses and pentoses comprising the majority of the useable carbon locked within this carbon source. The advent of biocatalysis and fermentation as potentially viable commercial-scale processes, and their rapid advancement over the past two decades has provided hope that molecules historically derived from petroleum can be obtained from renewable feedstocks in a cost effective manner. The synergistic coupling of biocatalysis and fermentation has seen the maturation of fermentation from simple beverage production to a commercial technology poised to incorporate renewable raw materials into mainstream chemical manufacture at the expense of petroleum.[8] Chief among the assets of biocatalytic processes are the lack of toxic byproducts, mild conditions, water as a solvent, and the renewable nature of their

feedstocks. Formidable process impediments challenge biocatalytic processes however, and include downstream product recovery, biocatalyst disposal, preventing introduction of genetically modified organisms into the environment, and public perception.

A number of industrially and commercially important chemicals have already benefited from commercial-scale, biocatalytic production, as several bulk industrial chemicals are biosynthesized. For example, biocatalytic ethanol production, mainly through sugar fermentation with *Saccharomyces cerevisiae* (Figure 1), has increased dramatically in the last two decades owing to the use of ethanol as a fuel additive. Although still subsidized, "bioethanol" has all but supplanted synthetic production of fuel-grade ethanol, and accounts for more than 13 million tons of ethanol production annually.[9] A more moderate-volume fermentation product is the amino acid L-lysine. The end market for this essential amino acid is primarily the food industry given the absence of L-lysine from most cereal grains. Fermentation routes to L-lysine include conversion of glucose by *Corynebacterium glutamicum*, with annual production of L-lysine in excess of 350,000 tons per year worldwide (Figure 1),[9] and fermentation titers in excess of 170 g/L.[10]

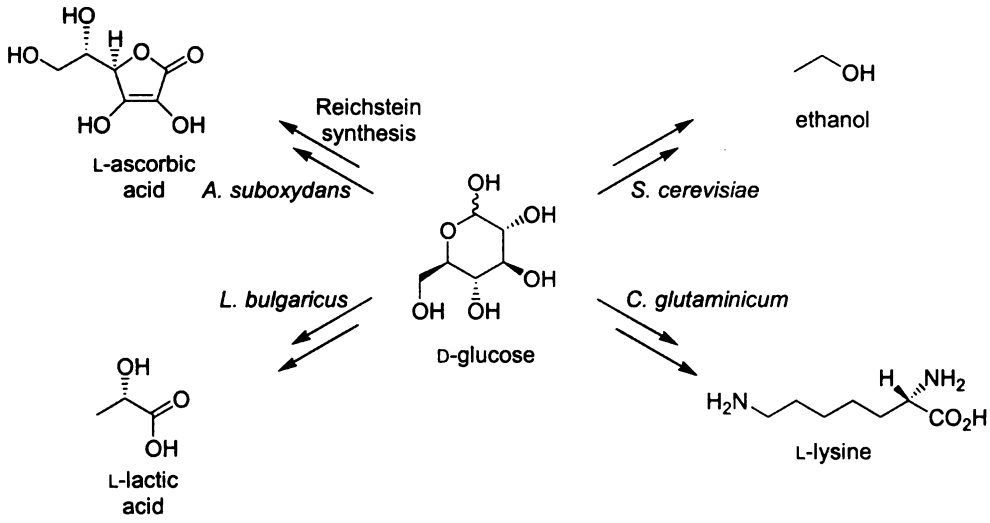

Figure 1. Select commercial fermentation products derived from glucose.

One moderate-volume fermentation product (70,000 ton per year) that possesses the capability to compete with or supplant its petroleum-derived counterparts is fermentative production of lactic acid for use in production of polylactides (Figure 1).[9] Lactic acid currently finds use as a food acidulant, which accounts for 85% of its use in the United States.[11] The modest production volume and current applications of lactic acid belie its potential as a feedstock however. A joint venture between Dow Chemical and Cargill led to the establishment of Cargill Dow Polymers in 1997, with the explicit purpose of producing biodegradable polylactic acid polymers to compete with petroleum-derived polyethylene, polypropylene, and polystyrene.[9] Anaerobic fermentative production of L-lactic acid by homolactic organisms such as *Lactobacillus bulgaricus* is accomplished at titers of 90 g/L and yields in excess of 90% from glucose, while utilizing starch in an enzymatic saccharification/fermentation process affords a 95% yield from the carbohydrate and achieves titers in excess of 100 g/L.[9,11]

The commercial production (Reichstein process) of L-ascorbic acid (vitamin C) has also benefited from biocatalysis (Figure 1). The coupling of chemical synthesis and biocatalysis is currently responsible for commercial L-ascorbic acid production at a rate of 60,000 tons per year.[9] The biocatalytic portion of the process relies on the oxidation of sorbitol to sorbose by the bacterium *Acetobacter suboxydans*, while the initial step of the chemical portion involves hydrogenation of glucose to sorbitol.

The Aromatic Amino Acid Biosynthesis Pathway.

The aromatic amino acid biosynthesis pathway (Figure 2), also referred to as the shikimate pathway, is responsible for the biosynthesis of L-phenylalanine, L-tyrosine, and L-tryptophan. This trio of amino acids is essential in mammalian diets since higher organisms lack the aromatic amino acid biosynthesis pathway. Aromatic amino acid metabolism and the metabolism of pathway intermediates leads to a miriad of essential biosynthetic aromatic compounds.[12] The intense mechanistic scrutiny afforded the aromatic amino acid biosynthesis pathway has resulted in elucidation of an apparently complete picture of metabolite intermediates and the enzymes responsible for their biosyntheses.

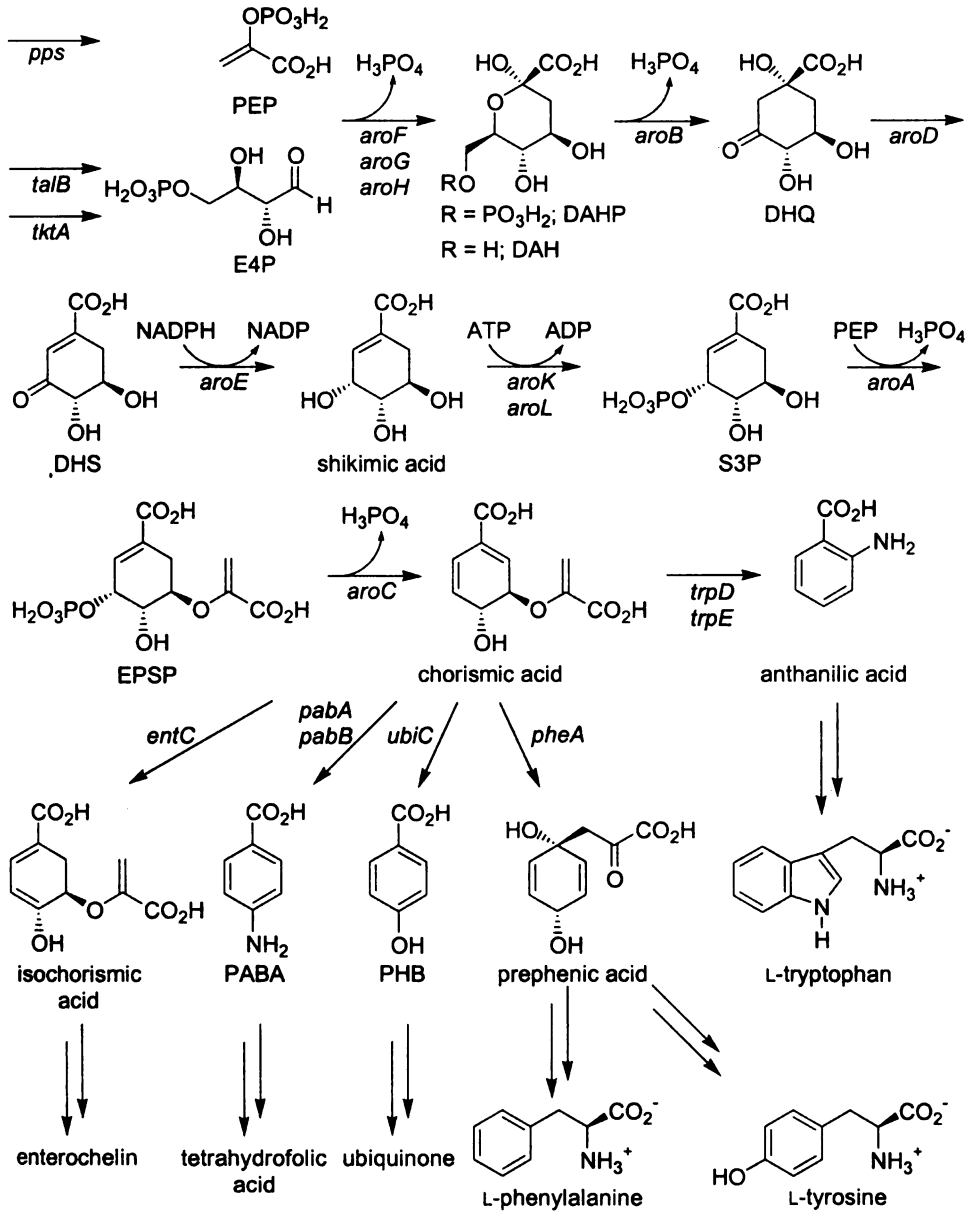

Figure 2. The aromatic amino acid biosynthesis pathway. Metabolite abbreviations: PEP, phosphoenolpyruvic acid; E4P, D-erythrose-4-phosphate; DAHP, 3-deoxy-D-*arabino*-heptulosonic acid 7-phosphate; DAH, 3-deoxy-D-*arabino*-heptulosonic acid; DHQ, 3-dehydroquinic acid; DHS, 3-dehydroshikimic acid; S3P, shikimate-3-phosphate; EPSP, 5-enolpyruvyl-shikimate-3-phosphate; PABA, *p*-aminobenzoic acid; PHB, *p*-hydroxybenzoic acid. Genetic loci abbreviations: *pps*, PEP synthase; *talB*, transaldolase; *tktA*, transketolase; *aroF*, *aroG*, *aroH*, DAHP synthase; *aroB*, DHQ synthase; *aroD*,

DHQ dehydratase; *aroE*, shikimate dehydrogenase; *aroK*, *aroL*, shikimate kinase; *aroA*, EPSP synthase; *aroC*, chorismate synthase; *trpD*, *trpE*, anthranilate synthase; *entC*, isochorismate synthase; *pabA*, *pabB*, *p*-aminobenzoic acid synthase; *ubiC*, chorismate lyase; *pheA*, chorismate mutase.

The aromatic amino acid biosynthesis pathway becomes of enhanced interest when its absence in humans is framed in the context of antibiotic or herbicidal-targeted enzymes to combat bacterial infection or agricultural pests. To this end a handful of compounds have met with success. The herbicide glyphosate (Figure 3) is the most notable compound to target the shikimate pathway. Marketed under the trade name Roundup®, glyphosate has been utilized as a herbicide for more than two decades. Glyphosate forms a ternary complex with EPSP synthase and either shikimate-3-phosphate or EPSP, competitively inhibiting EPSP synthase relative to PEP and uncompetitively inhibiting EPSP synthase relative to shikimate-3-phosphate,[13] resulting in the in vivo inhibition of aromatic amino acid and vitamin biosynthesis. Glyphosate has been so successful that hundreds of analogs and derivatives of it have been synthesized and tested for herbicidal activity.[14] In addition to herbicidal activity, glyphosate has also demonstrated biological activity in combating parasitic protozoa of the phylum Apicomplexa, including *Plasmodium* spp., which cause malaria, *Toxoplasma gondii*, which causes toxoplasmosis, and *Eimeria* spp., which cause avian coccidiosis.[15] Another chemotherapeutic agent to target the shikimate pathway is *N*-2-(6-methyl-pyridyl)-aminomethylene bisphosphonic acid (MAB). MAB (Figure 3) has been demonstrated to disrupt aromatic biosynthesis proceeding from the shikimate pathway by non-competitive inhibition of DAHP synthase.[14] Growth inhibition of *Nicotiana plumbaginifolia* was not completely reversed by supplementation with aromatic amino

acids, suggesting multiple modes of activity for MAB.[14] Finally (6S)-6-fluoroshikimic acid (Figure 3) has also proven to be an effective antimicrobial agent targeted at the shikimate pathway, however in depth discussion of this molecule will be deferred until Chapter 2.

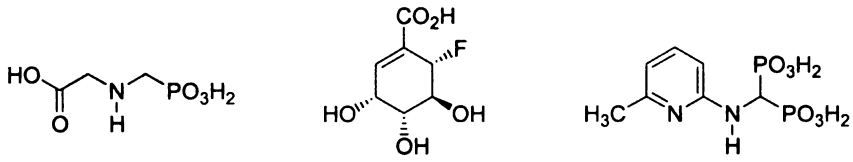

Figure 3. Structures of select aromatic amino acid biosynthesis pathway inhibitors.

Commercially Relevant Molecules Linked to the Shikimate Pathway.

In addition to the mid-volume to pseudo-commodity volume commercial molecules derived from glucose previously mentioned, several metabolites in the shikimate pathway (Figure 2) serve as portals to industrially relevant compounds. The manufacture of the polyamide nylon-6,6 is dependent upon the monomer adipic acid. As such, adipic acid is one of the top fifty chemicals produced in the United States in terms of volume, with worldwide production in excess of 1.9×10^6 tons in 1989.[16] Nylon-6,6 manufacture accounted for 88% of adipic acid produced in the United States in 1989. All current industrial routes to adipic acid require the use of nitric acid,[16] and the primary route currently employed requires cyclohexane[16] obtained from carcinogenic benzene. (Figure 4). Not only is the toxicity of benzene and cyclohexane problematic in terms of health and environmental impact, but the liberation of the known greenhouse gas nitrous oxide[17] during the oxidation step further argues a benign route should supplant the current process. Process shortcomings are further reinforced by the harsh conditions

required to obtain cyclohexane from benzene.[18] A fermentation route to adipic acid previously reported in literature[19] has recently been improved upon (Figure 4).[20] Beginning with renewable, benign glucose, adipic acid is converted to *cis,cis*-muconic acid via fermentation at 22% yield (mol/mol) and achieves titers of 37 g/L,[20] followed by a relatively mild hydrogenation (50 psig hydrogen) in the presence of platinum catalyst affords adipic acid in 97% yield from *cis,cis*-muconic acid. The fermentation process utilizes a heterologous *E. coli* biocatalyst expressing *aroZ*-encoded DHS dehydratase for the conversion of DHS to protocatechuic acid (PCA) from *K. pneumoniae, aroY*-encoded PCA decarboxylase for the conversion of PCA to catechol from *Klebsiella pneumoniae*, and *catA*-encoded catechol 1,2-dioxygenase for the conversion of catechol to *cis,cis*-muconic from *Acinetobacter calcoaceticus*.[19,20]

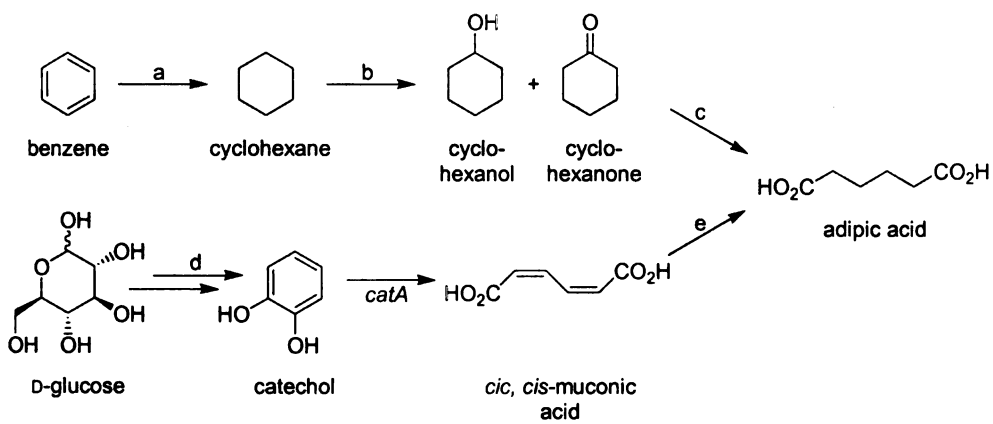

Figure 4. Synthetic and biosynthetic routes to adipic acid. Reaction conditions: (a) Ni-Al_2O_3, H_2, 370-800 psig, 150-250 °C, (b) Co, O_2, 120-140 psig, 150-160 °C (c) Cu, NH_4VO_3, 60% HNO_3, 60-80 °C. (d) *E. coli*. (e) 500 psig H_2, Pt.

The preceding biosynthesis of adipic acid necessarily routes through catechol. Catechol is currently manufactured in excess of 25,000 tons per year,[21] and provides another opportunity to examine a fermentation route beginning from the aromatic amino

acid biosynthesis pathway that could supplant an existing industrial process. Catechol usage encompasses a varied family of molecules, with pharmaceuticals (L-dopa, adrenaline, papavarine), flavors (vanillin, eugenol, isoeugenol), agrochemicals (carbofuran, propoxur), and polymerization inhibitors and antioxidants (4-*tert*-butylcatechol, veratrol) all being derived from this dihydroxylated benzene.[22] Synthesis from benzene constitutes the primary route to catechol currently (Figure 5),[22] and process shortcomings include high temperature and pressures coupled with several carcinogenic or toxic intermediates, as well as the reliance on explosive peroxides during the oxidation of phenol.

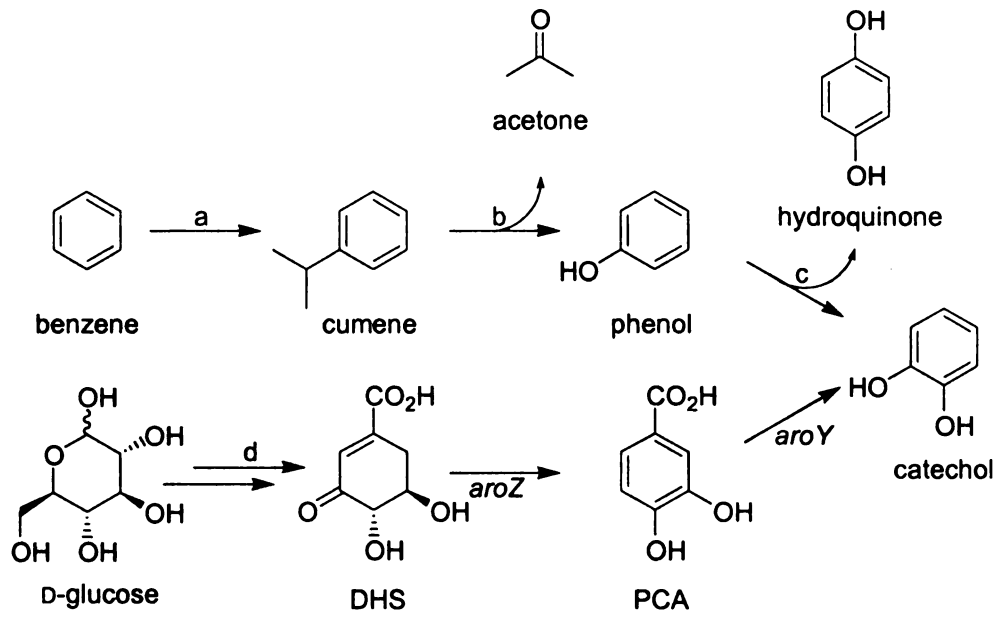

Figure 5. Synthetic and biosynthetic routes to catechol. Reaction conditions: (a) propylene, solid H_3PO_4 catalyst, 200-260 °C, 400-600 psig. (b) O_2, 80-130 °C; SO_2, 60-100 °C. (c) 70% H_2O_2, EDTA, Fe^{+2} or Co^{+2}, 70-80 °C. (d) *E. coli*.

Contrasting the chemical synthesis of catechol from benzene is the biocatalytic conversion of glucose to catechol (Figure 5).[23] The biocatalytic route forgoes not only carcinogenic, petroleum-derived benzene, but circumvents the toxicity of the cumene,

phenol, and hydroquinone intermediates employed to afford catechol. Additionally, mild reaction conditions are substituted for the high temperature and pressure necessitated to accomplish the synthetic conversion of benzene to catechol and peroxides are eliminated. The biocatalytic process employs *aroY* and *aroZ*, as previously described, to channel carbon from glucose-derived DHS to catechol, in an *aroE* deficient strain. Literature accounts of catechol biosynthesis from glucose report modest titers (2.0 g/L) and yields (33% mol/mol) in the absence of fed-batch fermentor cultivation.[23b] Biosynthetic production of catechol under fed-batch fermentor conditions might lead to titer enhancements in the absence of problematic microbial toxicity issues.

The biosynthesis of another molecule that stems from DHS and PCA is 3,4,5-trihydroxybenzoic acid, commonly known as gallic acid. This polyhydroxylated aromatic is currently obtained by the hydrolysis of tannins isolated from gallnuts, Aleppo galls, and tara powder obtained from the ground seeds of *Coulteria tinctoria*.[24] The annual production of gallic acid is estimated at 1.7×10^5 kg,[25] and gallic acid is the primary feedstock for synthesis of pyrogallol. Gallic acid and pyrogallol find use in the chemical syntheses of biologically active compounds that require trihydroxylated, aromatic rings, and their applications in this arena include the synthesis of the antibiotic trimethoprim (Figure 6), the muscle relaxant gallamine triethiodide, and the insecticide bendiocarb (Figure 6).[24,26] Additional uses of gallic acid include inks, tanning, dye preparation, lithography, a developer in photography, hair-dyeing, and medical application as a human urinary astringent and internal antihemorrageant in veterinary applications.[27] Pyrogallol is used commercially in pharmaceuticals and pesticides, and is considered one of the more versatile photographic developing agents currently in use.[27]

Although pyrogallol's antioxidant properties are superb, its acute toxicity precludes its use in food applications. Propyl gallate (Figure 6), however, is a commercial food antioxidant prepared from gallic acid that is typically used synergistically with 4-methyl-2,6-di-*tert*-butylphenol (BHT) and butylated hydroxyanisole (BHA).[27] Derivatization of pyrogallol can even yield mescaline, the hallucinogenic found in peyote and a potential psychotomimetic drug.[27]

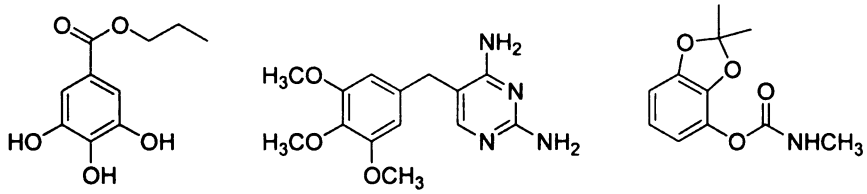

Figure 6. Select derivatives of gallic acid and pyrogallol.

The rich and varied uses of gallic acid, pyrogallol, and their derivatives suggest that a more dependable, cost-effective route to gallic acid relative to natural product isolation may be of significant industrial interest. Biosynthetic and coupled biosynthetic-synthetic processes for production of gallic acid and pyrogallol have recently been elaborated, and utilize chemically benign, renewable glucose as the feedstock (Figure 7).[26,28] Both routes utilize the common intermediate DHS. Purified DHS can be converted to gallic acid via Cu^{2+} or Zn^{2+} mediated oxidation (Figure 7).[28] Gallic acid biosynthesis proceeds from DHS to PCA by the enzymatic action of *aroZ*-encoded DHS dehydratase, followed by conversion of PCA to gallic acid by *pobA**, a mutant isozyme of *p*-hydroxybenzoate hydroxylase isolated from *Pseudomonas aeruginosa* possessing the ability to hydroxylate PCA.[29] Tandem expression of *aroZ* and *pobA** in a DHS

synthesizing construct leads to the accumulation of 20 g/L of gallic acid in fed-batch fermentation culture supernatants despite the toxicity associated with the biosynthetic product and byproducts toward the microbial host.[26]

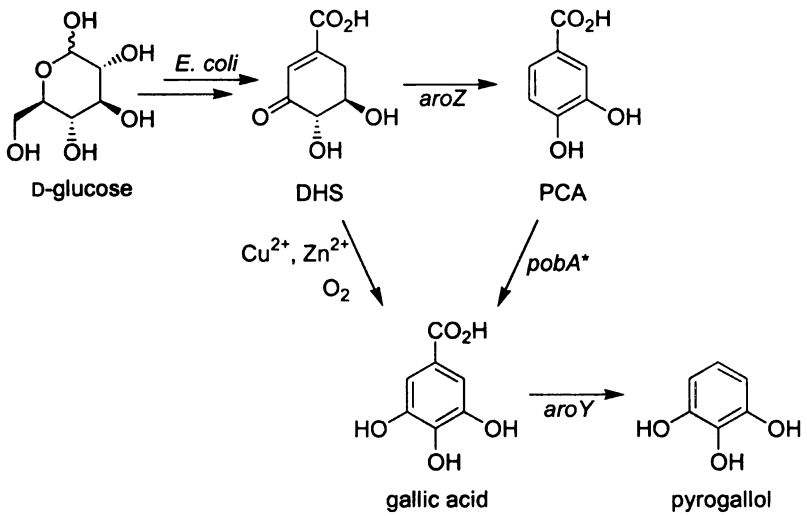

Figure 7. Synthetic and biosynthetic routes to gallic acid and pyrogallol.

Vanillin is one of the most important aromatic flavor compounds currently employed in foods, beverages, perfumes, and pharmaceuticals. Current industrial chemical syntheses result in an excess of 10,000 tons of vanillin production per year.[30] Synthetically derived vanillin cannot be referred to as "natural" and must bear the "nature-identical" moniker when used as a flavoring, and this represents a serious drawback in the utilization of synthetic vanillin. The current commercial route to vanillin proceeds from benzene-derived catechol through several toxic intermediates, and also utilizes dimethyl sulfate which is suspect as a cancer causative agent (Figure 8).[31]

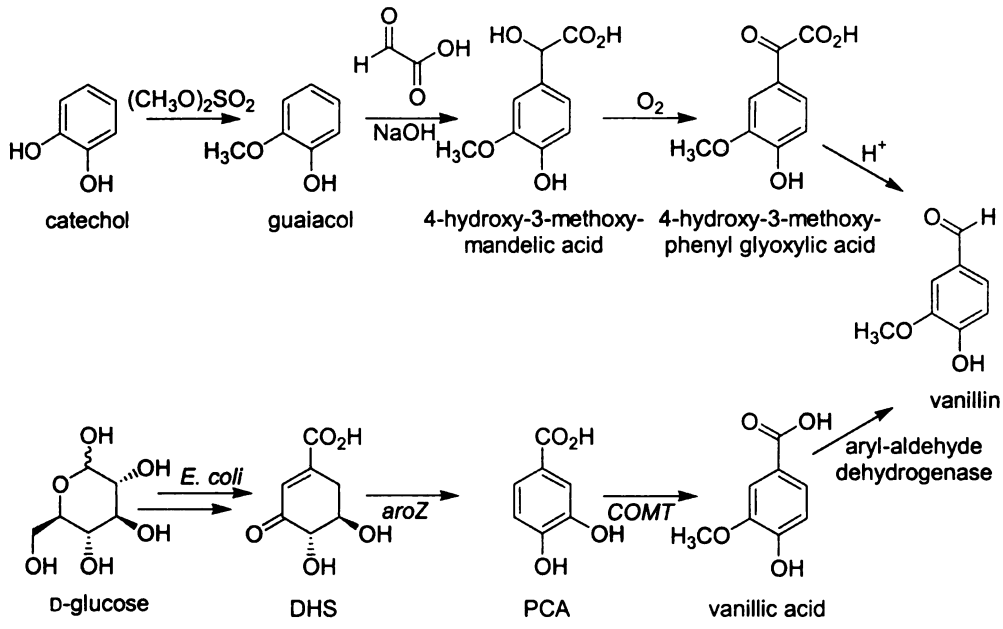

Figure 8. Synthetic and biosynthetic routes to vanillin.

In stark contrast to the synthetic route, biosynthesis of vanillic acid circumvents toxic or carcinogenic intermediates and feedstocks, relying on glucose as a starting molecule and proceeding through DHS to PCA, vanillic acid, and finally to the product of interest under mild reaction conditions employing water as the solvent (Figure 8). Heterologous expression of the *aroZ* locus in a DHS-producing biocatalyst leads to PCA as previously discussed. Coupling this heterologous expression with expression of rat-liver *COMT*-encoded catechol-*O*-methyltransferase in a recombinant host during fed-batch fermentation accumulates 5.0 g/L of vanillic acid.[32] Vanillic acid purified from crude culture supernatant is enzymatically converted to vanillin in 66% yield via partially purified aryl-aldehyde dehydrogenase isolated from the fungus *Neurospora crassa*.[32]

The preceding biosynthetic routes to adipic acid, catechol, gallic acid, and vanillin all proceed through the common intermediate DHS (Figure 4, Figure 5, Figure 7, and Figure 8). Although DHS is currently not produced industrially, its large-scale biosynthesis is feasible via scale-up of an existing process that converts glucose to DHS.[33] The bioconversion employs a recombinant *E. coli* strain auxotrophic in *aroE*-encoded shikimate dehydrogenase (Figure 2), permitting the accumulation of DHS in culture supernatants. The reported bioconversion DHS titer of 69 g/L in 30% yield (mol/mol) from glucose has subsequently been improved to permit a titer of 88 g/L DHS to accumulate in 48 h at 41% yield (mol/mol) from glucose.[34] Fed-batch fermentation is the source of DHS purified for use in the chemical catalysis to gallic acid previously discussed (Figure 7). DHS is also the most advanced intermediate common to the aromatic amino acid biosynthesis pathway and to the syntheses previously detailed, making it of central importance both metabolically and industrially. The central role of DHS in the syntheses discussed above is illustrated in Figure 9.

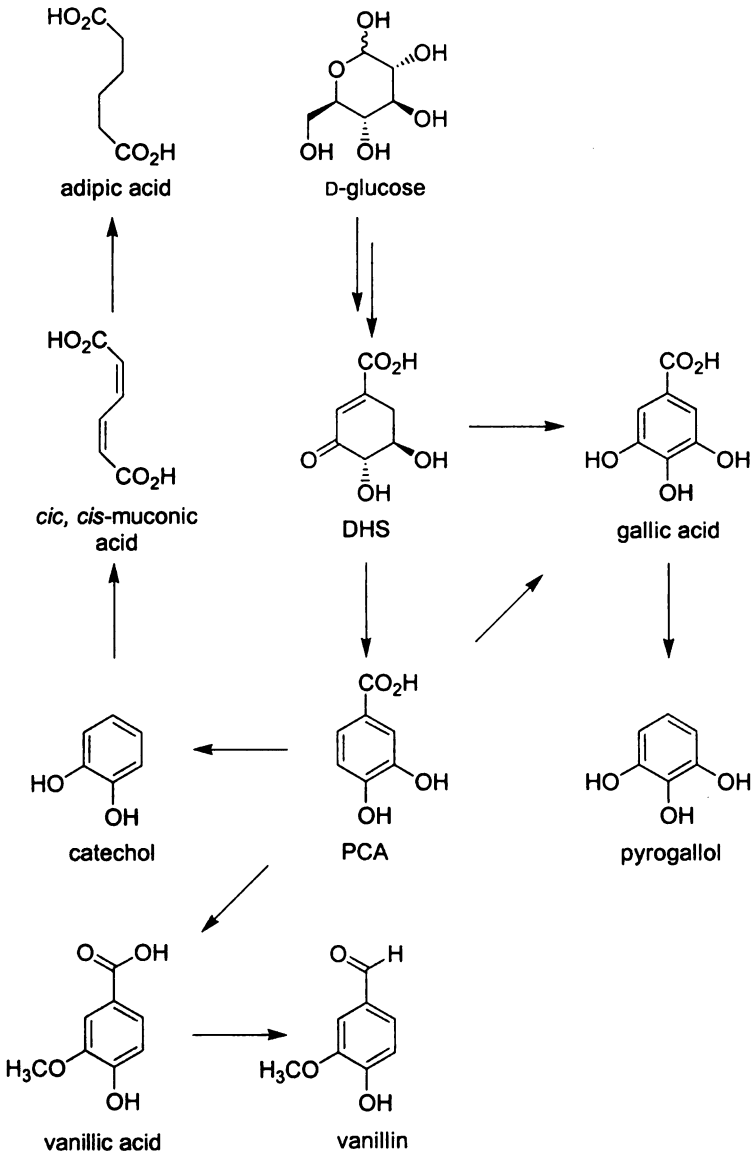

Figure 9. The central role of DHS in shikimate pathway-derived compounds.

In addition to industrially relevant chemicals tethered to the shikimate pathway via DHS intermediacy, several other prominent examples of key chemicals derived from different metabolites in the shikimate pathway are noteworthy. Indigo is the dye

responsible for the characteristic color of blue jeans, and their popularity has driven the worldwide production of indigo above 1 x 10^7 kg per year.[35a] As with the preceding discussions, both synthetic and biocatalytic routes to indigo are available. The current synthetic route commences with aniline and/or anthranilic acid and employs toxic, chlorinated, or cyanide containing reagents (Figure 10).[35b]

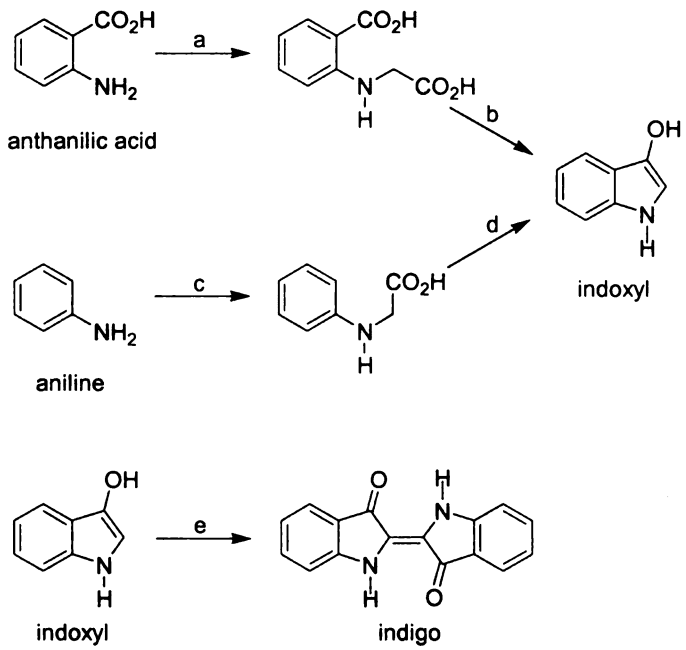

Figure 10. Synthetic indigo production. Reaction conditions: (a) $ClCH_2CO_2H$; (b) NaOH, Δ; (c) $ClCH_2CO_2H$; or HCHO, HCN, base; (d) $NaNH_2$, NaOH/KOH, 325 °C; (e) O_2, indoxyl.

Environmental and health hazards associated with the preceding synthesis of indigo can be circumvented by utilizing a biocatalytic route for the production of indigo. A microbial-catalyzed process for indigo production was recently elaborated (Figure 11). The bioprocess is capable of de novo indigo synthesis from glucose, and employs a heterologous *E. coli* biocatalyst that overexpresses tryptophanase and the *Pseudomonas*

putida-derived *NDO* operon responsible for naphthalene dioxygenase activity.[36] In the process, glucose is first converted to L-tryptophan (Figure 2). L-Tryptophan is then converted to indole by the action of a mutated *trp* operon (*trp20*) responsible for tryptophanase activity (Figure 11), with subsequent *NDO*-encoded naphthalene dioxygenase conversion to indoxyl and air oxidation to indigo. The bioprocess achieves very modest indigo accumulation (0.14 g/L). Although attempts to scale up biosynthetic indigo production have not proven cost effective thus far,[37] the potential for a commercially competitive fed-batch fermentation platform for indigo production remains an intriguing possibility.

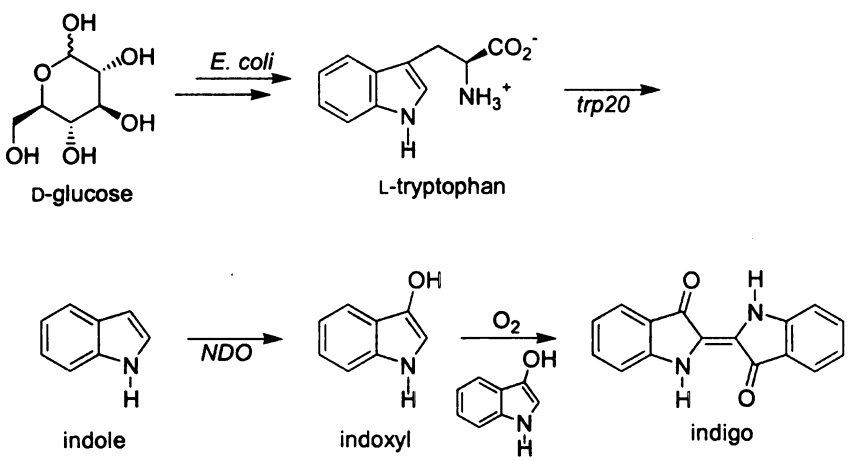

Figure 11. Biosynthesis of indigo from glucose.

p-Hydroxybenzoic acid (PHB) is a valuable intermediate in the biosynthesis of natural products and the chemical synthesis of several commercial goods. PHB finds its niche in the chemical industry as the starting material for parabens and liquid crystalline polymers (LCP's).[38] Parabens (PHB esters) are widely used in the cosmetics, food, and pharmaceutical markets as antimicrobial agents. PHB is also utilized as a monomer in

the LCP industry. While the paraben market consumes 1.4 x 10^6 kg of PHB annually, further expansion of LCP technology could raise the yearly demand to over 50 x 10^6 kg.[39]

Commercially, PHB is derived almost exclusively from benzene-derived phenol (Figure 12).[40] The drawbacks of this process include high temperature and pressure, and the toxic or carcinogenic characteristics of the feedstock and/or intermediates.

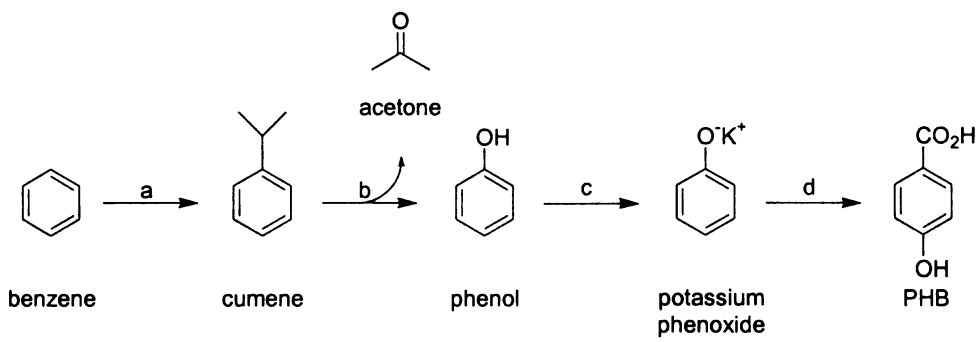

Figure 12. Synthesis of PHB. Reaction conditions: (a) propylene, solid H_3PO_4 catalyst, 200-260 °C, 400-600 psig. (b) O_2, 80-130 °C; SO_2, 60-100 °C. (c) KOH. (d) CO_2, 180-250 °C; H_2SO_4.

In an effort to employ milder reactions conditions, PHB has also been synthesized by enzyme-catalyzed carboxylation of phenol[41] and microbial oxidation of toluene.[42] However, these biocatalytic routes underscore petroleum dependence given their reliance upon either benzene or toluene. Alternatively, one can take advantage of PHB synthesis by recombinant microbes from renewable glucose (Figure 2). Overexpression of *ubiC*-encoded chorismate lyase in an *E. coli* host during fed-batch fermentation in conjunction with genomic modifications affords a PHB titer of 12 g/L from glucose in 13% yield (mol/mol).[39] Despite the precipitous decline in titer and yield relative to those reported for molecules such as DHS,[34] this process moves PHB bioproduction from proof-of-concept to the realm of scalable biocatalytic technology.

Aromatic Amino Acid Biosynthesis Pathway Metabolite Titer and Yield Enhancement via Metabolic Engineering.

Ultimately, the viability of any commercial process, be it synthetic or biosynthetic, is dictated by its economy versus competing processes. The rate and extent of bioprocess integration into mainstream chemical manufacture infrastructure will be dictated by process economics, rather than positive process aspects relative to established technologies. As conventional petroleum reserves dwindle, commanding a commensurate price premium, bioprocesses utilizing renewable feedstocks will play an increasingly prominent role amongst alternatives to supplant petroleum-based technologies. The yield of chemicals derived from the shikimate pathway, relative to the starting carbohydrate, and attainable titers are of paramount importance in determining bioprocess cost efficiency. To this end, the augmentation of shikimate pathway metabolites' titers and yields has been the focus of significant scrutiny.

Given its role as the first committed enzyme in the shikimate pathway, the extensive regulation of DAHP synthase is not surprising. In vivo DAHP synthase activity is subject to transcription repression, feedback inhibition, proteolytic degradation, thermal instability, and substrate availability. The first strategy typically employed to channel elevated carbon flow into the shikimate pathway is deregulation of DAHP transcriptional repression. Three DAHP synthase isozymes have been identified in *E. coli*, encoded by L-tyrosine-sensitive *aroF*, L-phenylalanine-sensitive *aroG*, and L-tryptophan-sensitive *aroH*. In excess of 99% of DAHP synthase activity is derived from the *aroF* and *aroG* isozymes,[43] and these isozymes are part of the *tyr* regulon, which also encompasses the *tyrR* gene. Control of the *tyrR* gene is dictated by accumulation of L-

tyrosine, L-phenylalanine, and L-tryptophan which operate as positive effectors for promotion of the *tyrR* gene.[43] The TyrR protein can then bind to *tyrR* box sequences in the promoter regions associated with *aroF* and *aroG* thereby preventing their transcription. L-Tyrosine and L-phenylalanine promote TyrR binding to *aroF*, while L-phenylalanine and L-tryptophan-mediated TyrR binding inhibit *aroG* transcription. Mutations in *tyrR*, which preclude an active gene product, result in derepression of *aroF* and *aroG* transcription.[44] Another viable option for transcriptional deregulation of *aroF* or *aroG* is simple titration via in vivo production of multiple TyrR binding sites through plasmid-localized overexpression of the DAHP isozyme of interest.

Feedback inhibition in the shikimate pathway was first demonstrated almost 30 years ago,[45] and feedback inhibition of DAHP synthase constitutes the most important factor controlling the flow of carbon into aromatic amino acid biosynthesis pathway in *E. coli*.[46] Indeed, the *E. coli aroF* and *aroG* isozymes can be inhibited in excess of 90% by sub-millimolar concentrations of L-tyrosine and L-phenylalanine respectively.[47] The following account therefore utilized a feedback-insensitive isozyme of *aroF*, denoted $aroF^{FBR}$, to circumvent feedback inhibition. The mutant allele was generated via UV mutagenesis, and is characterized by a point mutation that confers insensitivity to L-tyrosine.[48]

Once DAHP synthase expression is amplified to permit high shikimate pathway carbon throughput, the availability of substrate dictates the in vivo enzyme activity realized. The condensation of PEP and E4P by DAHP synthase to catalyze the formation of DAHP is therefore dependent on the intracellular pools of both substrates. The first limiting factor in shikimate pathway carbon flow, in the absence of DAHP synthase

activity constraints, is the availability of substrate E4P.[49] E4P availability is in turn dependent upon the pentose phosphate pathway enzymes *tktA* and *talB*. The low intracellular concentration of E4P maintained by *E. coli* at pseudo-steady state is theorized to result from its dimeric and trimeric forming tendencies.[50] Overexpression of either *tktA* or *talB* results in enhanced E4P production in theory, however *tktA* is a more attractive metabolic engineering target due to its catalysis of multiple E4P-forming reactions (Figure 13).[49b] The use of shikimate pathway metabolite titers as a litmus test for successful amplification of in vivo E4P concentration, via transketolase overexpression, has met with significant success.[49,51]

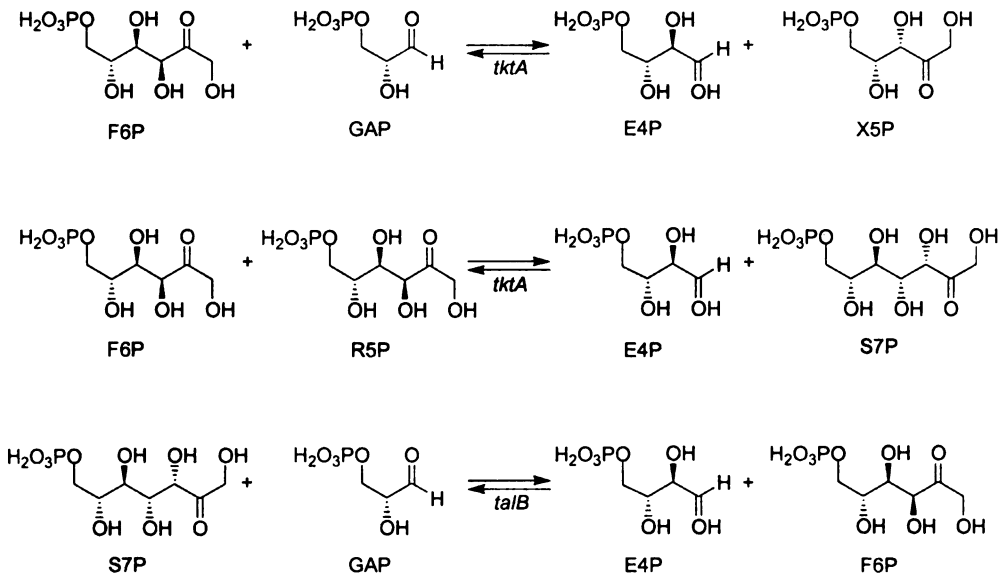

Figure 13. The role of *tktA* and *talB* in E4P formation. Metabolite abbreviations: F6P, D-fructose-6-phosphate; GAP, D-glyceraldehyde-3-phosphate; E4P, D-erythrose-4-phosphate; S7P, D-sedoheptulose-7-phosphate; X5P, D-xylulose-5-phosphate; R5P, ribose-5-phosphate.

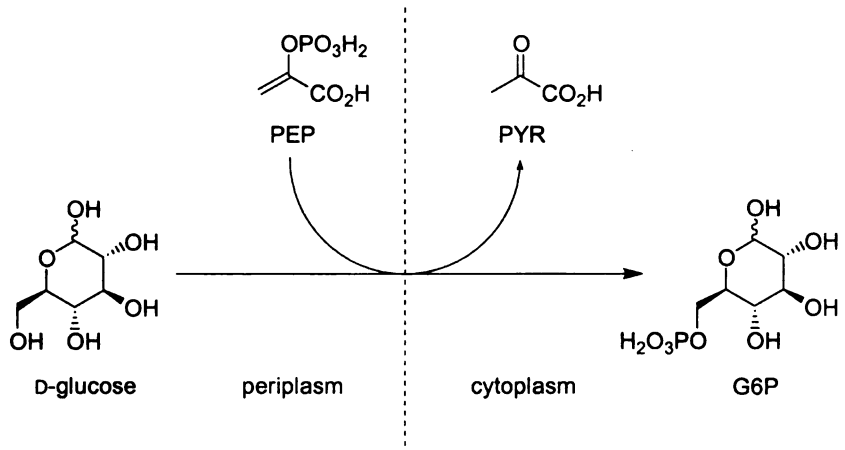

Figure 14. Import of glucose by the PTS system in *E. coli*. Metabolite abbreviations: PYR, pyruvate; G6P, glucose-6-phosphate.

PEP availability is the next limiting factor in shikimate pathway metabolite production in the absence of E4P limitation. The use of the phosphoenolpyruvate:carbohydrate phosphotransferase (PTS) system by *E. coli* for uptake and phosphorylation of glucose is inherently inefficient. One molecule of PEP is expended to transport and phosphorylate each molecule of glucose entering the cytoplasm, with concomitant PEP to pyruvate conversion (Figure 14). The net result of PTS-mediated glucose uptake and phosphorylation is a loss of three of the six carbons contained in glucose to perpetuating glucose uptake.[52] Competition for the intracellular PEP pool is further exacerbated by additional enzymes such as *ppc*-encoded PEP carboxylase[53] and *pykA*-encoded pyruvate kinase[54] that drain PEP for other cellular functions. Aromatic amino acid biosynthesis pathway intermediates distal to shikimate-3-phosphate require the incorporation of an additional PEP molecule, further reducing

PEP available for the import of glucose while simultaneously diminishing the theoretical yield from glucose of those metabolites.

What options exist for circumventing intracellular PEP limitations? Several authors have explored novel approaches to abolishing PEP constrained systems. One approach is to bypass the PTS entirely by utilizing pentose carbohydrate feedstocks for hydroaromatic biosynthesis. D-Xylose and L-arabinose have been utilized as the starting carbohydrate in microbe-catalyzed fed-batch fermentation DHS production, as part of an investigation exploring the feasibility of corn fiber feedstocks.[51a] The uptake of these pentoses is based on an ATP-permease system, permitting a theoretical yield of DHS from either pentose of 71% (mol/mol).[51] Another approach is to recycle pyruvate typically lost to CO_2 production in the tricarboxylic acid (TCA) cycle back to PEP by plasmid-mediated *pps* overexpression.[51b] The reaction requires the transfer of a high-energy phosphate from ATP to pyruvate and bolsters the theoretical maximum yield of shikimate pathway metabolites to 86% (mol/mol) from glucose.[52] This approach has met with significant success when DAHP has been the benchmark for increased pathway flux. Unfortunately, the robustness of *E. coli* recycling pyruvate in this fashion appeared questionable.[52] Subsequent studies utilizing fed-batch fermentation cultivation of *E. coli* with DHS and shikimic acid as markers for shikimate pathway carbon flow enhancement have not suffered the same fate though.[55] Other methods utilized to avoid in vivo PEP restriction include facilitated diffusion via heterologous *E. coli* gene expression of a glucose facilitator system (*glf*, *glk*) in a PTS deficient strain,[55b] upregulation of homologous glucose symports in *E. co*li,[56] and overexpression of *pck*-encoded PEP carboxykinase.[57]

Biochemical Engineering Considerations – Bioprocessing.

To this point, coupled biocatalysis-fermentation systems as benign routes to a diverse array of molecules traditionally obtained via natural product isolation or chemical syntheses rooted in petroleum have been discussed. In addition to the expense associated with natural product isolation, chemical syntheses are further hampered by harsh reaction conditions, toxic or carcinogenic intermediates or feedstocks, and byproduct waste stream generation. The alternate routes elaborated serve as a basis for comparison, typically employing mild reaction conditions in aqueous solutions with an absence of harmful intermediates and greatly reduced waste streams. Having lauded the benefits of biocatalytic processes to this point, one must question the inherent difficulties associated with these processes as well.

The challenges posed by biocatalytic processes are as diverse as the products derived from them. Batch, fed-batch, and continuous cultivation are all methodologies currently employed in the culture of microorganisms in the pursuit of carbohydrate bioconversion to value added chemicals, and animal cell cultivation for production of protein therapeutics. Of these methodologies, fed-batch fermentation dominates in the cultivation of bacteria, while continuous, or perfusion, culturing dominates in animal cell cultivation. Reactor design must take into account the specific nuances of the target cellular system. Bacterial systems frequently require high oxygen transfer and heat exchange rates to keep pace with prolific growth rates and the resulting high biomass densities. Eukaryotic and insect systems typically cannot tolerate excessive shear, experiencing extensive cell death in the presence of simple bubble bursting.[58]

A formidable challenge encountered in bacterial culture is the coupled problem of oxygen transfer rate (OTR) and heat transfer rate (HTR) limitations. For relatively small bioreactors (e.g., 1 m^3), an OTR of 8-10 $g \cdot L^{-1} \cdot h^{-1}$ becomes mechanically (impeller) rate limiting while HTR on the same scale does not typically become problematic until an OTR in excess of about 13 $g \cdot L^{-1} \cdot h^{-1}$ is achieved.[59] Examining a modest-sized reactor (in terms of production scale) of 10 m^3, the limiting OTR range remains unchanged. However HTR difficulties are magnified, becoming economically and mechanically limiting in the same OTR range.[59]

Three standard methodologies are employed for heat transfer in biochemical process vessels, jacketed vessels, baffles as heat transfer surfaces/coils (vertical), and heat transfer coils (helical).[60] Jacketed vessels rely on the external surface of the fermentor vessel as the heat transfer area, and the jacket covers the process vessel walls or the walls and the bottom of the vessel. Vertical coils are often employed in a dual capacity, serving both as baffles and as heat transfer vehicles. Unfortunately, the heat transfer capacity of both these systems is often outstripped by large scale, aerobic, bacterial cultures. Helical coils provide a much higher heat transfer surface area to process liquid volume ratio than either of the prior two heat transfer configurations, but their use is hampered by cost, leaks, enhanced cleaning difficulties, and mixing resistances. The capital expenditure for internal helical coils for a bioprocess vessel can augment the vessel cost by 15-25%.[61] Additionally, the potential for contamination of culture broth with non-sterile coolant increases as process vessels age and the coolant system welds deteriorate. Furthermore, internal coils foul, decreasing the overall HTR achievable by reducing the overall heat transfer coefficient. Coil cleaning is problematic as it must be

performed within the vessel. These shortcomings are further exacerbated as the HTR capacity of helical coils is still often challenged by rapidly growing bacterial cultures, necessitating the need for a chilled coolant if other process parameters are inflexible. The associated cost increment of such a bioprocess setup is typically exorbitant, and resulting process impediments include the freezing of lines and valves for coolants chilled to near or below freezing.[61]

The use of external heat exchangers for culture broth cooling appears an attractive alternative to internal heat exchange. External cooling would remove mixing inefficiencies imposed by helical coils, as well as the need to clean the coils within the process vessel. Standard tube-in-shell heat exchanger configurations typically provide reasonable cleaning capabilities, facilitating the removal of scale and maintaining the overall heat transfer coefficient near its maximum. Unfortunately, the potential for culture contamination is quite high. Additionally, pumping circulates the culture through substantially different process conditions than those experienced inside the process vessel. Finally, finding process pumps that are sterilizable/aseptic, mechanically reliable, easily cleanable, and capable of handling significant amount of entrained air while not harming the microorganisms being pumped is indeed a formidable challenge.[61]

The simplest process remedy for controlling highly exothermic fermentations therefore becomes reduction in culturing temperature. The growth rates of microorganisms such as *E. coli* are strongly temperature dependent.[62] Reducing the culturing temperature reduces the growth rate, and can preclude excessive enthalpy generation. Furthermore, reductions in culturing temperature do not necessarily diminish productivity, despite the reduction in growth rate and OTR requirements, or significantly

increased batch time in reaching stationary phase if the product of interest is a secondary metabolite.[59] Finally, reduction in broth temperature increases oxygen solubility,[63] providing a complimentary advantage in process OTR characteristics to that gained by slowed microbial growth.

In addition to the limiting OTR examples previously listed, numerous authors have investigated gas-liquid mass transfer in bioreactors ranging from bench to production scale.[64] Different processes dictate widely varying OTR requirements and capabilities. Traditionally, oxygen mass transfer has been enhanced by the action of mechanical agitation. The primary purpose of agitation is not to enhance turbulence and therefore increase k_L, the liquid mass transfer coefficient, but to reduce mean bubble diameter, thereby increasing the specific interfacial surface area (a) available for mass transfer and increasing gas hold up by decreasing bubble rise velocity.[64o] The specific power input to the culture required to drive bubble dispersion/disruption can ultimately becoming limiting from a cost or mechanical standpoint. Specific power inputs are exacerbated significantly in the presence of highly viscous, non-Newtonian broths[65] common in filamentous fungi cultures for industrial antibiotic fermentation.

A novel method for enhancing specific interfacial surface area in liquid-gas contactors without increased mechanical agitation is microbubble sparging.[64e,f,h,s,66] Microbubble generation and utilization was first described by Sebba, and typically involves the use of surfactant-stabilized, micron-sized diameter bubbles for liquid-gas mass transfer.[66] Microbubbles are typically generated external to the bioprocess vessel via a foam generator utilizing a bladeless, rotating disc at very high frequency for entrainment of the gas of interest from the headspace into the dilute surfactant

solution.[64e,f,h,s,66] The foam generated in this fashion is subsequently sparged to the bioprocess vessel via mechanical pumping. The void volumes of foams generated in this fashion typically range from 0.5-0.65, while microbubble diameters range from 20-1000 μm, conventional bubbles generated in fermentors via mechanical agitation are typically 3-5 mm in diameter.[64h]

The use of microbubble sparging can be especially beneficial for culturing animal cells, where the mechanical shear required for bubble disintegration can be extremely detrimental to the culture viability. In this instance however, the addition of surfactant to the medium can ultimately be as detrimental to the culture as enhanced shear, and in situ microbubble generation becomes necessary. This can be accomplished by employing porous metal frits of exceedingly small average pore diameter (e.g., less than 1 μm).[67] Although microbubbles generated in this fashion are subject to enhanced coalescence relative to surfactant-stabilized microbubbles, the lack of potentially harmful surfactant in the presence of enhanced OTR makes this method attractive.

Product recovery is another major consideration in the development of bioprocesses. Regardless of whether the fermentation product is a protein, a small molecule, gaseous, liquid, crystalline, or otherwise, its utility is obviated by the absence of an efficient recovery methodology. The recovery of fermentation products proceeds via steady and unsteady states, batch and continuous equipment, cocurrent and countercurrent contacting apparatuses.[68] A typical purification process for an antibiotic obtained via fermentation is listed in Table 1.[69]

Table 1. Example antibiotic recovery process.

Purification step	Product		
	Typical process	Concentration (g/L)	Quality (%)
Harvest broth	Fermentation	0.1-5	0.1-1.0
Removal of insolubles	Filtration	1.0-5	0.2-2.0
Isolation	Extraction	5-50	1-10
Purification	Chromatography	50-200	50-80
Polishing	Crystallization	50-200	90-100

Simple membrane filtration of biomass (e.g., removal of insoluble material) is typically precluded by the formation of an impermeable mat at the membrane.[70] Pretreatment of broths (e.g., heating, flocculation, etc.) assists in this process, however many primary separations are relegated to drum filtration or (semi)continuous centrifugation typically. Although continuous centrifugation tends to be rather effective, the associated capital and utility costs are significant, not to mention the maintenance requirements of such equipment. Drum filtration is also employed extensively. Although effective, drum filtration still requires the addition of a flocculating agent typically. Agents often employed range from simple acid and base for pH adjustment to filter aids such as diatomaceous earths and perlites.[71] One must take care in selecting a flocculating agent as it is often necessary to remove the agent at a downstream purification step.

Product isolation and purification can consist of several process steps, and selection of the appropriate methodology is typically critical in achieving success. Small molecule recovery is often accomplished through affinity chromatography, extraction or precipitation, while protein recovery methodologies can encompass affinity

chromatography, ultrafiltration, dialysis, or precipitation among others. Early steps in these processes are characterized by gross, relatively nonspecific processing, while latter processes are typified by highly selective screening for the bioproduct of interest.

Finally, polishing is carried out to convert the desired product to a useable form. Often crystallization and/or lyophilization are key polishing steps. Most bulk pharmaceuticals and organic fine chemicals are marketed as crystalline products.[72] Despite the rather simplistic steps involved in laboratory crystallization, production scale crystallization is more an art than science. Crystallization processes are often complicated by heat and mass transfer issues, the presence of trace impurities, and multiphase, multicomponent systems.[72] Lyophilization typically removes either water or solvent to levels acceptable in the specific process. The end result is a more stable product (e.g., increased longevity), preservation of activity (e.g., in enzymatic applications such as laundry detergents), or recovery of expensive/environmentally incompatible solvents.[73]

Substrate availability and expense can be problematic in the cost effective conversion of carbohydrates to value added chemicals. Purified carbon streams, although highly desirable in the culture of microorganisms, can be difficult to obtain at a cost conducive with conversion to small organic molecules such as PHB at an overall process cost on par with petroleum-derived routes. Substrate utilization at the commercial scale can be as diverse as the microorganisms employed and the products produced. Corn gluten-rich corn steeping liquor and coarse peanut meal are just two examples of substrates that can be employed as cost effective alternative carbon sources to refined hexose streams.

Recently, corn fiber has been examined as a potential source of hexoses and pentoses. Ammonia fiber explosion (AFEX) treatment has emerged as a viable method for unlocking the pentose and hexose streams sequestered in corn fiber as cellulose, hemicellulose, and starch.[74] AFEX treatment of lignocellulosic biomass begins with application of liquid ammonia at moderate temperatures and elevated pressures for less than 30 minutes.[74a] The rapid release of pressure allows a rapid phase change of the ammonia, exploding the fibrous biomass and permits an efficient recycling of ammonia (> 99%).[74a] Biomass treated in this fashion can be enzymatically hydrolyzed to hexoses and pentoses in high yield with subsequent bioconversion of these carbon sources to various products.[75] AFEX processing coupled with enzymatic hydrolysis circumvents hexose degredation often experienced during acid hydrolysis. Corn fiber becomes economically attractive as a carbon source in light of its total carbohydrate content (about 70%) and the prominent hexose (about 41%), pentose (about 29%), and starch (about 20%) carbohydrate components.[76]

Biochemical Engineering Considerations – Bioprocess Control and Modeling.

Fermentation operations pose formidable process modeling and control challenges due to their nonlinear nature and the lack of robust sensors for key metabolic variables. Prediction of substrate, biomass, and product concentrations in real-time is often hampered by inadequate process models, a lack of sensors for key variables, and sensor noise. Two "fuzzy" process control methods that have garnered significant attention in the past two decades are artificial neural networks (ANN) and Knowledge-Based (KB) control.

ANN have been widely used in predicting nonlinear process variables, both online and offline.[77] Real time control of fermentation variables is desirable, but can be difficult to achieve due to the highly nonlinear characteristics of fermentation processes and lack of reliable online information. ANN are attractive for prediction of fermentation processes because of their ability to learn and map highly nonlinear functions through training, without prior knowledge of the process.[77s] Historical data sets are used in the training process to obtain weight matrices, which serve as the basis for prediction when similar conditions are encountered.[77t] Recent examples of successful ANN applications in fermentation processes include a back propagation, multi-layer ANN constructed to overcome the difficulties of online monitoring of substrate consumption and product formation in lysine production,[77u] and a self-recurrent, multi-layer ANN used in conjunction with an Integrated System Optimization and Parameter Estimation algorithm for online prediction in 2,3-butanediol fermentations of *Klebsiella oxytoca*.[77f,gj] The powerful, non-parametric regression capabilities of ANN can be combined with the "first principles" knowledge of biochemical engineering to form so called "gray box" models that provide the capability to control ill-defined processes.[78]

Reviews and compilations of ANN literature as they pertain to control methodologies have been assembled in the last decade and provide the basis for the brief treatment here.[79] By definition, an ANN is a machine or program designed to model the way in which the brain performs a particular task or function of interest.[80] A nonlinear model of a neuron forms the basis of an ANN, and can be constructed with connecting links, weighting functions, a summing junction, and an activation function, to produce an output function (Figure 15).

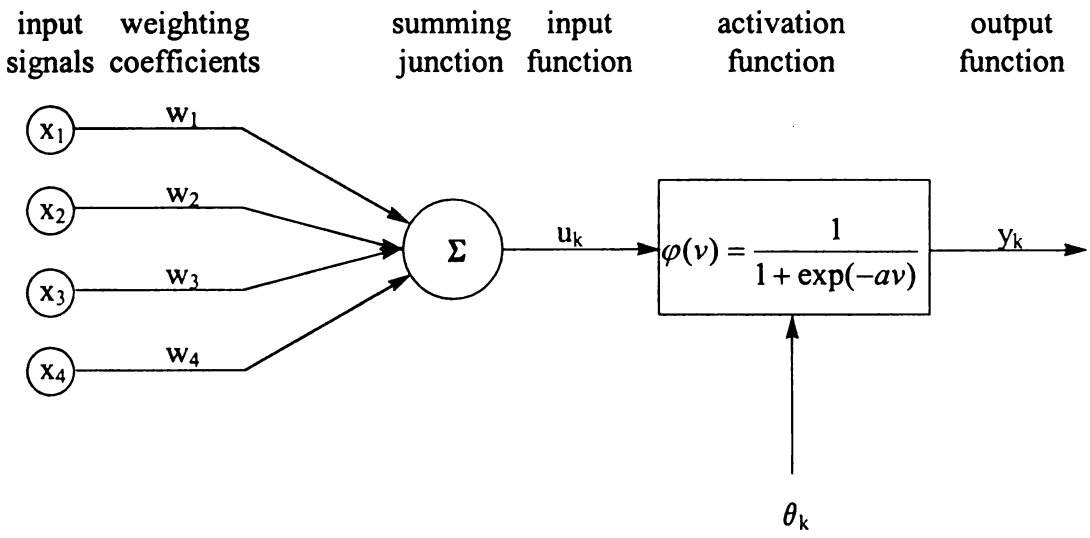

Figure 15. Schematic representation of a neural network neuron.

In the model, the input signals ($x_1...x_4$) are multiplied by the weighting factors ($w_1...w_4$) and summed to get an input function (u_k). The difference of the input function and the threshold (θ_k), multiplied by the activation function ($\varphi(v)$), produces an output (y_k). The mathematical representations of the input (Equation 1) and output (Equation 2) functions are given below.

Equation 1. $$u_k = \sum_{j=1}^{p} w_{kj} x_j$$

Equation 2. $$y_k = \varphi(u_k - \theta_k)$$

Each model neuron is a calculation node in the ANN, and the ANN can be comprised of numerous nodes assembled into multiple calculation layers (Figure 16). Figure 16 shows a simple ANN comprised of one input layer, one hidden layer, and one output layer. The ANN is initially trained with historic data, which determines the

strength (magnitude) of the weighting matrix elements, similar to the way the strength of some neuron connections in the brain are stronger than others.[80] After training, the neural network can then accept new input data, and make predictions based on prior knowledge.

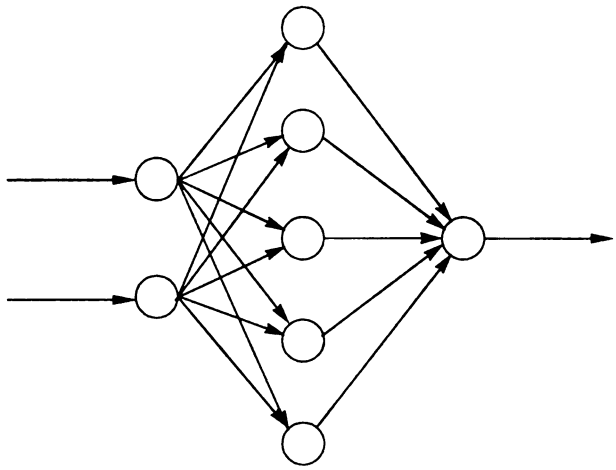

Figure 16. Example assembly of model neuron calculation nodes to form an ANN.

A second fuzzy control algorithm employed in fermentation processes is Knowledge-Based (KB) control.[81] KB, or expert system, control has increasingly been recognized as a viable method to supplement traditional controllers, such as PID control loops, in fermentation applications.[81] Expert systems have been likened to procedures that exhibit a degree of expertise in problem solving that is comparable to that of a human expert.[82] Expert systems typically consist of a searchable rule base. The prediction and control of the highly nonlinear behavior of many biological processes can be a daunting task if conventional algorithms are the sole source of control. Traditionally, the application of increasingly complex mathematical formalism for the modeling and control of fermentation processes has been pursued to accommodate nonlinear behavior.[81f] The complexity associated with many fermentation processes is not confined

to traditional mathematical frameworks however, and the resulting narrow scope of controllers implemented in this fashion often cannot distinguish between similar behaviors which might have strikingly different outcomes.[81f] In contrast, the implementation of KB control allows a control system to accommodate situations, process dynamics, etc. that might go unrecognized by conventional controllers. In this manner complex dynamics that could otherwise lead to undesired or even dangerous scenarios can be identified, and appropriate control action taken to ensure the process remains upon the desired trajectory.

KB control can be subdivided into two categories: direct control, and indirect (or supervisory) control. Direct control is typified by KB modules that operate at the level of standard PID controllers but are useful in realizing more complicated, nonlinear control algorithms and include such control methodologies as ANN.[81a] Direct KB control is referred to as fuzzy control,[81] and is accomplished by fuzzy controllers. Fuzzy control is based on fuzzy logic, developed to deal with problems lacking the ability to be solved by a simple 'yes' or 'no' answer.[83] Direct KB control incorporates its rule base into the control loop(s), and resembles conventional control in that actuators are directly manipulated in response to set point deviations, but more complex situations can also be managed. Direct KB control can be used in conjunction with, or in place of, conventional controllers. In contrast, indirect KB control is characterized by a division between the conventional controllers and the KB, supervisory system. In this configuration, measurement, data acquisition, etc. are performed by the conventional system, while the supervisory system issues commands to the conventional system, telling it when and what to do.[81a]

The searchable rule base that comprises the heart of a KB system is typified by the format: IF (condition 1) AND/OR (condition 2)...THEN (take action). Rule complexity can be arbitrarily increased with concatenations of the standard logical operators AND, OR, THEN, and ELSE to accommodate the specific behaviors, dynamics, and control nuances of a particular process control system. At-line control by the rule base is implemented by the use of an expert system development tool (ESDT). Unfortunately, ESDT specifically marketed for bioprocesses are currently unavailable, which makes ESDT selection critical in the development of bioprocess KB control, as many common functions must be assembled by the control system designer.[81a]

One mathematical modeling formalism prevalent in fermentation process analysis is stoichiometric modeling.[84] In the formulation of a stoichiometric model (SM), only the stoichiometry of known biochemical pathways is taken into account, and detailed kinetic rate data for enzymes are not required. The SM is a set of mass balances on metabolites involved in cellular metabolism, which can be posed via the formalism of matrices. Numerous authors have utilized SM in analyzing fermentation data to identify potentially rate-limiting enzymes, maximize carbon flux to desired pathways, or study the effects of arbitrary pathway flux manipulation.[84] The complexity of the SM can vary greatly, with integration of pathway fluxes for an entire fermentation[84p,q,r] giving way to optimizable objective functions for time dependent flux analyses.[84f,gj,k]

A SM may be underspecified, exactly specified, or overspecified. An underspecified SM is characterized by more unknown pathway fluxes than linearly independent metabolite balances. Such a system must have an optimizable objective function in order to determine the pathway flux distribution. An exactly specified system

is solved by a straightforward elimination process. An overspecified SM is characterized by more equations than unknowns, which permits a least squares solution method to be applied and gives a best fit solution to the flux distribution.[84q] The metabolite mass balances can be written in matrix form Equation 3.

Equation 3. $\frac{d\mathbf{v}}{dt} = \mathbf{A}\mathbf{x} - \mathbf{b}$

If the pseudo-steady-state assumption is invoked for non-excreted metabolites,[84h] then Equation 3 reduces to Equation 4. The **A** matrix is of m x n dimension, where m is the number of metabolites, n is the number of reactions, and $n \geq m$. The **b** vector is comprised of the metabolite production rates, and **x** is a vector containing the unknown fluxes. The pseudo-steady-state assumption can be justified by observing that intracellular volume is small compared to extracellular volume, and that intracellular metabolite concentrations are relatively constant compared to pathway fluxes.[84h] The unknown flux vector (**x**) can be solved for by taking the pseudo-inverse of **A**, which leads to a solution of the form given in Equation 5.

Equation 4. $\mathbf{A}\mathbf{x} = \mathbf{b}$

Equation 5. $\mathbf{x} = \left(\mathbf{A}^{\mathrm{T}}\mathbf{A}\right)^{-1}\mathbf{A}^{\mathrm{T}}\mathbf{b}$

The following chapters detail the obstacles attendant with hydroaromatic production from glucose, and utilize many relevant bioprocess aspects addressed in this introduction.

CHAPTER 2

Hydroaromatic Equilibration During Shikimic Acid Biosynthesis

Introduction

Shikimic acid (Figure 2) is a hydroaromatic intermediate in the common pathway of aromatic amino acid biosynthesis[85] found in plants,[86] microbes,[87] and parasites.[88] Shikimic acid possesses several characteristics that make it an attractive chiral molecule from which synthesis of biologically active compounds can proceed, including a highly functionalized, six-membered, carbocyclic ring with multiple asymmetric centers. Based on its chemical and chiral attributes, shikimic acid has attracted attention as the basis of a combinatorial library[89], and has recently been employed as the starting material in the synthesis of neuraminidase inhibitors such as the antiinfluenza drug GS4104[90] (Figure 17) developed by Gilead Sciences Inc. and marketed under the trade name Tamiflu™ by F. Hoffmann-La Roche Ltd.

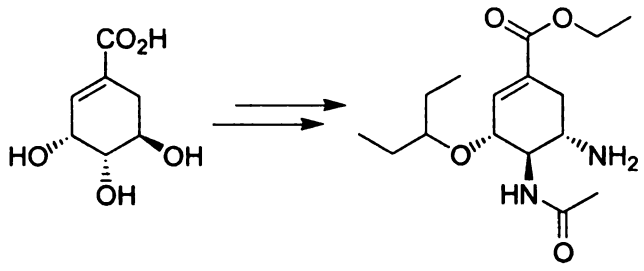

Figure 17. The structures of shikimic acid and neuraminidase inhibitor GS4104.

Unfortunately, the plentiful distribution of the shikimate pathway observed in nature does not translate into abundant availability of pathway intermediates such as shikimic acid. The tedious isolation of shikimic acid from *Illicium spp.*,[91] and resulting expense, have precluded its utilization in synthetic methodologies that require multi-ton, or even multi-kilogram, quantities. Furthermore, natural product isolation does not constitute a reliable source of material for the manufacture of pharmaceuticals. Shikimic acid availability limitations are further exacerbated by the lack of succinct or facile total syntheses of this synthon.[92]

The use of microbial biocatalysis for production of shikimate pathway intermediates and their derivatives has met with significant success in recent years,[33,51,93] and provides a potential route to shikimic acid that could supplant unreliable, laborious isolation from plants. The use of microbial biocatalysis is not without its hurdles however. As discussed in Chapter 1, carbon flow directed into the aromatic amino acid biosynthesis pathway is highly regulated, and the regulatory mechanisms responsible for this limitation must be addressed in order to accumulate significant concentrations of pathway metabolites. The success of any shikimic acid-producing process is contingent upon accumulating fed-batch fermentor titers substantial enough to make microbial shikimic acid biosynthesis economically viable at the commercial scale.

In this chapter, shikimic acid biosynthesis using *E. coli* is examined. The mechanism via which quinic acid is formed during shikimic acid biosynthesis is elucidated, and methodologies for suppressing or eliminating quinic acid contamination of shikimic acid cultures are elaborated.

Standard Fermentation Conditions and Oxygen Mass Transfer Rate Estimation.

The first issue addressed in fed-batch fermentations was the standard equipment conditions used to evaluate shikimic acid-producing constructs. Impeller spacing in the fermentor vessels was a critical factor in achieving the high oxygen transfer rates required to accommodate the oxygen demand of high density *E. coli* fermentations overexpressing shikimate pathway enzymes. The position of the impeller nearest the liquid surface in the standard impeller configuration for stirred vessels[94] was altered such that the surface of the initial liquid volume of fermentations fell in the center of the impeller blades. For the B. Braun Biotech (BBB) Biostat MD 2 L working volume system (M2 culture vessel), this was the center impeller. The bottom impeller was positioned as close to the sparger ring as possible, while the third impeller was spaced as close to equidistant from the middle impeller as possible. This procedure was repeated for the Dow 10 L working volume system. The impeller set up for the Bioflo IIc 1.25 L working volume system was modified slightly. Due to the reduced size of the Bioflo IIc vessel relative to the Biostat M2 culture vessel, use of three impellers was impractical and therefore only two impellers were employed. The top impeller was positioned such that the surface of the initial liquid volume of fermentations fell in the center of the impeller blades, and the bottom impeller was placed as close to the sparger ring as possible. The surface impeller in all three systems skimmed the liquid surface, enhancing aeration by entraining oxygen from the air present in the headspace of the fermentor.

The BBB Biostat MD k_La value attained at the standard maximum airflow rate and maximum impeller rate was estimated using an abiotic variation of the dynamic gassing-out method.[95] In gas-liquid contacting systems where the gas is only sparingly

soluble in the liquid, as in the case of oxygen and water, gas partitioning into a liquid is governed by the sum-of-resistances expression (Equation 6).

Equation 6. $$\frac{1}{K_L} = \frac{1}{k_L} + \frac{1}{Hk_G}$$

K_L is the overall mass transfer coefficient, k_L is the liquid side mass transfer coefficient, k_G is the gas side mass transfer coefficient, and H is Henry's Law constant for the gas-liquid system of interest. For sparingly soluble gasses, as in the case of oxygen, H is much greater than unity, and k_G is typically much larger than k_L.[96] Simplifying, we obtain Equation 7.

Equation 7. $$\frac{1}{K_L} \cong \frac{1}{k_L}$$

K_L is approximately equal to k_L from Equation 7. In practice, k_L is difficult to measure due to the uncertainty in determining the specific interfacial area (a) available for mass transfer.[96] Therefore, the combined quantity k_La was estimated. The liquid phase oxygen balance for a chemostat is given by Equation 8, where C is the liquid phase concentration of oxygen in the reactor, and thus the exit stream oxygen concentration as well. V is the volume of liquid in the reactor, F_{in} is the volumetric flow rate of liquid in with a corresponding oxygen concentration of C_{in}, and F_{out} and C are the analogous quantities for the outlet liquid stream. C_L^* is the liquid phase oxygen concentration in equilibrium with the gas phase at saturation, and k_La has been described previously. If V is constant, it can be extracted from the derivative term, and the equation divided by it. Assuming a constant V requires that the liquid inlet and outlet flow rates are identical, and therefore they collapse into a single, distributive term. At steady-state the derivative

can be set equal to zero, and Equation 8 can be rearranged to yield Equation 9 where D, the dilution rate, is given by Equation 10. Simple rearrangement of Equation 9 yields Equation 11, an expression for k_La in terms of easily measured quantities.

Equation 8. $$\left(\frac{d(CV)}{dt}\right) = F_{in}C_{in} - F_{out}C + k_La(C_L{}^* - C)V$$

Equation 9. $$D(C - C_{in}) = k_La(C_L{}^* - C)$$

Equation 10. $$D = \frac{F}{V}$$

Equation 11. $$k_La = \frac{D(C - C_{in})}{(C_L{}^* - C)}$$

Oxygen transfer experiments performed on the BBB MD units utilized the standard glucose-limited conditions' impeller rate (940 rpm) and airflow rate (1.0 L/(L·min)), and ambient temperature for the M2 culture vessels. The k_La values measured using this methodology were in the range of 500-550 h^{-1}. With k_La for the standard fermentation conditions known, Equation 11 can be rearranged to solved for C, yielding Equation 12, and a target C value to obtain similar oxygen mass transfer conditions could be calculated a priori when new conditions were being explored.

Equation 12. $$C = \frac{(k_LaC_L{}^* + DC_{in})}{(k_La + D)}$$

The unbaffled airflow rate was maintained, and baffles introduced into the M2 culture vessel. An impeller rate that provided a k_La within the unbaffled k_La range previously defined was sought for the baffled system. An impeller rate range of 750 – 775 rpm gave a comparable estimated k_La range to an impeller rate of 940 rpm in the

unbaffled system. Standard glucose-limited fermentation conditions are listed in Table 2. The same methodology was applied to determine cross-platform, standard, glucose-limited fermentation oxygen transfer conditions for the NBS Bioflo IIc (Chapter 4). The standard 8 L scale impeller rate was determined by trial and error to achieve a k_La and 48 h product titer (Chapter 4) similar to those observed on the smaller scale NBS and BBB equipment.

Table 2. Standard glucose-limited fermentation characteristics and set points.

Platform	BBB Biostat MD (DCU-1)	NBS Bioflo IIc	Dow Chemical
Laboratory	Dr. Frost	Dr. Worden	Dr. Worden
Maximum Impeller Rate	940 (750)	750	850
Baffled Reactor	No (Yes)	Yes	Yes
[a]Max. Airflow (vvm)	1.0	1.0	1.0
Temperature Set point	33 °C	33 °C	33.3 °C
pH Set point	7.0	7.0	7.0
Glucose Feed (g/L)	650	650	650
Glucose Feed Pump K_c	0.11	1.0	0.50
H_2SO_4 Concentration	2 N	6 N	18 N
NH_4OH Concentration	28-30 % w/v	28-30 % w/v	28-30 % w/v
Antifoam Concentration	Undiluted	Undiluted	Undiluted
Initial Liquid Volume	1.0 L	1.0 L	8.0 L

[a]vvm ≡ L air/(L culture·minute) = L/(L·min)

Background and Initial Shikimic Acid Fermentations.

The remainder of this chapter deals with standard, glucose-limited fermentation conditions in the Frost laboratory, or fermentation conditions which are modified from the standard conditions as indicated.

Shikimic acid-producing (SP) *E. coli* host strains were genetically engineered by Dr. Karen Draths of the Frost Group. All plasmids bearing the "pKD" prefix were constructed by Dr. Karen Draths. All plasmids bearing the "pDK" prefix were constructed by the author. All plasmids bearing the "pKL" prefix were constructed by Dr. Kai Li of the Frost Group. All plasmids bearing the "pLZ" prefix were constructed by Lingyan Zhu of the Frost Group.

Several genetic traits were shared by shikimic acid-synthesizing *E. coli* host biocatalysts. The absence of catalytically-active shikimate kinase provided for shikimic acid accumulation in culture supernatants by preventing enzymatic conversion of shikimic acid to shikimate-3-phosphate (Figure 2). Disruption of shikimate kinase activity was accomplished by disrupting shikimate kinase-encoding *aroL* and *aroK* via successive P1 phage-mediated transductions of *aroL478*::Tn*10* and *aroK17*::Cm^R.[97] The *aroL478*::Tn*10* mutation was a transposon-linked genetic element which encoded for tetracycline (Tc) resistance. The *aroK17*::Cm^R mutation was a transposon-linked genetic element which encoded for chloramphenicol (Cm) resistance. Due the absence of catalytically active shikimate kinase, growth of shikimic acid-synthesizing biocatalysts required supplementation with the aromatic amino acids L-phenylalanine, L-tyrosine, and L-tryptophan (Figure 2), along with aromatic vitamins potassium *p*-aminobenzoate, *p*-

hydroxybenzoic acid, and 2,3-dihydroxybenzoic acid for biosynthesis of protein, folic acid, coenzyme Q, and enterochelin.

Plasmids expressed a mutant *aroF* gene insensitive to feedback inhibition by L-tyrosine, denoted $aroF^{FBR}$, with its functional native promoter as described in Chapter 1.[48] DAHP synthase catalyzes the condensation of substrates E4P and PEP to form DAHP, the first committed intermediate in the aromatic amino acid biosynthesis pathway. Therefore, DAHP synthase activity levels are critical to the success of any hydroaromatic-synthesizing biocatalyst, and dictated the need for overexpression of this enzyme in all shikimic acid-producing biocatalysts.

Due to the increased carbon flow directed into the shikimate pathway (Figure 2) resulting from increased in vivo activity of DAHP synthase, wild-type expression levels of *aroB*-encoded DHQ synthase were inadequate to convert substrate DAHP into product DHQ at a rate sufficient to avoid substrate accumulation. DAHP undergoes dephosphorylation to 3-deoxy-D-*arabino*-heptulosonic acid (DAH), which accumulates in culture supernatants resulting in reductions in titer, yield, and purity of synthesized shikimic. Insertion of an extra copy of *aroB* into the *E. coli* genome has been found adequate to relieve the rate-limiting characteristic of DHQ synthase.[98]

The genomic modification responsible for increased DHQ synthase expression in shikimic acid-synthesizing biocatalysts resulted from the recombinant, site-specific insertion of a cassette consisting of *aroB* with flanking *serA* nucleotide sequences into the *serA* locus. The *serA* locus encodes 3-phosphoglycerate dehydrogenase, an enzyme necessary for biosynthesis of L-serine.[99] Growth in medium lacking L-serine supplementation requires expression of *serA* localized in all plasmids, therefore this

mutation was the basis for both plasmid maintenance and elevated *aroB*-encoded DHQ synthase activity.

The enzyme responsible for conversion of DHS to shikimic acid is *aroE*-encoded shikimate dehydrogenase (Figure 2). The feedback inhibition of the enzyme by shikimic acid represents the final metabolic impediment to shikimic acid synthesis in shikimic acid-synthesizing host strains.[98] Inhibition of shikimate dehydrogenase by synthesized shikimic acid prevents complete conversion of substrate DHS to shikimic acid. DHS substrate accumulation in culture supernatants results in a significant reduction in titer, yield, and purity of shikimic acid. Overexpression of shikimate dehydrogenase was accomplished by plasmid-localized P_{tac}*aroE* in constructs as indicated.

E. coli SP1.1 was derived from the parent strain *E. coli* RB791. RB791 is an *E. coli* variant that differs from the wild type *E. coli* K-12 isolate W3110 by a single mutation. Construction of SP1.1 began with the homologous recombination of the *aroB* gene into the *serA* locus of *E. coli* RB791, resulting in RB791 *serA*::*aroB*. The procedure for homologous recombination was based on methods described elsewhere.[33] RB791 *serA*::*aroB* was then subjected to two successive P1 phage-mediated transductions to transfer the *aroL478*::Tn*10* and *aroK*::Cm^R loci of ALO807[100] onto the genome, eliminating shikimate kinase activity. The RB791 *serA*::*aroB aroL478*::Tn*10 aroK*::Cm^R host was renamed SP1.1.

The construction of plasmid pKD12.112A began with PCR amplification of a 1.2-kb P_{tac}*aroE* fragment from pIA321,[101] digestion of the fragment with *Kpn*I and subsequent ligation with pKL4.20B (3.6-kb) that was linearized by *Kpn*I treatment, afforded the 4.8-kb plasmid pKD12.036A (Figure 18). Plasmid pKL4.20B had

previously been created in the Frost laboratory and bears the *aroF*^{FBR} locus on a pSU18 vector. Vector pSU18 is a 2.3-kb plasmid that harbors a *p15A* origin of replication, has a copy number of approximately 12 per cell,[102] contains a *lac* promoter, and also bears a genetic marker encoding for Cm resistance. The orientation of the P_{tac}*aroE* locus in pKD12.036A is in the opposite direction as that of *aroF*^{FBR}. The *serA* locus was obtained by digestion of pD2625[98] with *EcoR*V and *Dra*I. Blunt end ligation of this 1.9-kb fragment into pKD12.036, which had been linearized by *Sma*I digestion, afforded the 6.7-kb plasmid pKD12.047A (Figure 19). The orientation of the *serA* gene was in the same direction as that of P_{tac}*aroE*. The *β-lac* gene was amplified by PCR from pUC18, treated with *Nco*I and ligated into the *Nco*I site of pKD12.047A resulting in the 7.7-kb plasmid pKD12.112A (Figure 20).

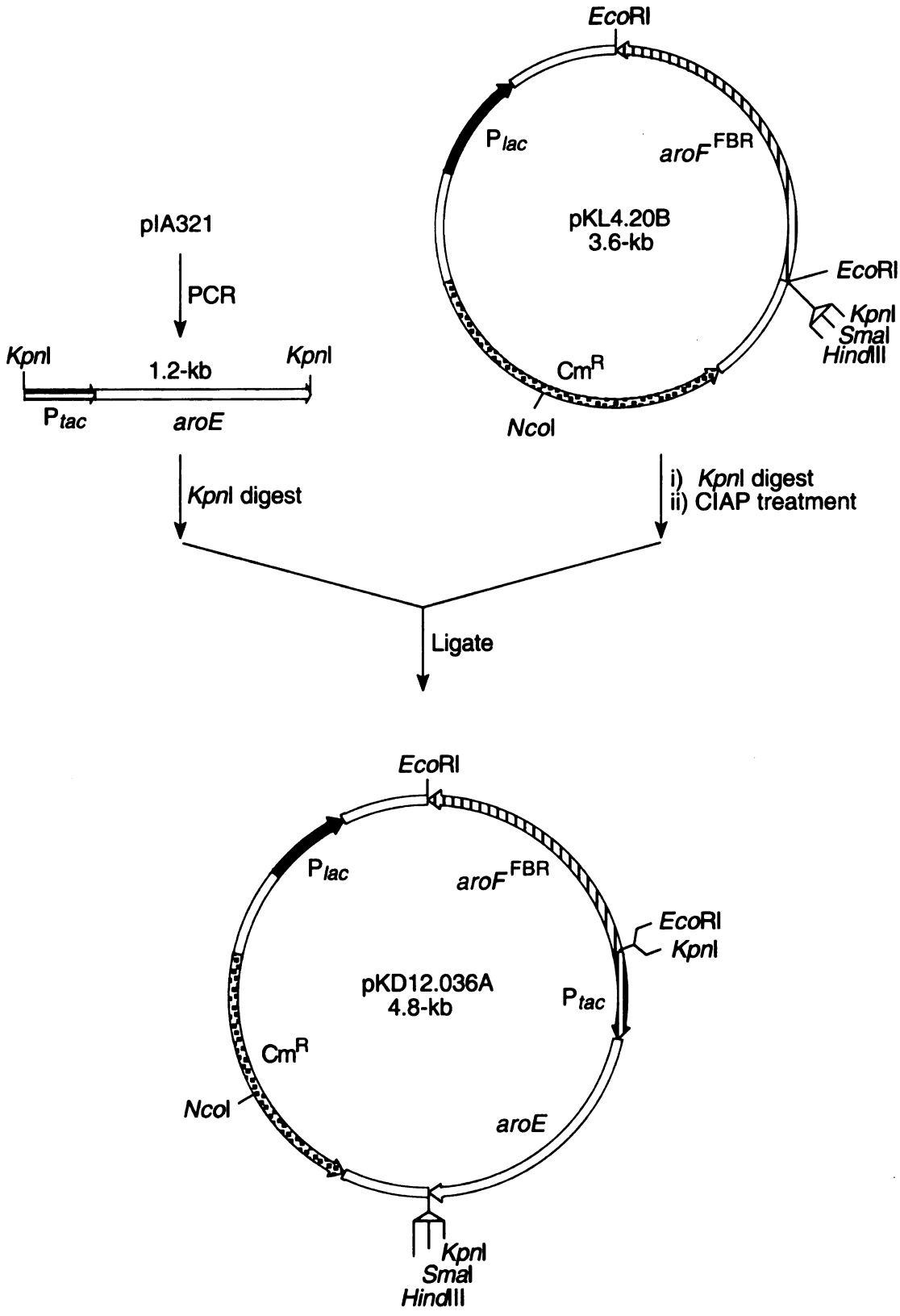

Figure 18. Plasmid pKD12.036A.

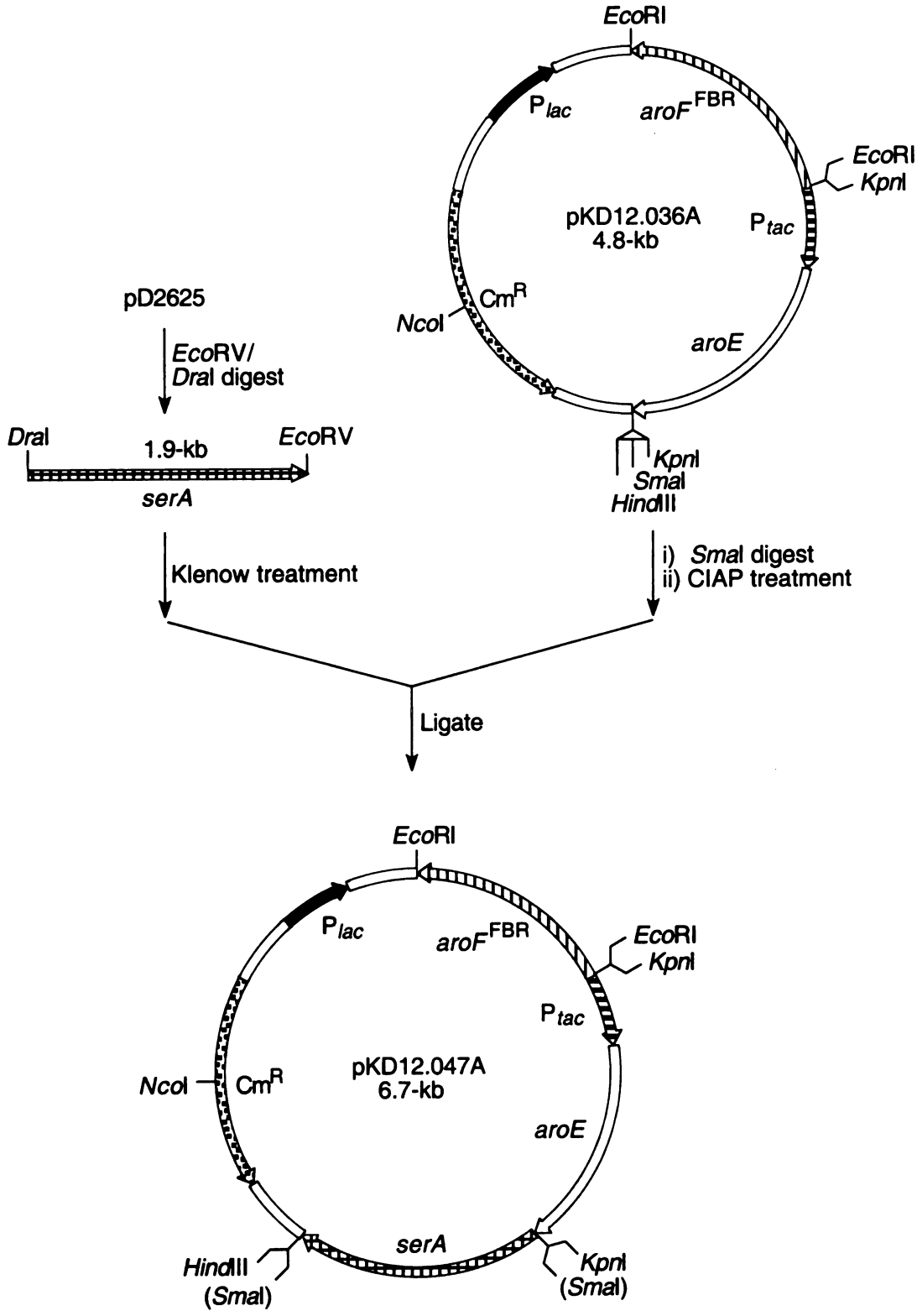

Figure 19. Plasmid pKD12.047A.

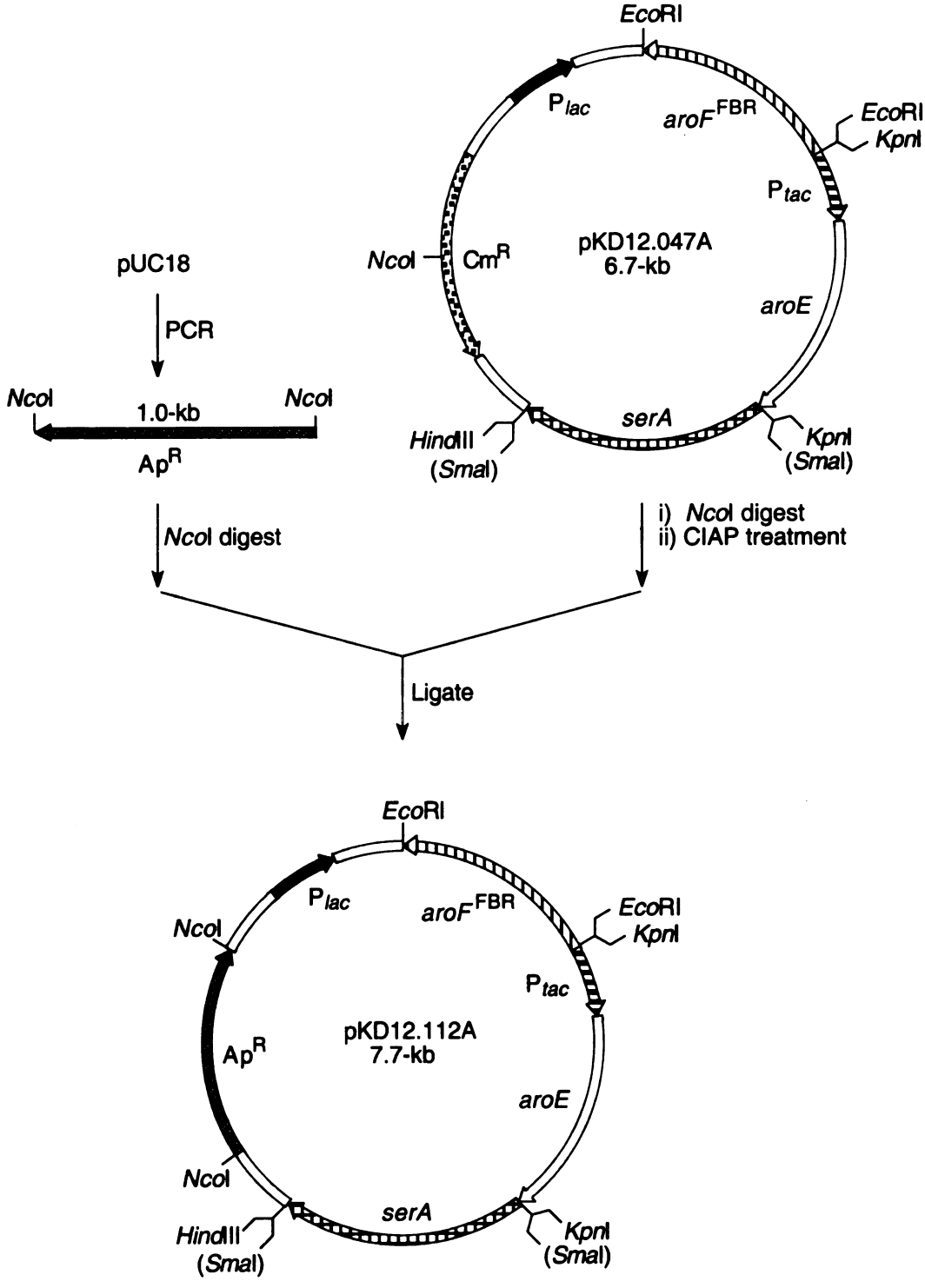

Figure 20. Plasmid pKD12.112A.

Initial shikimic acid fermentations performed by Dr. Karen Draths with *E. coli* SP1.1/pKD12.112A proceeded as expected, with shikimic acid as the major product and DHS as a significant byproduct. DHS formation was not surprising given shikimic acid was known to feedback inhibit shikimate dehydrogenase, the enzyme responsible for the DHS to shikimic acid conversion (Figure 2).[98] In addition to shikimic acid and DHS, ^{1}H NMR analysis of culture supernatants revealed that a significant concentration of another, unknown compound was present. The unknown compound was postulated to be quinic acid. The presence of quinic acid was subsequently confirmed by comparison of ^{1}H and ^{13}C NMR spectra of authentic quinic acid to spectra of fermentation supernatants. A typical product ratio observed for SP1.1/pKD12.112A was 8.8:2.3:1.0 shikimic acid:DHS:quinic acid (SA:DHS:QA, mol/mol/mol), with the onset of quinic acid formation typically occurring between 18 h and 24 h. Final product titers accumulated were 24 g/L shikimic acid, 6.0 g/L DHS, and 2.9 g/L quinic acid. The unexpected appearance of quinic acid in shikimic acid fermentations was puzzling given the absence of quinate dehydrogenase in *E. coli*, an oxidoreductase that interconverts DHQ and quinic acid in *K. pneumoniae*.[103] The appearance of quinic acid in shikimic acid fermentations was also perplexing given the difficulties associated with purifying contaminating quinic acid away from shikimic acid due to their structural similarities (Figure 21), which precluded complete removal of contaminating quinic acid from shikimic acid unless the SA:QA (mol/mol) was in excess of 10. Potential sources of quinic acid formation in shikimic acid fermentations were postulated to include homologous quinic acid formation by SP1.1/pKD12.112A or biosynthesis of quinic acid by a contaminating microbe.

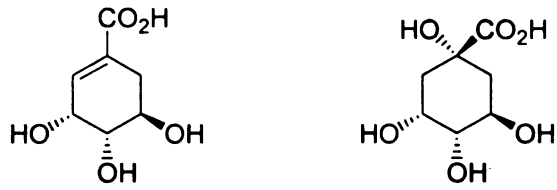

Figure 21. The structures of shikimic acid and quinic acid.

Preventing quinic acid formation initially focused on modification of the shikimic acid-producing construct. One hypothesis for quinic acid formation was that DHQ could be reduced to quinic acid by an unknown *E. coli* enzyme that competed for substrate DHQ with DHQ dehydratase. Overexpression of *aroD*-encoded DHQ dehydratase might reduce quinic acid formation by converting more DHQ to DHS before reduction of DHQ to quinic acid could occur. The *aroD* gene was overexpressed by introduction into plasmid pKD12.112A by first digesting plasmid pKD201 with *Cla*I to liberate the *aroD* gene. Following digestion of pKD12.112A with *Hind*III and Klenow treatment, the 1.8-kb *aroD* fragment was blunt ended using Klenow treatment and ligated into linearized pKD12.112A to afford the resulting 9.5-kb plasmid, pKD12.152A (Figure 22). The *aroD* gene is transcribed in the same direction as the *serA* gene.

Plasmid pKD12.152A was transformed into SP1.1 and the construct was examined under standard fed-batch fermentation conditions. Analysis of the fermentation supernatant by ^{1}H NMR revealed only trace levels of quinic acid, apparently due to the use of construct SP1.1/pKD12.152A. Overexpression of DHQ dehydratase by plasmid localization of *aroD* had seemingly alleviated the majority of quinic acid formation, suggesting excessive quinic acid formation was an artifact unique to the SP1.1/pKD12.112A construct's lack of *aroD* overexpression.

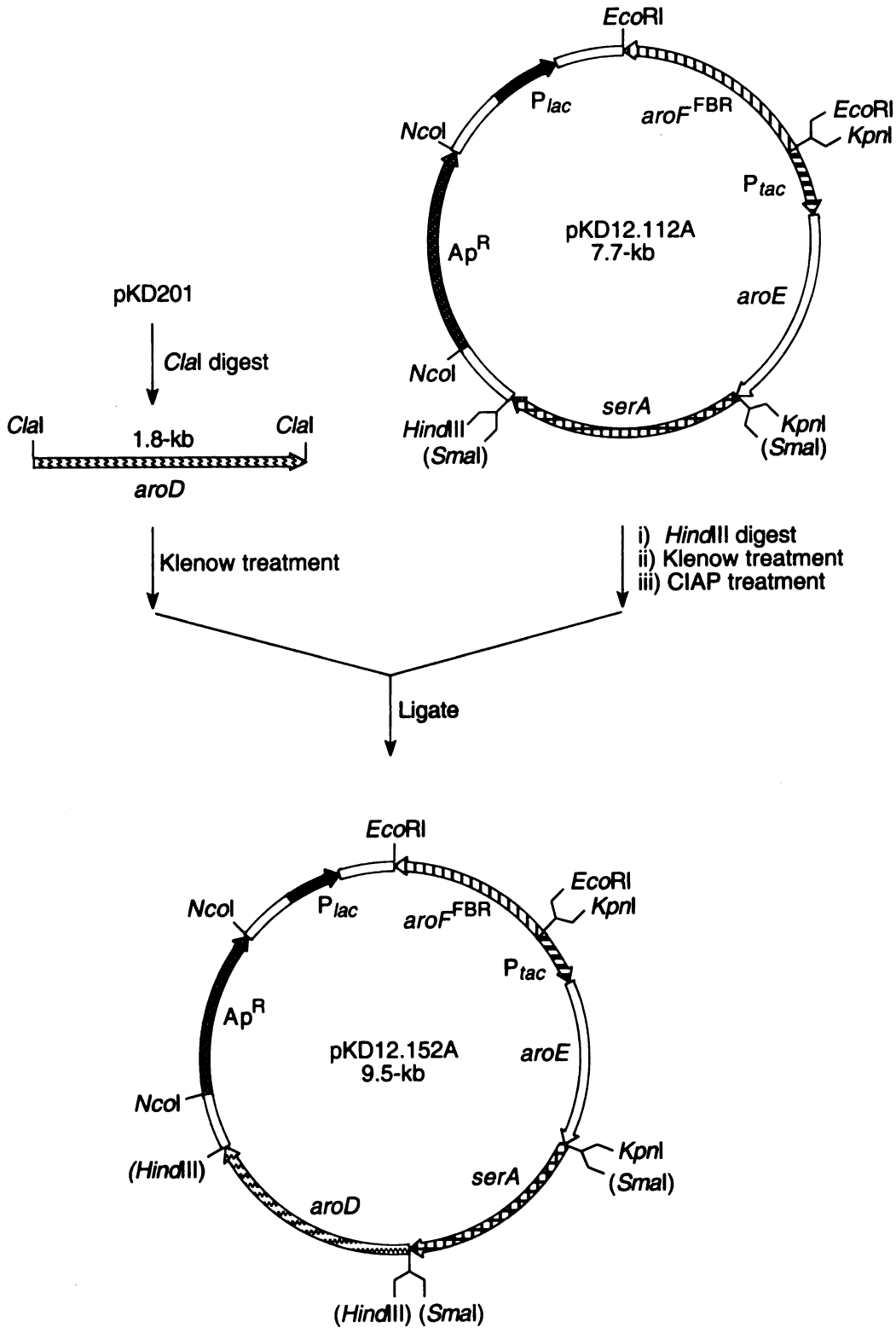

Figure 22. Plasmid pKD12.152A.

Reemergence of Quinic Acid Biosynthesis.

Thus far the standard glucose limited conditions in the Frost laboratory employed a D.O. concentration set point of 20% of air saturation and a maximum airflow rate of 3.0 vvm. At this point, responsibilities for performing shikimic acid fermentations shifted from Dr. Draths to the author. It appeared that problematic quinic acid formation was essentially eliminated, and thus the focus of shikimic acid fermentations shifted to optimization, in an effort to define more industrially viable conditions. The first changes implemented in fermentation conditions were the reduction of the maximum airflow rate from 3.0 vvm to 1.0 vvm, and an increase in the size of the primary exhaust gas filter employed from a diameter of 37 mm to 50 mm (Gelman, Acro37 and Acro50, respectively). The reduction in airflow rate was motivated by a desire to render the standard fed-batch fermentation conditions more industrially compatible, while the increase in the gas filter size was used to alleviate fermentor back pressure accumulation.

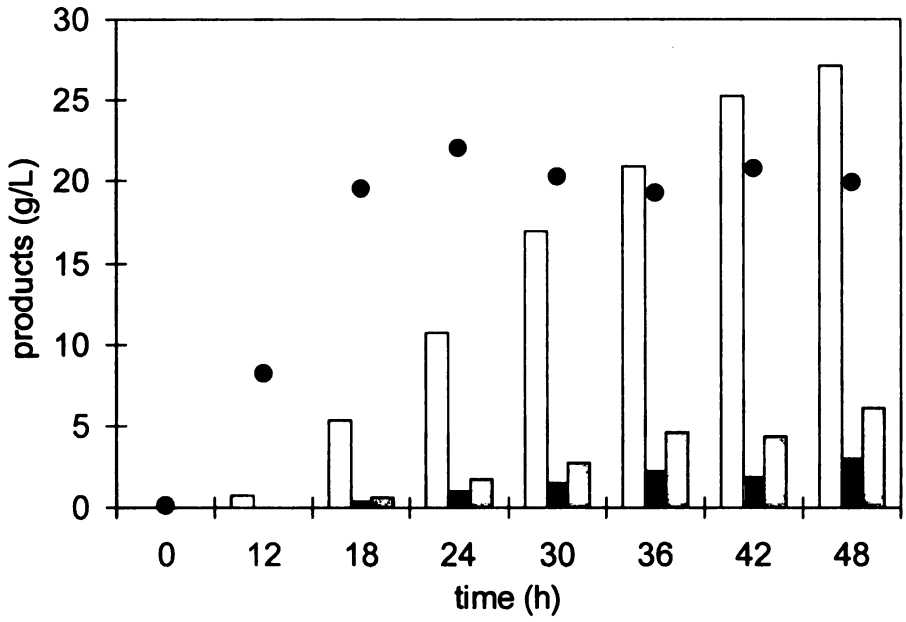

Figure 23. Fed-batch fermentation of SP1.1/pKD12.152A at an airflow rate of 3.0 vvm. Shikimic acid□, quinic acid■, DHS□, cell mass●, in g/L.

Dr. Draths's original fermentation conditions (3.0 vvm) were initially repeated with SP1.1/pKD12.152A to obtain baseline conditions for comparison with future fermentations utilizing altered process conditions. Surprisingly, the formation of quinic acid reappeared (Figure 23) at concentrations intermediate to those previously observed for SP1.1/pKD12.112A and SP1.1/pKD12.152A. Final product titers were 27 g/L shikimic acid, 6.1 g/L DHS, and 3.0 g/L quinic acid. Although the SA:QA was 10, permitting isolation of pure shikimic acid, the reemergence of quinic acid as a significant byproduct was troubling. Subsequently, the maximum airflow rate was reduced to 1.0 vvm and Acro50 filters were utilized for the primary exhaust gas outlet on fermentation

runs. A fermentation performed immediately following these changes, resulted in several noteworthy observations.

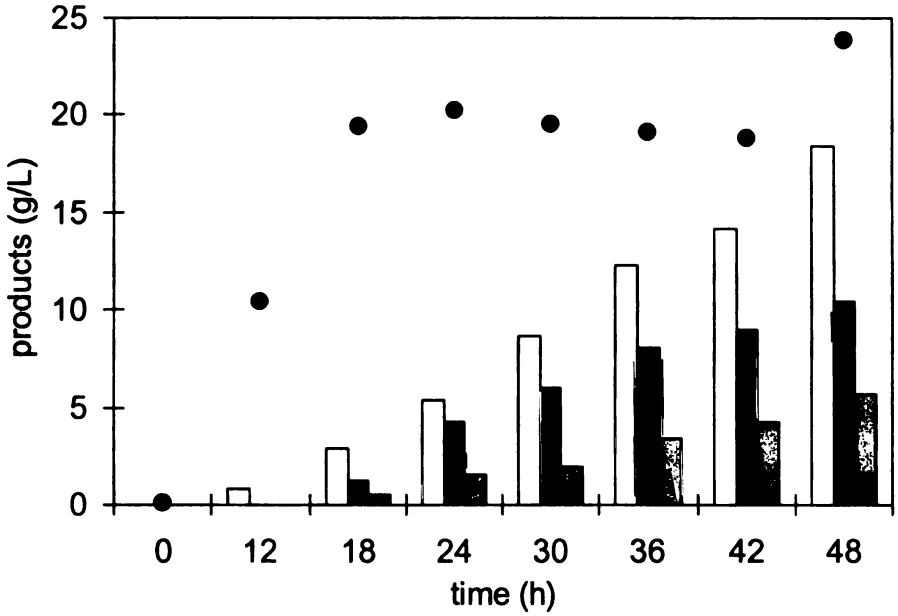

Figure 24. Fed-batch fermentation of SP1.1/pKD12.152A at an airflow rate of 1.0 vvm. Shikimic acid□, quinic acid■, DHS□, cell mass●, in g/L.

Firstly, neither the maximum biomass concentration achieved nor the resulting total accumulated product concentrations were deleteriously affected by the reduction in airflow rate. This suggested that the maximum impeller rate of 940 rpm was too slow for the oxygen transfer rate to be substantially enhanced by simply increasing the airflow rate above 1.0 vvm. This was not surprising given that the standard reactor configuration lacked baffles. Secondly, the backpressure accumulated in the reactor was virtually eliminated by the increase in the primary exhaust filter size. Lastly, the formation of quinic acid reemerged not only as an unwanted byproduct, but as a substantial fermentation supernatant constituent. Culturing SP1.1/pKD12.152A at 1.0 vvm resulted

in the formation of 18.4 g/L shikimic acid, 10.4 g/L quinic acid, 5.7 g/L DHS, and a SA:DHS:QA of 1.9:0.61:1.0. Not only had quinic acid formation increased dramatically, it had apparently done so at the expense of shikimic acid. Comparing the SP1.1/pKD12.152A fermentations in Figure 23 and Figure 24, shikimic acid titer dropped almost 9 g/L, while quinic acid concentration increased by 7.4 g/L, with DHS virtually unchanged. Given the lack of plausible rationale linking airflow rate to product mixture, and the seemingly unpredictable fashion in which quinic acid formation was enhanced or reduced, quinic acid biosynthesis was again postulated to be an artifact of contamination by a competing microbial population.

Anti-Contamination Measures Fail to Prevent Quinic Acid Biosynthesis.

Environment-born prokaryotic or fungal contamination was suspected as the source of quinic acid biosynthesis in fermentations. In such a scenario, shikimate pathway carbon flux which otherwise would be directed toward shikimic acid biosynthesis would be diverted to quinic acid biosynthesis by a contaminating species, potentially reducing the realizable titer and yield of shikimic acid from glucose. The theory that quinic acid biosynthesis was a result of prokaryotic contamination was plausible given that *K. pneumoniae* can interconvert quinic acid and DHQ via quinate dehydrogenase. Furthermore, in vitro experiments with extracts of *Aerobacter aerogenes* and *K. pneumoniae* had demonstrated that quinic acid could be converted to shikimic acid when the proper cofactors were present.[104] Similarly, fungal contamination was also a viable source of quinic acid biosynthesis given literature reports of *Neurospora crassa* mutants able to interconvert DHQ and quinic acid.[105]

The first approach undertaken to prevent quinic acid formation was improvement in aseptic technique. Prior to quinic acid appearing in shikimic acid fermentations, aromatic amino acid supplementation was accomplished by the addition of non-sterile, dry powders of L-tyrosine, L-phenylalanine, and L-tryptophan to the fermentor vessel immediately preceding inoculation. The procedure was modified to in situ aromatic amino acid sterilization in the fermentation medium. Pre-autoclaving and post-autoclaving ^1H NMR spectra of fermentation medium supplemented with the aromatic amino acids at the same concentrations employed in fermentation experiments revealed no apparent degradation products or decline in quantified concentrations. The fermentor air inlet filter was autoclaved in place on the vessel air inlet line. Previously the air inlet filter had not been autoclaved. Antifoam was autoclaved in a reagent addition bottle and added manually through the multi-addition port via a peristaltic pump instead of opening a head plate port and using a pipetman. An empty reagent addition bottle was autoclaved with the fermentor and used to transfer the inoculum to the fermentor. Previously the inoculum was poured from a growth flask into the fermentor through an open port in the head plate. The procedure was modified to transfer of the inoculum from the growth flask to the sterile reagent addition bottle in the laminar flow biological safety cabinet. The inoculum was then added from the reagent addition bottle into the fermentor through the multi-addition port via a peristaltic pump. An initial glucose solution was prepared and autoclaved in a reagent addition bottle. Just prior to the start of the fermentation, sterile solutions of trace minerals, $MgSO_4$, and aromatic vitamins were added to the initial glucose solution in the laminar flow biological safety cabinet. The combined solution was then added to the fermentor through the multi-addition port via a peristaltic

pump. The solutions had previously been added into the fermentor by pouring (initial glucose solution) or by a pipetman (trace minerals, $MgSO_4$, and aromatic vitamins) through an open port in the head plate.

Prevention of microbial contamination was further pursued by addition of antibiotics to inoculums and fermentations. Tetracycline (Tc) was a logical choice for antibiotic addition since the mutation employed to disrupt catalytically active *aroL*-encoded shikimate kinase II conferred Tc resistance upon SP1.1. Tc was added to inoculums, to the fermentor at the beginning of fermentations, and again at 18 h. Despite the presence of Tc, and the improvements in aseptic technique, quinic acid formation persisted in shikimic acid fermentations. This strongly suggested that quinic acid formation was either a host-dependent, homologous occurrence, or that a non-prokaryotic contamination such as *Neurospera crassa* was responsible for quinic acid formation.

Two key observations about shikimic acid producing cultures transpired shortly thereafter. First, when shikimic acid-producing cultures were grown in shake flasks, quinic acid formation was detected only subsequent to initial glucose depletion and appeared to progress at the expense of shikimic acid already present in the medium. This suggested that quinic acid formation might be a homologous, glucose-dependent phenomenon. Second, a SP1.1/pKD12.152A fermentation (Figure 25) in which a D.O. electrode malfunctioned during the fed-batch portion of the fermentation failed to accumulate detectable quinic acid. The malfunction manifested itself as an oscillatory D.O. concentration, hence the glucose feed rate to the fermentor oscillated as well. The shikimic acid (25 g/L) and DHS (6.5 g/L) titers were relatively unaffected by the

malfunction compared to prior fermentations (Figure 23), however the biomass concentration (16 g/L) developed was substantially lower.

The surprising decrease in quinic acid formation, relative to previous fermentations whose D.O. electrodes functioned properly (e.g., minimal D.O. concentration oscillations during the fed-batch portion of the fermentation), again implicated a homologous mechanism for quinic acid formation in shikimic acid-synthesizing cultures. These observations served as the starting point for optimizing shikimic acid fermentation selectivity conditions.

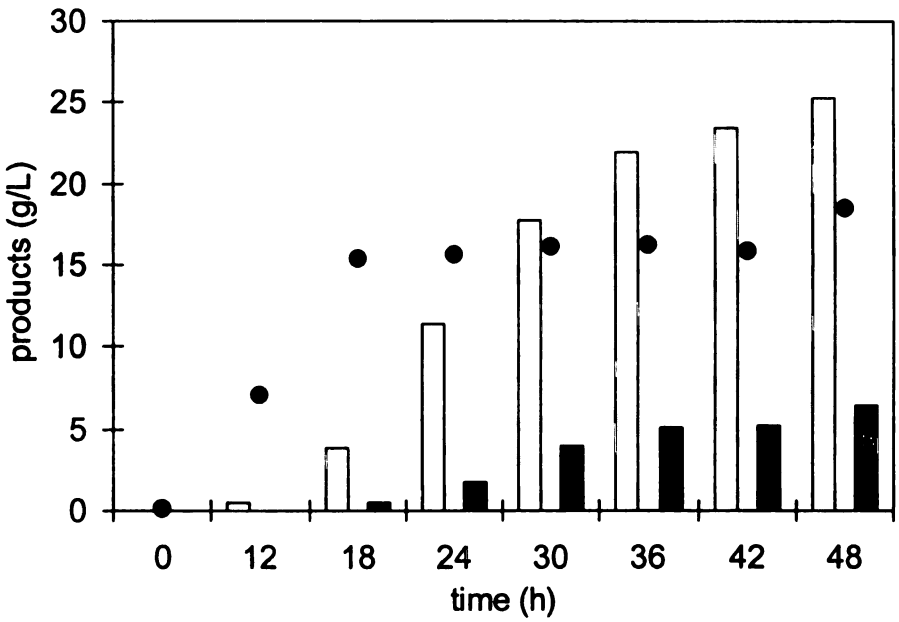

Figure 25. SP1.1/pKD12.152A fed-batch fermentation titers when D.O. oscillations resulted from a D.O. electrode malfunction. Shikimic acid □, quinic acid ■, DHS ❑, cell mass ●, in g/L.

Homologous Shikimic Acid-Quinic Acid Equilibration.

Quinic acid formation had apparently been suppressed by glucose-rich shake flask conditions while oscillatory control of fermentor D.O. concentration via glucose feeding

eliminated quinic acid formation. Quinic acid formation was hypothesized to be a competing reaction with shikimic acid formation and catabolic repression appeared to play a role in minimizing quinic acid formation given that the onset of its appearance in shake flasks coincided with the depletion of glucose from the growth medium. This hypothesis was further strengthened when the specific details of preliminary fermentation data were reexamined. SP1.1/pKD12.112A fermentations performed at an airflow rate of 3.0 vvm had a product mixture of 8.8:2.3:1.0 SA:DHS:QA while SP1.1/pKD12.152A fermentations done at 3.0 vvm exhibited quinic acid concentrations ranging from only trace levels to a product mixture of 1.9:0.61:1.0 SA:DHS:QA. The varying product ratios were consistent with homologous, glucose-dependent quinic acid formation. The initially low quinic acid production of fermentations was a result of an artificially high D.O. concentration due to reactor backpressure, induced by a high airflow rate (3.0 vvm) and an undersized primary exhaust gas filter. The resultant overestimation in measured D.O. concentration caused increased glucose feeding, which elevated the pseudo-steady state glucose concentration in the fermentor vessel relative to that experienced when reactor backpressure was eliminated. Since the fermentor vessel backpressure was unregulated, the same fermentation conditions which resulted in an almost undetectable quinic acid concentration for SP1.1/pKD12.152A fermentations (Figure 23) initially were unable to suppress quinic acid formation to the same degree in later fermentations. Once fermentation backpressure was eliminated by decreasing the maximum airflow rate, quinic acid formation increased significantly (Figure 24) due to the decrease in pseudo-steady-state fermentor glucose concentration. Motivated by the knowledge of glucose-

dependent quinic acid formation, alternate SP1.1/pKD12.152A fermentation conditions were explored in an effort to minimize quinic acid biosynthesis.

Table 3. SP1.1 shikimic acid fed-batch fermentation product titers, yields, and SA:QA when D.O. concentration set point and glucose feed pump K_c were varied.

Entry	Plasmid	D.O. Set Point	Temperature (°C)	SA yield (mol/mol)	[a]Total Yield (mol/mol)
1	pKD12.152A	20%	36	14%	18%
2	pKD12.152A	20%	36	10%	18%
3	pKD12.112A	10%	33	13%	20%
4	pKD12.152A	5%	36	15%	22%
5	pKD12.152A	5%	36	13%	20%
6	pKD12.152A	5%	36	11%	14%
7	pKD12.152A	10%	33	9.3%	12%
8	pKD12.112A	10%	33	10%	14%

Entry	K_c	SA (g/L)	QA (g/L)	DHS (g/L)	SA:QA (mol:mol)
1	0.1	27	3.0	6.1	10:1.0
2	0.1	18	10	5.7	1.9:1.0
3	0.1	26	8.1	6.5	3.1:1.0
4	0.1	27	6.6	7.5	4.5:1.0
5	0.3	25	5.8	7.4	4.7:1.0
6	0.6	20	0.0	6.8	N/A
7	0.8	16	1.2	4.3	15:1.0
8	0.8	14	1.2	4.6	13:1.0

Entry 1, 3.0 vvm; entries 2-8, 1.0 vvm. [a](mol SA + mol QA + mol DHS)/(mol glucose).

The original D.O. concentration set point of SP1.1/pKD12.152A cultures was 20%, and the steady-state glucose concentration of fermentations was initially increased by step-wise decreases in the D.O. concentration set point (Table 3) from 20% to 10% to 5%. Reductions in the D.O. concentration set point increased the SA:QA when a glucose feed pump K_c of 0.1 was employed (Table 3, entries 2-4). Unfortunately, D.O. concentration set point changes alone were unable to satisfactorily suppress quinic acid formation, and the highest SA:QA achieved was only 4.5 when the D.O. concentration set point was lowered to 5% (Table 3, entry 4).

Next, the proportional gain (K_c) of the glucose feed pump was increased step-wise, in lieu of direct glucose monitoring and control, until a product ratio was achieved that would permit isolation of pure shikimic acid. The glucose feed pump K_c was increased in an effort to mimic the phenomenon observed when the D.O. probe malfunctioned, and induced the glucose feed pump to continuously cycle. The glucose feed pump K_c was increased until the pump response was so rapid that a pulsed glucose addition regimen was assumed, which induced a pulsed D.O. concentration profile. D.O. concentrations remained near zero percent until a glucose pulse was consumed, then the D.O. concentration rose quickly. Once the D.O. concentration reached the set point (10%), the glucose pump turned on and its output ramped swiftly. The D.O. concentration typically peaked between 20% and 30%, coinciding with a peak in the glucose pump output. The D.O. concentration briefly remained at the peak before rapidly descending. As the D.O. concentration decreased, the glucose feed rate dwindled at a commensurate rate. The pump turned off once the D.O. concentration reached the set point (10%), and the D.O. concentration continued to decrease until it was at or near zero

percent. The D.O. concentration remained near zero for about a minute typically, depending on the age of the culture. When the glucose pulse was consumed, the cycle repeated. Fermentations carried out at a D.O. concentration of 5% (regardless of K_c) proved to be unstable and prone to unregulated glucose additions late in the runs, owing to the declining metabolic vigor of the cultures. Fermentations performed at a D.O. concentration of 20% were unable to attain a SA:QA in excess of 10, despite a large increase in K_c. An 8-fold increase in the glucose feed pump K_c at a D.O. concentration set point of 10% resulted in a SA:QA of 15:1 for SP1.1/pKD12.152A (Table 3, entry 7). SP1.1/pKD12.112A was then examined under the optimized fermentation conditions (Table 3, entry 8), and resulted in a 13:1 SA:QA for SP1.1/pKD12.112A, allowing shikimic acid purification from the SP1.1/pKD12.112A fermentation broths.

The previous inability of overexpressed DHQ dehydratase to reduce quinic acid formation coupled with the decrease in quinic acid production afforded by pulsed glucose addition suggested that quinic acid formation may not result from de novo biosynthesis, but rather from equilibration of initially synthesized shikimic acid. In such a scenario, glucose-induced catabolic repression of shikimic acid transport would preclude conversion to quinic acid. In lieu of direct measurement and control of glucose concentration, the pulsed glucose addition method was successful in obtaining purifiable shikimic acid.

Glucose was neither detectable in the ^1H NMR spectra of any fermentation condition listed in Table 3, nor in the spectra of previous fermentations (Figure 23, Figure 24, Figure 25). Glucose was only quantifiable when the control methodology failed and unregulated glucose addition proceeded. Unfortunately, the pulsed glucose addition

control scheme was prone to periods of unregulated glucose addition late in the fermentations. Additionally, the control scheme exacted a large metabolic toll on cultures during the progression of the feeding stage, requiring fermentations to be truncated (42 h) relative to fermentations utilizing a K_c of 0.1 (48 h). Truncating fermentations avoided the loss of D.O. concentration control by glucose feeding that typically transpired in fermentations with a K_c of 0.8 after 30 h and would result in unregulated glucose addition. Furthermore, the pulsed addition of glucose diminished the yields and titers of synthesized shikimic acid (Table 3).

A reduction in the standard fermentation temperature from 36 °C to 33 °C was required by a B. Braun Biotech upgrade of the fermentation equipment to expand fermentation capacity. Unfortunately, post-upgrade shikimic acid fermentation titers were only about two-thirds of their original measured values using identical fermentation set points (e.g., temperature, pH, D.O. concentration, airflow rate, impeller rate). A reduction in the standard fermentation temperature from 36 °C to 33 °C led to a modest increase in the post-upgrade shikimic acid fermentation titers achieved. The decrease in temperature may have helped stabilize the thermal-sensitive enzyme DAHP synthase during the course of the fermentations, thereby increasing the carbon flux directed into the shikimate pathway.

The optimized fermentation conditions of 10% D.O., 33 °C, and a glucose feed pump K_c of 0.8 for construct SP1.1/pKD12.152A were then applied to SP1.1/pKD12.112A with virtually identical results (Table 3, entries 7 and 8) obtained in shikimic acid titer and SA:QA. Since constructs SP1.1/pKD12.152A and SP1.1/pKD12.112A exhibited nearly identical shikimic acid titers and product ratios,

aroD overexpression was deemed unnecessary. SP1.1/pKD12.112A was used for further exploration of shikimic acid-quinic acid equilibration in fermentation experiments therefore.

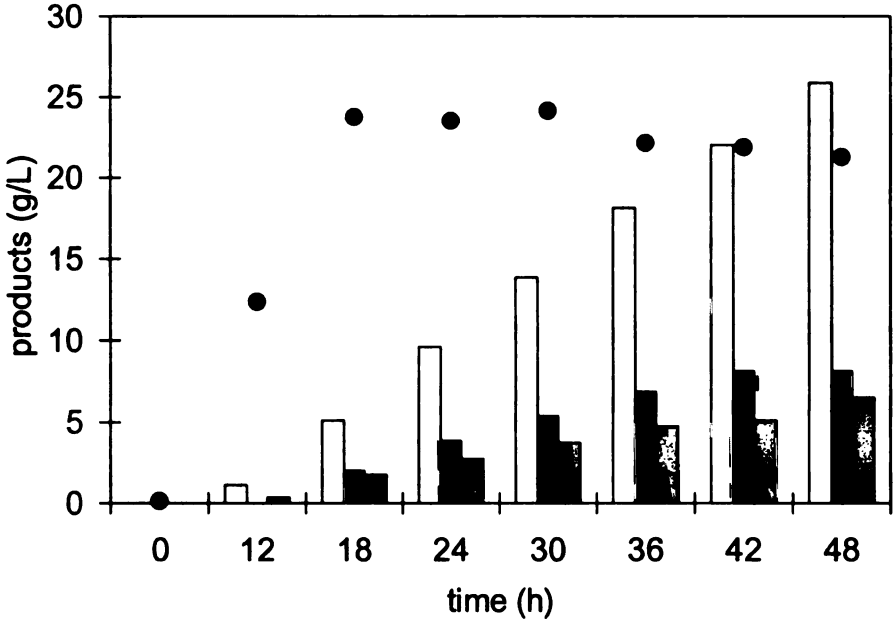

Figure 26. SP1.1/pKD12.112A cultured at 10% D.O. and a glucose feed pump K_c of 0.1. Shikimic acid □, quinic acid ■, DHS ❑, cell mass ●, in g/L.

Baseline conditions for shikimic acid-quinic acid equilibration for construct SP1.1/pKD12.112A were established by culturing at a D.O. concentration of 10%, and a glucose feed pump K_c of 0.1 (Table 3, entry 3). The resulting product time course (Figure 26) was similar to that of SP1.1/pKD12.152A (Figure 24), as expected. SP1.1/pKD12.112A accumulated 26 g/L shikimic acid, 8.1 g/L quinic acid, and 6.5 g/L DHS by 48 h with a SA:QA of 3.1. DAHP synthase and shikimate dehydrogenase enzyme activities were also measured for the SP1.1/pKD12.112A construct under the standard fed-batch fermentations conditions (Table 4).

Table 4. DAHP synthase and shikimate dehydrogenase specific enzyme activities (μmol/min/mg) for SP1.1/pKD12.112A.

		specific activity (μmol/min/mg)			
Entry	Enzyme	12 h	24 h	36 h	48 h
1	DAHP synthase	0.30	0.50	0.56	0.99
2	shikimate dehydrogenase	0.65	0.97	1.2	1.3

***tktA*-encoded Transketolase Overexpression.**

The in vivo DAHP synthase activity dependence upon PEP and E4P substrate availability was discussed in Chapter 1. E4P substrate limitation supercedes that of PEP,[49] with E4P availability dictated by the in vivo activity of *tktA*-encoded transketolase and *talB*-encoded transaldolase. Both enzymes operate in the non-oxidative pentose phosphate pathway and are responsible for the interconversion of C-4, C-5, C-6, and C-7 aldoses and ketoses (Figure 13). Overexpression of both *tktA*[49] and *talB*[55b,106] have previously been studied for use in enhancing shikimate pathway metabolite concentrations and yields under fed-batch fermentation conditions. Only *tktA* will be addressed in this work, however, given the apparent inability of *talB* to significantly enhance the titer or yield of shikimate pathway intermediates derived from glucose when *E. coli* is employed as the biocatalyst.[55b]

Overexpression of *tktA*-encoded transketolase (in the presence of DAHP synthase overexpression) had previously been shown to enhance both titers and yields of shikimate pathway metabolites produced under fed-batch fermentor conditions.[49b,51b,55b] Construct SP1.1/pKD12.138A overexpressed *tktA* via plasmid localization. Plasmid pKD12.138A (Figure 28) was constructed from plasmid pKD12.112A by cloning in the *tktA* locus,

which encodes for transketolase. Plasmid pKD12.112A was digested with *Hind*III and treated with Klenow fragment to make the restriction site blunt. Following digestion of pMF51A[107] with *Bam*HI, the 2.2-kb *tktA* fragment was blunt ended using Klenow fragment and ligated into linearized pKD12.112A using T4 ligase resulting in the 9.9-kb plasmid pKD12.138A. The *tktA* gene is transcribed in the same direction as the *serA* gene.

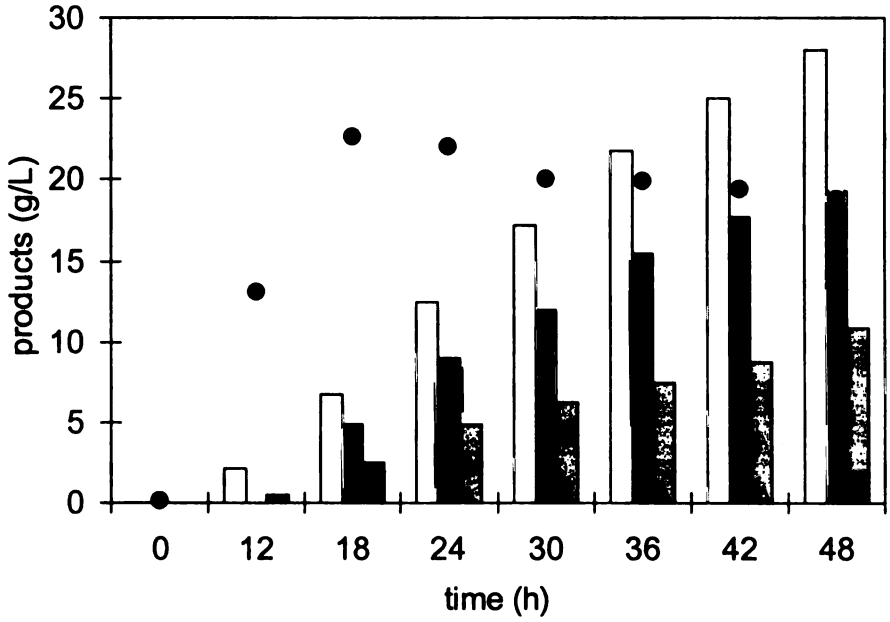

Figure 27. SP1.1/pKD12.138A cultured at 10% D.O. and a glucose feed pump K_c of 0.1. Shikimic acid □, quinic acid ■, DHS ❑, cell mass ●, in g/L.

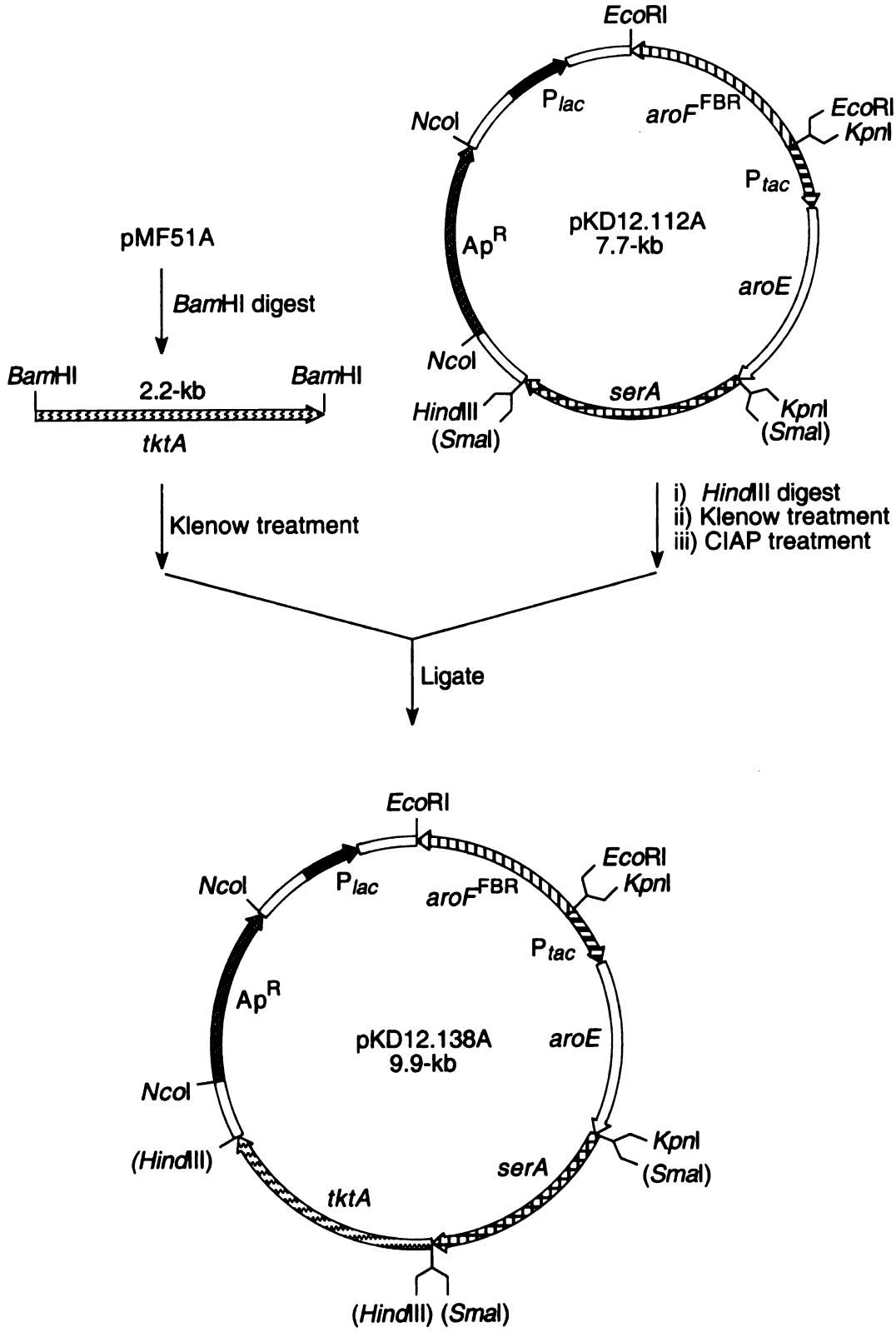

Figure 28. Construction of plasmid pKD12.138A.

Initially, construct SP1.1/pKD12.138A (Figure 27) was examined under non-oscillatory fermentation conditions (glucose feed pump K_c of 0.1), with the assumption that shikimic acid-quinic acid equilibration would result in a low (unpurifiable) SA:QA, but would significantly amplify metabolite titers relative to construct SP1.1/pKD12.112A (Figure 26) under the same conditions. The 28 g/L of shikimic acid, 19 g/L of quinic acid and 11 g/L of DHS were synthesized confirmed the expectation of enhanced shikimic acid-quinic acid equilibrium. The SA:QA ratio (1.6) was about half that of SP1.1/pKD12.112A (3.1) when cultured under the same conditions. DAHP synthase and shikimate dehydrogenase activity levels were fairly stable (Table 5).

Table 5. DAHP synthase and shikimate dehydrogenase specific enzyme activities (μmol/min/mg) for SP1.1/pKD12.138A.

		specific activity (μmol/min/mg)			
Entry	Enzyme	12 h	24 h	36 h	48 h
1	DAHP synthase	0.44	1.2	0.55	0.67
2	shikimate dehydrogenase	1.2	2.2	2.4	2.8

Next SP1.1/pKD12.138A was examined under the pulsed glucose addition fermentation conditions previously investigated for SP1.1/pKD12.112A. The same increase in K_c to 0.8 which afforded a purifiable SA:QA for construct SP1.1/pKD12.112A was unable to adequately suppress quinic acid formation for construct SP1.1/pKD12.138A (Table 6, entry 2) to provide a SA:QA in excess of 10. Proportional gains of 0.1 and 0.8 for SP1.1/pKD12.138A fermentations gave essentially an identical SA:QA (Table 6). Furthermore, the K_c of 0.8 detrimentally impacted titer and yield of synthesized shikimic acid (Table 6), as was the case for SP1.1/pKD12.112A

and SP1.1/pKD12.152A (Table 3, entries 1, 3, 7, 8). The overexpression of *tktA* appeared to increase the rate of glucose uptake, shortening the glucose pulse period significantly. The average glucose concentration experienced by SP1.1/pKD12.138A was therefore most likely decreased relative to that of SP1.1/pKD12.112A cultures, permitting quinic acid to reemerge as a substantial byproduct.

Table 6. Product titers and ratios for SP1.1/pKD12.138A when the glucose feed pump K_c is manipulated at 10% D.O.

[a]Entry	K_c	SA (g/L)	QA (g/L)	DHS (g/L)	SA:QA (mol:mol)	SA yield (mol/mol)	Total yield (mol/mol)
1	0.1	28	19	11	1.6	14%	29%
2	0.8	13	9.9	6.3	1.5	13%	26%

[a]Entry 1, 48h; entry 2, 42h.

Shikimic Acid Transport and Equilibration With Quinic Acid.

Quinic acid formation appeared to result from shikimic acid transport to this point, but definitive experimental evidence to substantiate this hypothesis was lacking. Could construct SP1.1/pKD12.112A transport exogenously-supplied shikimic acid into its cytoplasm in the absence of glucose? Could the biocatalyst convert transported shikimic acid to quinic acid? These questions were investigated via a standard glucose-limited SP1.1/pKD12.112A fermentation (10% D.O., 0.1 K_c, 33 °C). A portion (50 mL) of the fermentation's broth was harvested at 24 h (SA:QA of 2.8:1.0). The cells were collected by centrifugation and washed two times with sterile, fresh fermentation medium. The cells were again collected by centrifugation and resuspended in fresh fermentation medium in the presence of 80 mM shikimic acid. Figure 29 shows the resulting time course of the product mixture. Shikimic acid decreased with a

corresponding increase in quinic acid and DHS. The ability of SP1.1/pKD12.112A to transport exogenous shikimic acid was therefore established, but the mechanism by which shikimic acid was converted to quinic acid remained unclear.

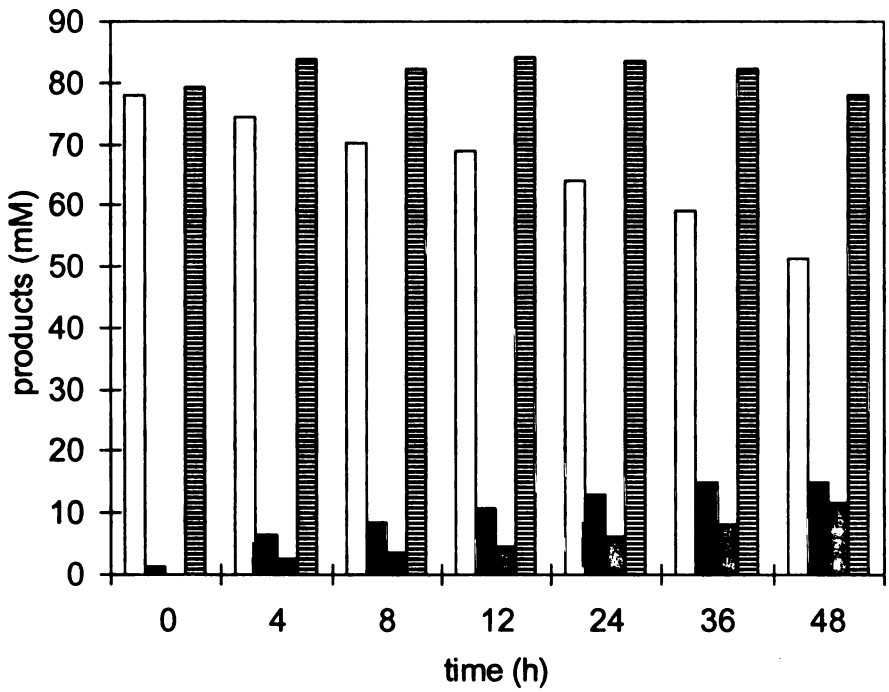

Figure 29. Shake flask transport and equilibration of exogenously supplied shikimic acid SP1.1/pKD12.112A at 37 °C. Shikimic acid □, quinic acid ■, DHS ❑, and total products ▤, in mM.

Inspection of the aromatic amino acid biosynthesis pathway reveals that DHQ and DHS bear a number of structural similarities (Figure 2). DHQ and DHS possess a 3-keto functionality, a carboxyl group, and multiple hydroxyl functionalities. With the structural similarity between DHQ and DHS in mind, Dr. Karen Draths purified shikimate dehydrogenase prepared from crude cellular lysate of AB2834/pIA321 shake flask cultures and incubated shikimate dehydrogenase in the presence of DHQ and an excess of $NADP^+$ in an attempt to form quinic acid. The AB2834/pIA321 construct was utilized due to its exceptionally high expression level of *aroE* and previous use as an

overproducer of shikimate dehydrogenase for purification purposes.[101] Shikimate dehydrogenase activity was measured under various conditions, the formation of product quinic acid from substrate DHQ in enzyme assay mixtures was established via ^{1}H NMR, and kinetic parameters for the conversion were determined. The following kinetic parameters were ascertained under identical assay conditions (e.g., the same temperature, substrate concentration, etc.): K_m=1.2 mM, and ν_{max}=0.096 mmol L^{-1} min^{-1} for shikimate dehydrogenase-catalyzed reduction of DHQ to quinic acid, compared to a K_m=0.11 mM and ν_{max}=0.11 mmol $L^{-1}min^{-1}$ for shikimate dehydrogenase-catalyzed reduction of DHS to shikimic acid.[97]

The newly elucidated ability of *aroE*-encoded shikimate dehydrogenase to reduce DHQ and DHS to quinic acid and shikimic acid respectively, confirmed the homologous capacity of *E. coli* to catalyze the formation of quinic acid. Quinic acid formation was the result of a two-fold problem it appeared. First, previously synthesized shikimic acid was transported back into the microbial cytoplasm, where reverse action of the shikimate pathway enzymes permitted in vivo formation of DHQ. Second, DHQ could be reduced to quinic acid by the enzymatic activity of native *E. coli* shikimate dehydrogenase. Transport of initially synthesized shikimic acid with subsequent equilibration to quinic acid was a more likely mechanistic explanation than de novo quinic acid biosynthesis for two reasons. First, overexpression of *aroD* in construct SP1.1/pKD12.152A was unable to decrease quinic acid formation by limiting the intracellular DHQ available for *aroE*-mediated reduction to quinic acid. Second, catabolite repression appeared to prevent circumvent the majority of quinic acid formation, suggesting quinic acid formation was linked to the transport of a carbon source such as shikimic acid. Quinic acid synthesized

by shikimic acid synthesizing biocatalysts continued to constitute a severe drain on realizable shikimic acid titers and yields while posing a significant purification impediment.

Host Strain Considerations.

The practical difficulties in applying the previously elucidated fed-batch fermentor conditions for production of purifiable shikimic acid suggested alternate methods to alleviate extensive shikimic acid-quinic acid equilibration be explored. Was the ability of SP1.1 to readily uptake exogenous shikimic acid unique to RB791-based *E. coli* constructs, or was shikimic acid uptake ubiquitous to *E. coli* K-12 derivatives? An investigation of alternate *E. coli* K-12-derived host strains for shikimic acid biocatalysis presented a potential opportunity to reduce quinic acid formation without the use of oscillatory fermentation conditions.

Table 7. Product ratios and titers for SP1.1/pKD12.152A (entry 1) and KL3sk$^-$/pKD12.152A (entry 2) at a glucose feed pump K_c of 0.6 and a D.O. concentration set point of 5%.

Entry	SA (g/L)	QA (g/L)	DHS (g/L)	SA:QA (mol:mol)	SA yield (mol/mol)	Total yield (mol/mol)
1	20	0.0	6.8	N/A	11%	14%
2	8.8	9.8	2.9	0.99:1.0	5.9%	14%

Entry 1, 36 °C; entry 2, 33 °C.

The first alternate host strain to SP1.1 examined was generated from *E. coli* KL3. KL3 is a variant of the chemical *aroE* auxotroph *E. coli* AB2834.[33] The genomic *aroL* and *aroK* of KL3 were inactivated by P1 phage-mediated transductions, as previously described, to yield KL3sk$^-$. The *aroE*-auxotrophic nature of KL3sk$^-$ was complemented

by plasmid-localized P_{tac}*aroE*. The capability of KL3sk$^-$ to interconvert shikimic and quinic acid was initially explored with the first fermentation conditions to prevented extensive shikimic acid-quinic acid equilibration in SP1.1/pKD12.152A (5% D.O. concentration and a glucose feed pump K_c of 0.6, Table 3, entry 6). The resulting shikimic acid titer (8.8 g/L) and SA:QA molar ratio (0.99:1.0) for KL3sk$^-$/pKD12.152A (Table 7, entry 2) exhibited significant decreases relative to SP1.1/pKD12.152A (Table 7, entry 1) under the similar culturing conditions. The poor selectivity towards shikimic acid production of the KL3-derived host strain precluded its further consideration as a shikimic acid-producing host. Despite the failure of KL3sk$^-$/pKD12.152A to improve the SA:QA, the fermentation result demonstrated that different *E. coli* K-12-derived host strains could exhibit substantially different shikimic acid-quinic acid equilibration properties under the same fermentation conditions, suggesting the use of an alternate host strain might be a viable strategy for minimizing quinic acid formation.

The next host strain investigated was *E. coli* SP2.1. SP2.1 was generated from the *aroD* auxotroph parent strain *E. coli* AB2848.[108] Homologous recombination of the *aroB* gene into the *serA* locus of AB2848, was followed by successive P1 phage-mediated transductions to transfer the *aroL478*::Tn*10* and *aroK*::Cm^R loci of ALO807[100] onto the genome and eliminate shikimate kinase activity. Finally, catalytically active *aroD*-encoded DHQ dehydratase activity was restored by transferring the *aroD* gene onto the genome via a P1 phage transduction. The AB2848 *serA*::*aroB* *aroL478*::Tn*10* *aroK*::Cm^R *aroD*$^+$ host was renamed SP2.1.

Table 8. Effect of host strain and glucose feed pump K_c on product titers and ratios when plasmid pKD12.112A is employed under fed-batch fermentation conditions.

Host	K_c	SA	QA	DHS	SA:QA	SA yield (mol/mol)	Total yield (mol/mol)
SP1.1	0.1	26	8.1	6.5	3.1:1.0	13%	20%
SP1.1	0.8	14	1.2	4.6	13:1.0	10%	14%
SP2.1	0.1	22	5.0	5.4	5.2:1.0	12%	18%
SP2.1	0.8	25	1.4	4.4	19:1.0	15%	18%

Construct SP2.1/pKD12.112A was evaluated under the same fermentation conditions that reduced shikimic acid-quinic acid equilibration in construct SP1.1/pKD12.112A (10% D.O. concentration and a glucose feed pump K_c of 0.8). Controllability was again an issue, and unregulated glucose addition was prone to occur between 32 h and 36 h. Fermentations were again truncated at 42 h due to feeding instabilities. The resulting average SA:QA was 19:1 (Table 8), but was most likely inflated due to the transient glucose-rich conditions that were typically experienced subsequent to loss of D.O. concentration control by glucose feeding (e.g, glucose accumulation in the fermentation medium). Applying fermentation conditions that employed a glucose feed pump K_c of 0.1 at a D.O. concentration of 10% to SP2.1/pKD12.112A (Table 8) resulted in a slight increase in SA:QA (5.2:1.0) relative to that of SP1.1/pKD12.112A fermentations (3.1:1.0) performed at the same conditions. Curiously, when SP2.1/pKD12.112A was subjected to pulsed glucose addition, the titer and yield of synthesized shikimic acid were not detrimentally impacted (Table 8), as was the case with SP1.1/pKD12.112A. SP2.1 proved to be a more robust host when subjected to the harsh culturing conditions attendant with glucose feeding that employed a pump K_c

of 0.8. The impact of *tktA*-encoded transketolase was not examined with SP2.1 using a glucose feed pump K_c of 0.8 given the deleterious impact on the SA:QA experienced when transketolase overexpression was explored with construct SP1.1/pKD12.138A (Table 6).

Shikimic Acid Transport and (6S)-6-Fluoro-Shikimic Acid Resistance.

Pittard was first to address shikimic acid transport by enterics, and others have since demonstrated the ability of *E. coli* to readily transport shikimic acid as well.[109] In this work, shikimic acid transport coupled with depressed substrate fidelity of shikimate dehydrogenase has been implicated as the source of quinic acid formation.[97] Previously, construct SP1.1/pKD12.112A was incubated in the presence of shikimic acid and observed to catalyze the formation of both DHS and quinic acid, with a commensurate reduction in shikimic acid concentration (Figure 29). Catabolic repression of shikimic acid uptake via oscillatory fed-batch fermentation conditions sharply curtailed quinic acid formation. Unfortunately, SP1.1/pKD12.112A shikimic acid titer and yield were both detrimentally impacted, and the inability to maintain control of the D.O. concentration by glucose feeding late in SP1.1/pKD12.112A and SP2.1/pKD12.112A fermentations was a motivation for alternate methods of preventing shikimic acid-quinic acid equilibration. One potential methodology for circumventing *aroE*-mediated quinic acid formation might be fed-batch fermentor cultivation of an *E. coli* strain incapable of shikimic acid import, removing the need for catabolic repression strategies.

The shikimic acid analog (6S)-6-fluoro-shikimic acid (FSA) was recently identified as a potent antimicrobial agent.[110] The biological mechanism by which FSA

exerts its antimicrobial properties is somewhat unclear, however FSA appears to be imported by *E. coli* via the same transport system responsible for shikimic acid uptake.[110b] FSA is then processed down the shikimate pathway to (6S)-6-fluoro-chorismic acid by the successive action of *aroK* and *aroL*-encoded shikimate kinase I and II respectively, *aroA*-encoded EPSP synthase, and *aroC*-encoded chorismate synthase (Figure 2). Biosynthesis of the aromatic vitamin *p*-aminobenzoic acid is believed to be disrupted given that supplementation with concentrations of *p*-aminobenzoic acid as low as 0.001 μg/mL can reverse growth inhibition.[110a] MIC values for *E. coli* K-12 ATCC strains NCTC 10538 and N99 were reported to be 0.5 and 0.1μg/mL, respectively, while the MIC for wild type *E. coli* B (ATCC 23226) was 0.25 μg/mL.[110a] The potency of FSA is tempered by the high rate of spontaneous mutation associated with its use and precludes its use as an antimicrobial agent.[110b]

The same mutational properties that precluded the use of FSA as an antimicrobial agent made it attractive as a potential resolution to problematic shikimic acid-quinic acid equilibration. It was hypothesized that the high rate of spontaneous mutation to FSA exhibited by *E. coli* could be utilized to genetically engineer a host strain incapable of importing shikimic given that FSA and shikimic acid shared the same transport system.[110b] Loss of FSA sensitivity might therefore coincide with a deficiency in shikimic acid transport capability. This was pursued with the generation of host strain SP1.1-4/3 by Dr. Draths and commenced with construction of plasmid pKD14.016A. Plasmid pKD14.016A was constructed to supply shikimate kinase activity to the shikimate kinase-deficient host strain SP1.1, and permitted FSA to be processed to 6-fluoro-chorismic acid, thereby allowing the antimicrobial effects of the FSA derivative to

be realized.[110] Construction of plasmid pKD14.016A began with digestion of plasmid pKAD31 with *Kpn*I and *Bam*HI. The 1.0-kb *aroL* fragment liberated was subsequently ligated with pCL1920 (4.6-kb) that had been linearized by treatment with *Kpn*I and *Bam*HI. to afford the 5.6-kb plasmid pKD14.016 (Figure 30). The pCL1920 plasmid bears a genetic marker encoding for spectinomycin (Sp) resistance, and has a relatively low copy number of approximately five.[111]

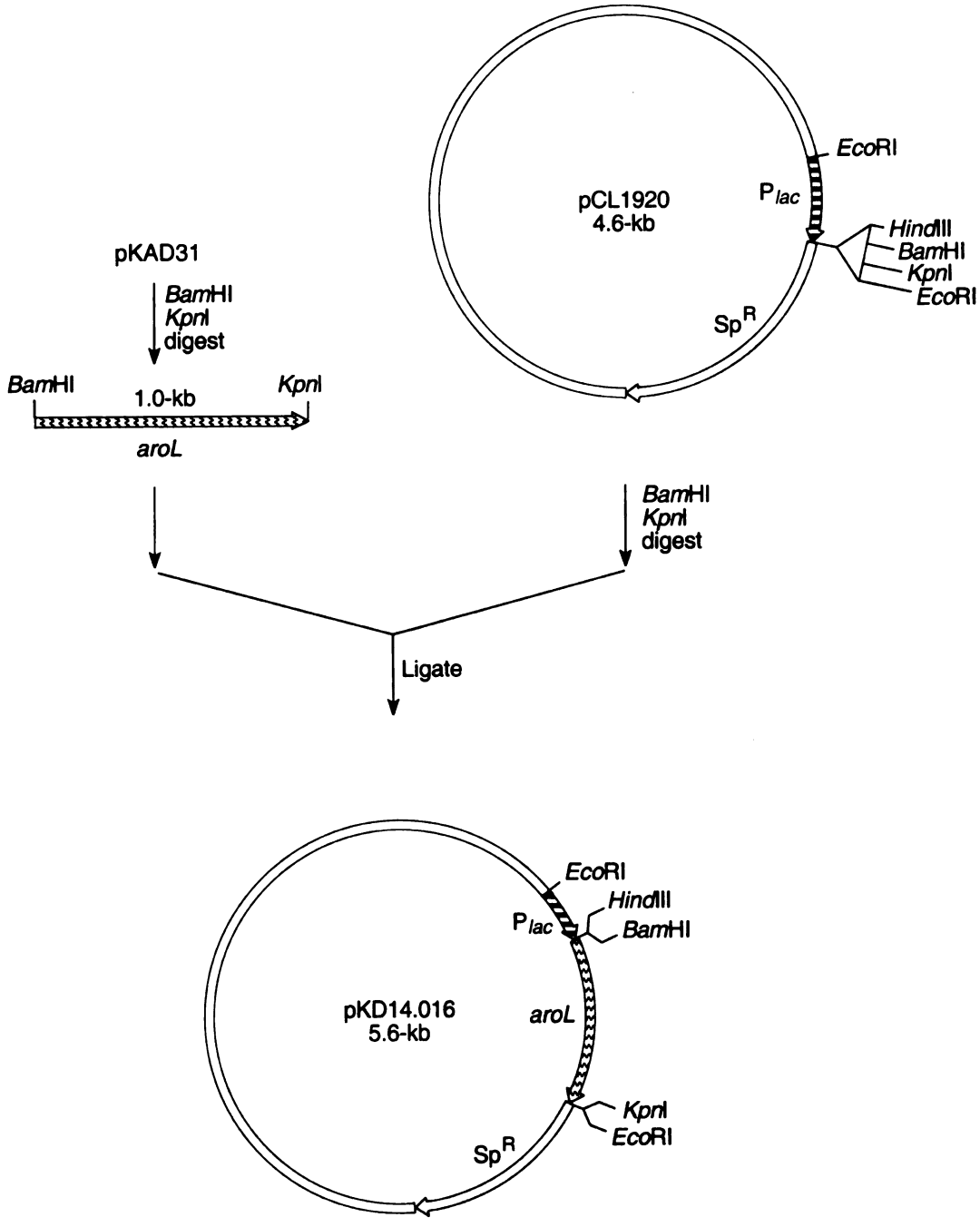

Figure 30. Construction of plasmid pKD14.016A.

E. coli SP1.1-4/3 was derived from parent strain SP1.1 via the following procedure. First, SP1.1 was transformed with plasmid pKD14.016 and grown on solid DM[109a] medium supplemented with varying concentrations of FSA. Candidate colonies were then replicate plated on solid DM medium containing 0-100 μg/mL of FSA. Mutant SP1.1-4/pKD14.016 was isolated from the 100 μg/mL FSA concentration based on its resistance to FSA characterized by rapid growth. Host SP1.1-4 was cured of plasmid pKD14.016A and mutant SP1.1-4/3 was isolated via replicate plating.

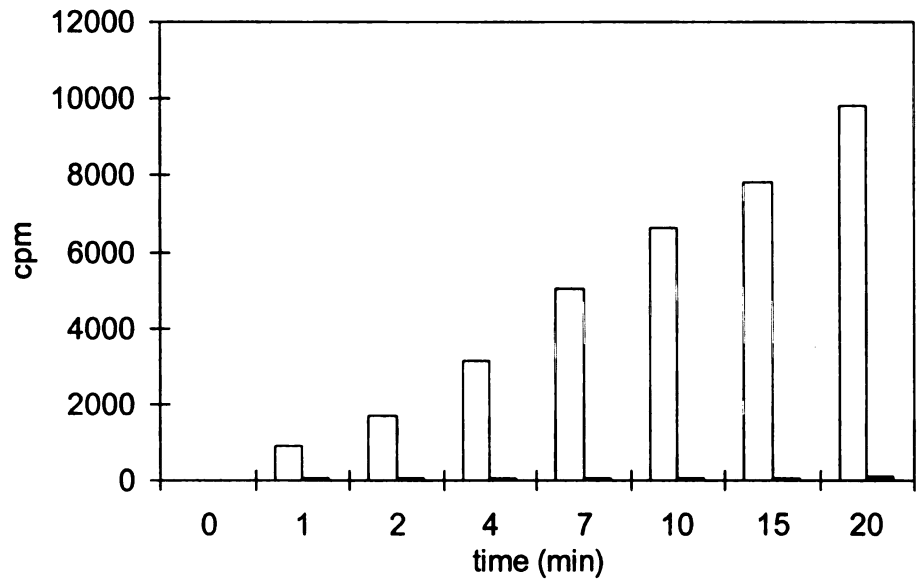

Figure 31. ^{14}C-labeled shikimic acid uptake by SP1.1-4/3/pKD14.016■, and SP1.1/pKD14.016□.

The ability of SP1.1-4/3 to transport shikimic acid was first examined by Dr. Draths with ^{14}C-labeled shikimic acid, using plasmid pKD14.016, following the procedure of Pittard and Wallace.[109a] The reintroduction of plasmid pKD14.016 into host SP1.1-4/3 was necessary to permit the conversion of ^{14}C-labeled shikimic acid to distal metabolites. SP1.1-4/3/pKD14.016 exhibited negligible intracellular ^{14}C-labeled

shikimic acid accumulation, while SP1.1/pKD14.016 exhibited significant shikimic acid transport affinity (Figure 31). The inability of SP1.1-4/3/pKD14.016 to uptake significant ^{14}C-labeled shikimic acid suggested the shikimic acid transport capability of SP1.1-4/3 had been impaired relative to that of host strain SP1.1.

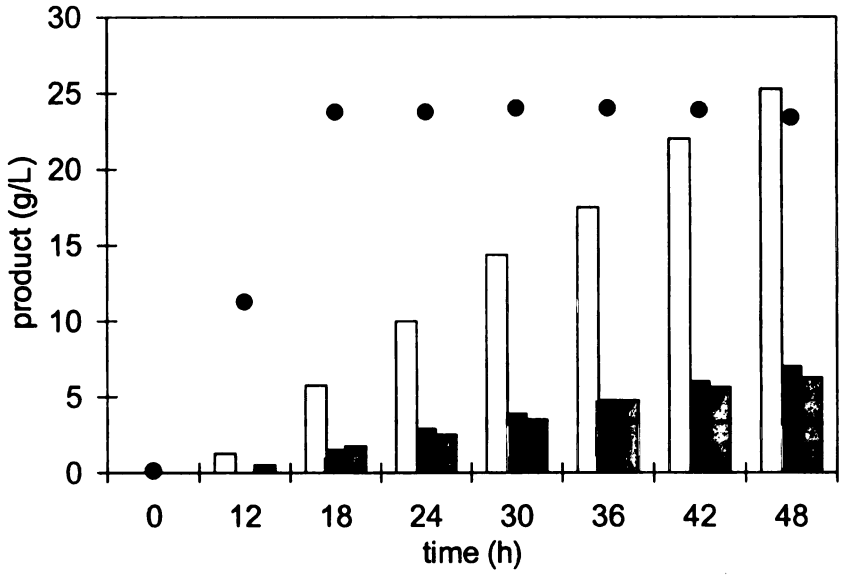

Figure 32. SP1.1-4/3/pKD12.112A cultured at 10% D.O. and a glucose feed pump K_c of 0.1. Shikimic acid□, quinic acid■, DHS□, cell mass●, in g/L.

Next, the SP1.1-4/3 host was transformed with plasmid pKD12.112A and evaluated under standard glucose-limited fermentation conditions. Unfortunately, culturing SP1.1-4/3/pKD12.112A under fed-batch conditions identical to those of SP1.1/pKD12.112A (10% D.O. concentration, glucose feed pump K_c of 0.1) did not result in a significant change in the SA:QA (Figure 32). The final shikimic acid titer (25 g/L), quinic acid titer (7.0 g/L), DHS titer (6.2 g/L), and the SA:QA (4.0:1.0) were all within experimental error of the values observed for SP1.1/pKD12.112A under the same fed-batch fermentation conditions (Table 3, entry 3; Figure 26). The DAHP synthase and

shikimate dehydrogenase enzyme activities of SP1.1-4/3/pKD12.112A (Table 9) were very similar to those of SP1.1/pKD12.112A (Table 4). The lack of a significant increase in the SA:QA between constructs SP1.1-4/3/pKD12.112A and SP1.1/pKD12.112A precluded further experimentation utilizing host strain SP1.1-4/3 for shikimic acid biosynthesis.

Table 9. DAHP synthase and shikimate dehydrogenase enzyme activities (μmol/min/mg) for SP1.1-4/3/pKD12.112A.

		specific activity (μmol/min/mg)			
Entry	Enzyme	12 h	24 h	36 h	48 h
1	DAHP synthase	0.25	0.43	0.34	0.27
2	shikimate dehydrogenase	0.50	0.86	1.2	1.3

Attenuation of Shikimate Dehydrogenase Activity.

Shikimate dehydrogenase overexpression by localizing *aroE* on plasmid pKD12.112A led to specific enzyme activities of 1.0 to 1.3 (μmol/min/mg) (Table 4, entry 2) by 48 h. Significant shikimate dehydrogenase overexpression was deemed critical to the conversion of substrate DHS to product shikimic acid given the feedback inhibition of the enzyme by shikimic acid. However, it was hypothesized that the increased expression level of shikimate dehydrogenase could also be responsible for quinic acid biosynthesis. Given the ability of shikimate dehydrogenase to catalyze the formation of both shikimic and quinic acids, an optimal *aroE* expression level might be possible where substantial DHS would not accumulate due to feedback inhibition and quinic acid formation might not be problematic.

The first avenue explored relative to manipulating *aroE* expression levels was utilization of a construct expressing only the genomic copy of *aroE*. This was accomplished by utilizing plasmid pDK3.117, which lacked the *aroE* gene. Construction of plasmid pDK3.117 was initiated by amplifying the *β-lac* gene via PCR from vector pUC18, and treating with *Nco*I. Ligation of the 1.0-kb fragment into pKL4.33A, which had been linearized by *Nco*I digestion, afforded the 6.4-kb plasmid (Figure 33).

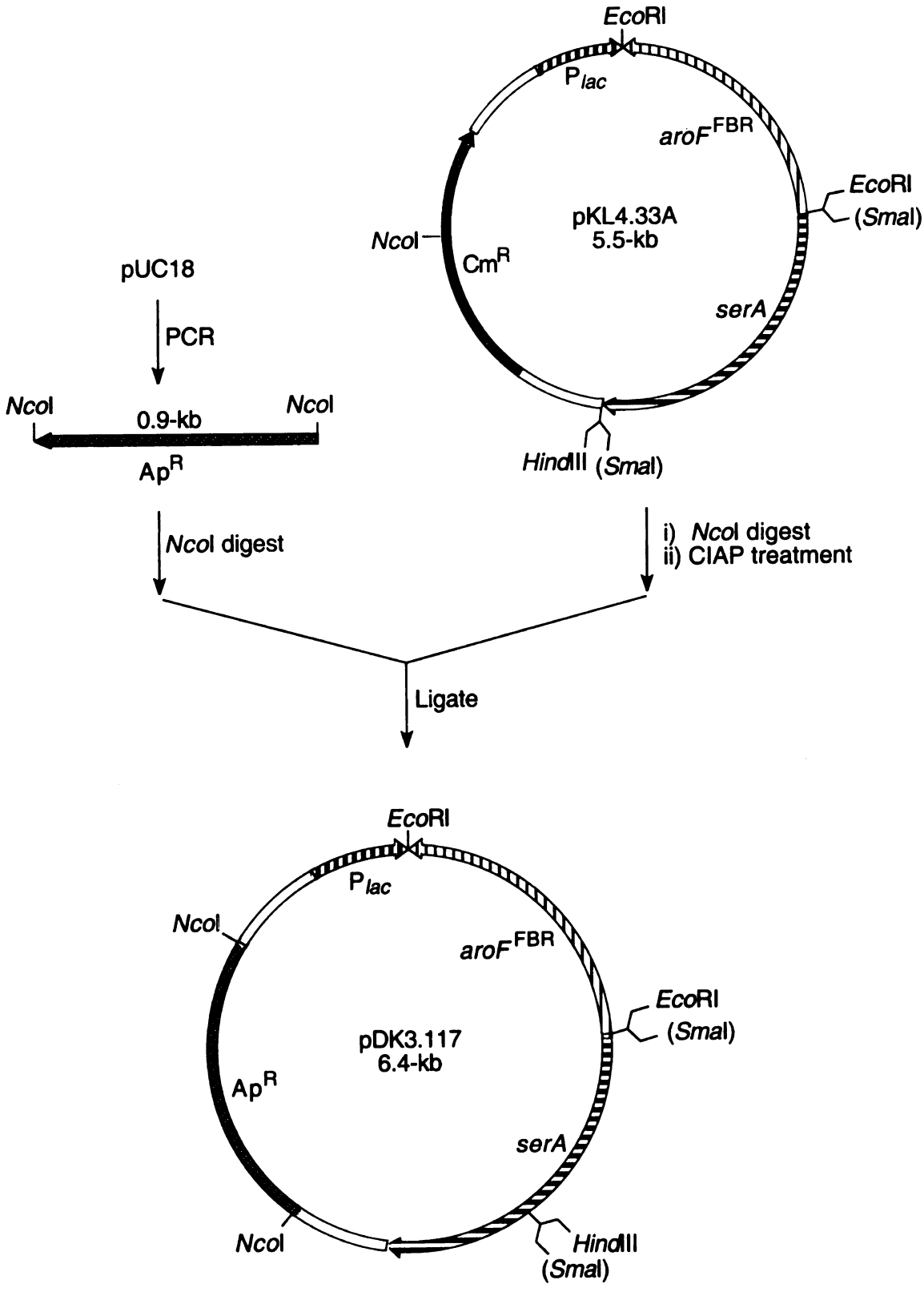

Figure 33. Construction of plasmid pDK3.117.

Plasmid pDK3.117 was transformed into SP1.1 and evaluated under standard glucose-limited fed-batch fermentor conditions. The growth characteristics of SP1.1/pDK3.117 were substantially different than those of construct SP1.1/pKD12.112A. The typical time required to attain an airflow rate of 1.0 vvm for construct SP1.1/pKD12.112A was about 11 h to 12 h, while construct SP1.1/pDK3.117 grew sluggishly, requiring 17 h to 18 h to attain the same airflow rate. Furthermore, all fermentations attempted with construct SP1.1/pDK3.117 resulted in unregulated glucose addition between 24 h and 36 h. A critical point in the fermentations was always achieved when glucose metabolism would rapidly decrease, resulting in a dramatic increase in D.O. concentration and a commensurate increase in the glucose feed rate. Substantial glucose concentrations were accumulated in the fermentor during these fermentations, most likely skewing the SA:QA towards shikimic acid and providing an inaccurate assessment of the strain's quinic acid forming capabilities. The repeated, catastrophic decrease in cellular metabolism and resulting glucose additions were perplexing given the stability of construct SP1.1/pKD12.112A and its similarity to SP1.1/pDK3.117. Analysis of enzymatic assay data from SP1.1/pDK3.117 suggested a cause for the control loss of fermentations. The DAHP synthase activities of SP1.1/pDK3.117 (Table 10, entry 1) were observed to dramatically increase as the fermentations progressed, and were about five-fold higher than SP1.1/pKD12.112A (Table 4, entry 1) under the same conditions by 36 h. The measured shikimate dehydrogenase activities (Table 10, entry 2) were about 20-fold lower than those measured for host SP1.1 when the enzyme was overexpressed by localization on plasmid pKD12.112A (Table 4, entry 2).

Table 10. DAHP synthase and shikimate dehydrogenase enzyme activities (μmol/min/mg) for SP1.1/pDK3.117.

		specific activity (μmol/min/mg)		
Entry	Enzyme	12 h	24 h	36 h
1	DAHP synthase	0.91	1.9	2.5
2	shikimate dehydrogenase	0.060	0.047	0.047

Removing the $P_{tac}aroE$ portion of the pKD12.112A plasmid apparently permitted excessive overexpression of the plasmid-localized $aroF^{FBR}$ gene, overwhelming the cell's ability to readily oxidize substrate at a level commensurate with the oxygen transfer rate. The large overproduction of DAHP synthase may have diverted cellular resources critical to maintaining the high glucose and oxygen uptake rates associated with the fermentation conditions, precluding control of D.O. concentration by substrate addition. Typically $aroF^{FBR}$ expression levels decline during the course of a fermentation, resulting in a decline in the measured specific activity of DAHP synthase. However, the SP1.1/pDK3.117 construct exhibited the reverse trend, with DAHP synthase specific activity increasing throughout the progression of the fermentation until oxygen sensor-controlled glucose feeding became unregulated and the fermentation had to be terminated.

Next, the effect of manipulating *aroE* expression levels on the SA:DHS:QA product mixture was explored via construct SP1.1/pKD14.074A. Plasmid pKD14.074A construction began with *Xba*I digestion of pJB2.277A to liberate the 1.2-kb $lacI^q$ fragment. Linearization of plasmid pLZ1.169A (7.1-kb) with *Xba*I, treatment with T4 ligase, and subsequent ligation with the $lacI^q$ fragment afforded the 8.3-kb plasmid

pKD14.074A. Plasmid pLZ1.169A, and therefore plasmid pKD14.074A, possessed the *aroE* gene optimally spaced behind a P_{tac} promoter for maximal gene expression.

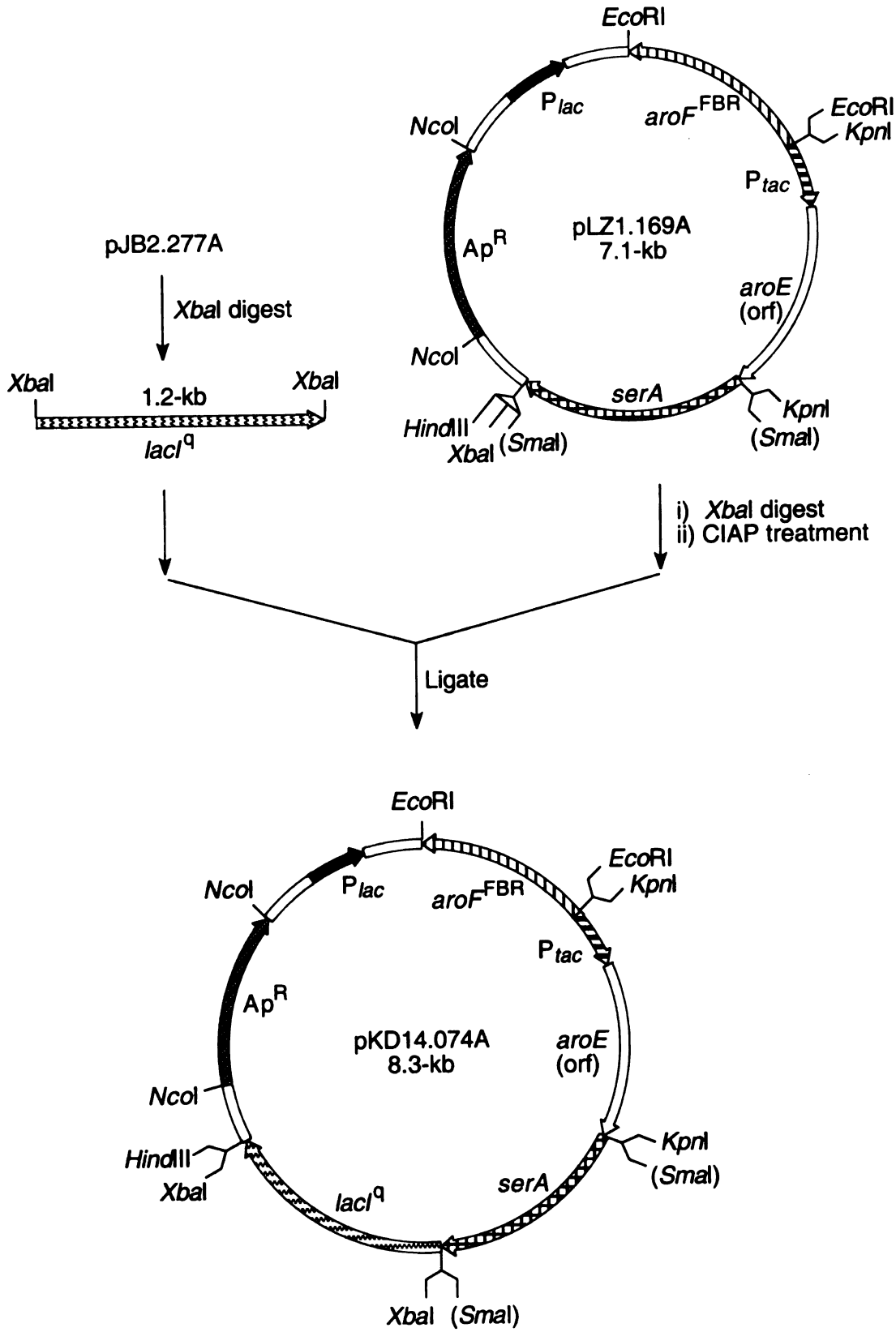

Figure 34. Construction of plasmid pKD14.074.

Table 11. Shikimate dehydrogenase activities (μmol/min/mg) and product ratios for SP1.1/pKD14.074 at various IPTG addition regimens.

	specific activity (μmol/min/mg)					
[a]IPTG	12 h	24 h	36 h	48 h	SA:QA (mol:mol)	SA:DHS (mol:mol)
0.0	0.12	0.19	0.21	0.20	0.82	1.2
2.5	0.38	3.1	3.4	4.0	1.9	5.1
5.0	0.10	5.7	6.6	6.6	2.1	5.4
10	1.4	11	12	13	1.7	4.1

[a]mg IPTG added at 11 or 12 h, 18 h, 24 h, 30 h, 36 h, and 42 h.

Attenuation of shikimate dehydrogenase activity was accomplished by periodic isopropyl-β-D-thiogalactopyranoside (IPTG) addition during fed-batch fermentor cultivation of SP1.1/pKD14.074A, and the effect on the SA:QA was observed. Fed-batch fermentations performed with IPTG addition at the indicated intervals and amounts (Table 11) did not elucidate an addition regimen with an acceptable SA:QA (>10:1), despite an approximately 60-fold increase in assayable shikimate dehydrogenase activity in crude lysate. Increasing IPTG additions above 2.5 mg/6 h showed no further increase in the SA:QA. The absence of IPTG addition (Table 11, entry 1) permitted substantial feedback inhibition of shikimate dehydrogenase by shikimic acid and led to a low SA:DHS (0.82). The SA:DHS did not significantly increase at IPTG additions greater than 2.5 mg/6 h, suggesting further overexpression did not substantially affect the equilibrium of shikimic acid and DHS. This points to the need for a feedback insensitive, mutant isozyme of shikimate dehydrogenase if the SA:DHS is to be significantly increased.

Catabolic Repression Revisited: Methyl-α-D-Glucopyranoside

The failure of alternate host strains to eliminate the need for pulsed glucose addition coupled with the undesired consequences and difficulty in application of this control method suggested future titer and yield improvements in shikimic acid fermentations would be very difficult to achieve. An intriguing solution to shikimic acid-quinic acid equilibration would be to maintain a fermentation medium glucose concentration high enough to catabolically repress shikimic acid transport and conversion to quinic acid, yet low enough to prevent excessive acetate excretion. Such a glucose concentration might also circumvent the need for excessive oxygen transfer rates that may not be industrially viable. Literature precedent and fermentation data to this point suggested that fermentation conditions deviating from a glucose-limited environment were ill advised due to acetate excretion.[112] One alternative to enhanced glucose conditions would be the introduction of a compound structurally similar to glucose that could mimic the catabolic repression effects that glucose exhibits. One well precedented paradigm for the desired glucose-mimic behavior is induction of the *lac* operon genes whose expression is governed by the *lacI*^{q} repressor gene. Lactose serves as an inducer for genes repressed by the gene product of *lacI*^{q} by binding to the repressor molecule, thereby preventing repressor binding to the operon's operator sequence. Lactose induction is problematic since it is catabolized and therefore cannot sustain gene induction without repeated or continuous addition. IPTG circumvents this problem because it is able to bind to the *lacI*^{q} gene protein product, mimicking the affects of lactose in the absence of substrate catabolism. Furthermore, the inability of *E. coli* to metabolize IPTG precludes the need for substantial addition of the molecule in the

absence of hydrolytic instability. These were also desirable characteristics in a glucose analog as well.

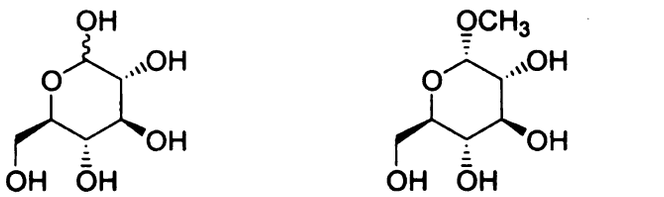

D-glucose methyl-α-D-glucopyranoside

Figure 35. The structures of D-glucose and methyl-α-D-glucopyranoside.

Research directed toward elucidating and understanding the proteins and transport mechanisms involved in the phosphoenolpyruvate:carbohydrate phosphotransferase (PTS) system of enterics have utilized the molecule methyl-α-D-glucopyranoside (MGP) extensively, particularly when investigating *Salmonella typhimurium* and *E. coli*. Numerous authors have explored the catabolic repression effects of MGP on the PTS system in *S. typhimurium* and *E. coli*.[113] Studies of MGP influx into these organisms has helped elucidate enzyme II complex subunit specificity in the PTS system. The cytoplasmic proteins enzyme I and Hpr, and the carbohydrate-specific, integral and cytosolic enzyme II proteins are responsible for the PTS-mediated carbohydrate uptake and phosphorylation in *S. typhimurium* and *E. coli*.[113j] Protein IIA^{Glc} (formerly III^{Glc}) of enzyme II plays a key role in catabolite repression because of its glucose-specific uptake capacity in the PTS system.[113k] MGP can serve as a substrate for IIA^{Glc}, reducing the rate of glucose phosphorylation in enterics by 40% when a 1 mM concentration is present.[113d] Mirroring glucose uptake by the PTS system, MGP is phosphorylated during transport into the cytoplasm, concomitantly converting PEP to pyruvate. However, phosphorylated MGP cannot be catabolized further by enterics and is hypothesized to undergo

dephosphorylation by cytosolic phosphatases, with eventual export of the free methyl-glucoside to the supernatant. Additionally, MGP was not observed to be hydrolyzed in solution, and was not observed to degrade when subjected to sterilization via autoclaving.

The preceding rationale suggested MGP would be an ideal candidate molecule to mimic the catabolic repression effects of glucose in glucose-limited fed-batch fermentations. MGP addition (10 mM) to SP1.1/pKD12.112A standard fed-batch fermentations at inoculation dramatically shifted hydroaromatic selectivity in favor of shikimic acid such that no quinic acid was detectable by ^{1}H NMR (Table 12, entry 1). The MGP appeared to induce the same catabolic repression of shikimic acid transport that increased glucose concentrations achieved. MGP addition circumvented the pulsed glucose regimen previously employed to reduce quinic acid formation while relegating quinic acid biosynthesis to an undetectable level. The shikimic acid titer at 48 h was 18 g/L while 3.1 g/L DHS accumulated. This constituted a significant increase in shikimic acid titer relative to the oscillatory conditions previously employed to culture SP1.1/pKD12.112 (Table 3, entry 8). The yield of shikimic acid (9.8%) was essentially unchanged however, and the total yield (11%) was actually lower than the pulsed glucose addition conditions, mainly due to the absence of quinic acid.

Unfortunately, the MGP-induced catabolic repression that prevented quinic acid formation also resulted in a significant reduction in total carbon flux through the shikimate pathway. The average shikimic acid titer produced by SP1.1/pKD12.112A when non-oscillatory fermentation conditions were employed in the absence of MGP addition was 26 g/L, while the total hydroaromatics produced (40 g/L) was almost double that of SP1.1/pKD12.112A cultured in the presence of 10 mM MGP (22 g/L). Could an

optimal MGP concentration be determined that reduced quinic acid biosynthesis to an acceptable concentration, yet attenuated catabolic repression effects to a level that permitted significant increases in hydroaromatic titers? Table 12 shows the hydroaromatic titers biosynthesized by SP1.1/pKD12.112A as a function of MGP concentration. Figure 36 shows a typical shikimic acid fermentation time course when MGP (1.0 mM) was present and a glucose feed pump K_c of 0.1 is employed. A MGP concentration of 1.0 mM was optimal (Table 12, entry 2), resulting in complete suppression of quinic acid formation while permitting shikimic acid and DHS final titers to increase relative to the 10 mM MGP addition. SP1.1/pKD12.112A shikimate dehydrogenase enzyme activities (Table 4) were not significantly altered by the addition of MGP (Table 13) to fermentation culture supernatants. DAHP synthase activities were not adversely affected by MGP, remaining at a level adequate to channel sufficient carbon into the shikimate pathway.

Table 12. SP1.1/pKD12.112A product titers, ratio, and yields as a function of MGP concentration.

Entry	MGP (mM)	SA (g/L)	QA (g/L)	DHS (g/L)	SA:QA	SA yield (mol/mol)	Total yield (mol/mol)
1	10	18	0.0	3.1	N/A	9.8%	11%
2	1.0	27	0.0	5.3	N/A	15%	18%
3	0.50	19	4.2	3.7	4.9 :1.0	12%	18%
4	0.0	26	8.1	6.5	3.1 :1.0	13%	20%

Table 13. DAHP synthase and shikimate dehydrogenase specific enzyme activities (μmol/min/mg) for SP1.1/pKD12.112A in the presence of 1.0 mM MGP.

		specific activity (μmol/min/mg)			
Entry	Enzyme	12 h	24 h	36 h	48 h
1	DAHP synthase	0.40	0.24	0.26	0.24
2	shikimate dehydrogenase	0.53	0.83	1.0	1.1

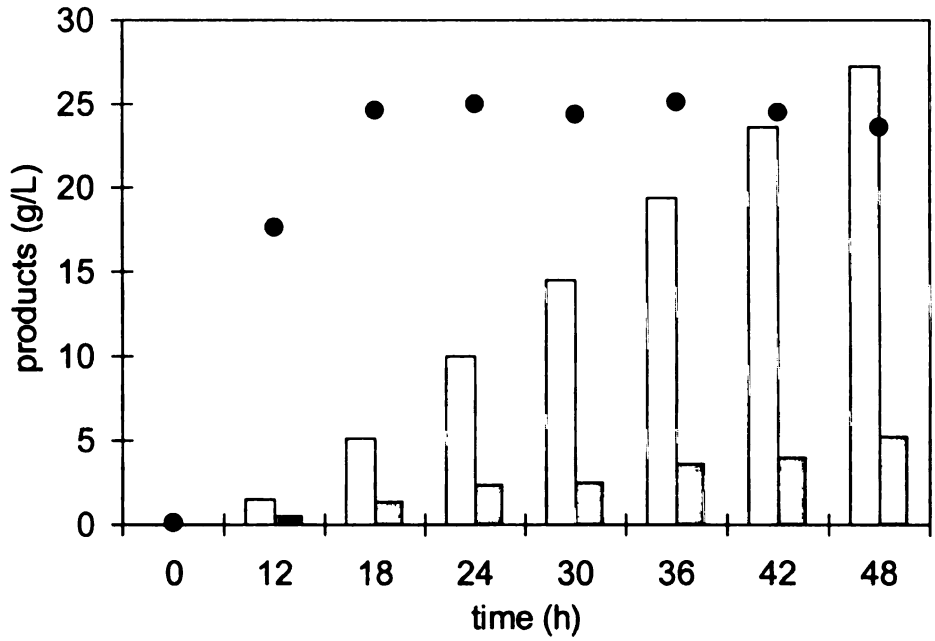

Figure 36. SP1.1/pKD12.112A cultured in the presence of 1 mM MGP. Shikimic acid□, quinic acid■, DHS□, cell mass●, in g/L.

Next, MGP addition was investigated in SP2.1/pKD12.112A fermentations, and optimized in the same fashion as for SP1.1/pKD12.112A. MGP addition was expected to suppress hydroaromatic equilibration better in SP2.1/pKD12.112A than in SP1.1/pKD12.112A since use of construct SP2.1/pKD12.112A had already resulted in a better SA:QA under both low (0.1) and high (0.8) glucose feed pump K_c conditions.

Starting with the optimized SP1.1/pKD12.112A MGP concentration (1.0 mM), the dependence of hydroaromatic equilibration was investigated by decreasing the MGP concentration present in SP2.1/pKD12.112A fermentations. Table 14 shows hydroaromatic concentrations and ratios formed under fed-batch fermentation conditions as a function of MGP concentration. The optimal MGP concentration for SP2.1/pKD12.112A was 0.5 mM, based on the SA:QA. Fermentations with MGP concentrations of 0.5 mM and 1.0 mM were essentially identical in final product titers and ratios, therefore the lower concentration was selected as optimal. As the MGP concentration was reduced, the SA:QA of SP2.1/pKD12.112A fermentations became unacceptable (<10) at concentrations below 0.5 mM (Table 14). MGP addition did not adversely affect either DAHP synthase or shikimate dehydrogenase measured enzyme activities (Table 15).

Table 14. SP2.1/pKD12.112A fed-batch fermentation product titers and ratios as a function of MGP concentration.

MGP (mM)	SA (g/L)	QA (g/L)	DHS (g/L)	SA:QA (mol:mol)	SA yield (mol/mol)	Total yield (mol/mol)
1.0	26	2.6	4.6	11:1.0	16%	20%
0.50	27	2.6	4.8	11:1.0	15%	19%
0.25	25	3.3	3.4	8.3:1.0	14%	18%
0.0	22	5.0	5.4	5.2:1.0	12%	18%

Table 15. DAHP synthase and shikimate dehydrogenase specific enzyme activities (μmol/min/mg) for SP2.1/pKD12.112A in the presence and absence of 0.5 mM MGP.

		specific activity (μmol/min/mg)			
[a]Entry	Enzyme	12 h	24 h	36 h	48 h
1	DAHP synthase	0.73	0.20	0.18	0.26
2	shikimate dehydrogenase	12	9.2	11	13
3	DAHP synthase	0.38	0.20	0.14	0.15
4	shikimate dehydrogenase	11	9.5	9.6	11

[a]Entries 1 and 2, no MGP; entries 3 and 4, 0.50 mM MGP.

Transketolase Revisited

The overexpression of transketolase by plasmid-localized *tktA* in construct SP1.1/pKD12.138A under pulsed glucose (K_c of 0.8) fermentor conditions led to a SA:QA nearly identical to that of SP1.1/pKD12.138A evaluated under standard (K_c of 0.1) fermentor control conditions (Table 6). Furthermore, the inability of pulsed glucose fermentor conditions to prevent quinic acid formation in SP1.1/pKD12.138A fermentations dissuaded evaluation of SP2.1/pKD12.138A. Recognizing that MGP addition to fed-batch fermentations prevented shikimic acid-quinic acid equilibration renewed interest in transketolase overexpression for enhancing shikimic acid titers and yields.

Table 16. SP1.1 product titers, yields, and ratios without (pKD12.112A) and with (pKD12.138A) transketolase overexpression in the presence of 1.0 mM MGP.

Entry	Plasmid	SA (g/L)	QA (g/L)	DHS (g/L)	SA:QA (mol:mol)	SA yield (mol/mol)	Total yield (mol/mol)
1	pKD12.112A	27	0.0	5.3	N/A	15%	18%
2	pKD12.138A	35	2.8	8.8	14:1.0	19%	25%

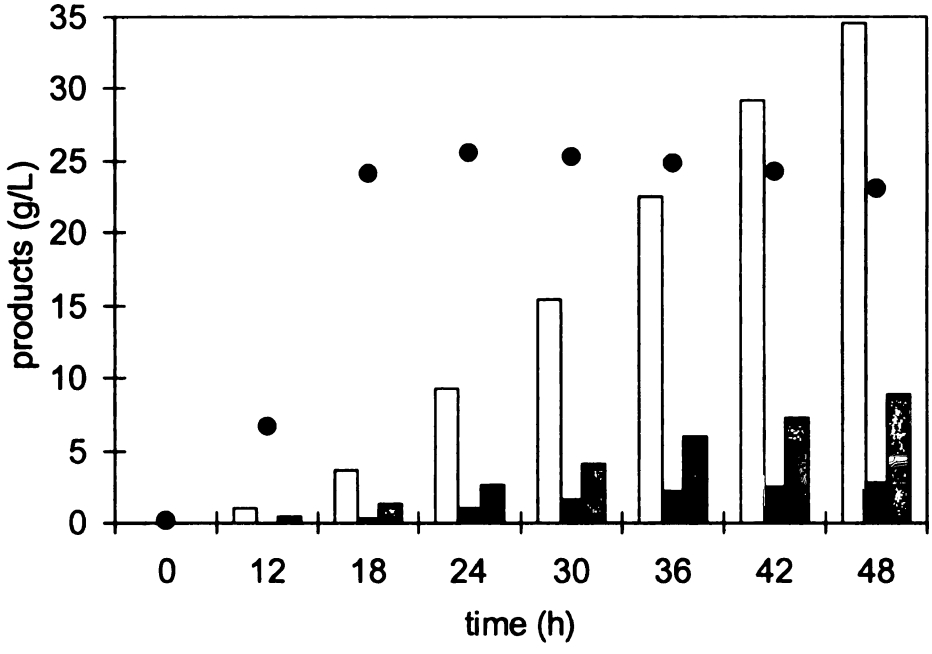

Figure 37. SP1.1/pKD12.138A cultured at 10% D.O., 0.1 K_c, in the presence of 1.0 mM MGP. Shikimic acid □, quinic acid ■, DHS ❑, cell mass ●, in g/L.

SP1.1/pKD12.138A (Figure 37) was cultured under standard glucose-limited, fed-batch fermentor conditions in the presence of 1.0 mM MGP. Quinic acid reemerged as a quantifiable byproduct, however the resulting product mixture had a SA:QA of 14:1.0, affording facile shikimic acid purification from fermentation broths. The final shikimic acid titer of 35 g/L and yield of 19% (Table 16, entry 2) represented substantial increases relative to the shikimic acid titer (27 g/L) and yield (15%) when SP1.1/pKD12.112A (Table 16, entry 1) was cultured under the same fermentor conditions. The final DHS titer accumulated (8.8 g/L) by SP1.1/pKD12.138A revealed a significant portion of the increased carbon flux directed into the shikimate pathway by transketolase overexpression was diverted to DHS synthesis. This suggested that transketolase overexpression exacerbated feedback inhibition of shikimate dehydrogenase by shikimic acid, which was not surprising given the increase in shikimic acid titer. DAHP synthase

and shikimate dehydrogenase activities (Table 17) were similar to those measured for SP1.1/pKD12.138A cultured in the absence of MGP addition (Table 5).

Table 17. DAHP synthase and shikimate dehydrogenase specific enzyme activities (μmol/min/mg) for SP1.1/pKD12.138A in the presence of 1.0 mM MGP.

		specific activity (μmol/min/mg)			
Entry	Enzyme	12 h	24 h	36 h	48 h
1	DAHP synthase	0.31	0.20	0.17	0.25
2	shikimate dehydrogenase	0.60	0.87	1.2	1.1

Table 18. SP2.1 product titers, yields, and ratios without (pKD12.112A) and with (pKD12.138A) transketolase overexpression in the presence of 0.5 mM MGP.

[a]Entry	Plasmid	SA (g/L)	QA (g/L)	DHS (g/L)	SA:QA (mol:mol)	SA yield (mol/mol)	Total yield (mol/mol)
1	pKD12.112A	27	2.6	4.8	11:1.0	15%	19%
2	pKD12.138A	30	2.0	13	17:1.0	15%	22%

[a]Entry 2, 36 °C.

Similarly, SP2.1/pKD12.138A was cultured under standard glucose-limited, fed-batch fermentor conditions, but in the presence of 0.50 mM MGP (Table 18, entry 2). An increase in temperature, from 33 °C to 36 °C was necessitated in order to accommodate the sluggish growth characteristics exhibited by construct SP2.1/pKD12.138A relative to SP1.1/pKD12.112A. An increase in titer and yield of shikimic acid relative to the same host strain bearing the pKD12.112A plasmid was observed. Although the final shikimic acid titer (30 g/L) improved relative to that of SP2.1/pKD12.112A (27 g/L), the increment was less than that realized when SP1.1 was evaluated with the same plasmids and fermentation conditions. The shikimic acid yield (15%) was identical for both

SP2.1/pKD12.112A and SP2.1/pKD12.138A, while the total yield had a modest improvement from 19% to 22%, respectively (Table 18). The SA:QA increased when transketolase was overexpressed (17) relative to when it was not (11). Previous precedent had suggested SA:QA could be temperature dependent in such a fashion during shikimic acid biosynthesis by *E. coli*.[39]

The product mixture of SP2.1/pKD12.138A was unfavorable when compared to SP1.1/pKD12.138A. Although both constructs demonstrated an acceptable SA:QA, SP2.1/pKD12.138A generated a significantly larger DHS concentration than SP1.1/pKD12.138A. The increased DHS titer accounted for the lack of increased shikimic acid yield and modest gain in shikimic acid titer. This was somewhat unexpected since the shikimate dehydrogenase activity of SP2.1/pKD12.138A (Table 19) was about 8 to 18-fold greater than that of SP1.1/pKD12.138A (Table 17). The DAHP synthase activity levels of the two constructs were approximately the same (Table 17, entry 1 and Table 19, entry 1), and did not deviate significantly from constructs utilizing plasmid pKD12.112A cultured in the absence of MGP.

Table 19. DAHP synthase and shikimate dehydrogenase specific enzyme activities (μmol/min/mg) for SP2.1/pKD12.138A in the presence of 0.5 mM MGP.

		specific activity (μmol/min/mg)			
Entry	Enzyme	12 h	24 h	36 h	48 h
1	DAHP synthase	0.32	0.13	0.21	0.26
2	shikimate dehydrogenase	11	12	10	11

Shikimic Acid Biosynthesis and Unlimited Glucose Availability.

Until this point, several methodologies for preventing shikimic acid uptake and subsequent conversion to quinic acid where investigated. However, exploration of fed-batch fermentation conditions unlimited in glucose supply had been avoided. Instead of supplying fermentations with a glucose-mimic to induce catabolic repression of quinic acid formation, the glucose concentration of fermentations could be maintained at a level sufficient to accomplish the same result. Unfortunately, literature precedent suggested the implementation of such a control scheme would result in organic acid excretion by *E. coli*, particularly acetic acid.[112] The use of "inappropriate" glucose feeding strategies for aerobic *E. coli* cultures have been characterized by feed rates that exceed the respiration capacity of the cultures to oxidatively metabolize glucose.[112b] Inhibition of high-density *E. coli* cultures by excreted acetate has served as a daunting process impediment at both small and large scale alike, and has been vigorously scrutinized.[112] However, process scale fermentation equipment is often hampered by oxygen mass transfer limitations and/or non-ideal mixing, and acetate formation in many literature accounts is the result of excess glucose metabolism in the absence of sufficient oxygen to fully oxidize the available substrate. Contrary to literature precedent, F. Hoffmann-La Roche communicated to the Frost Group that they had experienced success in suppressing quinic acid formation in their shikimic acid cultures by employing glucose-rich conditions at scales of up to 1000 liters. The departure from literature observations that poor culture productivity and acetate excretion were synonymous with fermentation conditions with elevated glucose levels suggested investigation of a glucose-rich fermentation environment might be successful.

The standard glucose-limited fermentation conditions were altered to a glucose-rich environment by a modification in fermentation control methodology, and introduction of baffles into the reactor system. The initial staged control of impeller rate and airflow rate to maintain the D.O. concentration at the set point remained unchanged, however glucose feeding was no longer computer-controlled to maintain the desired D.O. concentration once the maximum airflow rate was achieved. Instead, the order of the impeller-airflow rate cascade loop was reversed when the maximum airflow rate was achieved, and the control loop remained active. The glucose feed rate was manually adjusted to maintain a glucose concentration of 20-30 g/L, while the impeller rate varied to maintain the D.O. concentration at 10% of air saturation.

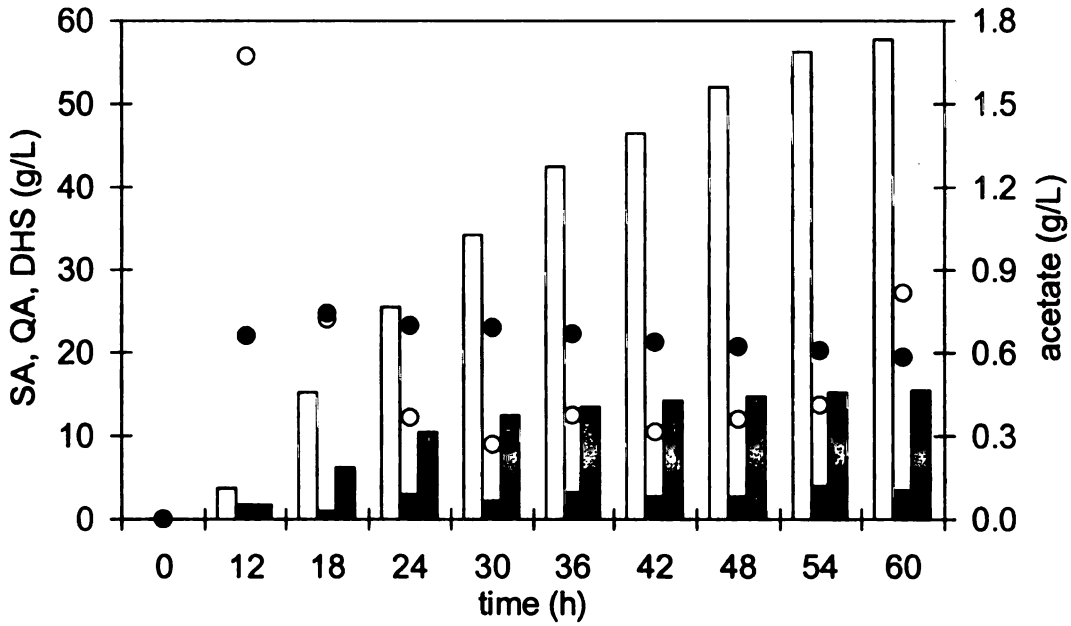

Figure 38. SP1.1/pKD12.138A glucose rich fed-batch fermentation product time course. Shikimic acid□, quinic acid■, DHS ⬚, cell mass●, in g/L.

The final shikimic acid concentration (58 g/L) at 60 h represented a 23 g/L increase relative to that achieved under glucose-limited conditions in the presence of 1.0

mM MGP. Unfortunately, the final titer of DHS (15 g/L) was almost double that observed under glucose-limited fermentation conditions with MGP (8.8 g/L). A marginal increase in quinic acid titer (3.6 g/L) was observed relative to glucose-limited conditions with MGP added (2.8 g/L). The feedback inhibition of *aroE*-encoded shikimate dehydrogenase was now the limiting factor in shikimic acid production, with DHS accumulation accounting for about 20% of the total carbon directed into the shikimate pathway. Furthermore, DAHP synthase and shikimate dehydrogenase enzyme activities (Table 20) did not exhibit significant reductions due to the glucose-rich culturing environment relative to SP1.1/pKD12.138A cultured under glucose-limited conditions in the presence of 1.0 mM MGP (Table 19).

When SP1.1/pKD12.138A was cultured under the glucose-rich conditions, shikimic acid biosynthesis was not detrimentally impacted by excreted acetate. Acetate excretion was observed to increase relative to glucose-limited conditions, however the increase was not excessive, and the acetate concentration accumulated by 60 h (0.82 g/L) constituted neither a major fermentation product, nor a significant drain of carbon through metabolic overflow.[112h,i]

Table 20. DAHP synthase and shikimate dehydrogenase specific enzyme activities (μmol/min/mg) for SP1.1/pKD12.138A cultured under glucose-rich fermentation conditions.

		specific activity (μmol/min/mg)					
Entry	Enzyme	12 h	24 h	36 h	48 h	54 h	60 h
1	DAHP synthase	0.16	0.25	0.31	0.16	0.17	0.19
2	shikimate dehydrogenase	0.57	0.90	1.3	1.4	1.4	1.6

Discussion

Hydroaromatic equilibration.

Formation of quinic acid results from the *aroE*-mediated reduction of DHQ. Delineating the source of the DHQ that is reduced therefore is paramount to understanding the mechanism responsible for byproduct formation during shikimic acid biosynthesis. Two mechanisms are possible. DHQ synthesized from glucose may be reduced by *aroE*-encoded shikimate dehydrogenase prior to its conversion to DHS catalyzed by *aroD*-encoded DHQ dehydratase (Figure 2). Alternatively, microbe-synthesized shikimic acid that accumulates in the culture supernatant may be transported back into the microbial cytoplasm followed by microbe-catalyzed equilibration. Conversion of transported shikimic acid into DHQ would require shikimate dehydrogenase-catalyzed oxidation of shikimic acid to DHS followed by hydration of this hydroaromatic catalyzed by DHQ dehydratase.

Demonstrating the ability of *E. coli* to catalyze the formation of DHS and quinic acid from transported shikimic acid (Figure 29) was essential to establishing that hydroaromatic equilibration was a possible mechanism to explain the formation of quinic acid during shikimic acid biosynthesis. However, demonstration of hydroaromatic equilibration does not necessarily establish shikimic acid transport as the mechanism responsible for quinic acid formation during fermentor-controlled, microbial synthesis of shikimic acid from glucose. Delineation of the role of shikimic acid transport in quinic acid formation provided an essential second line of mechanistic information. Continued formation of quinic acid in shikimate-synthesizing *E. coli* constructs deficient in shikimic acid transport would be consistent with a mechanism involving shikimate dehydrogenase-

catalyzed reduction of intermediate DHQ prior to synthesis of shikimic acid. A pronounced decline or the absence of quinic acid generated by this same *E. coli* construct lacking the ability to transport shikimic acid from its growth medium to its cytoplasm would be indicative of equilibration of initially synthesized shikimic acid.

Transport of shikimic acid in *E. coli* has been linked to the *shiA* locus.[109] Therefore, the construction of a shikimate-synthesizing *E. coli* strain incapable of shikimic acid transport was guided by literature precedent for spontaneous mutations associated with the shikimic acid transport system of enterics resulting from exposure to FSA.[110] One such construct phenotypically deficient in *shiA*-encoded transport of shikimic acid, *E. coli* SP1.1-4/3/pKD12.112A, produced quinic acid and DHS during de novo biosynthesis of shikimic acid from glucose (Figure 32). Upon first inspection, quinic acid and DHS production appeared consistent with a mechanism for quinic acid formation involving reduction of intermediate DHQ prior to formation of shikimic acid. However, subsequent evaluation of several genotypic *shiA*-deficient *E. coli* strains[55b,114] generated via transposon mutagenesis[55b,109c] suggested quinic acid and DHS were formed when shikimic acid was added to these constructs' culture media.[114]

The observation that quinic acid and DHS were formed by SP1.1-4/3/pKD12.112A when shikimic acid transport should have been disrupted has several plausible explanations. First, ^{14}C-labeled shikimic acid uptake experiments were performed according to Pittard and Wallace.[109a] The ability of SP1.1/4-3/pKD12.112 to produce both shikimic and quinic acids, despite being a *shiA*$^-$ phenotype, might be attributable to residual shikimic acid transport capability. Experiments performed to validate the *shiA*$^-$ phenotype of SP1.1/4-3 employed a much lower biomass concentration

(0.11 g/L) relative to those observed in fed-batch fermentations (about 25 g/L, Figure 32). Perhaps the greater than 200-fold increase in cell concentration resulted in a corresponding amplification of any residual shikimic acid uptake ability retained by host SP1.1-4/3. The statistically negligible difference in the SA:QA between SP1.1/pKD12.112A (3.1:1.0) and SP1.1/4-3/pKD12.112A (4.0:1.0) might therefore be explained. A contributing factor to residual shikimic acid transport might be the time scale discrepancy between the two experimental protocols. ^{14}C-labeled shikimic acid uptake experiments were concluded by 30 minutes, while glucose-limited, fed-batch fermentations (K_c of 0.1) were often subjected to glucose-limited conditions in excess of 36 h during feeding. The stability of the spontaneous mutation induced by FSA has yet to be confirmed, and therefore spontaneous reversion to a *shiA*$^+$ phenotype might also be plausible. Finally, quinic acid accumulation in SP1.1-4/3/pKD12.112A culture supernatants could result from non-*shiA*-mediated shikimic acid transport if *E. coli* employs multiple transport systems for shikimic acid. Transport of shikimic acid has been theorized to result from multiple loci,[108,109] consistent with the multiple transport systems that bacteria often employ for uptake of carbon sources. Hydroaromatic equilibration would therefore be a good candidate for catabolic repression of shikimic acid transport.

MGP addition and catabolite repression.

Additional insight into the role of shikimic acid transport and formation of quinic acid came from consideration of shikimic acid's role as a source of carbon for microbial growth and metabolism. Numerous microbes can use hydroaromatics such as shikimic

acid as a sole source of carbon during growth.[115] One of these species, *Klebsiella spp.*, is evolutionarily related to *E. coli*.[116] Although unable to utilize shikimic acid as a sole source of carbon for growth, shikimic acid transport in *E. coli* may be an evolutionary remnant of a former capacity to catabolize shikimic acid and may also reflect the multiple transport systems microbes often possess for transport of carbon sources. Consideration of shikimic acid as a source of carbon for growth and metabolism also leads to a possible strategy for repression of shikimate transport. When another carbon source (e.g. lactose, arabinose, mannose etc.) in addition to glucose is available at any one time for growth of microbes such as *E. coli*, glucose is frequently consumed first.[117,118] Expression of genes required for transport and metabolism of non-glucose carbon sources can be prevented by catabolite repression.[117] The mechanism of catabolite repression encompasses a complex cascade of cellular processes. The traditional hallmarks of catabolite repression are a decrease in intracellular cAMP concentration, and an increase in the intercellular molar ratio of ATP:ADP. Studies of the PTS system in enterics have revealed that MGP increases the molar ratio of ATP:ADP[113k] and decreases the intercellular cAMP[113o] concentration despite its inability to be catabolized.

Both low (0.50-1.0 mM) concentrations of MGP under glucose-limited culture conditions (about 0.20 mM glucose for a K_c of 0.1) and glucose-rich (140 mM glucose) culture conditions successfully inhibited quinic acid biosynthesis. These observations are consistent with catabolic repression of all systems employed by *E. coli* to transport shikimic acid. Inhibition of quinic acid formation attendant with repression of shikimic acid transport, in turn, indicates that quinic acid formation during shikimic acid biosynthesis is best viewed as an equilibration of initially synthesized shikimic acid as

opposed to reduction of intermediate DHQ prior to formation of shikimic acid. In essence, the shikimate pathway is operating in an intact organism in the reverse of its normal biosynthetic direction.

The relatively low concentration of MGP (0.5-1.0 mM) required to mimic catabolite repression was not surprising since the PTS system of enterics has been reported to have a similar affinity for glucose and MGP. The reactions of the PTS can be subdivided into transport and phosphorylation, each with its own apparent K_m values for glucose and MGP, which are subject to assay conditions, the carbon source used for generating biomass, and so on. Therefore, kinetic data for MGP in *S. typhimurium* and *E. coli* can be somewhat ambiguous. The apparent K_m value for the protein $IIBC^{Glc}$-dependent transport and phosphorylation of MGP has been reported as 6 to 28 μM,[113e,m] compared to 3 to 10 μM for glucose,[113e,f] while the K_m for the protein IIA^{Glc}-dependent phosphate transfer to protein IIB^{Glc} when either MGP or glucose is the substrate has been reported as 2 to 5 μM.[113i,m,n]

Yield and Titer Considerations.

Determining the theoretical maximum yield for biocatalytic synthesis of shikimic acid begins with a carbon balance (Equation 13) for PEP and E4P inputs and shikimic acid and byproducts. The PEP and E4P inputs are then equated to the amount of glucose required to form these substrates (Equation 14). Because *E. coli* relies on the PTS system for glucose uptake, a pyruvic acid term is included in Equation 14 to reflect the conversion of one molecule of PEP into pyruvic acid for each molecule of glucose transported into the cytoplasm as glucose-6-phosphate. Equation 14 reflects the effective

absence of pyruvic acid recycling back to PEP that would be catalyzed by PEP synthase.[52] PTS-generated pyruvic acid is often considered to be the carbon source for the anabolism and catabolism required for generation of *E. coli* biomass.[33]

Equation 13. PEP + E4P ⟶ 2 H_3PO_4 + H_2O + shikimic acid

Equation 14. x glucose ⟶ PEP + E4P + x PYR

Equation 15. x 6(C) ⟶ 3(C) + 4(C) + x 3(C)

A coefficient is determined (Equation 15) to balance the number of carbon atoms in the glucose starting material with the total number of carbon atoms formed in PEP, E4P, and pyruvic acid. The determined coefficient of 2.33 leads to a maximum theoretical yield of 43% (mole shikimic acid/mole glucose) for synthesis of shikimic acid from glucose. SP1.1/pKD12.138A, the construct producing the highest yields and titers of shikimic acid, synthesized shikimic acid at 54% of the theoretical maximum yield under glucose-rich conditions. In considering the performance of SP1.1/pKD12.138A, synthesis of quinic acid and DHS must be also be taken into consideration. Including quinic acid and DHS synthesis, SP1.1/pKD12.138A channeled a total of 71% of the theoretical maximum amount of carbon that can be directed into aromatic amino acid biosynthesis (Figure 38).

Alleviating E4P limitation during shikimic acid biosynthesis via transketolase overexpression resulted in a dramatic increase in shikimic acid titer and yield. Comparing SP1.1/pKD12.112A and SP1.1/pKD12.138A cultured under the same fed-batch fermentor conditions (1.0 mM MGP, Table 16, entries 1 and 2 respectively), overexpression of *tktA*-encoded transketolase provided a significant increase in shikimic

acid titer (from 27 g/L to 35 g/L), total hydroaromatic titer (from 33 g/L to 46 g/L), shikimic acid yield (from 15% to 19%) and total yield of hydroaromatics (from 18% to 25%). The dramatic increase in total yield between SP1.1/pKD12.112A and SP1.1/pKD12.138A was a result of both increased shikimic acid production and the reemergence of quinic acid as a quantifiable byproduct (2.8 g/L). The significant enhancement in DHS titer (from 5.3 g/L to 8.8 g/L) via transketolase overexpression presumably reflected an increase in feedback inhibition of shikimate dehydrogenase from the increased shikimic acid titer accumulated. Comparing SP1.1/pKD12.112A[55b] and SP1.1/pKD12.138A cultured under glucose-rich conditions, titer enhancements were greater still, while shikimic acid yield improvement was slightly less. SP1.1/pKD12.112A produced 38 g/L shikimic acid in 18% yield,[55b] while SP1.1/pKD12.138A produced 58 g/L shikimic acid in 23% yield from glucose (Figure 38). The large accumulation of DHS during glucose-rich cultivation of SP1.1/pKD12.138A demonstrates the crucial role that feedback inhibition of shikimate dehydrogenase exerts during biosynthesis of shikimic acid. DHS formation constituted about 20% of the total carbon channeled into the shikimate pathway, and comprises a significant drain on realizable shikimic acid titers and yields.

Glucose-Rich Conditions and Acetate Biosynthesis.

The extensive pursuit of mechanistic insight into acetate biosynthesis via fed-batch and batch aerobic fermentation, analytic instrumentation, and modeling are a testament to the gravity of its metabolic consequences.[112] The electron transport chain has been implicated as the rate-limiting step in metabolism responsible for acetate

accumulation during aerobic growth,[119] and nutrient limitation credited with curtailing acetate biosynthesis.[112d] Subsequent studies have shown that acetate formation is highly strain dependent however, and not necessarily a function of the carbon source feeding strategy adopted or peripheral nutrient availability alone.[112c,e,f,g,i]

During fermentor-controlled shikimic acid biosynthesis, acetate accumulation (0.82 g/L) during glucose-rich fermentation conditions did not appear to adversely affect the cultures. Pseudo-steady state acetate levels were maintained between 0.30 and 0.40 g/L up to 54 h, at which time acetate excretion began to rise slightly. By comparison, the 48 h acetate accumulation during SP1.1/pKD12.138A glucose-limited fermentations (0.14 g/L) in the presence of MGP was somewhat lower. Literature accounts of high acetate production during fed-batch fermentation typically involve systems with a set oxygen transfer rate where nutrients are limiting.[112b,c] Accounts of batch fermentations, or pseudo-fed-batch fermentations that add nutrients only when their concentrations have been reduced to a threshold value (but non-limiting), that are limited neither in nutrients nor in oxygen have highly strain-dependent results for acetate accumulation.[112f,g] Therefore it is not entirely surprising that acetate formation was not problematic in the aerobic, glucose-rich culturing of shikimic acid-synthesizing SP1.1/pKD12.138A. The lack of acetate excretion may reflect RB791's absence of significant mutations. RB791, the parent strain of SP1.1, and differs form wild type *E. coli* by single mutation. The success of this culturing methodology has permitted the process to be scaled to 60 m^3 by F. Hoffmann-La Roche Ltd.

CHAPTER 3

Homologous Quinic Acid Biosynthesis

Introduction

Although the source of quinic acid has historically been *Cinchona* bark,[120] a less exotic source of quinic acid was established in 1992 with the construction of a transgenic *E. coli* strain that synthesized quinic acid from glucose under shake flask conditions.[103] Quinic acid utilization as a synthetic backbone has benefited from greater availability relative to shikimic acid, resulting in the application of quinic acid as the starting molecule in a remarkably large array of chiral molecule and natural product syntheses.[121] Quinic acid has also garnered attention as a polyoxygenated scaffold for combinatorial synthesis.[122] Numerous biologically active molecules have been constructed in whole, or in part, from quinic acid. The diversity of these molecules encompasses the tubulin stabilizing antitumoral agent taxol (the 2-iodocyclohexenone acetal portion)[123] which has proven effective against metastatic carcinoma of the ovary, advanced ovarian carcinoma and AIDS-related Kaposi's sarcoma;[124] the Lewis lung carcinoma and Walker intramuscular carcinosarcoma tumor-inhibitor (+)-crotepoxide (Figure 39);[125] the bicyclic core structure of the enediyne antitumoral agent esperimicin-A_1 effective against melanoma, several carcinomas, and leukemia;[126] model compounds for the cyclohexenone moiety of scyphostatin which is a powerful inhibitor of neutral sphongomyelinase for treatment of ceramide-mediated pathogenic states;[127] (+)-eutypoxide B which is a secondary metabolite of the fungus *Eutypa lata* implicated as a

potential causative agent in pathogenic vineyard die-back disease (Figure 39);[128] the C_{20} to C_{34} segment of the immunosuppressant FK-506 (Figure 39);[129] and the anti-influenza drug GS4104 (Figure 17, Figure 39)[89] just to name a few.

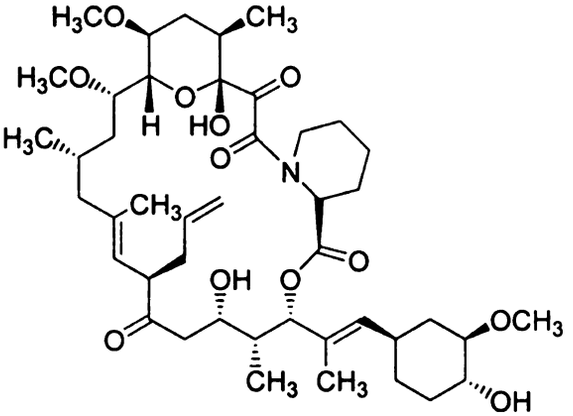

immunosuppressant FK-506

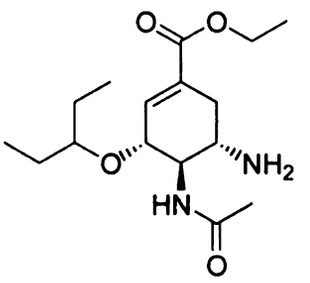

GS4104

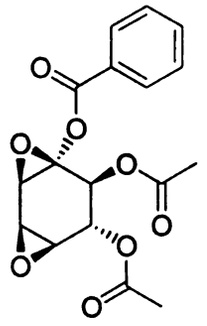

(+)-crotepoxide

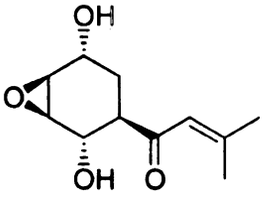

(+)-eutypoxide B

Figure 39. Select biologically active molecules derived from quinic acid.

Quinic acid has not previously been considered a normal intermediate of the shikimate pathway in *E. coli*.[130] Subsequent to the identification of quinic acid as a homologous metabolite in *E. coli*, the shikimate pathway (Figure 2) must be modified to include biosynthesis of quinic acid (Figure 40).

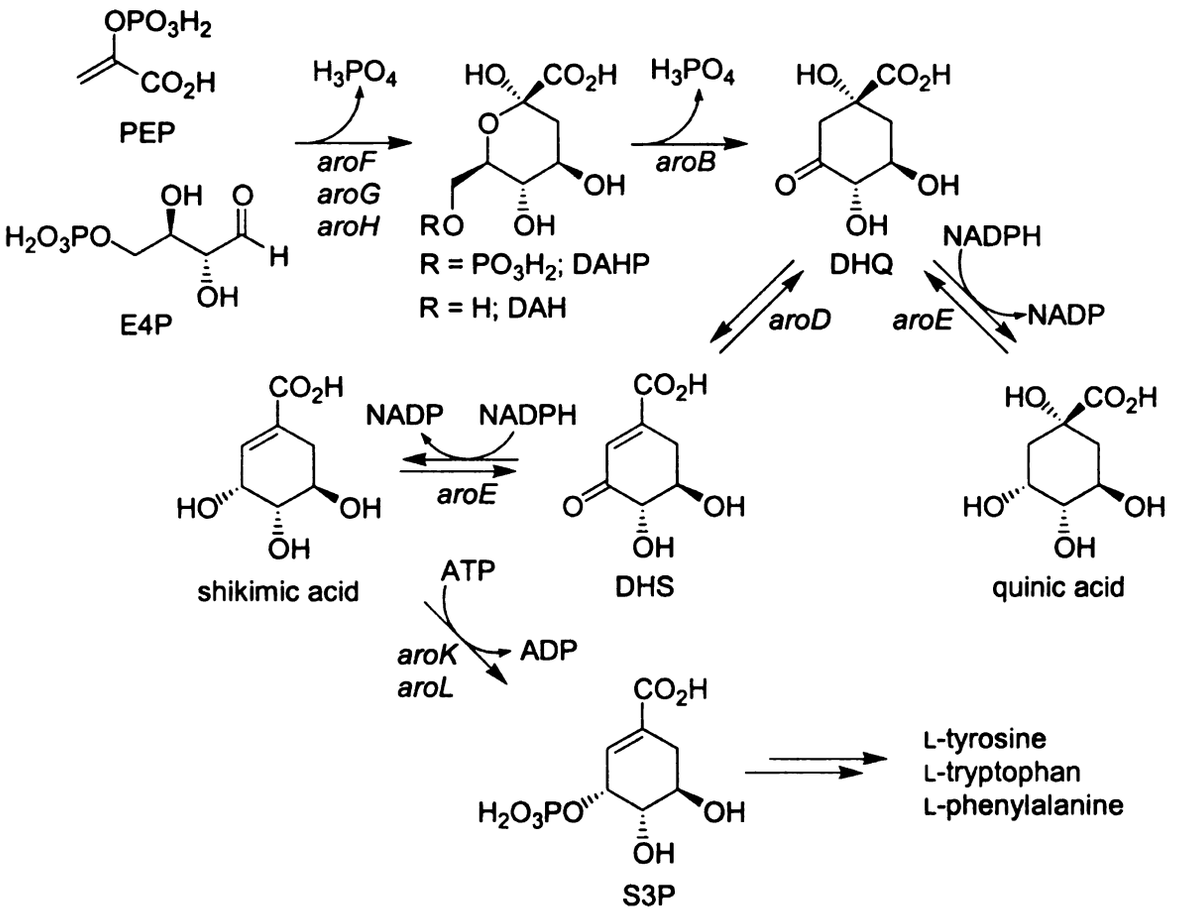

Figure 40. The truncated aromatic amino acid biosynthesis pathway with quinic acid biosynthesis. Metabolite and genetic loci abbreviations are per Figure 2.

Conspicuously absent from the Chapter 1 discussion of molecules obtained from shikimate pathway metabolites was a treatise of hydroquinone. The results of Chapter 2 established that homologous conversion of glucose to quinic acid by *E. coli* constructs could be achieved. The Chapter 2 results might be exploited to develop quinic acid biosynthesizing *E. coli* constructs that lacked the requirement for plasmid maintenance with antibiotics or relied on foreign gene expression.[103] Furthermore, potential improvement in yield and culturing conditions relative to prior work might substantially increases quinic acid titers.[103] Improvements in the biosynthetic route to quinic acid from glucose could be coupled to recent improvements in synthetic methodologies for the

conversion of quinic acid to hydroquinone (Figure 41).[131] Enhanced abiotic or biotic conversion of quinic acid to hydroquinone could constitute an important industrial route to this dihydroxylated aromatic. Woskresensky first synthesized hydroquinone from quinic acid in 1838,[132] and hydroquinone now commands a central role in photographic development and also finds use in polymerization inhibitors, rubber antioxidants, food antioxidants, and water treatment.[133] Hydroquinone is even employed in the insect kingdom as a chemical defense by species such as the bombardier beetle (*Brachinus* spp.) for repelling predators.[134] The demand for hydroquinone was estimated at 40,000 tons per year in 1992, with worldwide production capacity approaching 50,000 tons per year recently.[133] Current industrial syntheses of hydroquinone suffer from the same process shortcomings of similar processes discussed in Chapter 1. The three industrial routes to hydroquinone in widespread use are aniline oxidation, phenol hydroxylation, and *p*-diisopropylbenzene hydroperoxidation (Figure 41). Aniline oxidation results in an immense amount of environmentally problematic byproduct salt streams, including manganese sulfate, ammonium sulfate, or iron oxides. Hydroxylation of toxic phenol requires explosive peroxide reagents and *p*-diisopropylbenzene hydroperoxidation proceeds through peroxide intermediates. The genesis of all three synthetic methodologies is carcinogenic benzene as well. Is fed-batch fermentation biosynthesis of quinic acid viable? If so, are titers that make it an economically attractive molecule from which the synthesis of hydroquinone can proceed achievable? This chapter will address the biocatalytic conversion of glucose to quinic acid by recombinant *E. coli* under fed-batch fermentation conditions.

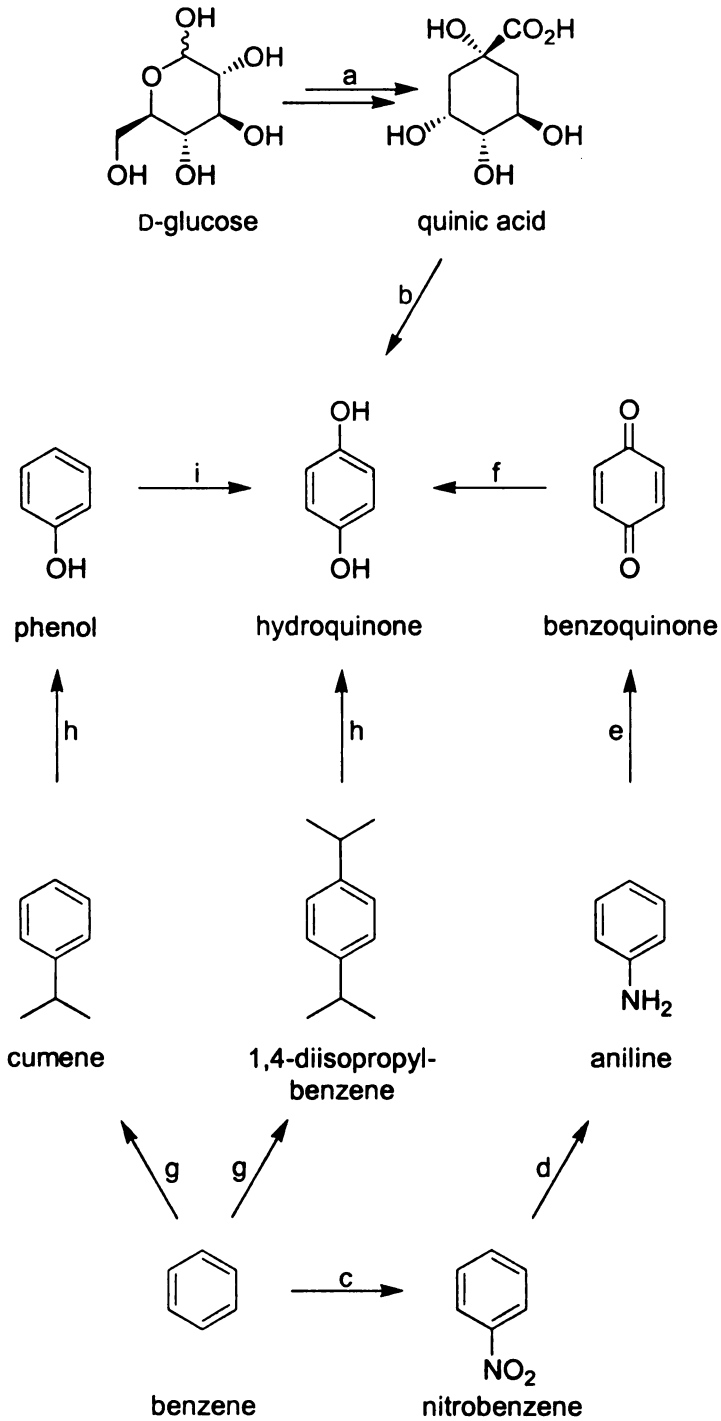

Figure 41. Synthetic and biosynthetic routes to hydroquinone. Reaction conditions: (a) *E. coli*. (b) HOCl or $Ag_3PO_4/K_2S_2O_8$. (c) HNO_3, H_2SO_4; (d) Cu/SiO_2, H_2. (e) MnO_2, H_2SO_4. (f) Fe^0. (g) 2-propene, HZSM-12. (h) (i) O_2, NaOH, (ii) H_2SO_4. (i) HCO_2H, HCO_3H.

Fermentation Conditions

Fed-batch fermentation results reported in this chapter are for standard glucose-limited conditions in the laboratory of Dr. John Frost. Fermentation conditions which deviated from the standard conditions (e.g., different D.O. concentration set point, glucose-rich conditions, etc.) are explicitly stated.

Homologous Quinic Acid Biosynthesis and Fed-Batch Fermentation.

The capability of SP1.1 constructs to homologously biosynthesize quinic acid presented an intriguing opportunity for biocatalytic production of this molecule. Quinic acid formation in shikimic acid-synthesizing cultures was demonstrated to be an equilibrium between shikimic acid and quinic acid resulting from reverse operation of the shikimate pathway in Chapter 2, with *aroE*-encoded shikimate dehydrogenase catalyzing the conversion of intercellular DHQ to quinic acid. Could biocatalytic quinic acid formation be exploited as a fermentation route to this widely utilized chiral synthon? Inspection of the shikimate pathway (Figure 40) reveals that the absence of catalytically-active *aroD*-encoded DHQ dehydratase should provide for accumulation of DHQ in fermentation culture supernatants. However, overexpression of *aroE* in an *aroD*-deficient construct might capitalize upon the ability of *aroE*-encoded shikimate dehydrogenase to reduce substrate DHQ to product quinic acid, affording a homologous quinic acid producing construct. Exploration of homologous quinic acid formation was initiated with construction of host strain QP1.1.

E. coli QP1.1 was constructed by the site-specific insertion of *aroB* into the *serA* locus of *E. coli* AB2848 via homologous recombination. AB2848 lacks catalytically

active DHQ dehydratase due to a mutation in its *aroD* locus and therefore cannot convert substrate DHQ to product DHS.[108] QP1.1 constructs required supplementation with L-phenylalanine, L-tyrosine, L-tryptophan, *p*-hydroxybenzoic acid, *p*-aminobenzoic acid, and 2,3-dihydroxybenzoic acid due to their lack of DHQ dehydratase activity.

Initial Fed-Batch Quinic Acid Fermentations.

The first construct evaluated for biocatalytic formation of quinic acid under fed-batch fermentation conditions was QP1.1/pKD12.112A. The construction of, and structural genes harbored by, plasmid pKD12.112A were elaborated in Chapter 2 (Figure 20). Fed-batch fermentation of construct QP1.1/pKD12.112A resulted in quinic acid as the major fermentation product, with a low level of contaminating DHQ accumulation. Initial fed-batch fermentation conditions employed a D.O. set point of 20% of air saturation, as did initial shikimic acid fermentations described in Chapter 2. Additionally, catabolite repression methodologies required during fed-batch fermentation of shikimic acid-synthesizing constructs were not required during cultivation of QP1.1/pKD12.112A.

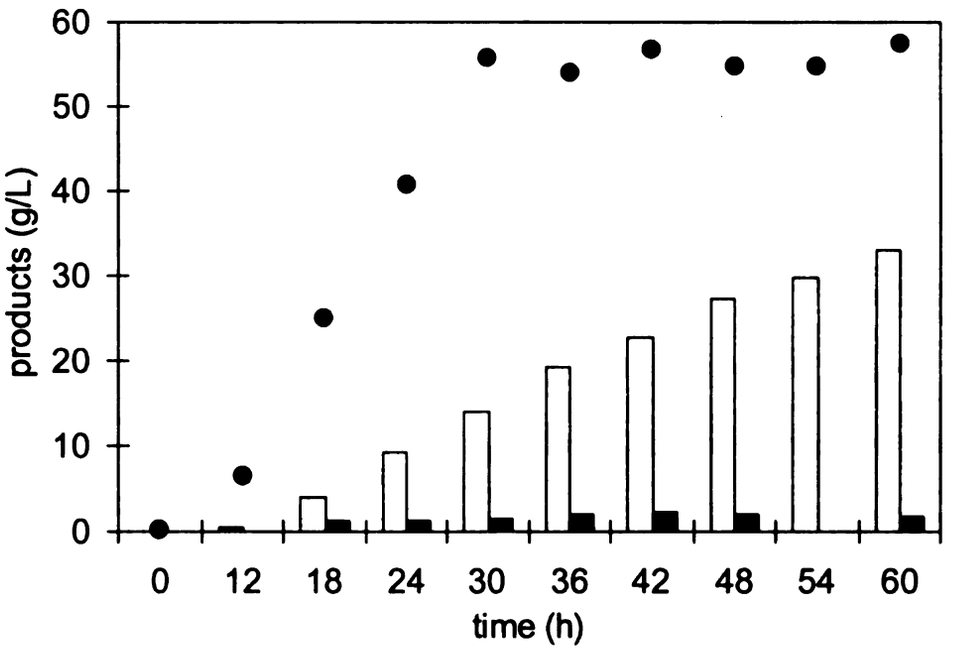

Figure 42. Fed-batch fermentation of QP1.1/pKD12.112A at 20% D.O. Quinic acid□, DHQ■, cell mass●, in g/L.

Fed-batch fermentations of QP1.1/pKD12.112A produced quinic acid for 60 h, resulting in a final quinic acid titer of 33 g/L in a 14% yield (mol/mol) from glucose. This titer was almost a 7-fold increase relative to a prior literature account of quinic acid production by *E. coli*, and required neither heterologous gene expression nor a multiple plasmid expression system.[103] The lack of catabolite repression methodologies permitted extended controllability of QP1.1/pKD12.112A cultures without the fear of unregulated glucose addition. The biocatalyst had worked as conceived: instead of accumulating DHQ as the major fermentation product, DHQ was reduced to quinic acid by shikimate dehydrogenase and accumulated as the major supernatant constituent. In addition to quinic acid, DHQ accumulated at low levels in fermentation supernatants (1.8 g/L by 60 h) and was relatively constant subsequent to 18 h, ranging between 1.3 and 2.1 g/L.

DHQ accumulation was not necessarily surprising, given the utilization of shikimate dehydrogenase for a non-native conversion. The final QA:DHQ was 18.

Fed-batch fermentation conditions for QP1.1/pKD12.112A were then permuted to the standard fed-batch fermentation conditions for shikimic acid-producing constructs, namely a D.O. set point of 10%. Culturing QP1.1/pKD12.112A at the standard conditions resulted in an incremental increase in quinic production (Figure 43). Quinic acid titer increased to 40 g/L while the yield from glucose was essentially unchanged at 15% (mol/mol). The concentration of DHQ varied between 1.0 g/L and 2.3 g/L between 18 h and 60 h. The final DHQ concentration of 2.3 g/L accounted for only a modest drain on the quinic acid titer and yield. The final QA:DHQ was 17. The previously unprecedented ability of shikimate dehydrogenase to reduce DHQ to quinic acid had now successfully been employed in the production of quinic acid with only marginal accumulation of DHQ. DHQ is easily purified away from quinic acid and is described elsewhere.[135]

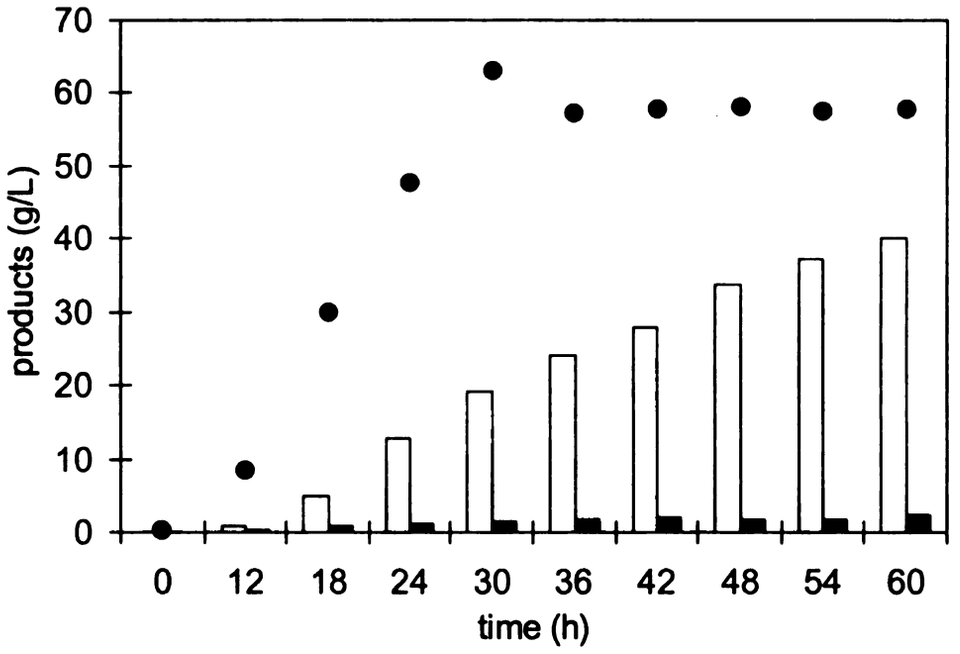

Figure 43. QP1.1/pKD12.112A cultured under standard fed-batch fermentation conditions (10% D.O.). Quinic acid □, DHQ ■, cell mass ●, in g/L.

Transketolase Overexpression and Quinic Acid Biosynthesis.

Given the success of *tktA* overexpression in increasing both shikimic acid titer and yield from glucose by alleviating E4P limitation, attempting to enhance quinic acid titers and yield from glucose by *tktA* overexpression was the next logical step in the quinic acid culturing progression. QP1.1 was transformed with plasmid pKD12.138A and examined under standard glucose-limited fed-batch fermentation conditions. As expected, titer and yield of quinic acid from glucose were enhanced (Figure 44) relative to the absence of *tktA* overexpression. Although preliminary fermentations of QP1.1/pKD12.138A were cultured for 60 h, a precipitous decline in quinic acid productivity was observed subsequent to 48 h. QP1.1/pKD12.138A fermentations were therefore truncated at 48 h.

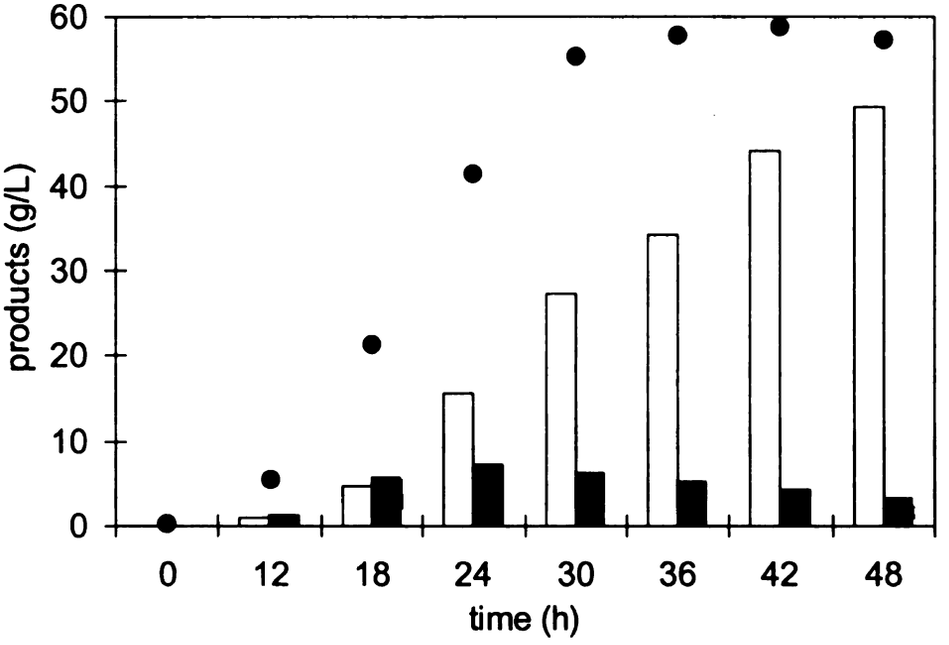

Figure 44. Fed-batch fermentation of QP1.1/pKD12.138A at standard conditions. Quinic acid □, DHQ ■, cell mass ●, in g/L.

QP1.1/pKD12.138A accumulated 49 g/L quinic acid by 48 h, at a yield of 20% from glucose (mol/mol). DHQ accumulation increased from 2.3 g/L at 48 h (Figure 43) to 3.3 g/L (Figure 44), and the final QA:DHQ molar ratio was 15. More important perhaps was the shift in DHQ profile from initially increasing up to 24 h followed by an approximately constant titer for the duration of the fermentation (Figure 43), to increasing for 24 h to a maximum of 7.1 g/L followed by a steady decline to 3.3 g/L at 48 h. The increase in DHQ concentration prompted examination of DAHP synthase and shikimate dehydrogenase enzyme activity levels (Table 21). The DAHP synthase activity profile was similar to that of SP2.1/pKD12.112A (Table 19, entry 1) which was not surprising given that both hosts were derived from the same parent strain. The increase in shikimate dehydrogenase activity relative to SP2.1 constructs was somewhat

unexpected since expression levels of this enzyme were initially similar (12 h), but increased to about threefold that of SP2.1 constructs by 48 h (Table 19, entry 2; Table 21, entry 2). The fortuitously high expression of shikimate dehydrogenase may have accounted for the success of QP1.1/pKD12.138A in converting DHQ to quinic acid and the resultant high titer.

Table 21. DAHP synthase and shikimate dehydrogenase enzyme activities (μmol/min/mg) for QP1.1/pKD12.138A.

		specific activity (μmol/min/mg)			
Entry	Enzyme	12 h	24 h	36 h	48 h
1	DAHP synthase	0.94	0.40	0.22	0.11
2	shikimate dehydrogenase	14	16	22	29

Recycling Pyruvate to PEP.

In the absence of E4P restrictions on DAHP synthase, PEP availability becomes limiting. Recycling of pyruvate to PEP to circumvent in vivo PEP limitations via PEP synthase overexpression was discussed in Chapter 1, and has been successfully exploited in the production of the shikimate pathway intermediates DAHP,[51b,52] DHS,[55a] and shikimic acid.[55b] Increasing the intercellular PEP pool was pursued by plasmid localization of the pps gene (Figure 45). Digestion of pKL1.87B[136] with *EcoR*I and *Hind*III afforded the 3.0-kb *pps* gene, which was subsequently treated with Klenow fragment. Plasmid pKD12.138A was digested with *Nco*I and the resulting 8.9-kb fragment was treated with Klenow fragment. Ligation of the *pps* gene into linearized pKD12.138A afforded pKD15.071B. Transcription of the *pps* gene is in the opposite orientation of the *tktA* gene.

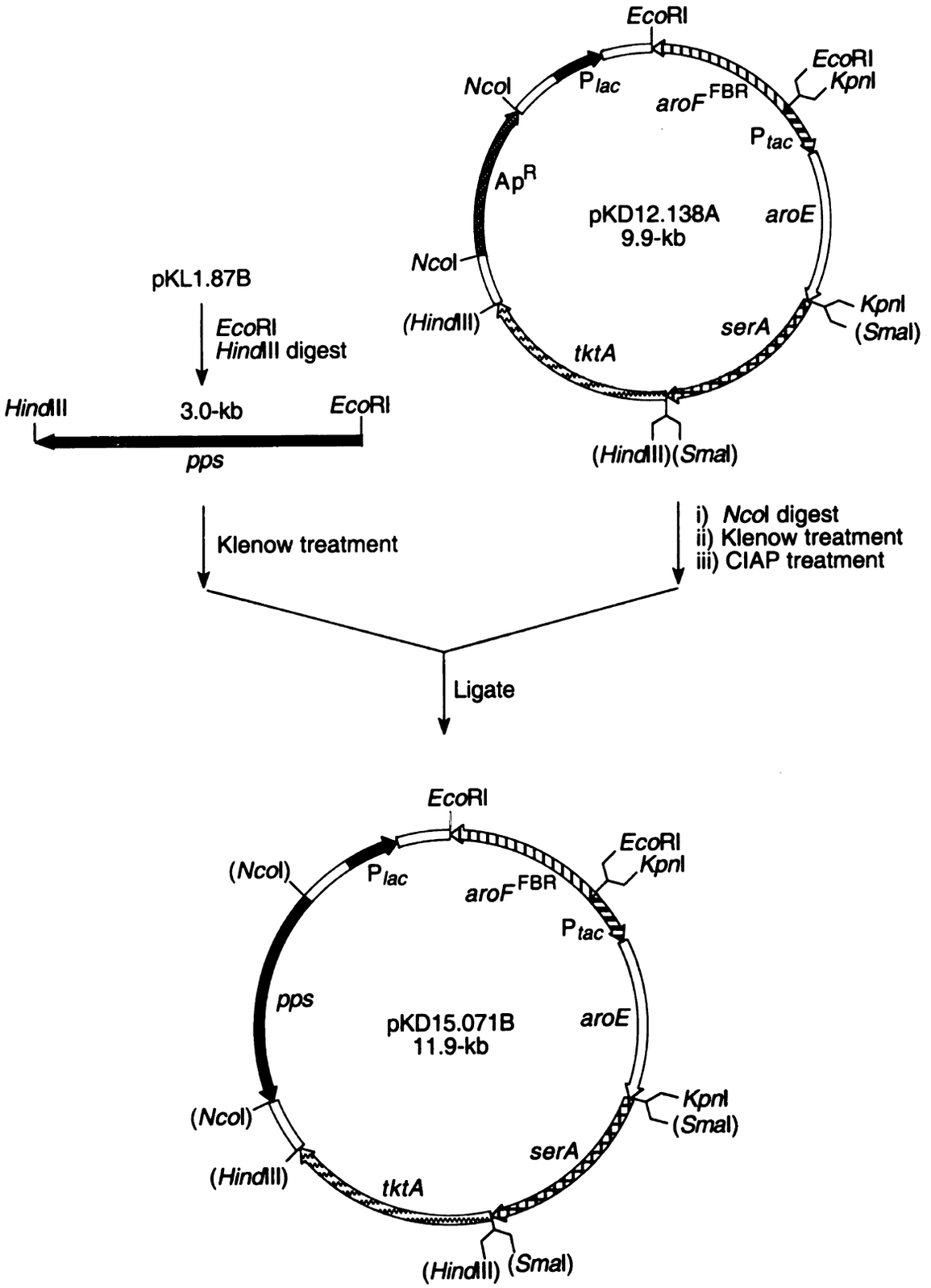

Figure 45. Construction of plasmid pKD15.071B.

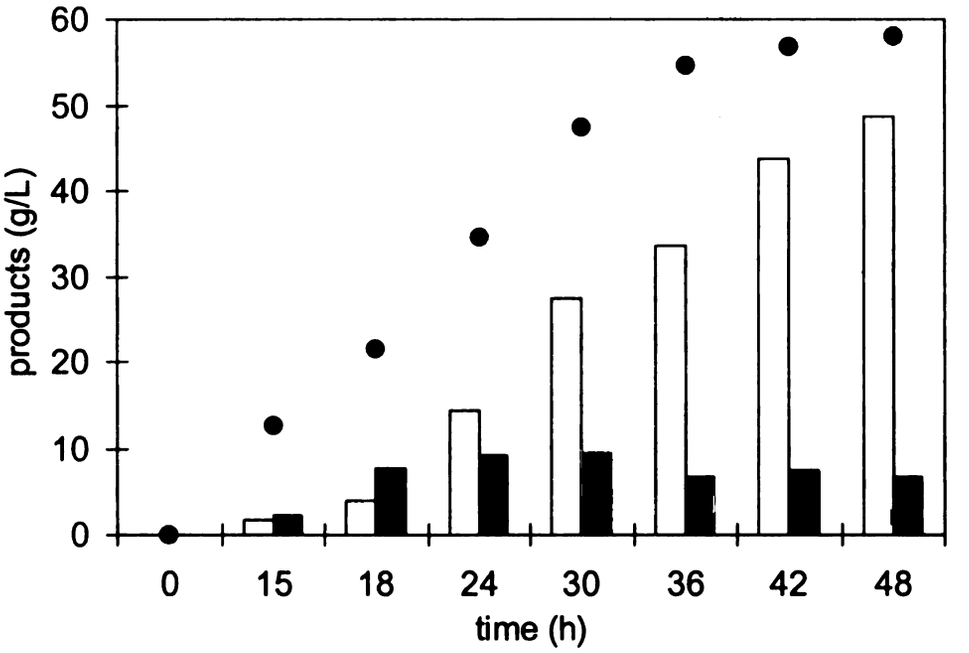

Figure 46. QP1.1/pKD15.071B fed-batch fermentation time course. Quinic acid □, DHQ ■, cell mass ●, in g/L.

QP1.1 was transformed with plasmid pKD15.071B and examined under standard fed-batch fermentation conditions (Figure 46). The resulting 49 g/L quinic acid titer was identical to that observed for QP1.1/pKD12.138A, while the 21% quinic acid yield from glucose (mol/mol) was only a marginal increase relative to QP1.1/pKD12.138A. The 48 h DHQ concentration was 6.7 g/L, resulting in a final QA:DHQ of 7.2. Comparison of the PEP synthase specific activity levels for constructs QP1.1/pKD12.138A and QP1.1/pKD15.071B revealed that *pps* overexpression by simple plasmid-localization in host QP1.1 only achieved about a one to five-fold increase in assayable *pps* activity (Table 22). Unfortunately this was substantially less than prior work utilizing *pps* overexpression by plasmid-localization when *pps* was transcribed from its native promoter.[137] QP1.1/pKD15.071B biomass production appeared to slow relative to

QP1.1/pKD12.138A. Comparing the biomass concentration at 30 h, QP1.1/pKD12.138A (Figure 44) achieved a concentration of 55 g/L while QP1.1/pKD15.071B (Figure 46) accumulated 47 g/L biomass.

Table 22. PEP synthase specific activities (μmol/min/mg) without (QP1.1/pKD12.138A) and with (QP1.1/pKD15.071B) *pps* overexpression.

		specific activity (μmol/min/mg)			
Entry	Construct	12 h	24 h	36 h	48 h
1	QP1.1/pKD12.138A	0.0080	0.0070	0.0066	0.013
2	QP1.1/pKD15.071B	0.018	0.038	0.020	0.014

Quinic Acid Biosynthesis and Unlimited Glucose Availability.

The success of glucose-rich conditions in bolstering carbon funneled into the shikimate pathway during SP1.1/pKD12.138A fed-batch fermentations suggested QP1.1/pKD12.138A might also benefit from application of these conditions. Surprisingly, when QP1.1/pKD12.138A was cultured under glucose-rich conditions, hydroaromatic distribution shifted dramatically. Only 28 g/L of quinic acid was biosynthesized by 48 h while 38 g/L of DHQ accumulated (Figure 47). The maximum DHQ titer of 40 g/L was achieved at 42 h. The final QA:DHQ was 0.74, or about 20-fold lower than QP1.1/pKD12.138A under glucose-limited conditions. Examining the specific enzyme activities for these conditions (Table 23) revealed nothing atypical for DAHP synthase (entry 1), however shikimate dehydrogenase activities (entry 2) declined significantly relative to glucose-limited conditions (Table 21, entry 2). Acetate excretion was again observed to be highly strain dependent, as 2.3 g/L of acetate was accumulated by 48 h. The developed acetate concentration was not observed to inhibit hydroaromatic

formation as substantially enhanced total hydroaromatic (quinic acid + DHQ) concentrations were synthesized relative to glucose-limited conditions.

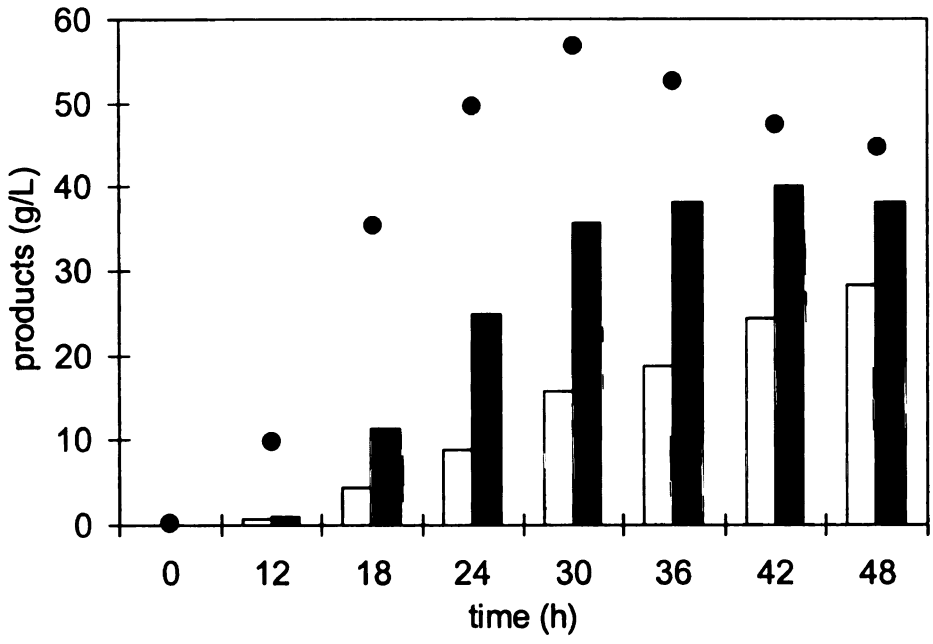

Figure 47. QP1.1/pKD12.138A glucose-rich, fed-batch fermentation time course. Quinic acid □, DHQ ■, cell mass ●, in g/L.

Table 23. DAHP synthase and shikimate dehydrogenase enzyme activities (μmol/min/mg) for QP1.1/pKD12.138A cultured under glucose-rich conditions.

		specific activity (μmol/min/mg)			
Entry	Enzyme	12 h	24 h	36 h	48 h
1	DAHP synthase	0.58	1.7	0.85	0.43
2	shikimate dehydrogenase	9.1	11	12	11

Biomass Considerations.

The nearly 60 g/L of biomass developed by constructs QP1.1/pKD12.112A (Figure 43), QP1.1/pKD12.138A (Figure 44), and QP1.1/pKD15.071B (Figure 46) constituted an enormous carbon sink. The total biomass accumulated in a typical 1 L QP1.1/pKD12.138A fed-batch fermentation was about 85 g, accounting for 3.5 moles of carbon (carbon moles or Cmol), while total quinic acid production (about 74 g) accounted for only about 2.7 Cmol using a conversion factor of 24.6 g/Cmol biomass for *E. coli*.[138] By comparison, the best shikimic acid producing construct and conditions (SP1.1/pKD12.138A, glucose-rich, Figure 38) yielded less than 1.2 Cmol biomass while biosynthesizing in excess of 3.4 Cmol of shikimic acid. Glucose-limited fed-batch fermentation of SP1.1/pKD12.138A (Figure 37) still resulted in less than 1.2 Cmol biomass, while more than 1.7 Cmol of shikimic acid was produced.

Why were QP1.1 constructs able to divert so much carbon to biomass accumulation? Inspection of culture supernatant ^{1}H NMR spectra used to quantify quinic acid and DHQ accumulation revealed significant L-phenylalanine (δ 7.4, m, 5 H) and L-tyrosine (δ 7.2, d, 2 H; δ 6.9, d, 2 H) accumulation. Aromatic amino acid biosynthesis was inconsistent with the notion that QP1.1 was an *aroD* auxotroph, and suggested that catalytically active DHQ dehydratase activity must be present in the host. Attempts to grow QP1.1 constructs without aromatic amino acid and vitamin supplementation were unsuccessful despite the accumulation of terminal pathway products. Therefore, biomass titration appeared a reasonable approach for controlling the flux of carbon to biocatalyst formation.

Biomass titration required the tunable expression of *aroD*. Modulation of *aroD* was accomplished by construction of plasmid pKD14.186A. Construction of pKD14.186A began with digestion of plasmid pD2625 with *EcoR*V and *Dra*I followed by treatment with Klenow fragment to liberate the blunt 1.9-kb *serA* fragment. The *serA* fragment was ligated with plasmid pKD14.140B, which had been linearized by digestion with *Sma*I, to afford the 8.5-kb plasmid (Figure 48). The new plasmid bore a copy of *aroD* preceded by the P_{lac} promoter, and regulated by the $lacI^q$ repressor gene.

QP1.1/pKD14.186A fed-batch fermentations were problematic insomuch as the P_{tac} promoter responsible for plasmid-encoded *aroE* transcription was simultaneously regulated by the $lacI^q$ gene product. IPTG addition for attenuation of *aroD* expression necessarily modulated *aroE* expression. Furthermore, even when a very high IPTG concentration (1.0 mM) was present from the time of inoculation, assayable *aroE* activities were diminished (Table 24, entry 2) relative to plasmid pKD12.138A (Table 21, entry 2). Modest quinic acid (3.4 g/L) and DHQ (3.8 g/L) concentrations were synthesized. Moreover, *aroD* activity was unmeasurable despite a large biomass accumulation (almost 50 g/L), and further pursuit of QP1.1/pKD14.186A was suspended.

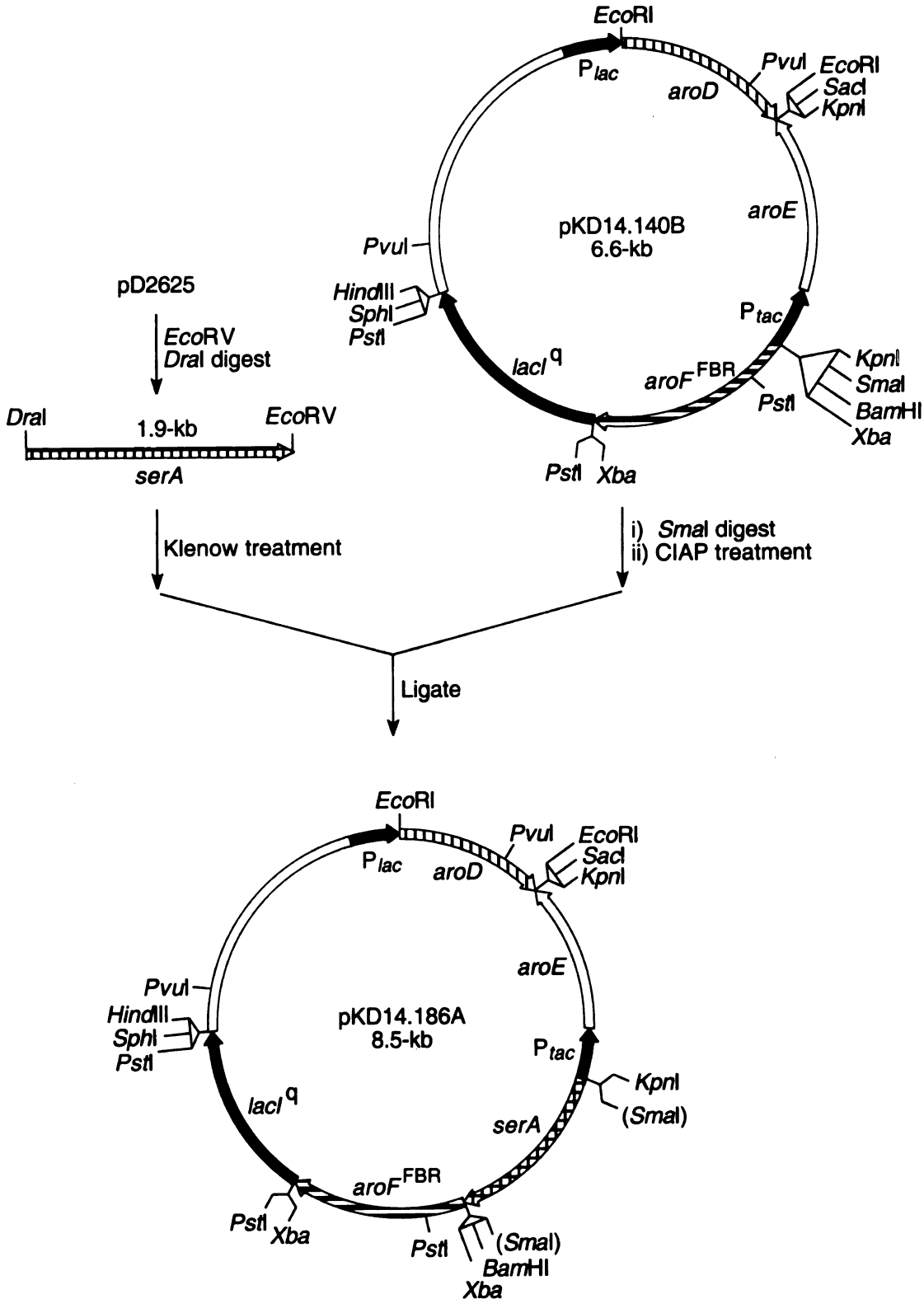

Figure 48. Construction of plasmid pKD14.186A.

Table 24. DAHP synthase and shikimate dehydrogenase enzyme activities (μmol/min/mg) for QP1.1/pKD14.186A induced with 1.0 mM IPTG.

		specific activity (μmol/min/mg)			
Entry	Enzyme	12 h	24 h	36 h	48 h
1	DAHP synthase	1.7	0.67	0.32	0.19
2	shikimate dehydrogenase	0.14	0.14	0.17	0.23

The inability of QP1.1/pKD12.138A to grow in the absence of aromatic amino acid and vitamin supplementation was perplexing given that L-tyrosine and L-phenylalanine accumulated, and the significant carbon siphoned to biomass. If the current plasmid system was ineffective for biomass titration, could a more cost-effective supplement than aromatic amino acids be exploited? The known capacity for shikimic acid transport by *E. coli* suggested shikimic acid could be employed as a growth supplement. The fermentation processes elaborated in Chapter 2 alleviated shikimic acid supply and expense concerns, making it an attractive alternative to aromatic amino acid usage.

QP1.1/pKD12.138A was initially supplemented with sterile, unpurified shikimic acid fermentation supernatant, but fermentations supplemented in this fashion failed to grow. QP1.1/pKD12.138A fed-batch fermentations supplemented with purified shikimic acid[39,135,139] met with increased success. Substitution of shikimic acid for aromatic amino acid supplementation appeared to slow the biocatalyst growth considerably, permitting a biomass concentration of only 46 g/L by 30 h (Figure 49). By comparison, QP1.1/pKD12.138A supplemented with aromatic amino acids and vitamins typically achieved 55 g/L of biomass by 30 h. The quinic acid titer time course lagged behind that

previously observed for QP1.1/pKD12.138A as well, with only 41 g/L quinic acid being accumulated by 48 h, in 18% yield from glucose (mol/mol).

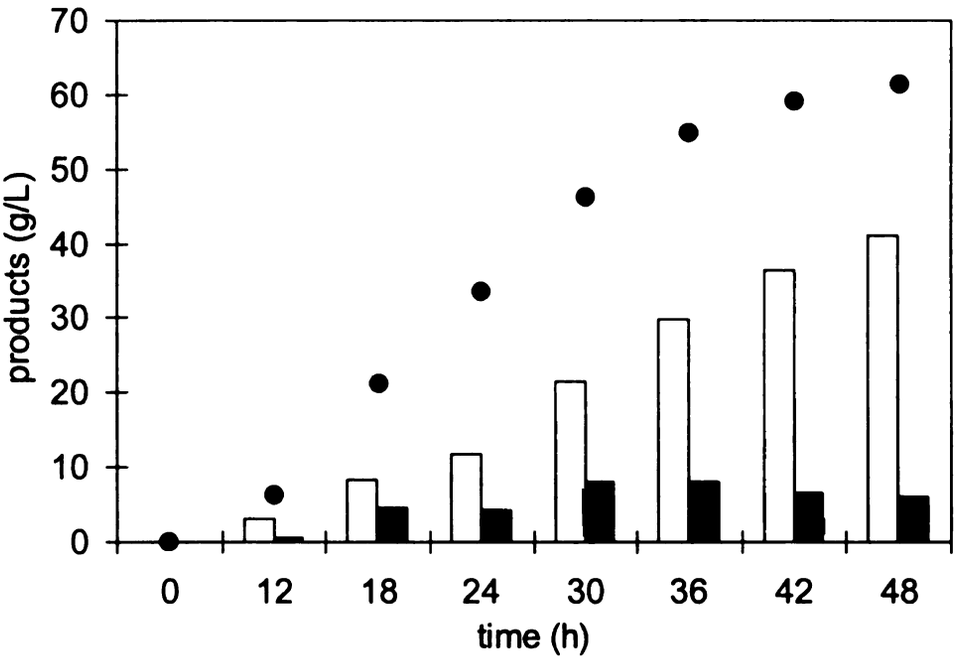

Figure 49. Purified, shikimic acid-supplemented QP1.1/pKD12.138A fed-batch fermentation time course. Quinic acid□, DHQ■, cell mass●, in g/L.

The use of partially purified shikimic acid fermentation supernatant was also examined as a QP1.1/pKD12.138A supplement (Figure 50). Deproteinized, refluxed shikimic acid fermentation supernatant[135] was incubated for 1 h with 20 g/L Darco KB-B 100 to remove PCA. The resulting partially purified supernatant was used directly as a supplement for QP1.1/pKD12.138A fed-batch fermentations after sterile filtering. Supplementing in this fashion resulted in a marked increase (relative to aromatic amino acid supplementation) in lag phase between inoculation and the onset of PID-controlled impeller ramping for D.O. level maintenance from about 1/2 h to about 6 h. Less than 36 g/L of biomass accumulated by 30 h, a substantial decrease relative to

QP1.1/pKD12.138A supplemented with purified shikimic acid (46 g/L) or with aromatic amino acids and vitamins (55 g/L) in the same time frame. Somewhat surprisingly, the final quinic acid titer of 45 g/L and yield of 23% from glucose (mol/mol) both improved relative to when purified shikimic acid was the supplement, and were similar to the values obtained for aromatic amino acid supplemented QP1.1/pKD12.138A fermentations despite the decrease in biomass titer.

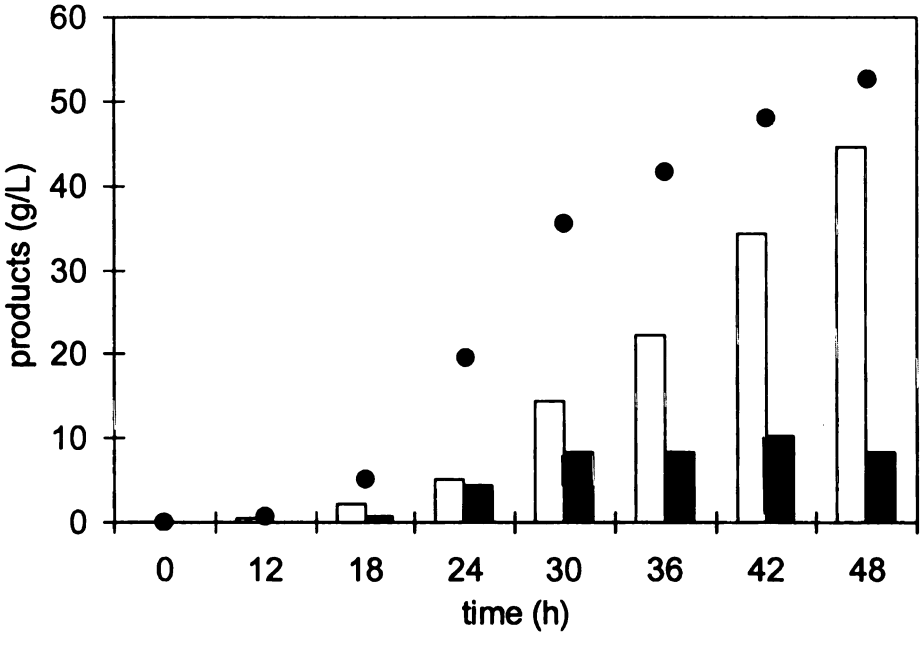

Figure 50. Partially-purified, shikimic acid-supplemented QP1.1/pKD12.138A fed-batch fermentation time course. Quinic acid□, DHQ■, cell mass●, in g/L.

Discussion

Glucose-Limited, Microbial Quinic Acid Biosynthesis.

The success of microbial quinic acid biosynthesis by QP1.1/pKD12.112A (Figure 42, Figure 43) and QP1.1/pKD12.138A (Figure 44) was not necessarily surprising given the significant quinic acid byproduct concentration accumulated during fed-batch cultivation of SP1.1 constructs in the absence of a catabolite repression methodology. Nonetheless, successful homologous quinic acid biosynthesis was not assured since shikimate dehydrogenase was employed in a bioconversion absent of its native substrate. In the previously reported microbe-catalyzed synthesis of quinic acid from glucose, DHQ was reduced to quinic acid in *E. coli* AB2848/pKD136/pTW8090A by heterologous expression of *qad*-encoded quinate dehydrogenase isolated from *K. pneumoniae*.[103] *E. coli* QP1.1/pKD12.112 and QP1.1/pKD12.138 utilized *aroE*-encoded shikimate dehydrogenase isolated from *E. coli*. Promoter compatibility and codon usage were completely avoided as factors requiring consideration in route to achieving adequate overexpression of the enzyme that reduced DHQ to quinic acid consequently. *E. coli* AB2848/pKD136/pTW8090A was cultured under shake flask conditions and stable plasmid maintenance required the presence of antibiotics in its culture medium. Fed-batch fermentor cultivation of quinate-synthesizing constructs *E. coli* QP1.1/pKD12.112 and QP1.1/pKD12.138 relied on nutritional pressure as opposed to resistance to antibiotics for plasmid maintenance. While the previously reported *E. coli* AB2848/pKD136/pTW8090A synthesized only 4.8 g/L of quinic acid,[103] *E. coli* QP1.1/pKD12.138 synthesized 49 g/L of quinic acid. The conversion of glucose (80 mM) into quinic acid (20 mM) catalyzed by *E. coli* AB2848/pKD136/pTW8090A

suggests an apparent yield for synthesis of quinic acid from glucose that is higher than the 20% yield achieved using *E. coli* QP1.1/pKD12.138. However, this comparison is not meaningful since *E. coli* AB2848/pKD136/pTW8090A was first cultured in rich medium, harvested, and then resuspended in minimal salts medium where synthesis of quinic acid transpired. The yield of quinic acid synthesized by *E. coli* QP1.1/pKD12.112 (15%) and QP1.1/pKD12.138 (20%) reflects both the amount of glucose consumed to form biomass as well as the amount of glucose consumed to synthesize quinic acid. Nonetheless, significant improvement in the yield of quinic acid microbially synthesized from glucose remains to be achieved. The theoretical maximum yield for synthesis of quinic acid from glucose with *E. coli* is 43% (mol/mol), per Chapter 2.

Pps-Mediated Pyruvate Recycling.

The lack of significant *pps* overexpression by QP1.1/pKD15.071A was not surprising since gene expression levels can be highly strain dependent. Indeed, subsequent evaluation of *pps* overexpression in shikimic acid and DHS producing constructs in the Frost lab has afforded significant gains in titers and yields from glucose relative to titers and yields achieved in the absence of pyruvate recycling.[55b,137] The impact of *pps*-encoded PEP synthase on shikimic acid and DHS titers and yields has not been realized in the absence of glucose-rich conditions, however.[55b,137] The standard glucose-limited fed-batch fermentation conditions may not constrain intracellular PEP availability to a level that impedes its use as substrate by DAHP synthase, thereby preventing the impact of PEP synthase overexpression from being realized under the glucose uptake rates currently achieved. Titration of *pps* specific activity has also been

investigated, and has resulted in amplified carbon flux into the shikimate pathway during quinic acid biosynthesis under glucose-rich conditions.[140]

Glucose-Dependent Metabolite Mixture.

Glucose-rich culturing of QP1.1/pKD12.138A resulted in a significant enhancement in carbon channeled into the shikimate pathway. *E. coli* QP1.1/pKD12.138A accumulated 51 g/L total hydroaromatics by 30 h under glucose-rich fermentation conditions (Figure 47), while glucose-limited conditions resulted in only 33 g/L of total pathway metabolites (Figure 44) in the same time frame. Unfortunately the product distribution was skewed toward DHQ. The 20-fold shift in QA:DHQ from glucose-limited conditions (15:1) to glucose-rich conditions (0.74:1) by 48 h was puzzling. The deleterious influence of glucose-rich culturing conditions on shikimate dehydrogenase expression relative to glucose-limited conditions may have resulted in insufficient enzymatic activity for conversion of DHQ to quinic acid. Enhanced carbon flux through the shikimate pathway as a result of glucose-rich conditions would further exacerbate this problem, potentially saturating the enzyme. The slight decrease in DHQ concentration between 42 h and 48 h was consistent with previous fermentation data where DHQ was accumulated to high titers, and most likely reflected the antioxidant characteristics of DHQ.[25]

An intriguing idea also stemming from possible rate-limiting conversion of DHQ to quinic acid by shikimate dehydrogenase is the notion of cofactor availability. The concomitant conversion of NADPH to NADP during the *aroE*-mediated reduction of DHQ to quinic acid would not typically be considered a determining factor of in vivo

enzyme activity. However, the excessive biomass formation associated with QP1.1 constructs may tax the intracellular NADPH pool at a rate greater than that of its replenishment during peak biomass and hydroaromatic biosynthesis. NADPH is considered a significant component of fueling reactions that provide for biomass assembly through protein production.[141] As such, the biosynthetic commitment to biomass assembly would divert NADPH prior to its availability for the non-essential production of quinic acid, and might render NADPH availability a limiting factor in the reduction of DHQ to quinic acid. However, this notion might be more applicable to the observation of initially increasing DHQ titers until 24 h followed by a subsequently declining DHQ profile in QP1.1/pKD12.138A glucose-limited fed-batch fermentations (Figure 44). Limited NADPH availability resulting from biomass production up to 24 h would preclude complete conversion of intracellular DHQ to quinic acid. The relaxed biosynthetic requirement of NADPH for biomass assembly subsequent to 24 h would alleviate NADPH limitations on shikimate dehydrogenase-mediated reduction of DHQ to quinic acid, thereby preventing further DHQ accumulation. The decline in measured DHQ titer might therefore result from oxidative degradation or microbial DHQ transport.

A second, equally plausible explanation for the considerable DHQ titer synthesized by QP1.1/pKD12.138A under a glucose-rich environment was catabolite repression of DHQ transport. The observation of declining DHQ titer during glucose-limited conditions raised the possibility that some portion of the quinic acid synthesized by *E. coli* QP1.1/pKD12.138A was derived via transport back into the cytoplasm and subsequent reduction of DHQ that had been initially synthesized and exported into the culture supernatant. Such a mechanism would be reminiscent of shikimic acid transport

and subsequent conversion to quinic acid discussed in Chapter 2. Glucose-rich culturing conditions of SP1.1/pKD12.138A in Chapter 2 resulted in a drastic reduction in quinic acid biosynthesis. Modest quinic acid titers were still accumulated even in the absence of microbial shikimic acid transport however. The continued accumulation of quinic acid suggested in vivo microbial reduction of DHQ to quinic acid was transpiring, albeit at a rate eclipsed by DHS reduction to shikimic acid by greater than an order of magnitude (as suggested by the respective K_m's in Chapter 2). Despite the apparent glucose-induced reduction in measured shikimate dehydrogenase activity, substantial activity was still developed. The enzyme activity may have been adequate to convert substrate DHQ to quinic acid in the absence of possible glucose-repressed DHQ transport. Viewing the cellular membrane as permeable with respect to DHQ, microbially transported DHQ would provide multiple opportunities for shikimate dehydrogenase to catalyze the reduction of DHQ to quinic acid, essentially circumventing the enzyme's low affinity (K_m=1.2 mM) for substrate DHQ. Cessation of DHQ transport would constrain the capability of shikimate dehydrogenase to catalyze the reduction of intracellular DHQ to quinic acid. However if ample enzymatic activity was present, significant quinic acid would still be expected to accumulate, albeit at a reduced concentration relative to when DHQ transport was active. Competition between DHQ export and reduction to quinic acid would then dictate the final QA:DHQ, and appears a likely explanation of the 28 g/L of quinic acid accumulated during glucose-rich cultivation of QP1.1/pKD12.138A (Figure 47). Independent examination of the effects of shikimate dehydrogenase enzymatic activity and DHQ transport on DHQ-quinic acid equilibrium may ultimately

be required to further delineate the source of enhanced DHQ biosynthesis during glucose-rich fed-batch fermentor cultivation of QP1.1/pKD12.138A.

Biomass Considerations and Shikimic Acid Supplementation.

The ability of QP1.1 constructs to develop biomass concentrations in excess of 60 g/L presents significant process engineering challenges in the form of oxygen transfer and heat removal consideration upon scale up. Furthermore, the disposal of spent biomass can pose significant regulatory and monetary constraints on an industrial process. The yield of quinic acid typically achieved by QP1.1/pKD12.138A under glucose-limited fed-batch fermentation conditions (20%) constitutes less than half that of the theoretical maximum yield (43%). Biomass becomes a carbon sink, channeling significant carbon that might otherwise be funneled into the shikimate pathway for quinic acid biosynthesis and limits realizable hydroaromatic titers and yields.

The sluggish microbial growth observed when shikimic acid was utilized as a growth supplement for QP1.1/pKD12.138A may have resulted from rate-limiting transport of shikimic acid, rate-limiting conversion of shikimic acid to distal metabolites, inhibitory molecules (in partially purified or unpurified supernatant supplementation) or inhibitory proteins (in unpurified supernatant supplementation). For example, the inhibitory affects of PCA on log phase microbes has previously been reported,[25] and could account for the significant lag phase encountered when partially purified shikimic acid supernatant was employed as a growth supplement. PCA formation is a consequence of shikimic acid fermentation broth purification in which subsequent dehydrations under reflux conditions convert DHQ to DHS, and DHS to PCA.[135]

Incomplete removal of PCA during activated carbon treatment of supernatant during purification might lead to a substantial inhibitory affect upon log phase QP1.1/pKD12.138A, resulting in the observed increase in lag phase.

Failure of QP1.1/pKD12.138A to grow when supplemented with unpurified shikimic acid supernatant could be a result of an excreted signaling metabolite or protein that triggers a starvation response, prompting the onset of stationary phase. One such proposed metabolite is homoserine lactone.[142] Despite the lack of literature precedent for excretion of homoserine lactone and intercellular signaling, intracellular induction of the σ^S regulon by homoserine lactone has been demonstrated.[143] The σ^S regulon is one of many genetic elements responsible for the onset of stationary phase in *E. coli*.[142] The presence of homoserine lactone or another stationary phase-inducing compound in crude shikimic acid supernatant is possible given cell lysis could release non-excreted, inhibitory metabolites or proteins that could then prevent growth when the supernatant was employed as a growth supplement.

Slowed growth of QP1.1/pKD12.138A utilizing shikimic acid as a supplement relative to aromatic amino acid supplementation could result from transport affinity differences between the supplements. The K_m values for proteins associated with general (0.4 μM) and specific transport (2 μM) of L-phenylalanine, L-tyrosine, and L-tryptophan reveal a high affinity for their substrates.[144] The kinetics of shikimic acid transport have yet to be established, however it is unlikely that *E. coli* would have such a strong affinity for shikimic acid given its inability to be utilized as a sole carbon source.

The failure of QP1.1/pKD14.186A to accumulate DHQ or quinic acid in substantial concentrations suggested the IPTG addition should be lowered.

Unfortunately, even a 1.0 mM IPTG addition resulted in diminished shikimate dehydrogenase activities in the presence of the *lacI*^{q} repressor gene product. The maximum induction of *aroD* allowed almost all the carbon channeled into the shikimate pathway to proceed to biomass through aromatic amino acid formation despite the lack of assayable *aroD* activity. Independent modulation of enzymatic activities may ultimately provide for titratable biomass in QP1.1, and is a potential area for further investigation.

Conversion of Quinic Acid to Hydroquinone.

Reaction methodology previously employed for the chemical conversion of quinic acid to hydroquinone (Figure 41) required stoichiometric amounts of MnO_2.[103] In addition to the toxic intermediate generation inherent to the process, byproduct salt stream generation results from stoichiometric reaction of quinic acid with MnO_2. The same problem is associated with the commercial route to hydroquinone where stoichiometric amounts of MnO_2 are used to oxidize aniline (Figure 41).[133] The improvements elaborated in biocatalytic conversion of glucose to quinic acid in this dissertation have permitted the improvement of companion chemical methodology for conversion of quinic acid into hydroquinone.[131] High-yielding conversion of quinic acid to hydroquinone utilizing hypochlorite under mild conditions (87%) and chlorine-free conditions where either $(NH_4)_2Ce(SO_4)_3$ (91%) or V_2O_5 (85%) is the oxidant have been recently been elaborated in literature.[131]

Exposure to benzene, which has been linked to both acute myeloid leukemia and non-Hodgkin's lymphoma,[145] continues to create challenges to the chemical industry. With annual production of benzene in the U.S. at approximately $8x10^9$ kg,[146] high costs

have been cited by the U.S. chemical industry to be a major impediment to reducing exposure limits for benzene.[147] Ultimately, the most effective way of dealing with benzene's human health risk may be to circumvent its use. Such a solution, although conceptually simple, requires the elaboration of fundamentally new syntheses for aromatic chemicals and products derived from aromatics. The synthesis of hydroquinone via chemical oxidation of microbe-synthesized quinic acid can be viewed as being part of this process. The microbially-based conversion of glucose to quinic acid facilitates the development of one such process, may be industrially viable with continued improvement, and moves the synthesis of hydroquinone from glucose from a proof-of-concept conversion to a route with prospects for supplanting currently employed syntheses of hydroquinone where benzene serves as the starting material.

CHAPTER 4

Physiological State Variable/Knowledge-Based Monitoring and Control of Fed-Batch Quinic Acid Fermentations

Introduction.

The DHQ profile of QP1.1/pKD12.138A glucose-limited fed-batch fermentations (Figure 44) observed in Chapter 3 left several unanswered questions. Was the increasing DHQ concentration prior to 24 h due to biomass-induced intracellular NADPH limitations, insufficient shikimate dehydrogenase activity to facilitate conversion of substrate DHQ to product quinic acid, or some other phenomenon? Was the decreasing DHQ concentration subsequent to 24 h an artifact of DHQ degradation, microbial transport of synthesized DHQ and conversion to quinic acid, or an unknown mechanism? Furthermore, was the large DHQ accumulation of QP1.1/pKD12.138A under glucose-rich culturing conditions (Figure 47) a result of depressed shikimate dehydrogenase activity, glucose-induced catabolic repression of microbial DHQ transport, or a third, undisclosed mechanistic possibility? In addressing these questions, the adaptability of the control methodologies previously presented must be challenged, as standard glucose-limited and glucose-rich fed-batch fermentation conditions were inadequate to fully resolve these questions.

Physiological State (PS) variable and KB control have been employed to enhance L-phenylalanine titers, yields, and volumetric productivity during fed-batch fermentation

of recombinant *E. coli*.[112a,b,148] The use of PS variable monitoring and control in fermentations[148,149] dictates a requisite level of intelligent (e.g., KB) control, and leads to the manipulation of non-environmental variables during culturing. Traditional fed-batch fermentation control methodologies employ PID control of such environmental factors as pH, temperature, OTR, and glucose feed rate (GFR). While the optimal control of these variables may be key to successful culturing, the impact of these variables in relation to the culture physiology is necessarily ignored.

The fundamental drawback of many traditional bioprocess control methodologies is their emphasis on the cell environment, in lieu of the actual cell state.[148] The concept of PS control was first proposed by Konstantinov and Yoshida over a decade ago, and mandates both the explicit estimation of the current culture state and the drive of this state toward maximum efficiency by an intelligent control scheme.[148] To this end, the acquisition of PS information and PS variable calculation is critical to a successful control system. PS variables, in contrast to environmental variables, quantify a particular metabolic property of a culture. For example, the specific oxygen uptake rate (SOUR) of a culture can be calculated online by normalizing the oxygen uptake rate (OUR) by the total cell population (Equation 16). In a D.O. stat,[112c] where the pseudo-steady-state assumption of balanced OUR and OTR can be invoked, the SOUR can be calculated if an oxygen balance around the bioreactor is performed to obtain the volumetric OTR (g $O_2 \cdot L^{-1} \cdot h^{-1}$), and online information regarding volume (V) and biomass concentration (X) is available.

Equation 16. $$SOUR = \frac{OUR}{X} = \frac{OTR}{X}$$

One common control dilemma that can be corrected by utilizing PS variables is misinterpreted D.O. concentration data. If the D.O. concentration is utilized for control of the GFR with a set OTR, the OTR can exceed the oxygen requirement of the culture as the metabolic vigor of the cell population declines.[112b] The D.O. concentration would increase in the absence of attenuated OTR, and a standard PID control loop which manipulates GFR in response to D.O. concentration would therefore increase the GFR when it should actually be decreased. In the same scenario, monitoring and control of a PS variable such as SOUR through OTR, coupled with standard PID control loop maintenance of D.O. concentration via GFR, would alleviate the control problem. The SOUR would necessarily need to be controlled relative to experience, in conjunction with a KB control system for intelligent manipulation of the SOUR set point should it become inappropriate for the current PS of the culture.

Could KB and PS variable control methodologies be employed to facilitate quinic acid production enhancement in the absence of amplified carbon flux to DHQ? In this chapter, the details of an integrated KB, PS variable, and pseudo-online stoichiometric model (SM) monitoring and control system are elaborated, with the resulting affects upon quinic acid biosynthesis and product ratios discussed. All fermentations reported in this chapter employed the quinic acid biosynthesizing construct QP1.1/pKD12.138A reported in Chapter 3.

ANN model.

A custom ANN prediction program was encoded by Mr. Kun Xu in C++ for the pseudo-online prediction of biomass, quinic acid, and DHQ concentrations (Appendix

A). The ANN prediction program was modified by the author as required, including the addition of online acetate prediction capability. The topology (node configuration) of all neural networks within the program was 2-5-1, corresponding to two nodes in the input layer, one hidden layer with five nodes, and one node (prediction) in the output layer (Figure 51). The network was feedforward in nature, meaning no output from any node looped back to the same node or to nodes contained in prior layers.

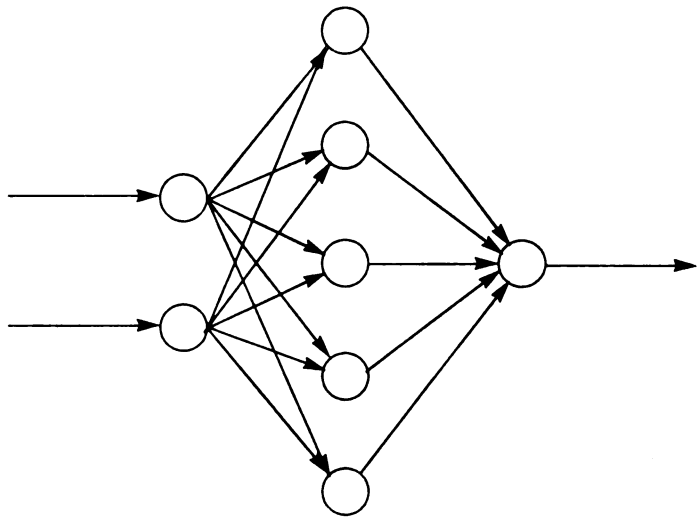

Figure 51. Feedforward, three-layer ANN configuration with two inputs and one output.

Inputs to the ANN consisted of biomass concentration (OD_{600nm}) and either reactor offgas CO_2% or GFR. Initiation of the GFR was noisy both initially and for the first couple hours of its operation in both standard and KB-controlled fed-batch fermentations typically. Therefore, CO_2% was used as one of the inputs to the ANN before the GFR noise dampened to an acceptable level, at which time the GFR replaced CO_2% as an input to the ANN. The man-machine interface (MMI) of the pseudo-online prediction program contained a manual toggle for switching between the inputs. The

ANN topologies were assembled to produce a feedback structure as shown in Figure 52, where the previous biomass concentration prediction (t_{i-1}) served as an input for predicting the current biomass concentration (t_i). The MMI of all OptoControl strategies (see below) contained an icon for reinitializing the ANN biomass concentration prediction should large deviations (e.g., > 5%) between predicted and actual biomass concentrations arise during fermentations. The ability to recalibrate the ANN "on the fly" was useful in maintaining accurate pseudo-online biomass predictions and in executing subsequent control actions based on biomass concentration values. The model was trained using a backpropagation method.[79a] The ANN prediction interval for all fermentations was 0.25 h.

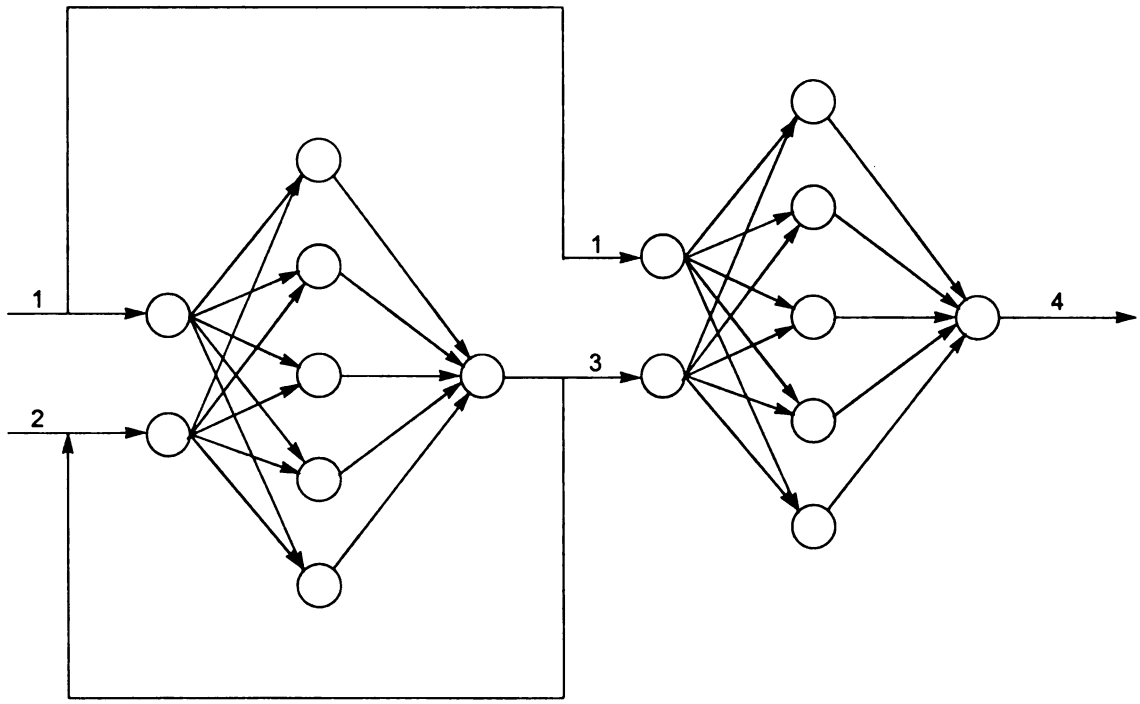

Figure 52. Feedforward neural network topology with feedback structure. Inputs and outputs were 1) $CO_2\%(t_i)$ or $GFR(t_i)$; 2) $OD_{600nm}(t_{i-1})$; 3) $OD_{600nm}(t_i)$; 4) quinic acid (g/L), DHQ (g/L), or acetate (g/L).

Stoichiometric Model Development.

An overspecified SM[84a,c,d,q,h] was developed using the known molar stoichiometries of the pentose phosphate, glycolysis, tricarboxylic acid (TCA) cycle, and aromatic amino acid biosynthesis biochemical pathway reactions of *E. coli* (Figure 53 and Appendix B). Reactor balances were calculated in the OptoControl strategies as part of the KB control system and are discussed below. ANN-derived inputs to the SM included molar consumption/production of quinic acid, DHQ, and biomass determined from pseudo-online ANN metabolite concentration predictions and a reactor volume balance. Moles of metabolites generated or consumed were calculated as the difference of the current concentration prediction (t_i) and previous concentration prediction (t_{i-1}). The molar GFR to the reactor was calculated from the online GFR signal. The carbon dioxide evolution rate (CER) from the reactor in moles was calculated from offgas analysis utilizing a CO_2 mass balance discussed below. The SM was encoded in C++ and assimilated into the existing ANN/DDE C++ program. As such, the SM calculated biochemical pathway fluxes each time the ANN predictions were executed (e.g., in 0.25 h intervals) based on the molar generation or consumption of metabolites. The SM accepted glucose, CO_2, DHQ, quinic acid, and biomass fluxes as inputs.

Several assumptions were made in formulating the SM. First, the pseudo-steady-state assumption was invoked for all non-excreted metabolites.[84h,q] This assumption is predicated on the low intracellular accumulation of metabolites relative to the carbon flux through the pathways that form them. The formation of pentose phosphate pathway intermediates from D-fructose-6-phosphate (F6P) and D-glyceraldehyde-3-phosphate (GAP) was assumed to predominate rather than D-glucose-6-phosphate (G6P) conversion

to D-ribulose-5-phosphate (Ru5P) due to the plasmid-localized *tktA* overexpression of transketolase (J4, Figure 53) in the quinic acid producing construct QP1.1/pKD12.138A. Therefore negligible carbon flux was assumed to proceed from G6P to Ru5P. The glyoxylate shunt was assumed inactive due to glucose utilization as the carbon source, which precludes expression of glyoxylate shunt enzymes.[150] NADH and NADPH were considered equivalent in the model due to their interconversion by transhydrogenases. The P/O ratio was assumed to be 2.0.[84h] Unbranched fluxes were simplified into single fluxes, as is customary with SM.[84]

The coefficient matrix **A** (Appendix B) encompassed the stoichiometries of the pathway reactions, including the reactions for biomass assembly for *E. coli*.[84h,141] A fundamental indicator of the coefficient matrix stability is the condition number. The condition number of a matrix is a measure of the intrinsic difficulty in solving the linear system. The coefficient matrix condition number was 73, suggesting the system was "well posed" (e.g., condition number less than 100).[84q]

The overspecified nature of the SM dictated the formulation of a non-square coefficient matrix. The linear system **Ax=b** was solved per Equation 5, which is reproduced in Equation 17 for the reader's convenience. The static calculation of the generalized inverse, or pseudo-inverse, of the coefficient matrix ($\mathbf{A}^{+}$) was performed offline to circumvent unnecessary computational requirements (Equation 18). The dynamic portion (Equation 19) of the linear system was solved online each time the ANN executed concentration predictions.

Equation 17. $\mathbf{x} = \left(\mathbf{A}^{T}\mathbf{A}\right)^{-1}\mathbf{A}^{T}\mathbf{b}$

Equation 18. $\mathbf{A}^{+} = \left(\mathbf{A}^{T}\mathbf{A}\right)^{-1}\mathbf{A}^{T}$

Equation 19. $\mathbf{x} = \mathbf{A}^{+}\mathbf{b}$

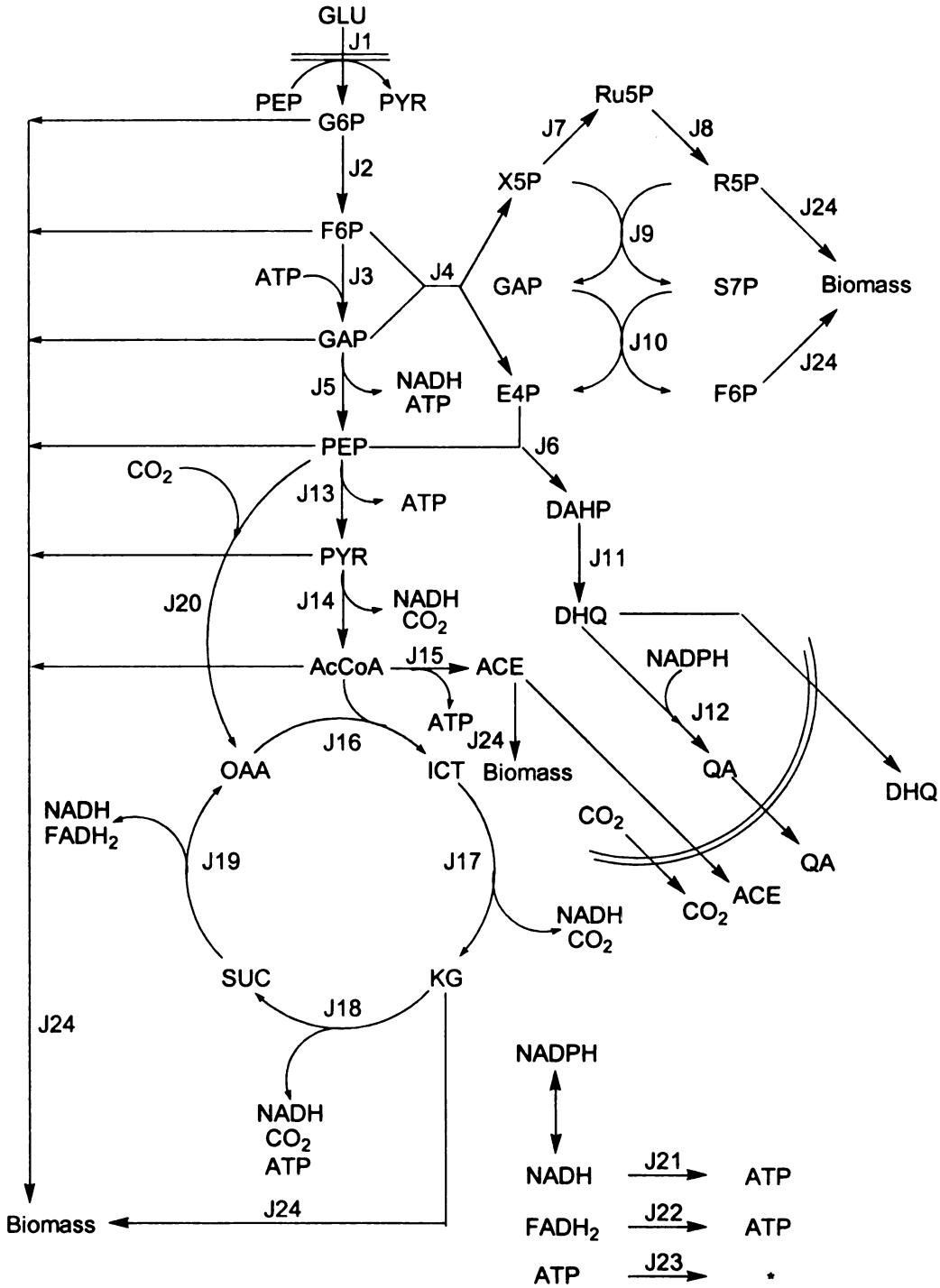

Figure 53. The simplified reaction network encompassed by the SM.

KB Control System Development: General Information.

The Opto22 Factory Floor® software encompasses several programs, three of which were utilized in the development of the KB control and MMI system described here. OptoControl is the program responsible for the actual control methodology development and implementation, and control schemes constructed utilizing this program are referred to as strategies. OptoDisplay was the program responsible for MMI development and implementation. OptoServer was the program responsible for inter-program communication. Dynamic Data Exchange (DDE) was used to interface the ANN model to the KB control strategy. DDE is a message protocol embedded in the Windows operating system environment that is used for inter-process communication. In DDE, the client is the process that requests data and/or executes commands. The server is the process that responds to a request. A C++ program was utilized for DDE between the OptoControl (client) program and the OptoServer (server). The OptoServer program ferried data between the C++ encoded ANN model and the OptoControl strategies (Figure 54).

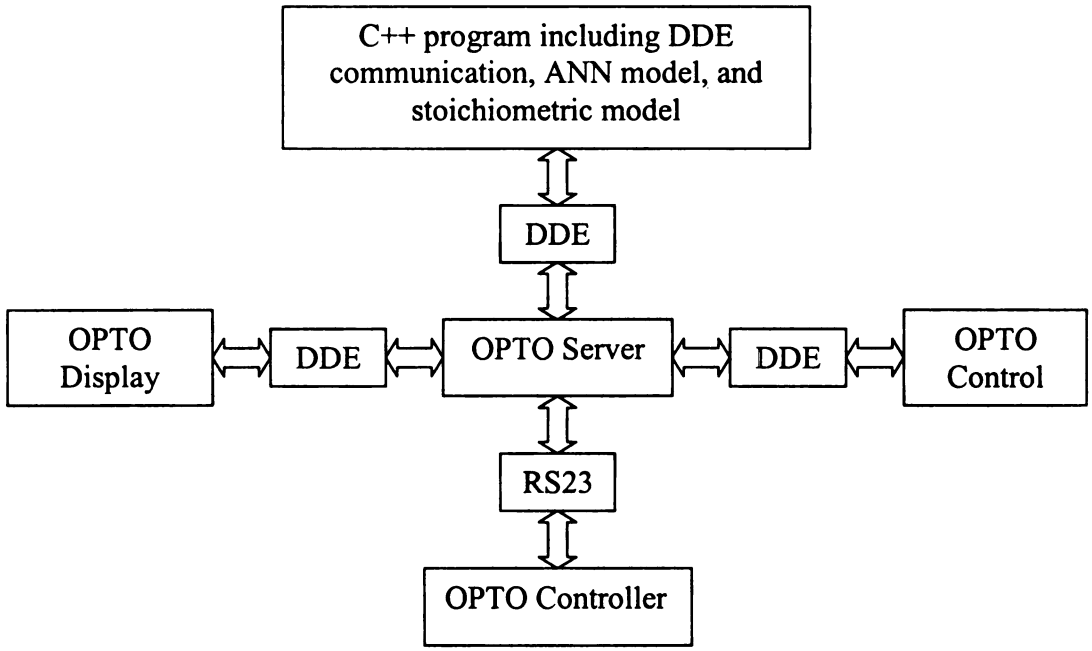

Figure 54. DDE protocol and information exchange during fermentations controlled using the Opto22 Factory Floor® software package.

The requisite features of a biologically dedicated KB control system include supervisory control (e.g., supervision of conventional control), identification of the state of the cell population (e.g., the "phase"), identification of the process equipment state, advanced communication with the user, handling of "fuzzy" information, and real-time control capabilities.[81a] The KB control systems developed here utilized the Opto22 Factory Floor® v. 3.1d control package. Use of the Opto22 software as an ESDT permitted implementation of the essential KB attributes listed above. Control charts (top-down design) can operate independent of one another, or they can be linked through various variables or control actions in the Opto22 software. In the case of the KB control system, this permitted the rule base to be implemented in an indirect (supervisory) fashion. This hierarchy structure is more desirable than direct KB control, and took

action only when required. The indirect methodology was implemented by simply dividing all KB-related control tasks into control charts separate from those responsible for at-line PID control. The state of the cell population was identified via the culture age, biomass concentration, current PS variable values, and current environmental variable values. The process equipment state was continuously evaluated by a dedicated control chart (8 L scale only) which examined process signals for evidence of acid or base pump failures, heating or cooling loop failures, attainment of the process equipment physical limitations, and so on. The charts responsible for KB control supervised the standard PID control by automatically changing PID control loop set points or disabling/enabling PID control loops (e.g., changing the culture control methodology) based on the PS of the culture. Descriptions of control system actions/decisions were communicated to the user via a MMI that reported the number of times a specific action/rule had been taken/executed, the time the action was taken, the reason for action being taken, the current phase of the fermentation, and so on. Processing of fuzzy information[81] (e.g., is the GFR too high for the current control scheme and fermentation age?) was manifested in multiple rules. The terminology (e.g., too high, too low, etc.) used to expound the KB control rules is consistent with literature precedent, and reflects the need to interpret qualitative data.[81] Finally, the real-time control requirement of the KB control system was achieved through the use of the Opto22 software. The software allocates the same amount of time for each chart configured in the control strategy, and therefore the KB control system chart(s) were executed at the same speed and frequency afforded the conventional control charts. The prioritization of KB control strategy rules is often of paramount importance, particularly when the rule base cannot execute at speeds on par

with that of standard control processes.[81] Although the rules were prioritized in the KB control schemes, this was not a critical consideration given the rule base execution occurred simultaneously with that of the conventional control strategy.

All KB control system derivatives, d(variable)/dt, were approximated by Δ(variable)/Δt. Derivative time scales (Δt) were evaluated on a rule-by-rule basis in relation to the process signal and associated noise. The biomass prediction interval was maintained by the control strategy, and predictions occurred every 0.25 h after the ANN was initialized. Many rules in both Phase 3 and Phase 4 keyed off the prediction interval timer (PIVT) to ensure integrity of the acquired data.

Fed-batch fermentations began in batch mode with an initial glucose charge. An example of a KB rule that recognizes a common occurrence not correctable with simple PID control is the depletion of the initial glucose charge prior to attaining the maximum desired airflow. PID control of the D.O. concentration by airflow views glucose depletion, and the subsequent spike in the D.O. concentration, as a cause for decreasing the airflow rate to the reactor, when more glucose should be added and airflow should actually be increasing. This common problem can be overcome by a straightforward rule that monitors the D.O. concentration during airflow ramp up, compares it to the set point, and adds glucose to the reactor (without suspending the airflow PID loop control) if the D.O. concentration suddenly increases to some arbitrary amount, say two times the set point for example. Furthermore, the amount of glucose added could be dependent upon the airflow rate at the instant of glucose depletion, adding less if the airflow is near the maximum desired value, or more if the airflow requires a significant increase to attain the

maximum value. Such a rule is diagrammed in Figure 55, and is presented in the context of a control scheme below as well.

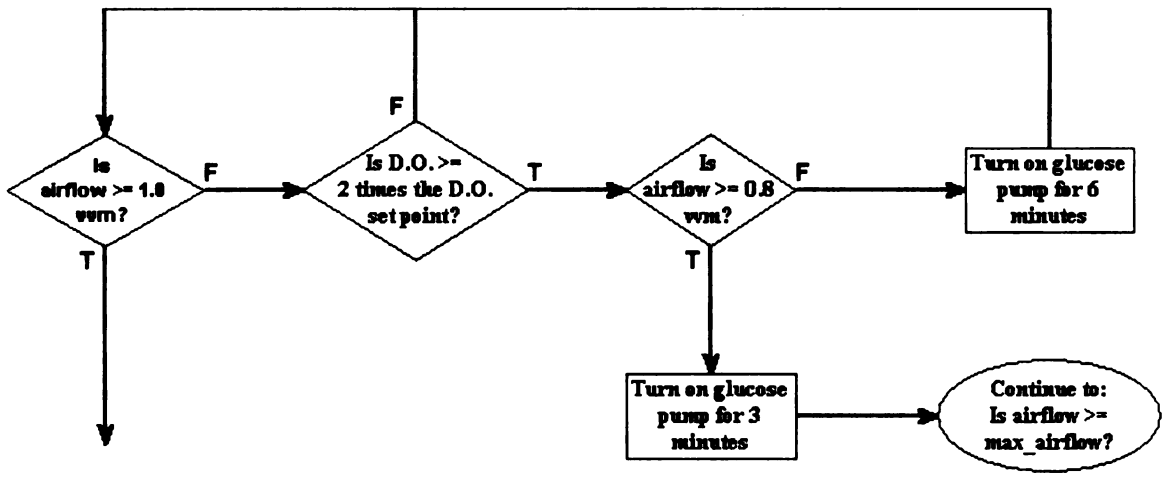

Figure 55. Simple KB rule for detection and correction of glucose depletion during airflow ramp during the batch phase of a fed-batch fermentation.

The KB control methodologies and rules were predicated upon the definition of a PS vector (Equation 20). PS variables encompassed by the PS vector were monitored in real-time by calculating their values from the pseudo-online prediction of biomass concentration (X) and appropriate peripheral information as indicated. The online monitoring and control of PS variables in real-time required the implementation of a simple linear extrapolation technique to estimate biomass concentration within the 0.25 h prediction interval void of the ANN. Equation 21 provides the formula utilized to estimate the real-time biomass concentration from the ANN biomass predictions. A fraction of the difference between the most recent biomass concentration prediction (X_t) and previous prediction (X_{t-1}) was calculated and added to X_t by calculating the fraction of the prediction interval (PIV) that had expired from the PIVT. Equation 16 provided the mathematical formalism utilized for online SOUR calculation. The OTR of

fermentations was calculated by a fermentor oxygen balance (Equation 22) and a nitrogen balance (Equation 23) that utilized the conservation expression in Equation 24. Online biomass concentration data were supplied as previously described. The reactor liquid volume was calculated online with a volume balance (Equation 25 and Equation 26), where F_T is the total liquid flow rate to the vessel and "b" was a correction factor to account for the water fraction of the glucose feed. The 8 L correction factor (b) was 0.64. The ammonium hydroxide feed rate (F_{NH4OH}) could not be calculated on the 1 L scale (e.g., set to zero). Therefore the 1 L scale "b" (0.75) was increased to compensate for volume increases due to both glucose and NH_4OH feeding. The specific glucose uptake rate (SGUR), in g glucose/g biomass/h, ($g \cdot g^{-1} \cdot h^{-1}$) was calculated online using Equation 27, which invoked the pseudo-steady-state assumption that the GFR was equal to the glucose uptake rate (GUR) if glucose was not accumulating in the culture supernatant. The specific carbon dioxide evolution rate (SCER), in g CO_2/g biomass/h, ($g \cdot g^{-1} \cdot h^{-1}$) was calculated per Equation 28, where the CER, in g CO_2/h was calculated from the offgas flow rate (converted to mol gas/h) and CO_2% (Equation 29). The specific growth rate (SGR or μ) was calculated, in units of h^{-1}, from Equation 30 by assuming dX/dt, the change in biomass concentration with respect to time, was constant over each 0.25 h prediction interval, and equal to the difference between the current and last biomass concentration predictions. The SGR was then solved for by simple rearrangement. The specific acetate excretion rate (SAER) was calculated, in g acetate/g biomass/h, by normalizing the difference of the most current and previous ANN acetate concentration predictions to the biomass concentration multiplied by the prediction interval (Equation 31).

Equation 20. $\mathbf{PS} = [SOUR, SGUR, SCER, SGR, SAER]^{T}$

Equation 21. $X_{current} = X_{t} + \left(\frac{X_{t} - X_{t-1}}{PIV}\right)(PIV - PIVT)$

Equation 22. $OTR = \frac{(F_{IN}O_{IN} - F_{OUT}O_{OUT})}{V}$

Equation 23. $F_{IN}N_{IN} = F_{OUT}N_{OUT}$

Equation 24. $1 = \frac{(O_2\% + N_2\% + CO_2\%)}{100\%}$

Equation 25. $\frac{dV}{dt} = F_T$

Equation 26. $F_T = bF_G + F_{NH4OH}$

Equation 27. $SGUR = \frac{GUR}{V \cdot X} = \frac{GFR}{V \cdot X}$

Equation 28. $SCER = \frac{CER}{V \cdot X}$

Equation 29. $$CER = MW_{CO2}\left(\frac{CO_2\%}{100\%}\right)F_{OUT}$$

Equation 30. $$\frac{dX}{dt} = \left(\mu - \frac{F_T}{V}\right)X$$

Equation 31. $$\frac{([acetate]_t - [acetate]_{t-1})}{X_t \cdot (PIV)}$$

KB Control System: 1 L Scale.

The objective of the PS variable/KB control system developed was to culture QP1.1 strains under glucose-limited conditions while approximating the OTR ramp observed when glucose-rich conditions were employed. To this end, a scaled-back version of the KB control system developed for the control of 8 L fermentations (detailed below) was implemented on the 1 L scale to afford similar culturing conditions while permitting scale up of the control strategy. The KB control scheme was divided into four phases. Individual control charts were dedicated to continuous PS variable calculation, KB control (all four phases), DDE management, and conventional control. Environmental variables (pH and temperature) were monitored and controlled per standard quinic acid fed-batch fermentation conditions and set points (Chapter 5). The phases were demarcated by the control methodologies active (Table 25), and were automatically advanced by the KB control system based on the PS of the culture.

Table 25. 1 L quinic acid fed-batch fermentation KB control phases.

Phase	Control methodologies
1	PID control of D.O. by impeller rate, fixed airflow rate (0.1 vvm)
2	PID control of D.O. by airflow rate, fixed impeller rate (750 rpm)
3	PID control of SOUR by GFR, PID control of D.O. by impeller rate, variable airflow rate (2.0 vvm maximum)
4	PID control of CER by GFR, PID control of D.O. by impeller rate, variable airflow rate (2.0 vvm maximum)

The transfer of control between Phase 1 and Phase 2 simply required the activation/deactivation of PID control loops. The Phase 2 to Phase 3 switch was implemented when the maximum Phase 2 airflow rate was attained, but was delayed until the control strategy detected the initialization of the ANN biomass concentration by the operator if the ANN had not been initialized prior to the onset of Phase 3. In the interim, the KB control system switched to standard glucose-limited control of the fermentation until the ANN was initialized. The PS variable control strategy was automatically invoked by the KB control system once the ANN was initialized, provided Phase 2 was complete. The initial Phase 3 SOUR set point of KB-controlled fermentations ranged between 0.13 and 0.15 $g \cdot g^{-1} \cdot h^{-1}$. The transfer of control between Phase 3 and Phase 4 occurred once a user defined biomass concentration was attained (40 g/L default), and transitioned between the control methodologies by a gradual set point ramp. The CER set point was ramped from its initial value (e.g., value at the onset of Phase 4, average of 5.2 g/h) to the Phase 4 CER set point (4.0 g/h default) value over the course of an hour.

The rules for the KB control scheme are listed below. Rules are listed in their assigned priority in the control strategy. Note that the physical limits on OTR were an

impeller rate of 1000 rpm and an airflow rate of 2.0 Lpm (2.0 vvm with 1.0 L of culture). Rules referenced during the explanation of another rule are confined to the current phase discussion unless otherwise specified. The marker of glucose accumulation (MGA)[81b,112a] was evaluated by suspending the control loop action responsible for glucose addition in Phase 3 (SOUR PID) or Phase 4 (CER PID). The impeller rate adjustments to maintain D.O. concentration constant could not be suspended (as they were in the 8 L KB control strategy below), however the PID control parameters of the Bioflo IIc were sufficiently sluggish to preclude significant variance in the impeller rate. Once the GFR was interrupted, a timer was initialized and monitored. The time required for the D.O. concentration to reach two times the D.O. concentration set point was then monitored and subsequently used to evaluate potential glucose overfeeding. A MGA value of 23 seconds was used in Phase 3 and 35 seconds was used in Phase 4 as determined by operator-initiated GFR interruptions of standard glucose-limited fed-batch fermentations. The MMI informed the operator when the MGA was being checked, the suspension of control loop action, and the time elapsed since the cessation of glucose feeding. After MGA determination, glucose feeding was resumed at its previous level if glucose had not been accumulating.

Phase 1:

Rule 1: *IF the impeller rate is too high, THEN switch to Phase 2.*

The rule was implemented with a single conditional block that compared the current impeller rate with the maximum Phase 1 impeller rate of 750 rpm. If the impeller rate was greater than or equal to 750, the control system advanced to Phase 2, otherwise

Phase 1 remained active. Switching to Phase 2 dictated a change in control algorithms as described in Table 25. The MMI informed the operator of the phase change and the time that it occurred.

Phase 2:

Rule 1: *If glucose is depleted, THEN add more glucose.*

The rule detected premature initial glucose charge exhaustion and was implemented by comparing the current D.O. concentration to that of a variable equal to double the D.O. concentration set point. Glucose exhaustion was defined as an increase in the D.O. concentration to greater than twice its set point. This caused glucose to be added to the reactor to a final concentration of 4.5 g/L if the airflow rate was between 0.8 vvm and 1.0 vvm, or 9 g/L if the airflow rate was less than 0.8 vvm. This is the rule presented in Figure 55, with the glucose pump duration converted to grams of glucose given the known flow rate (1.5 mL/min) and concentration (650 g/L) of glucose dispensed by the Bioflo IIc nutrient pump. The MMI informed the operator of glucose depletion, the addition of more glucose by the control scheme, and the time remaining until the required glucose addition was finished.

Rule 2: *IF the airflow rate is too high, THEN switch to Phase 3.*

The rule was implemented with a single conditional block that compared the current airflow rate with the maximum Phase 2 airflow rate (1.0 vvm). If the airflow rate was greater than or equal to 1.0 vvm, the control system advanced to Phase 3, otherwise Phase 2 remained active. Switching to Phase 3 dictated a change in control algorithms as

described in Table 25. The MMI informed the operator of the phase switch and the time it occurred.

Phase 3:

Rule 1: *IF the OTR requirements cannot be met, THEN decrease the SOUR set point.*

This rule was utilized to automatically reduce the SOUR set point if the OTR demanded by the culture became physically impossible to meet. The rule was implemented with two conditional blocks. The first checked if the maximum Phase 3 impeller rate (975 rpm) had been exceeded. If it had, the second conditional block would then check if previous airflow rate adjustments had incremented the airflow rate above 1.8 vvm. If both these conditions were met, the SOUR set point was decreased by 10% so that Phase 3 could continue aerobically. The rule was linked to a timer which expired every 10 minutes, permitting time for the effect of the airflow rate increment to be realized in the D.O. concentration, thereby lowering the impeller rate. The MMI informed the operator of the number of times the SOUR had been decremented due to OTR limitations.

Rule 2: *IF the impeller rate is too high, THEN increase the airflow rate.*

This rule was utilized in conjunction with the previous rule. If the airflow rate was not greater than 1.8 vvm when the impeller rate attained 975 rpm, then the airflow rate was incremented 0.2 vvm in order to maintain the culture in an aerobic state. The MMI presented graphical information to inform the operator of the current airflow rate and the impeller rate status in addition to displaying the current numeric values.

Rule 3: *IF the MGA check has been disabled, THEN suspended the MGA check.*

This rule consisted of a single conditional block that verified the value of a logical variable. If the variable was set false via an operator-initiated MMI override, then all MGA logic was bypassed until the user reset the variable to true.

Rule 4: *IF time has expired, THEN check the MGA.*

The rule keyed off the PIVT. Each time the timer ran out a variable was incremented. Once the variable value was greater than or equal to three (45 minute interval), the variable was reset to zero and the logic to measure the MGA was triggered. The MMI informed the operator as previously described.

Rule 5: *IF the MGA is too high, THEN decrease the SOUR set point.*

The rule utilized a condition block to compare the measured MGA to the maximum allowable value. If the MGA exceeded the maximum, then the SOUR set point was decreased by 10%, as this indicated the metabolic capacity of the culture to oxidize substrate was being exceeded and glucose was accumulating in the medium. Glucose feeding was resumed only after accumulated glucose had been depleted, and at 90% of the previous feed rate. The MMI informed the operator as previously described.

Rule 6: *IF the current culturing methodology becomes inappropriate, THEN switch to Phase 4.*

The rule was implemented in conjunction with Rule 5. A counter was incremented each time the MGA exceeded the maximum value. If this occurred three times during Phase 3,

then SOUR control was deemed an inappropriate control methodology. The variable used to evaluate rule 7 was then set to the current biomass concentration, forcing an immediate phase change. The MMI informed the operator of the time and nature of the phase change if it occurred.

Rule 7: *IF the biomass concentration is too high, THEN switch to Phase 4.*

The rule was implemented with a single conditional block that compared the current biomass concentration prediction to a variable. A biomass concentration of 40 g/L was the default to trigger a Phase 3 to Phase 4 switch. Switching to Phase 4 dictated a change in control algorithms as described in Table 25. The MMI informed the operator of the phase change and time that it occurred.

Rule 8: *IF the DDE fails, THEN switch to back up biomass concentration prediction.*

The rule monitored the time required for a response (prediction) to be received from the ANN prediction program once the OptoControl strategy requested a prediction (e.g., the prediction interval timer expired). If the response took greater than 10 seconds, biomass concentration was no longer predicted based on fermentation inputs to the ANN model. Instead, biomass concentration was internally updated in 15 minute intervals by the control strategy as a function of the previous biomass concentration according to a polynomial fit to the most recent fermentation done under the same control strategy. Upon reestablishing communication with the ANN, internal biomass concentration updating was immediately discontinued, and normal biomass concentration prediction by the ANN resumed. The MMI informed the operator of the DDE failure by displaying a

timer that indicated the elapsed time since the failure of the DDE, as well as displaying the internal OptoControl timer used to execute backup predictions.

Phase 4:

Rule 1: *If the OTR requirements cannot be met, THEN decrease the CER set point.*

The rule was utilized to automatically reduce the CER set point if the OUR demands of the culture became physically impossible to meet. The rule was implemented with the same logic used in rule 1 of Phase 3, but with the CER set point being decremented, instead of the SOUR set point, 10% at a time. The MMI informed the operator of the number of times the CER set point had been decremented due to OTR limitations.

Rule 2: *If the impeller rate is too high, THEN increase the airflow rate.*

The rule was utilized in conjunction with the previous rule. If the airflow rate was not greater than 1.8 vvm when the impeller rate attained 975 rpm, then the airflow rate was incremented 0.2 vvm in order to maintain the culture in an aerobic state. The MMI presented graphical information to inform the operator of the current airflow rate and impeller rate status in addition to displaying the current numeric values.

Rule 3: *IF the MGA check has been disabled, THEN suspended the MGA check.*

The rule consisted of a single conditional block that verified the value of a logical variable. If the variable was set false by the operator (via the MMI) then all MGA logic was skipped (e.g., rules 4-6) until the user reset the variable to true.

Rule 4: *IF d(GFR)/dt is positive, THEN check the MGA.*

The rule keyed off the PIVT. When the timer expired, the GFR during the timer interval (total time pump was on in seconds during the 0.25 h PIV) was moved to a storage table. The values were then compared. If $(\text{GFR seconds})_{t=0\ min} > (\text{GFR seconds})_{t=-15min} > (\text{GFR seconds})_{t=-30\ min} > (\text{GFR seconds})_{t=-45\ min} > (\text{GFR seconds})_{t=-60\ min}$ then the MGA was evaluated. The MMI informed the operator of the MGA check as previously described.

Rule 5: *IF time has elapsed, THEN check MGA.*

The rule keyed off the PIVT, incrementing a variable each time the timer expired. When the variable value reached 10 or more (2.5 h), the MGA was automatically checked and the variable was reset to zero.

Rule 6: *IF the MGA is too high, THEN decrease the CER set point.*

The rule utilized a condition block to compare the measured MGA to the maximum allowable value. If the MGA exceeded the maximum, then the CER set point was decreased by 5%, as this indicated the metabolic capacity of the culture to oxidize substrate was being exceeded and glucose was accumulating in the medium. Glucose feeding was resumed only after accumulated glucose had been depleted, and at 90% of the previous feed rate. The MMI informed the operator of both the magnitude and number of times the CER set point had been decremented.

Rule 7: *IF the DDE fails, THEN switch to back up biomass concentration prediction.*

This rule was identical to rule 8 of Phase 3.

KB Control System: 8 L Scale.

The maximum OTR capabilities of the 8 L scale were 10 L/min (1.25 vvm) of conventional airflow, 10 L/min of microsparger airflow (1.25 vvm), and an impeller rate of 1020 rpm. The KB control scheme was divided into four phases. Individual control charts were dedicated to continuous PS variable calculation, KB control (all four phases), KB monitoring of equipment and phase-independent rules, DDE management, digital control (pH and temperature), and analog control (PID control) in the strategy. Environmental variables (pH and temperature) were monitored and controlled per standard quinic acid fed-batch fermentations (Chapter 5). The phases were demarcated by the control methodologies active (Table 26), and were automatically advanced by the KB control system based on the PS of the culture. The MMI consisted of dedicated windows for: process values (e.g., airflow rate, temperature, impeller rate, etc.), trend lines (e.g., data sampled in 7 second intervals for the last hour for D.O. concentration, airflow rate, impeller rate, etc.), history plots (e.g., data sampled in 7 second intervals for the last 50 h), messages sent by the KB rules to advise the operator of actions taken, KB control overrides that provided the operator the ability to turn on or off specific rules or calculations, DDE information, and PID parameters.

Table 26. 8 L quinic acid fed-batch fermentation KB control phases.

Phase	Control methodologies
1	PID control of D.O. concentration by impeller rate, fixed airflow rate (0.1 vvm)
2	PID control of D.O. concentration by airflow rate, fixed impeller rate (850 rpm)
3	PID control of SOUR by impeller rate, PID control of D.O. concentration by GFR, variable air (1.25 vvm maximum) and microsparger (1.25 vvm maximum) flow rates
4	PID control of CER by GFR, PID control of D.O. concentration by impeller rate, variable air (1.25 vvm maximum) and microsparger (1.25 vvm maximum) flow rates

The Phase 3 SOUR set point of 8 L KB-controlled fermentations ranged between 0.17 and 0.18 $g \cdot g^{-1} \cdot h^{-1}$. The transfer of control between Phase 3 and Phase 4 occurred once a user defined biomass concentration was attained (40 g/L default) or the KB control system detected multiple SOUR set point decrements indicating the current control method was no longer effective. The transition between control methodologies (Phase 3 and Phase 4) was executed by a set point ramp. The CER set point was ramped from its initial value (e.g., value at the onset of Phase 4, average of 44 g/h) to the Phase 4 CER set point (43 g/h default) value over the course of an hour.

Rules referenced during the explanation of another rule are confined to the current phase discussion unless otherwise specified. The MGA was evaluated by suspending the control loop action responsible for glucose addition in Phase 3 (GFR PID) or Phase 4 (CER PID). The PID control of the impeller rate (SOUR PID in Phase 3 and D.O. concentration PID in Phase 4) was suspended and the impeller rate set at the current value for the duration of the MGA check rate. A timer was immediately started to

monitor the time required for the D.O. concentration to attain twice its set point, and was subsequently used to evaluate potential glucose overfeeding. A MGA value of 10 seconds or less, or 35 seconds or greater was used in Phase 3. A MGA value of 10 seconds or less, or 45 seconds or greater was used in Phase 4. The use of a minimum value prevented the failure of the MGA check to identify glucose overfeeding if reactor backpressure or decreased metabolic capacity of the culture had already resulted in an increase of the D.O. concentration significantly above the set point (e.g., the D.O. concentration was already greater than twice the set point) subsequent to the previous MGA check. The increase in the maximum MGA seconds between Phase 3 and Phase 4 reflected the decreased vigor of the cell population typically seen in Phase 4 relative to Phase 3. After the MGA was determined, glucose feeding was resumed at its previous level if glucose had not been accumulating. The MMI informed the operator when the MGA was being checked, the suspension of the relevant control loop action(s), and the time elapsed since the cessation of glucose feeding.

All Phase 4 rules responsible for automatic fermentation shutdown followed the same logic. First the glucose feed to the reactor was shutoff. When the D.O. concentration reached four times the D.O. concentration set point, indicating residual glucose depletion, all PID loops were disabled, all analog outputs (airflow rate, impeller rate, etc.) were ramped to zero, and all digital control loops were disabled. The operator was informed of the shutdown time and reason by the rule that triggered the shutdown. The always-running rules had a 1 h delay from the onset of the fermentation before becoming active, allowing pseudo-steady-state to be achieved. The logic of the rules responsible for fermentor shutdowns triggered by the always-running rule set were the

same as Phase 4 shutdown rules, but took effect immediately (e.g., no glucose depletion period) due to safety concerns.

Phase 1:

Rule 1: *IF the impeller rate is too low for too long, THEN switch to a historic impeller ramp profile.*

The goal of this rule was to detect a D.O. probe malfunction via the impeller rate value. The rule contained a conditional block that permitted user override capability from the MMI. A conditional block compared the elapsed time since the start of the fermentation to three hours. If the time was greater than three hours, the current impeller rate was examined. If the current impeller rate was less than or equal to 200 rpm after three hours, denoting a lack of impeller ramp due to a D.O. probe malfunction, then the rule started sampling the impeller rate at one minute intervals for a period of a half hour. If all the impeller rate values sampled were still at or below 200 rpm at the end of a half hour, then the rule disabled the PID control loop responsible for feedback control of the D.O. concentration by impeller rate, and ramped the impeller rate as a function of time based on a composite historical profile obtained from prior successful fermentations. The MMI warned the operator of the D.O. probe failure and the nature of the corrective action.

Rule 2: *IF pseudo-steady state has been achieved, THEN turn on the impeller rate oscillation calculation.*

The rule was implemented by moving 3 h to a timer. When the timer expired, the current impeller rate was moved to element zero of a storage table every two minutes, and the

timer reset. The calculation initiated once the table was full, and transpired each time the timer expired. The MMI informed the operator of the status of the impeller rate oscillation calculation.

Rule 3: *IF antifoam is being added, THEN suspend the impeller rate oscillation calculation.*

The rule was implemented by evaluating whether the antifoam pump was on or off prior to checking for expiration of the impeller rate oscillation calculation timer. If the antifoam pump was on, the impeller rate oscillation calculation timer was reset to 600 seconds. The MMI informed the operator of both antifoam addition and the impeller rate oscillation status.

Rule 4: *IF the impeller PID loop integral term is too low, THEN suspend the impeller rate oscillation calculation.*

The rule was implemented by a pre-test conditional statement that checked how many times the impeller rate PID control loop integral term had been decremented. If the integral term was already decremented five times, then the calculation was bypassed thereafter and the MMI informed the operator.

Rule 5: *IF the impeller rate is oscillating, THEN reduce the impeller PID loop integral term.*

The rule was implemented in several steps. First, impeller rates were acquired every two minutes and stored in a four-position table. Each time a new impeller rate value was

acquired, an average and limits of the currently stored values were calculated. The limits were defined as the average of the current table values +/- 1.5% of the maximum Phase 1 impeller rate (850 rpm). Next, the impeller rates were checked to verify they were within the limits. Rule execution terminated and the timer was reset if all the impeller rate values were within the calculated limits. If any impeller rate values fell outside the specified limits, then the values were checked for the qualitative trends of oscillation to ensure the impeller rate was not simply increasing or decreasing. This was accomplished by checking both the conditions (rate 1< rate 2 > rate 3 < rate 4) and (rate 1 > rate 2 < rate 3 > rate 4), if either condition was true, then the impeller rate was deemed oscillatory, and the integral term of the PID control loop responsible for D.O. concentration control via the impeller rate was reduced by 10% of its current value. The MMI informed the operator of the number of times the impeller rate had been diagnosed as oscillating and the number of times the integral term had been decremented.

Rule 6: *IF the impeller rate is too high, THEN switch to Phase 2.*

The rule was implemented with a conditional block that verified the current impeller rate was less than the maximum Phase 1 impeller rate (850 rpm). If the impeller rate was below the threshold value, the Phase 1 rules check began again with rule one. If the impeller rate was equal to or exceeded the threshold value, the impeller rate was set to the Phase 1 maximum impeller rate and the fermentation phase was switched to Phase 2. The MMI informed the operator of the time at which the phase change took place.

Rule 7: *IF the antifoam addition timer has expired, BUT the impeller rate is high, THEN delay antifoam addition, ELSE add antifoam.*

The rule was implemented by initiating an antifoam interval timer (6 h) at the inception of the fermentation, and then checking for expiration of the timer. The antifoam pump was turned on once the timer expired, unless the impeller rate was within 50 rpm of the maximum Phase 1 impeller rate (850 rpm), in which case antifoam addition was delayed for 1/2 hour. Delaying antifoam addition prevented premature advancement to Phase 2 due to an artificial increase in impeller rate caused by an antifoam-induced drop in the D.O. concentration. The default antifoam addition duration was 120 seconds. The MMI informed the operator that antifoam addition was in progress.

Phase 2:

Rule 1: *IF the glucose is depleted, THEN add more glucose.*

The rule detected premature initial glucose charge exhaustion and was implemented by comparing the current D.O. concentration to that of a variable equal to double the D.O. set point. Glucose exhaustion was defined as an increase in the D.O. concentration to greater than or equal to twice its set point. This caused glucose addition to the reactor on a sliding scale based upon the airflow rate at the time of glucose depletion. If the airflow rate was at or below 0.5 vvm (4 L/min), glucose was added to a final concentration of 27.4 g/L (pump on for 30 minutes). If the airflow rate was between 0.5 vvm and 1.0 vvm (8 L/min), the glucose pump was turned on for a duration inversely proportional to the airflow (e.g., 30 minutes for 0.5 vvm, zero minutes for 1.0 vvm) to prevent excessive glucose accumulation prior to the onset of glucose feeding. The rule triggered a warning

in the MMI that informed the operator glucose had been depleted, additional glucose was being added, and the duration of glucose addition.

Rule 2: *IF antifoam addition is occurring, THEN suspend the airflow oscillation calculation.*

The rule was implemented by evaluating whether the antifoam pump was on or off prior to checking for airflow rate oscillation calculation timer expiration. If the antifoam pump was found to be on, the airflow rate oscillation calculation timer was reset to 10 minutes, to avoid detection of false airflow oscillations induced by antifoam addition. The MMI informed the operator of the status of the calculation and if antifoam addition was in progress.

Rule 3: *IF Phase 2 has reached pseudo-steady-state, THEN initiate the airflow oscillation calculation.*

The rule was implemented by moving 1 h to a timer when Phase 2 commenced with subsequent timer expiration checking. Once the initial time expired, the current airflow rate was moved to element zero of a storage table, and the timer reset to 120 seconds. The calculation initiated once the table was full, and transpired each time the timer expired. Delaying the onset of the calculation prevented premature detection of oscillations that might result from Phase 2 initiation. The MMI informed the operator of the airflow oscillation calculation status.

Rule 4: *IF the airflow PID loop integral term is too low, THEN suspend the airflow rate oscillation calculation.*

The rule was implemented by a pre-test conditional block that checked the number of times the airflow rate PID control loop integral term had been decremented. If the airflow integral term was already decremented five or more times, then the calculation was bypassed and the MMI informed the operator of the calculation status.

Rule 5: *IF the airflow rate is oscillating, THEN reduce the airflow PID loop integral value.*

The rule was implemented in several steps. First, airflow rates were acquired every two minutes and stored in a four-position table. Each time a new airflow rate value was acquired, an average of the values and limits for the values were calculated. The limits were defined as the average of the current table values +/- 5.0% of the maximum Phase 2 airflow rate (8 L/min). Next, the airflow rates were checked to verify they were within the limits. Rule execution ended, and the timer was reset if no values were outside the calculation limits. If any airflow rates fell outside the specified limits, then they were checked for the qualitative trends of oscillation to ensure the airflow rate was not simply increasing or decreasing. This was accomplished by checking both the conditions (rate 1< rate 2 > rate 3 < rate 4) and (rate 1 > rate 2 < rate 3 > rate 4), if either condition was true, then the airflow rate was deemed oscillatory, and the integral term of the PID loop that controlled the D.O. concentration via airflow rate was reduced by 10% of its current value. The MMI notified the operator when airflow oscillations were detected and the number of times the integral term was decremented.

Rule 6: *IF the airflow rate is too high, THEN switch to Phase 3.*

The rule was implemented with a conditional block that verified the current airflow rate was less than the maximum Phase 2 airflow rate (8 L/min). If the airflow rate was below the threshold value, the Phase 2 rules check began again with rule one. If the airflow rate was equal to or exceeded the threshold value, the airflow rate was set to the Phase 2 maximum airflow rate and the fermentation phase was switched to Phase 3. The MMI informed the operator of the phase switch, and the time of the switch.

Rule 7: *IF enough time has elapsed, BUT the airflow rate is high, THEN delay antifoam addition, ELSE add antifoam.*

The rule was implemented by checking for expiration of the antifoam interval timer. The antifoam pump was turned on once the timer expired, unless the airflow rate was within 1 L/min or closer to the maximum Phase 2 airflow rate, in which case antifoam addition was delay 1/2 h. Delaying antifoam addition prevented premature advancement to Phase 3 due to an artificial increase in airflow rate. The MMI informed the operator if antifoam addition was in progress.

Phase 3:

Rule 1: *IF the ANN has been initialized, THEN switch to SOUR control, ELSE use standard glucose-limited control.*

The rule was implemented with a single conditional block. The D.O. concentration was controlled by the addition of glucose at a fixed impeller rate until the ANN was

initialized with a biomass concentration. Inputting an initial biomass concentration started the ANN predictions and initiated the execution of Phase 3 rules, activating the PID control of SOUR via impeller rate, and PID control of the D.O. concentration via glucose feeding remained active. The MMI informed the operator that standard glucose-limited control was being utilized if the ANN had not been initialized.

Rule 2: *IF the airflow rate or the microsparger flow rate were incremented, or if the SOUR set point was decremented, THEN wait before checking if the impeller rate is high.* The rule was implemented by moving 180 seconds to a timer after the microsparger flow rate was incremented, the airflow rate was incremented, or the SOUR set point was decremented. This rule superceded rules 3-6 via checking for timer expiration prior to the action blocks that rectified excessive impeller rates. This provided a delay for corrective action taken to affect the impeller rate before its value was checked again. The timer value was viewable and/or overridable in the MMI.

Rule 3: *IF the OTR requirements cannot be met, THEN decrease the SOUR set point .* The rule was implemented by checking the current impeller rate, current airflow rate, and current microsparger flow rate. The default maximum microsparger and airflow rates were 8 L/min, but could be manually input from the MMI by the operator to permit maximums between 0 and 10 L/min. If the impeller rate was greater than the maximum Phase 3 impeller rate (1020 rpm) less 50 rpm, after the microsparger flow rate had reached its maximum and the airflow had reached its maximum, the SOUR set point was reduced 10% because the maximum physical OTR was attained and could no longer meet

the OUR demand of the culture at the current SOUR set point. The MMI informed the operator of the decrement in SOUR set point and the number of times it had occurred.

Rule 4: *IF the microsparger flow rate is not too high, AND the airflow and impeller rates are too high, THEN increase the microsparger flow rate.*

The rule was implemented by checking the current impeller rate, current airflow rate, and current microsparger flow rate. If the impeller rate was greater than the maximum impeller rate (1020 rpm) less 50 rpm and the airflow rate had reached its maximum after the microsparger flow rate attained 6 L/min, then the microsparger flow rate was incremented by 1 L/min. The MMI informed the operator of airflow, microsparger, and impeller rates both graphically and via text.

Rule 5: *IF the microsparger flow rate is high and the impeller rate is too high, THEN increase the airflow rate.*

The rule was implemented by checking the current impeller rate, current airflow rate, and current microsparger flow rate. If the impeller rate was greater than the maximum impeller rate (1020 rpm) less 50 rpm and the microsparger flow rate had reached 6 L/min already, then the airflow rate was incremented 1 L/min. Conventional sparging was increased after the microsparger flow rate reached 6 L/min due to gas hold up considerations. The MMI informed the operator of airflow, microsparger, and impeller rates both graphically and via text.

Rule 6: *IF the impeller rate is too high, THEN substitute microsparging for conventional sparging.*

The rule was implemented by checking the current impeller rate. If the impeller rate was within 50 rpm of the maximum impeller rate (1020 rpm), the airflow rate was decremented by 1.0 L/min and the microsparger flow rate was incremented by 1.0 L/min. This allowed for an increase in the k_La, by increasing the specific interfacial surface area, without an increase in the overall airflow rate to the reactor. The MMI informed the operator that the microsparger was activated and informed the operator of the airflow, microsparger, and impeller rates both graphically and via text.

Rule 7: *IF antifoam addition is occurring, THEN suspend the MGA check.*

The rule was implemented by a conditional block that verified the antifoam pump was off before progressing to the MGA check logic. If the antifoam pump was on, the strategy bypassed rules 8-10 until the antifoam pump was turned off. If the antifoam pump was off, rules 8-10 were executed. The MMI informed the operator that antifoam addition was occurring.

Rule 8: *IF the MGA check has been manually disabled, THEN suspended MGA check.*

This rule consisted of a single conditional block that verified the value of a logical variable. If the variable was set false by the operator (via the MMI) then all MGA logic was skipped (e.g., rules 9-11) until the user reset the variable to true.

Rule 9: *IF enough time has elapsed, THEN check the MGA.*

The rule was implemented by incrementing a counter when the prediction timer ran out. A pre-increment conditional block checked if the counter had reached one. If the counter was less than one, the MGA calculation was bypassed. If the counter was equal to one, it was reset to zero and then the MGA was checked (e.g., the MGA was automatically checked every 1/2 h).

Rule 10: *IF the MGA is too high, THEN decrease the SOUR set point.*

The rule was implemented by comparing the MGA to the limits previously elaborated. If the MGA was outside the limits, the SOUR set point was decremented by 10%, otherwise no corrective action was taken. Control of the GFR and impeller rate were then returned to the appropriate PID loops. If the MGA was exceeded, the GFR resumed at 90% of its original value.

Rule 11: *IF the SAER is too high, THEN warn the operator.*

The rule was implemented by a conditional block that compared the current calculated SAER to the maximum SAER. If the SAER was greater than or equal to the maximum (0.0018 g acetate·g biomass^{-1}·h^{-1}), the MMI warned the operator. This rule was linked to the MGA (rules 8-10), but took no corrective action. The maximum SAER was calculated from previous 1 L fermentations where oxygen-sensor controlled glucose feeding resulted in excess glucose addition, and excessive acetate excretion occurred.

Rule 12: *IF the SGR is less than or equal to zero, THEN warn the operator an ANN prediction error may have occurred.*

The rule was implemented with a single conditional block that verified the current calculated SGR was not less than zero. If the SGR was less than zero, the MMI warned the operator that an ANN problem might have occurred, and rules 13-17 were bypassed.

Rule 13: *IF enough time has elapsed, THEN check if the SGR is within its limits.*

The rule was implemented by moving the current calculated SGR to a four-position table each time the prediction timer expired. A single conditional block verified whether the last four SGR values were within the SGR limits (0.10/h minimum, 0.40/h maximum). If all the SGR values were outside the limits, then rules 14-17 were permitted to execute as required. If any SGR values were within the limits then rules 14-17 were bypassed.

Rule 14: *IF the temperature set point is too high, THEN suspend the low SGR temperature correction.*

The rule was implemented with a pre-test conditional block that verified the temperature set point had not previously been incremented to or past the maximum allowable set point. If the temperature set point was greater than or equal to the original temperature set point plus 3.0 °C, the low SGR corrective action was suspended and the MMI warned the operator.

Rule 15: *IF the SGR is too low, THEN increase the temperature.*

The rule was implemented with a conditional block that compared the last four calculated SGR values to the minimum allowable SGR. If all four SGR values were less than or equal to the minimum, the temperature set point was incremented by 0.5 °C and the MMI

informed the operator, otherwise the SGR was deemed greater than or equal to the maximum allowable SGR since rule 13 established the SGR was outside the allowable limits.

Rule 16: *IF the temperature set point is too low, THEN suspend the maximum SGR temperature correction.*

The rule was implemented with a pre-test conditional block that verified the temperature set point had not previously been decremented to or past the minimum allowable set point. If the temperature set point was less than or equal to the original temperature set point minus 3.0 °C, further temperature reductions were suspended and the MMI warned the operator.

Rule 17: *IF the SGR is too high, THEN decrease the temperature.*

The rule was implemented with the same control structure used for rule 13 and 15. If the last four SGR values were outside the limits, but not too low, the values were too high. SGR values in excess of the maximum SGR resulted in a temperature set point reduction of 0.5 °C, and the MMI informed the operator of the set point change.

Rule 18: *IF the DDE fails, THEN switch to back up biomass concentration prediction.*

The rule was identical to rule 8 of the 1 L KB control system Phase 3.

Rule 19: *IF the current culturing method is inappropriate, THEN switch to Phase 4.*

The rule was defined by checking the number of times the SOUR set point had been decremented due to OTR limitations and/or MGA checks. If the set point was decremented four times or more then the fermentation was switched to the Phase 4 rule set and the MMI informed the operator of the phase switch and the time that it occurred.

Rule 20: *IF the fermentor biomass concentration is too high, THEN switch to Phase 4.*

The rule was implemented with a single conditional block that verified the current biomass concentration was still less than 40 g/L. If the biomass was less than 40 g/L, the Phase 3 rule evaluations began again, otherwise the fermentation was switched to the Phase 4 rule set and the MMI informed the operator of the phase switch and the time that it occurred.

Rule 20: *IF enough time has elapsed, THEN add antifoam.*

The rule was implemented by checking for expiration of the antifoam interval timer. Antifoam was added if the timer was expired. The timer was reset to 3 h and the MMI informed the operator of the antifoam addition.

Phase 4:

Rule 1: *IF the airflow rate or the microsparger flow rate were incremented, or if the CER set point was decremented, THEN wait before checking if the impeller rate is too high.*

The rule was implemented by moving five minutes to the timer responsible for checking the current impeller rate after the microsparger flow rate set point was incremented, the

airflow rate set point was incremented, or the CER set point was decremented. This rule superceded rules 2-5 by checking for timer expiration prior to the action blocks that rectified excessive impeller rates. This provided a delay for corrective action taken to affect the impeller rate before its value was rechecked. The timer was visible to the operator in the MMI.

Rule 2: *IF the OTR requirements cannot be met, THEN decrease the CER set point.*

The rule was implemented by checking the current impeller rate, current airflow rate, and current microsparger flow rate. If the impeller rate was greater than the maximum impeller rate (1020 rpm) less 50 rpm, after the microsparger flow rate had reached its maximum (8 L/min default) and the airflow has reached its maximum (8 L/min default), the CER set point was reduced 10% because the maximum OTR was attained and could no longer meet the OUR demand of the culture at the current CER set point. The MMI informed the operator of the decrement in CER set point and the number of times it had occurred. The MMI informed the operator of airflow, microsparger, and impeller rates both graphically and via text.

Rule 3: *IF the microsparger flow rate is not too high AND the airflow and impeller rates are too high, THEN increase the microsparger flow rate.*

The rule was implemented by checking the current impeller rate, current airflow rate, and current microsparger flow rate. If the impeller rate was greater than the maximum impeller rate (1020 rpm) less 50 rpm and the airflow had reached its maximum after the

microsparger flow rate reached 6 L/min, the microsparger flow rate set point was increment by 1 L/min.

Rule 4: *IF the microsparger flow rate is high AND the impeller rate is too high, THEN increase the airflow rate.*

The rule was implemented by checking the current impeller rate, current airflow rate, and current microsparger flow rate. If the impeller rate was greater than the maximum impeller rate (1020 rpm) less 50 rpm and the microsparger flow rate had already attained 6 L/min, then the airflow rate set point was incremented 1 L/min. Conventional sparging was increased after the microsparger flow rate reached 6 L/min due to gas hold up considerations.

Rule 5: *IF the impeller rate is too high, THEN substitute microsparging for conventional sparging.*

The rule was implemented by checking the current impeller rate. If the impeller rate was within 50 rpm of the maximum impeller rate (1020 rpm), the airflow rate set point was decremented by 1.0 L/min and the microsparger flow rate set point was incremented by 1.0 L/min. This allowed for an increase in the k_La, by increasing the interfacial surface area, without an increase in the overall airflow rate to the reactor. The MMI informed the operator that the microsparger was active.

Rule 6: *IF antifoam is being added, THEN bypass the GFR calculations, the MGA check, the QA productivity calculation, and the SAER check until antifoam addition is complete.*

The rule was implemented by a single conditional block that preceded the logic responsible for rules 7-15. If the antifoam pump was on, rules 7-15 were bypassed until the antifoam was turned off, and the rule execution resumed. The MMI informed the operator if antifoam addition was in progress.

Rule 7: *IF MGA check has been disabled by the operator, THEN suspended MGA check.*

This rule consisted of a single conditional block that verified the value of a logical variable. If the variable was set false by the operator (via the MMI) then all MGA logic was bypassed until the user reset the variable to true.

Rule 8: *If the GFR is very high, THEN check the MGA.*

This rule was implemented by a conditional block that compared the current GFR to a user-defined value. The rule keyed off the prediction interval timer and could be executed up to every 15 minutes. The user-defined maximum GFR could be input via the MMI and was dependent upon strain, phase age, and overall fermentation age. If the GFR was in excess of the user-defined value, then the MGA check was initiated. This rule was defined to recognize an excessively high GFR that may have increased very rapidly due to vessel pressurization, massive cell death (e.g., extreme vessel temperature shift), glucose reservoir depletion, etc. The default GFR value associated with this rule was 3.0 mL/min.

Rule 9: *If the MGA is too high AND the fermentation is too old, THEN permit residual glucose consumption and shutdown the fermentation.*

The rule was implemented by checking the elapsed time since the fermentation commenced if the MGA was exceeded. If the user-defined criterion of an old fermentation was met or exceeded (46 h default), the fermentor was automatically shutdown. The MMI informed the operator when and why the system was being shutdown.

Rule 10: *If the MGA is too high AND the fermentation is not too old, THEN reduce the CER set point.*

The rule decreased the CER set point by 5% if the MGA was exceeded but the fermentation was still viable for quinic acid production. The MMI informed the operator of the set point decrement and the origin of the corrective action.

Rule 11: *IF the quinic acid productivity, d(QA)/dt, is negative, AND the fermentation is too old, and the SAER is too high, THEN shutdown the fermentation.*

The rule was implemented by moving the current quinic acid concentration (g/L) prediction to element zero of a five position table each time the prediction interval timer expired, and calculating $(\text{quinic acid concentration})_{t=0\text{min}}$-$(\text{quinic acid concentration})_{t=-60\text{min}}$. If the difference was less than zero, the operator was warned via the MMI and had to acknowledge the message in order to remove it from the MMI. ANN experience dictated that declining quinic acid concentration predictions in Phase 4 (e.g., negative d(QA)/dt) suggested that the GFR was increasing. An increasing GFR was contrary to typical Phase 4 behavior and triggered an automatic fermentation shutdown if the

fermentation was too old and the calculated SAER had continuously exceeded the maximum for longer than 2 h, otherwise the MGA was checked.

Rule 12: *IF the d(QA)/dt is too low, AND the fermentation is too old, THEN shutdown the fermentation.*

This rule was implemented by calculating the quinic acid productivity per rule 11, and then checking if it was at or above the user-defined quinic acid productivity threshold (default 0.30 $g \cdot L^{-1} \cdot h^{-1}$) required to continue the fermentation. If the productivity fell between 0.0 $g \cdot L^{-1} \cdot h^{-1}$ and 0.30 $g \cdot L^{-1} \cdot h^{-1}$, and the fermentation was too old as previously defined, then the fermentation was shutdown and the operator informed via the MMI. The minimum requirement to trigger fermentation shutdown was two continuous hours of substandard productivity.

Rule 13: *IF the SAER is too high, AND the fermentation is too old, THEN shutdown the fermentation.*

The rule was implemented by a conditional block that compared the calculated SAER with the user-defined maximum SAER (0.0018 $g \cdot g^{-1} \cdot L^{-1}$ default) whenever the PIVT expired. If the SAER was continuously greater than or equal to the maximum for two hours or more, a second conditional block evaluated if the fermentation was too old. If both conditions were true, the fermentation was shutdown via the method previously described and the MMI informed the operator of the shutdown time and reason.

Rule 14: *IF the SAER is too high, THEN decrease the CER set point AND disable the rule.*

The rule was implemented in conjunction with the first condition in rule 13. If the fermentation was not too old, the CER set point was decremented 5%, and rules 13 and 14 were deactivated to prevent excessive set point changes. The user was informed of the rule deactivation, the set point decrement, and the number of times the set point had been decremented by the rule in the MMI. The rules could be reactivated by the operator using MMI overrides.

Rule 15: *If the GFR is high AND the d(GFR)/dt is positive, THEN check the MGA.*

The rule was implemented with a timer, a table, and two conditional blocks. A timer expired every 6 minutes and the current GFR was stored in the first position of a five-position table. If the current GFR was greater than or equal to a user-defined (via the MMI) threshold (2.2 mL/min default), then the rule checked if $(GFR)_{t=0min} > (GFR)_{t=-6min} > (GFR)_{t=-12min} > (GFR)_{t=-18min} > (GFR)_{t=-24min}$. If the condition was true, then d(GFR)/dt was positive and the MGA check was triggered. The MMI informed the operator that the d(GFR)/dt was positive and the time at which it occurred. The operator had to acknowledge the message to remove it from the MMI display. The rule was designed to identify the gradual increase in GFR associated with declining metabolic vigor and the resulting increase in GFR due to increased D.O. concentration.

Rule 16: *IF the CER set point has been decremented, THEN suspend the SGUR minimum check.*

The rule monitored for CER set point decrements by any rule and disabled the system's ability to increase the CER set point based on a low SGUR if the CER set point was decremented for any reason. The MMI informed the operator when and if the SGUR minimum calculation had been disabled.

Rule 17: *IF the SGUR is too low, AND the fermentation is too old, THEN shutdown the fermentation.*

The rule was implemented by a conditional block that compared the calculated SGUR with the user-defined minimum SGUR (0.04 $g \cdot g^{-1} \cdot L^{-1}$ default). If the SGUR was continuously too low for two hours, and the fermentation was too old, then the fermentation was automatically shutdown and the operator informed of the reason and time of the shutdown in the MMI.

Rule 18: *IF the SGUR is too low, AND the CER set point has not previously been decremented, THEN increase the CER set point.*

The same conditional block utilized in rule 17 was utilized for this rule. If the fermentation was not too old, then the CER set point was incremented 5% in order to increase the GFR to the reactor and therefore the SGUR as well. The MMI informed the operator of the low SGUR, the number of times the CER set point was incremented due to a low SGUR, and the time at which the most recent CER set point increment occurred.

Rule 19: *IF the SCER is too low, THEN inform the operator.*

The rule was implemented by a conditional block that compared the calculated SCER with the user-defined minimum SCER (0.03 $g \cdot g^{-1} \cdot L^{-1}$ default) every fourth prediction interval timer expiration. If the SCER decreased below the minimum SCER, the MMI informed the operator, but no corrective action was taken since rule 18 was also active and coupled to metabolic performance.

Rule 20: *IF the antifoam addition interval has elapsed, THEN add antifoam.*

The rule was implemented by checking for expiration of the antifoam interval timer. Antifoam was added if the timer was expired and the timer reset. The antifoam addition interval was user-definable (0 to 6 h) in the MMI, as was the addition duration (0 to 5 minutes). The default antifoam addition interval was 4 h. The default antifoam addition duration was 2 minutes.

Rule 21: *IF the fermentation is too old, THEN shutdown the fermentor.*

The rule was implemented by a conditional block that compared the current fermentation age to the user-defined maximum fermentation age. If the fermentation age was older than the user-defined maximum (48 h default), then the fermentation was automatically shutdown as previously described.

Rule 22: *IF the DDE fails, THEN switch to back up biomass concentration prediction.*

This rule was identical to rule 8 of the 1 L KB control system Phase 3, but also turned off all metabolic calculations (e.g., low SGUR, quinic acid productivity calculation, etc.)

capable of automatic fermentation shutdown. All equipment-related automatic fermentation shutdown rules were unaffected.

Always-Running Rules:

Rule 1: *IF the reactor volume is high, THEN warn the operator.*

The rule checked the current calculated reactor volume against a user-defined value (default 12.0 L) to prevent excessive volume accumulation. If the reactor reached the high volume mark, the MMI warned the operator that fermentor shutdown was imminent.

Rule 2: *IF the reactor volume exceeds the safe level, THEN shutdown the fermentor.*

The rule checked the current calculated reactor volume against that defined by the user in the MMI as safe. If the safe volume was exceeded (12.3 L default) then the reactor was shutdown.

Rule 3: *IF the CO_2 meter fails, THEN switch to standard glucose limited control.*

The rule was evaluated each time the prediction interval timer expired. First, if the CO_2% reading was outside the known instrument limits (0%-15% CO_2) when the timer expired then a meter failure was detected. Secondly, the offgas CO_2% value was stored in a table each time the timer ran out, and all values were compared to the MMI user-defined CO_2% minimum (1.3% default). If all the values were less than the minimum, signaling the meter reading had been incorrect for an hour or more, then a meter failure was detected. In the event of a meter failure detection, the rule switched the control of the fermentation to the standard glucose-limited fed-batch fermentation control

conditions for the 8 L scale and the MMI informed the operator of the meter failure, the switch in the control methodology, and the time of the control methodology switch. The meter failure could be overridden by the operator in the manual override window (Table 27, see below) via re-enabling the CER control methodology. This rule, although in the always-running rule set, got enabled automatically only after the ANN was initialized.

Rule 4: *IF the base addition rate is too high, THEN disable the base pump.*

The rule was implemented by calculating the base added to the fermentor over the last five minutes. If the average base addition rate was greater than the maximum normal base addition rate (5 mL/min) then a base pump failure was detected and the pump was disabled. The MMI warned the operator that the base pump was disable, and the time at which the failure occurred.

Rule 5: *IF the acid addition rate is too high, THEN disable the acid pump.*

The rule was implemented by calculating the acid added to the fermentor over the last five minutes. If the average acid addition rate was greater than the maximum normal acid addition rate (5 mL/min) then an acid pump failure was detected and the pump was disabled. The MMI warned the operator that the acid pump was disable, and the time at which the failure occurred.

Rule 6: *IF the temperature is too high, THEN warn the operator.*

The rule sampled and saved the temperature every two minutes to a storage table. If the temperature was greater than or equal to the maximum permissible temperature (current

temperature set point plus 3 °C default) for 10 minutes, then the MMI warned the operator of a possible cooling water failure. An operator-visible countdown from 10 minutes was started in the MMI that warned the operator the fermentor would be shutdown due to a cooling water failure at the end of the countdown.

Rule 7: *IF the temperature is too high too long, THEN shutdown the fermentor.*

The rule shut the fermentor down if the countdown in rule 6 reached zero. The MMI informed the operator the fermentor was shutdown due to a cooling water failure, and also informed the operator of the shutdown time.

Rule 8: *IF the temperature is too low, THEN warn the operator.*

The same storage table utilized in rules 6 and 7 was utilized for rules 8 and 9. If the temperature was less than or equal to the minimum permissible temperature (current temperature set point minus 3 °C default) for 10 minutes, then the MMI warned the operator of a possible heater failure. An operator-visible countdown from 10 minutes was started in the MMI that warned the operator the fermentor would be shutdown due to a heater failure at the end of the countdown.

Rule 9: *IF the temperature is too low for too long, THEN shutdown the fermentor.*

This rule shut the fermentor down if the countdown in rule 8 reached zero. The MMI informed the operator the fermentor was shutdown due to a heater failure, and also informed the operator of the shutdown time.

Rule 10: *IF pH control fails, THEN shutdown the fermentor.*

The rule was implemented by adding or subtracting a tolerance (default 1.0 pH unit) to or from the current pH set point in real-time. If the pH fell outside the limits so derived continuously for longer than an hour then the fermentor was shutdown and the operator was informed of the shutdown time and cause (failed pH probe or corrective pump).

Rule 11: *IF the impeller rate is too high, THEN warn the operator.*

The rule was implemented with a single conditional block that checked the current impeller rate against the equipment limit (1020 rpm). If the impeller rate was at the maximum the MMI warned the operator.

In addition to the preceding rules, the KB system had several operator-usable manual overrides built into the MMI. Table 27 lists the manual overrides available to the operator, and whether the override was a phase-dependent rule or an always-running (AR) rule. Note that the rules could be deactivated or reactivated regardless of whether the rule was set to its current state by the operator (manually) or automatically by the KB control system. Disabling a calculation disabled all control actions based on that calculation as well as the calculation itself.

Table 27. 8 L KB control system MMI operator override actions.

Entry	Phase	Override Action
1	1	Disable/enable the impeller rate oscillation calculation
2	1	Disable/enable the D.O. probe failure calculation
3	2	Disable/enable the airflow rate oscillation calculation
4	3	Disable/enable the MGA calculation
5	3	Force a MGA calculation
6	4	Disable/enable the MGA calculation
7	4	Force a MGA calculation
8	4	Disable/enable the quinic acid productivity calculation
9	4	Disable/enable the (SAER) $\geq$ $(SAER)_{max}$ calculation
10	4	Disable/enable the CER control of glucose feeding
11	AR	Disable/enable the CO_2 meter failure check
12	AR	Disable/enable the base pump failure check
13	AR	Disable/enable the acid pump failure check
14	AR	Disable/enable the temperature (heating and cooling) failure check
15	AR	Disable/enable all automatic shutdown rules

Most overrides in Table 27 are self-explanatory, however a few are of particular interest. Entries 4 and 6 describe overrides that precluded the evaluation of the MGA. This was useful in Phase 3 of the 8 L scale since OTR limitations were always encountered prior to exceeding the maximum OUR capacity of the cultures. Manually disabling the MGA check prevented unnecessary interruption of the GFR. The overrides

denoted by entries 5 and 7 permitted the user to check the MGA on demand if fermentation behavior appeared consistent with glucose accumulation, although as previously mentioned this was typically not the case in Phase 3. The ability to re-enable actuators such as the acid and base pumps if they were automatically disabled was useful in extending the productivity of fermentations. These overrides permitted simple and time efficient equipment repairs to transpire in the absence of significant fermentation interruptions. After rectifying actuator problems, actuators could be brought back online from the software MMI with minimal impact on fermentations. The rule in entry 15 of Table 27 was global in nature. As it states, all rules responsible for triggering the automatic shutdown of a fermentation could be disabled with a single override, excluding fermentation shutdown due to high volume given the gravity of exceeding the physical capacity of the fermentation vessel.

Standard 1 L and 8 L Fed-Batch Fermentations.

Initial fed-batch fermentations performed in the Worden laboratory utilized standard glucose-limited fed-batch fermentation conditions adapted from the BBB Biostat MD units in the Frost laboratory to the NBS Bioflo IIc platform (Table 2). The standard glucose-limited fermentation conditions for the NBS Bioflo IIc were estimated using the dilution method employed in Chapter 2 for the baffled and unbaffled BBB Biostat MD vessels. The airflow rate (1.0 vvm) and impeller rate (750 rpm) used on the Bioflo IIc were identical to the rates employed on the Biostat MD units. QP1.1/pKD12.138A was evaluated under the standard glucose-limited fermentation OTR conditions for the NBS Bioflo IIc platform. It should be noted that oversized impellers

(D_i of 5.5 cm, L of 1.9 cm, W of 1.1 cm) were required on the Bioflo IIc to attain the desired OTR characteristics due to the inability of the standard Bioflo IIc impellers (D_i of 4.9 cm, L of 1.2, W of 0.9) to attain an acceptable OTR even at the maximum impeller rate (1000 rpm).[151]

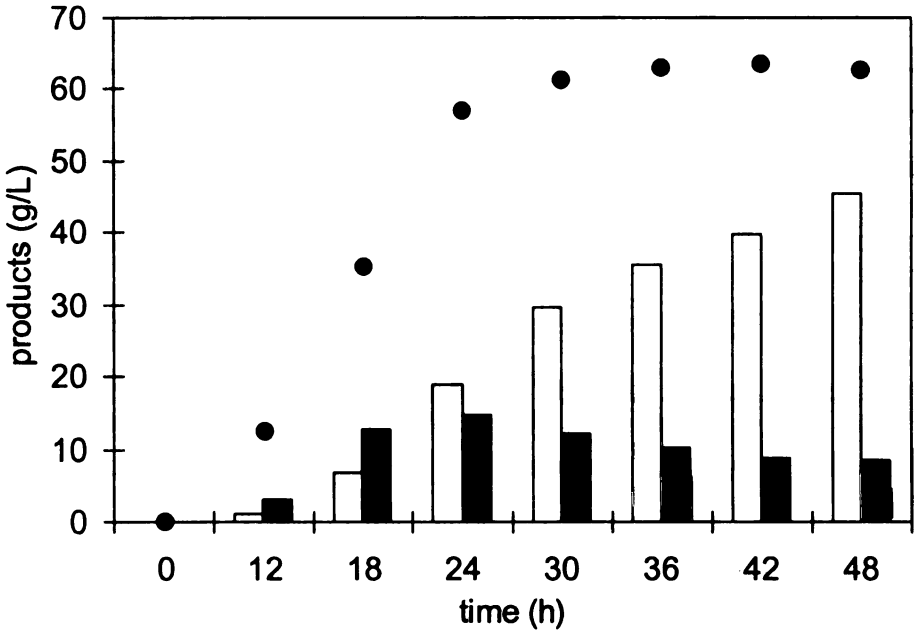

Figure 56. Standard 1 L QP1.1/pKD12.138A glucose-limited fed-batch fermentation product time course. Quinic acid □, DHQ ■, cell mass ●, in g/L.

Table 28. Standard glucose-limited fed-batch fermentation titers and yields for QP1.1/pKD12.138A on different equipment platforms.

Entry	Platform	QA (g/L)	DHQ (g/L)	QA:DHQ (mol:mol)	QA yield (mol/mol)	Total yield (mol/mol)
1	BBB Biostat MD	49	3.3	15	20%	21%
2	NBS Bioflo IIc	45	8.5	5.3	17%	21%

Table 29. DAHP synthase and shikimate dehydrogenase enzyme activities (μmol/min/mg) for standard 1 L QP1.1/pKD12.138A fed-batch fermentation conditions.

		specific activity (μmol/min/mg)			
Entry	Enzyme	12 h	24 h	36 h	48 h
1	DAHP synthase	0.47	0.31	0.17	0.12
2	shikimate dehydrogenase	7.2	15	22	31

Comparing the fermentation results to those obtained under the standard OTR conditions of the BBB Biostat MD units utilized in Chapter 3, the final quinic acid titer (45 g/L) was 4 g/L lower, while the DHQ titer (8.5 g/L) was enhanced by about 5 g/L (Table 28). The resulting QA:DHQ was 5.3. The yields of quinic acid and DHQ were 17% (mol/mol) and 3.7% (mol/mol) from glucose respectively. The magnitude of the DHQ profile (Figure 56) increased relative that previously observed (Figure 44), while the relevant enzyme activities (Table 29) measured on the NBS Bioflo IIc system did not deviate significantly from the BBB Biostat MD platform (Table 21). The quinic acid and DHQ profiles (Figure 56) were the baseline at the 1 L scale from which enhanced 1 L OTR experiments and scale up to 8 L proceeded.

The ANN was trained using previous concentration data for quinic acid, DHQ, biomass, and acetate from standard glucose-limited fed-batch fermentations performed on the Bioflo IIc, and used to make pseudo-online predictions for the fermentation (Figure 57). Note that under the standard conditions the predictions were not utilized for control action. The ANN predictions approximated the concentration profiles of the various fermentation supernatant components closely. The particularly good agreement between

predicted and actual biomass concentrations permitted accurate online calculation of PS variables (Figure 58).

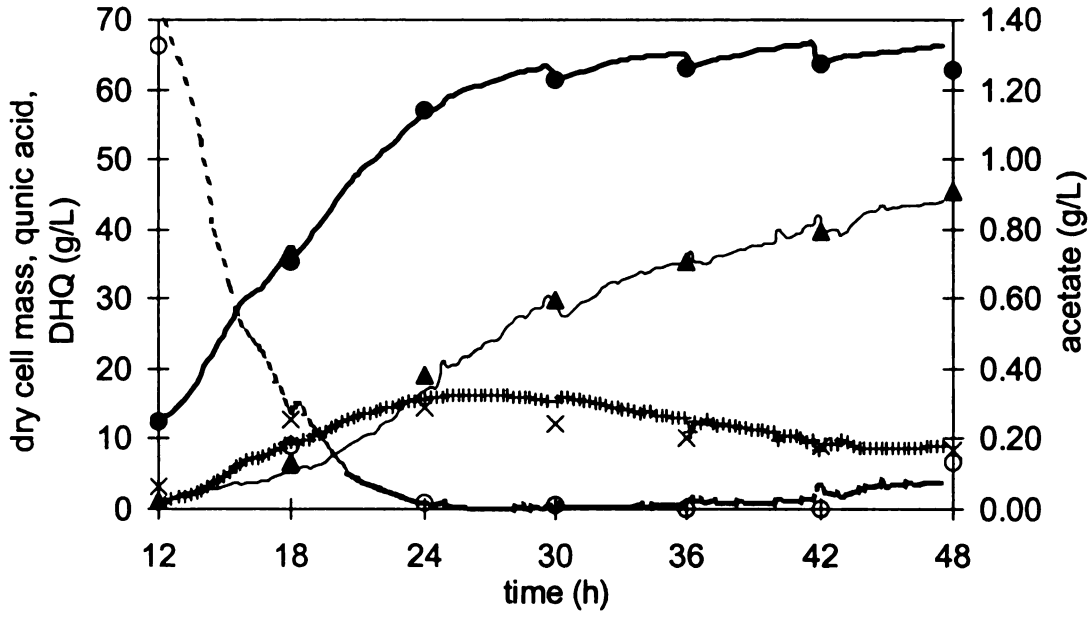

Figure 57. Actual (symbol) and ANN-predicted (line) concentration profiles for quinic acid (▲, ——), DHQ (×, ⋕⋕⋕), cell mass (●, ——), and acetate (○, ·····) in g/L for standard 1 L glucose-limited fed-batch fermentation of QP1.1/pKD12.138A.

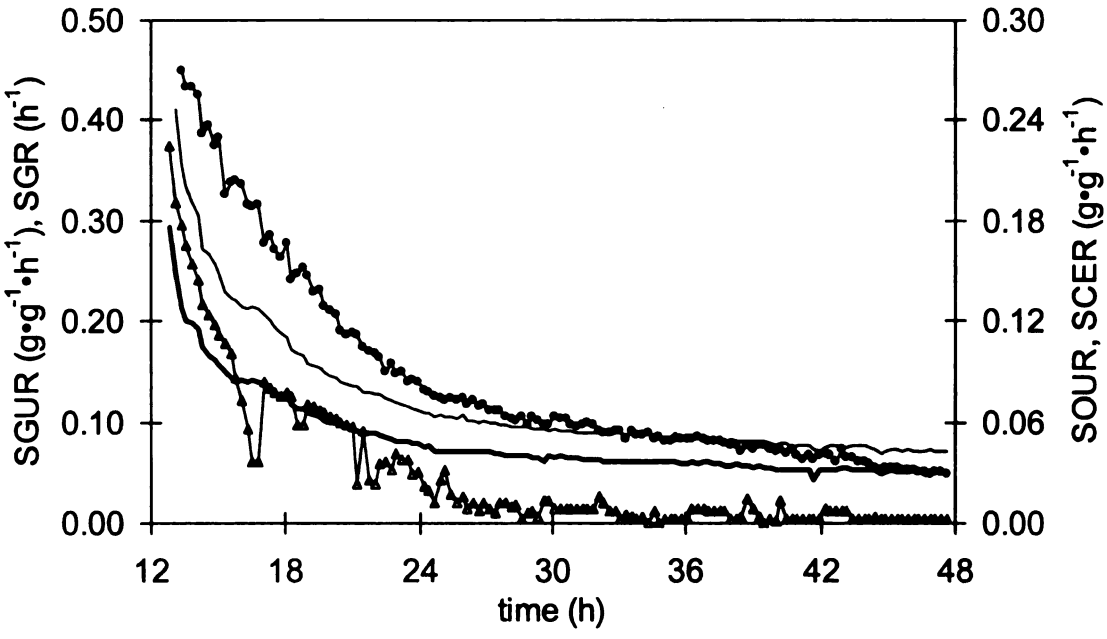

Figure 58. Select 1 L QP1.1/pKD12.138A PS variable profiles for standard glucose-limited fed-batch fermentation. SOUR —, SCER —, SGUR —•—, SGR —▲—.

The standard glucose-limited fed-batch fermentation OTR conditions were initially defined on the 8 L scale by trial and error. The OTR conditions (Dow platform, Table 2) were determined by picking an impeller rate (650 rpm) and airflow rate (1.0 vvm), and performing a fermentation. Concentration profiles for biomass, quinic acid, and DHQ were diminished relative to their 1 L scale counterparts. Low product and biomass concentrations were indicative of insufficient glucose feeding due to a low OTR. The OTR was increased by increasing the maximum impeller rate and another fermentation was done to test the affects. This process was repeated until the standard impeller rate for the 8 L scale (850 rpm) was determined which provided essentially identical quinic acid (45 g/L) and biomass (about 60 g/L) concentrations by 48 h relative to the 1 L scale. Direct estimation of the 8 L OTR conditions based upon standard,

relevant criteria (e.g., k_La) was not possible due to geometric (e.g., vessel dimensions and ratios) and hardware (e.g., sparger configuration) variation between the two equipment platforms. The previous method (Chapter 2) for OTR condition determination was impractical due to the pump flow rates and buffer volume requirements imposed by the 8 L scale.

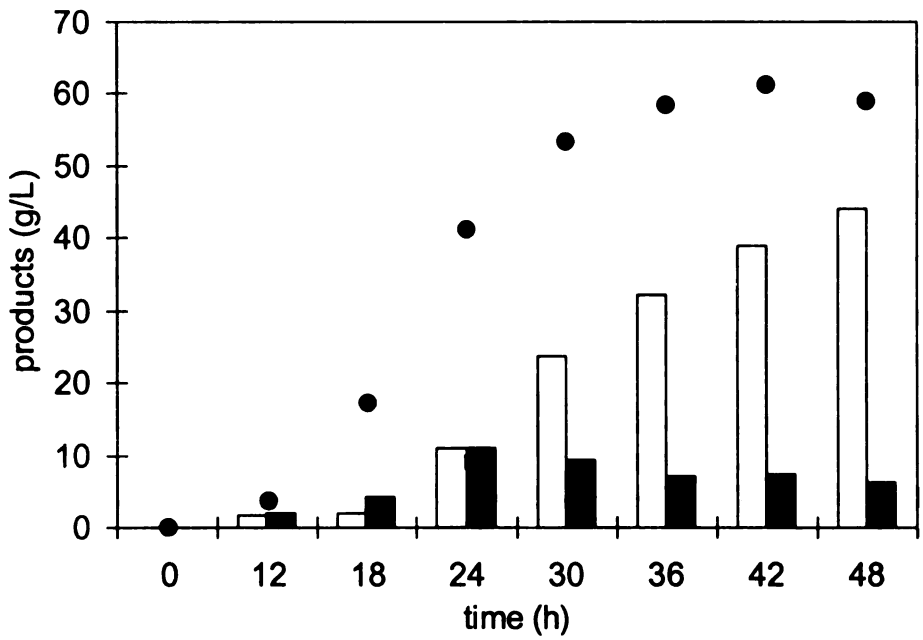

Figure 59. Standard 8 L QP1.1/pKD12.138A glucose-limited fed-batch fermentation product time course. Quinic acid □, DHQ ■, cell mass ●, in g/L.

The final quinic acid concentration of 44 g/L, DHQ concentration of 6.1 g/L, and biomass concentration of 59 g/L were all within experimental error of the standard 1 L fed-batch fermentation conditions. The 18% yield of quinic acid (mol/mol) and 2.8% yield of DHQ (mol/mol) from glucose were also very similar. The final QA:DHQ was 7.2. The slight increase in QA:DHQ relative to the 1 L scale was due to a decrease in the final DHQ concentration from 8.5 g/L (1 L) to 6.1 g/L (g/L) while the quinic acid

concentration developed remained essentially constant. Enzymatic data were within experimental variation of 1 L fermentation data (Table 29) for DAHP synthase (Table 30, entry 1) specific activities, and nearly identical for shikimate dehydrogenase (Table 30, entry 2) specific activities.

Table 30. DAHP synthase and shikimate dehydrogenase enzyme activities (μmol/min/mg) for standard 8 L QP1.1/pKD12.138A fed-batch fermentation conditions.

		specific activity (μmol/min/mg)			
Entry	Enzyme	12 h	24 h	36 h	48 h
1	DAHP synthase	0.49	0.19	0.098	0.096
2	shikimate dehydrogenase	11	15	21	31

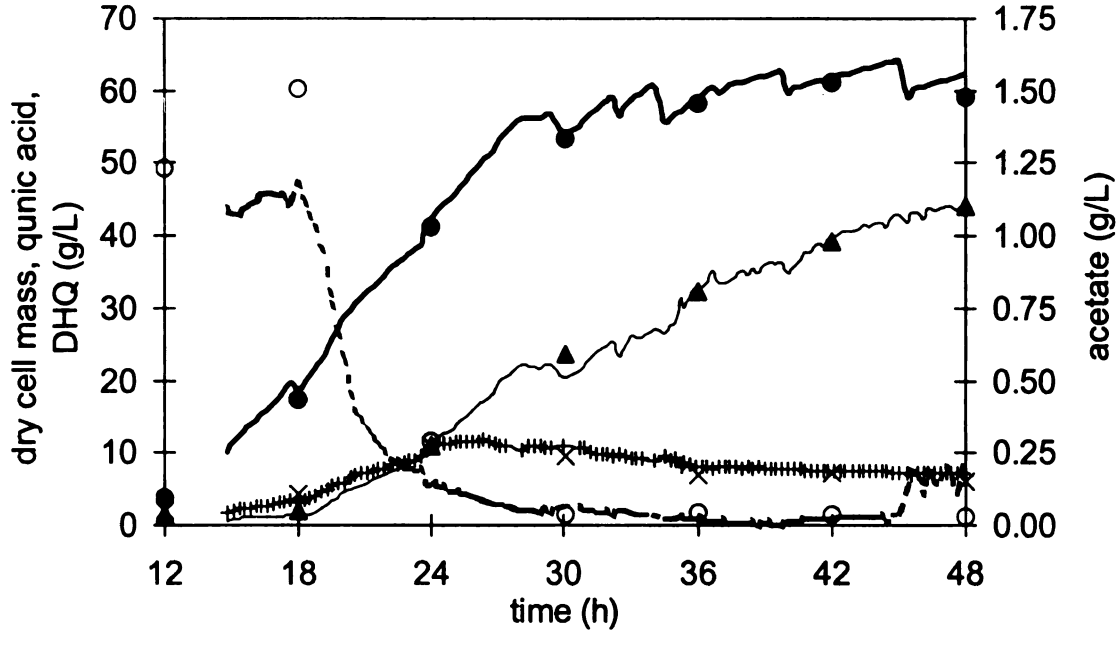

Figure 60. Actual (symbol) and ANN-predicted (line) concentration profiles for quinic acid (▲, ——), DHQ (× , ++++), cell mass (● , ——), and acetate (○ , ·····) in g/L for standard 8 L glucose-limited fed-batch fermentation of QP1.1/pKD12.138A.

The ANN quinic acid and DHQ concentration predictions were virtually identical to the actual concentration data. The biomass concentration prediction was reinitialized several times due to a slight decrease in the final biomass concentration developed relative to the training data set used. Frequent reinitialization of the biomass concentration and the resulting concentration spikes were propagated through the PS variable calculations (Figure 61). The acetate prediction was qualitatively correct, but was 0.33 g/L lower than the actual value at 18 h. Acetate concentration accumulation varied from run to run at the completion of the batch (glucose-rich) portion of the fermentations, and this variation was reflected in the discrepancy between the predicted and actual acetate concentrations.

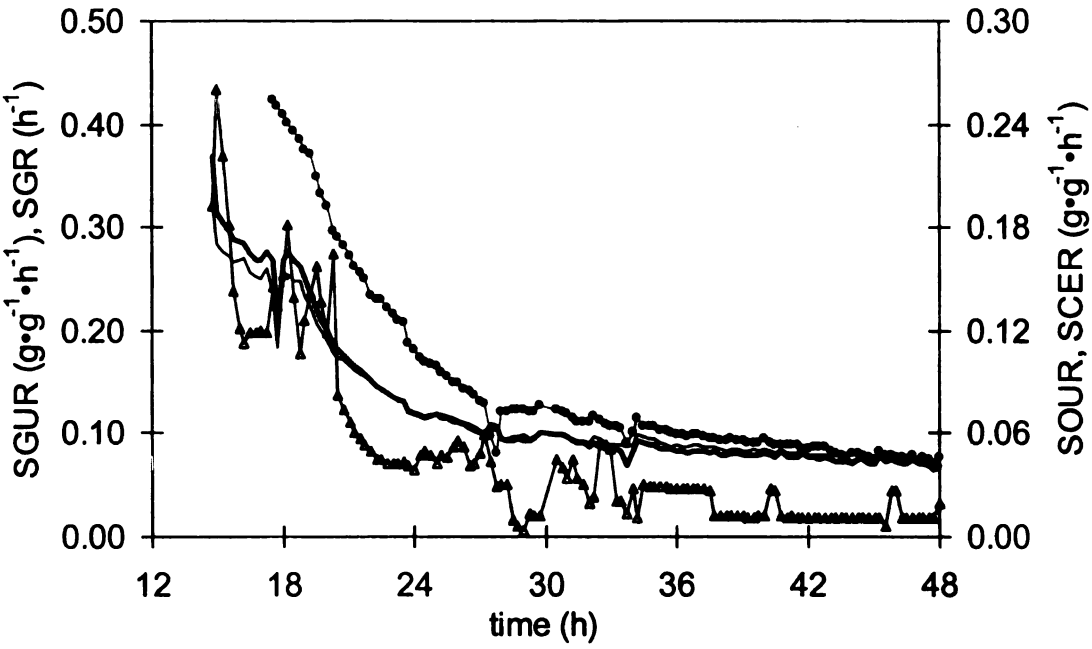

Figure 61. Select online-calculated 8 L QP1.1/pKD12.138A PS variable profiles for standard glucose-limited fed-batch fermentations. SOUR —— , SCER —— , SGUR —•— , SGR —▲— .

1 L KB and PS Variable Controlled Fermentations.

The KB control system developed for the 1 L scale described above was implemented for fed-batch fermentation control. The objective of the PS variable control was to provide a similar OTR ramp to that previously observed under glucose-rich fermentation conditions (Chapters 2 and 3), while permitting a glucose-limited culturing environment. The Phase 1 and Phase 2 control methodologies of the KB control system were identical to those utilized in the standard glucose-limited culturing of QP1.1/pKD12.138A, with the addition of relevant rules. Phase 3 maintained the SOUR (Equation 16) constant by compensating for increasing biomass concentration with an increasing OTR. Due to the inability to isolate PID control of the impeller rate from the Bioflo IIc unit, GFR was used to maintain the SOUR constant. As the SOUR declined due to increased biomass concentration (Equation 16), an increasing GFR caused a decrease in the D.O. concentration. As the D.O. concentration declined, the impeller rate was increased by the Bioflo IIc to maintain the D.O. concentration constant at the set point. The control system automatically increased the airflow rate as required to maintain the culture aerobic if the impeller rate approached the physical maximum of the system. SOUR set point changes were automatically made based on glucose accumulation, OTR considerations, etc. The initial SOUR set point (0.13-0.15 $g \cdot g^{-1} \cdot h^{-1}$) was automatically set by the control system. Phase 4 maintained the CER (g CO_2/h) constant via PID manipulation of the GFR. At the onset of Phase 4, the CER set point was ramped from the final Phase 3 value (typically about 5-5.3 g/h, or a SCER of about 0.13 $g \cdot g^{-1} \cdot h^{-1}$) to the initial Phase 4 CER set point value of 4 g/h (SCER of about 0.10 $g \cdot g^{-1} \cdot h^{-1}$) in the span of an hour.

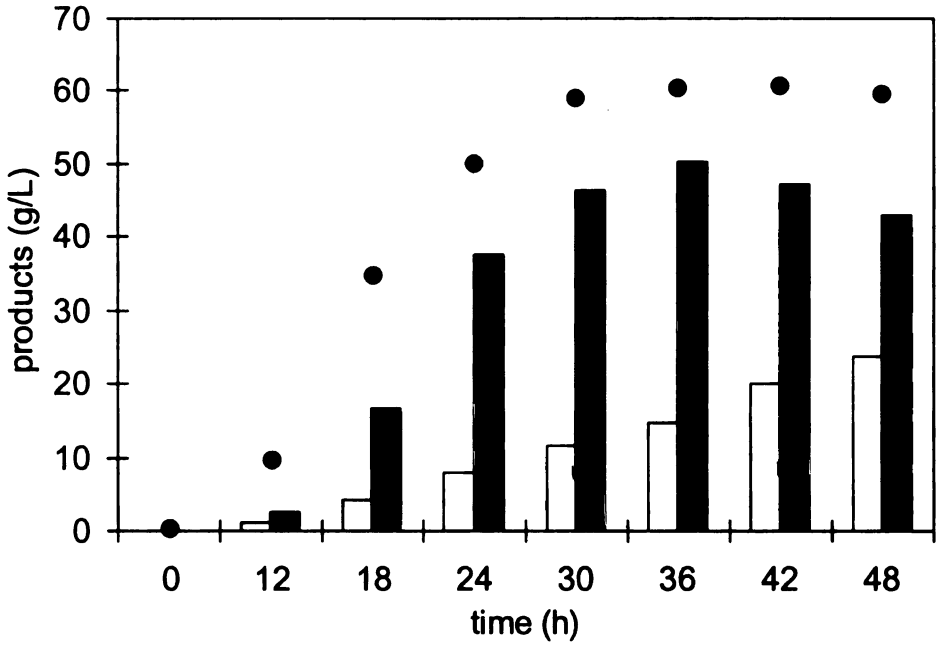

Figure 62. 1 L QP1.1/pKD12.138A PS variable/KB-controlled fed-batch fermentation time course. Quinic acid□, DHQ■, cell mass●, in g/L.

Table 31. DAHP synthase and shikimate dehydrogenase enzyme activities (μmol/min/mg) for 1 L PS variable/KB-controlled QP1.1/pKD12.138A.

		specific activity (μmol/min/mg)			
Entry	Enzyme	12 h	24 h	36 h	48 h
1	DAHP synthase	0.94	2.1	0.75	0.30
2	shikimate dehydrogenase	13	11	14	16

Despite the use of the advanced control methodology, DHQ formation predominated during the culturing of QP1.1/pKD12.138A. The final DHQ titer of 43 g/L (maximum of 50 g/L at 36 h) and quinic acid titer of 24 g/L were similar to the concentrations observed under glucose-rich culturing conditions (Figure 47). The 8.3% yield (mol/mol) of quinic acid and 17% yield (mol/mol) of DHQ reflected the shift in

product mixture as well. The QA:DHQ (0.54) was diminished an order of magnitude relative to that previously observed (Figure 56), and was even lower than that observed for glucose-rich culturing conditions (0.74, Figure 47). The shikimate dehydrogenase activities (Table 31, entry 2) were again diminished relative to those observed for standard glucose-limited conditions (Table 29), while DAHP synthase activity increased markedly.

The data acquired from the fermentation in Figure 62 was used to train the ANN and the fermentation was subsequently repeated. The resulting time courses of the fermentation products were similar to those in Figure 62, and afforded close approximation of fermentation concentrations by online ANN predictions (Figure 63).

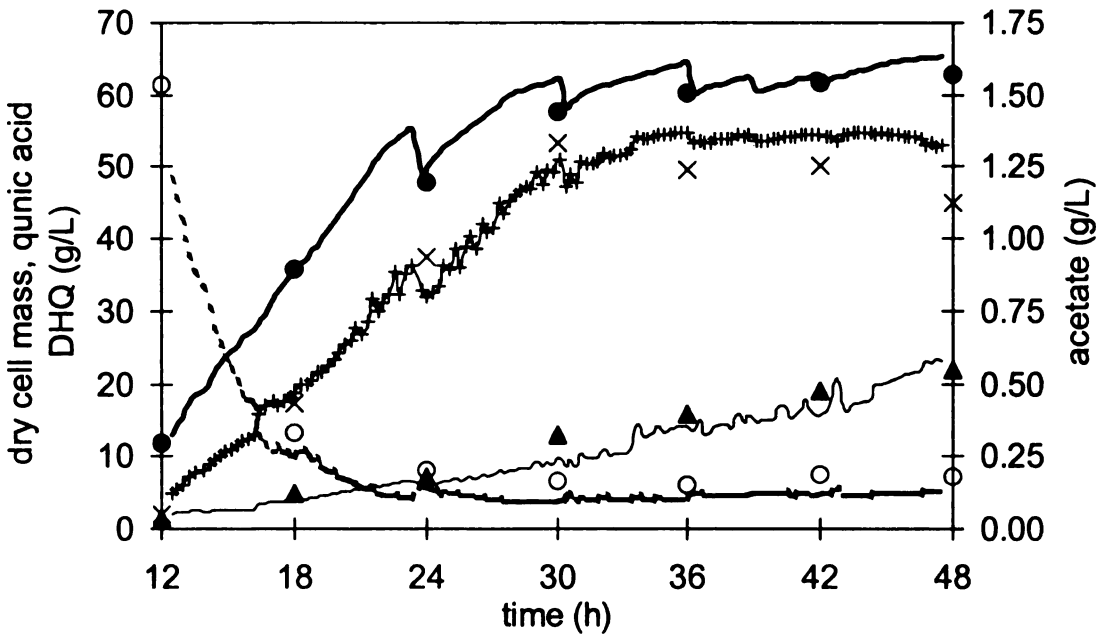

Figure 63. Actual (symbol) and ANN-predicted (line) concentration profiles for quinic acid (▲, ——), DHQ (× , ++++), cell mass (● , ——), and acetate (○ , ·····) in g/L for PS variable/KB-controlled 1 L fed-batch fermentation of QP1.1/pKD12.138A.

The dramatic drop in QA:DHQ was perplexing given the confirmation of glucose-limited conditions during the KB control of fed-batch fermentations via automatic and operator initiated MGA checks throughout Phase 3 and Phase 4. Furthermore, the decrease in shikimate dehydrogenase activity seemed consistent with glucose-rich conditions as well. These observations led to an investigation of the pseudo-steady-state glucose concentrations during the various culturing conditions examined to this point.

Despite the persistent metabolite equilibrium problem, the control system accomplished an OTR profile similar in shape, albeit reduced in magnitude, to that of the glucose-rich conditions while maintaining a glucose-limited environment (Figure 64). Additionally, the magnitude of the typical GFR profile (Figure 65) for glucose-limited fermentations was increased for the duration of the fermentation, commensurate with the

enhanced OTR. Enhanced glucose feeding was particularly prevalent during Phase 3 (between 12 h and 18 h). The decrease in the KB-controlled OTR prior to the onset of Phase 4 (X of 40 g/L) was mediated by MGA checks that automatically adjusted the SOUR set point to prevent glucose accumulation in the medium, maintaining glucose-limited conditions for the duration of the control phase.

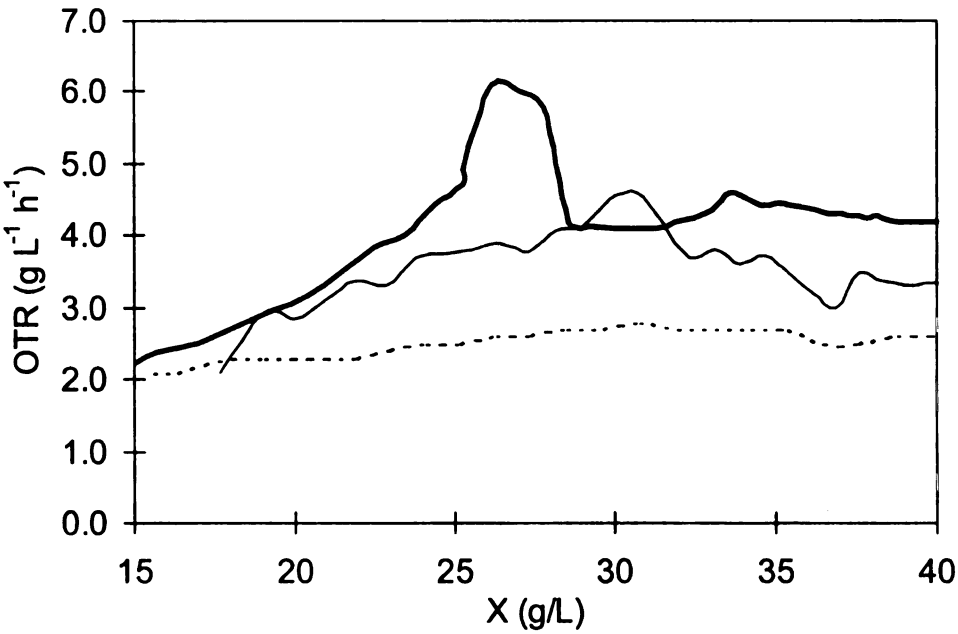

Figure 64. Oxygen transfer rate profiles as a function of biomass concentration (X) for glucose-rich —— , KB-controlled (Phase 3) —— , and standard glucose-limited ----, fed-batch fermentation of QP1.1/pKD12.138A.

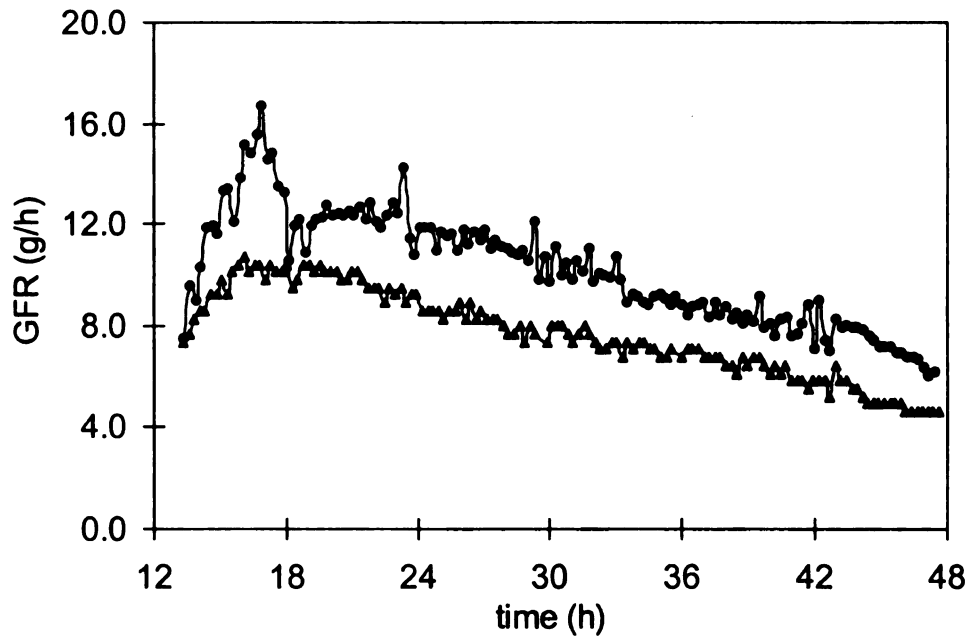

Figure 65. Typical GFR profiles for standard glucose-limited —▲—, and KB/PS variable controlled —●—, fed-batch fermentations.

Revisiting the Glucose-Dependent Nature of Metabolite Equilibrium.

To this point, two events had led to significant shifts in the QA:DHQ under glucose-limited fed-batch fermentation conditions from the original QA:DHQ observed for QP1.1/pKD12.138A (Figure 44). The first was the switch from the BBB Biostat MD platform to the NBS Bioflo IIc platform. The second was the utilization of the KB control system instead of the standard glucose-limited control scheme on the Bioflo IIc platform. Since the glucose-limited to glucose-rich culturing condition change on the BBB Biostat MD had resulted in a large shift in the QA:DHQ, glucose was once again suspect as the causative agent in the unfavorable equilibrium observed.

It was hypothesized that platform and control strategy changes may have influenced the pseudo-steady-state glucose concentration profiles of fermentations. To

this end, the pseudo-steady-state glucose concentration profiles of the various control schemes and platforms (Figure 66) were quantified from culture supernatant samples removed for product assays using a YSI 2700 Biochemical Analyzer.

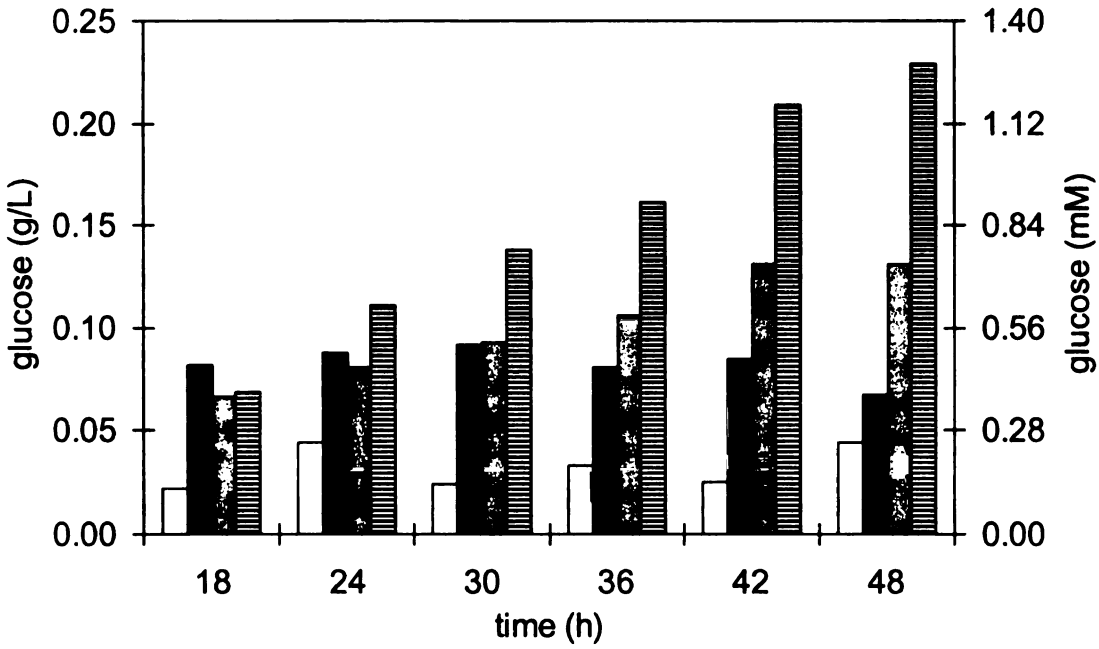

Figure 66. Typical QP1.1/pKD12.138A glucose concentration profiles for glucose-limited (□, 15:1.0 QA:DHQ) 1 L BBB Biostat MD fermentations, glucose-limited (■, 5.3:1.0 QA:DHQ), modified KB-controlled (□, 2.4:1.0 QA:DHQ), and KB-controlled (▤, 0.54:1.0 QA:DHQ) 1 L NBS Bioflo IIc fermentations.

Based on these results, it was hypothesized that if the KB control scheme could be modified to reduce the pseudo-steady-state glucose concentration profile to a level intermediate to those previously observed on the Bioflo IIc, then the metabolite equilibrium might shift back towards quinic acid, at least in part, at the expense of DHQ. The KB control scheme was subsequently modified to this end, such that the Phase 4 control of CER had a dynamic, linearly declining set point. The set point was still subject to rule intervention/decrements and the control system was otherwise unchanged. The

initial CER set point was again derived from the end of Phase 3 and was about 4.8 g/h. The control strategy linearly ramped the set point from 4.8 g/L at 20 h to 3.4 g/h by 46 h before the KB control system intervened to prevent glucose accumulation and fixed the CER set point at 3.2 g/h for the remainder of the fermentation. Evaluation of QP1.1/pKD12.138A under this new set of fermentation conditions (Figure 67) largely realized the expectations set forth. The pseudo-steady-state glucose concentration profile (Figure 66) was observed to decrease relative to the previous KB control conditions. Quinic acid accumulation increased from 24 g/L (Figure 62) to 47 g/L, while DHQ decreased from 43 g/L at 48 h (Figure 62) to 19 g/L. As such, the QA:DHQ (2.4) was intermediate to that previous observed for standard glucose-limited conditions (5.3) and KB-controlled conditions (0.54) on the Bioflo IIc. In addition to the shift in metabolite equilibrium, the shikimate dehydrogenase activities for QP1.1/pKD12.138A (Table 32, entry 2) recovered to a level similar to standard glucose-limited conditions (Table 29, entry 2).

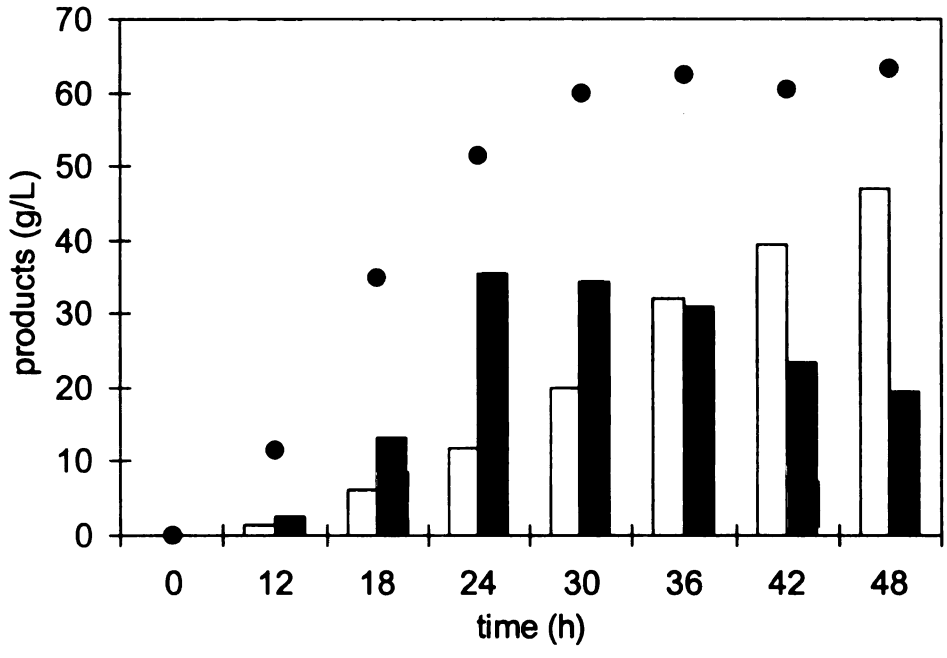

Figure 67. QP1.1/pKD12.138A 1 L modified PS variable/KB-controlled fed-batch fermentation time course. Quinic acid□, DHQ■, cell mass●, in g/L.

Table 32. DAHP synthase and shikimate dehydrogenase enzyme activities (μmol/min/mg) for modified 1 L PS variable/KB-controlled QP1.1/pKD12.138A.

		specific activity (μmol/min/mg)			
Entry	Enzyme	12 h	24 h	36 h	48 h
1	DAHP synthase	0.29	0.48	0.11	0.081
2	shikimate dehydrogenase	15	15	22	28

Dynamic Fed-Batch Fermentation Model.

The dependence of glucose concentration (S) on OTR is evident if the coupled, conventional fed-batch fermentation mass balances for glucose (Equation 32) and oxygen (Equation 33) are written in terms of Monod kinetics.[112i,152]

Equation 32.

$$\frac{dS}{dt} = \left(\frac{F_G}{V}\right)(S_f - S) - SGUR_{\max}\left(\frac{S}{K_S + S}\right)\left(\frac{C_O}{K_O + C_O}\right)X$$

Equation 33.

$$\frac{dC_O}{dt} = \left(\frac{F_G}{V}\right)(C_{Of} - C_O) + k_L a(C_L^* - C_O) - SOUR_{\max}\left(\frac{S}{K_S + S}\right)\left(\frac{C_O}{K_O + C_O}\right)X$$

Equation 34.

$$F_G = F_{SS} + K_C\left(E(t) + \frac{1}{\tau_I}\int E(t)\right)$$

Equation 35.

$$\frac{dV}{dt} = 0.6F_G$$

Equation 32 and Equation 33 were incorporated into a previously developed dynamic fed-batch fermentation model.[153] The model was encoded in MATLAB® (Appendix C) and solved numerically. Model parameters are defined in Appendix C. The model consisted of three coupled ordinary differential equation mass balances, a glucose balance (Equation 32), an oxygen balance (Equation 33), and a volume balance (Equation 35). The model included a PID control equation (Equation 34) to calculate the glucose feed rate. Model assumptions included Monod kinetics for substrate and oxygen consumption, an approximate exponential decay for the maximum SGUR ($SGUR_{max}$),[112b] and that the biomass formation rate was independent of the glucose and oxygen concentrations observed under the conditions examined. The parameter "b" accounted

for the liquid fraction of the glucose feed. The model was solved for glucose-limited fed-batch fermentation conditions altered from the standard conditions by increasing the impeller rate to increase the OTR and compared to experimental data. The model predicted that the pseudo-steady-state glucose concentration should increase with increasing k_La (Figure 68 and Figure 69). The model also predicted that glucose concentrations would increase over time at fixed OTR (k_La) conditions (Figure 68 and Figure 69). If the k_La and controller gain were sufficiently high (e.g., 650 h^{-1} and 0.8 respectively), glucose was predicted to accumulate (1.5 g/L) late in the fermentation (Figure 69). The prediction trend agreed with the experimental observation of glucose accumulation by 48 h (14 g/L, point not shown) at an estimated k_La of 650 h^{-1}. The results suggest the pseudo-steady-state glucose concentration increases with increasing OTR, which agrees with the experimental data in Figure 66.

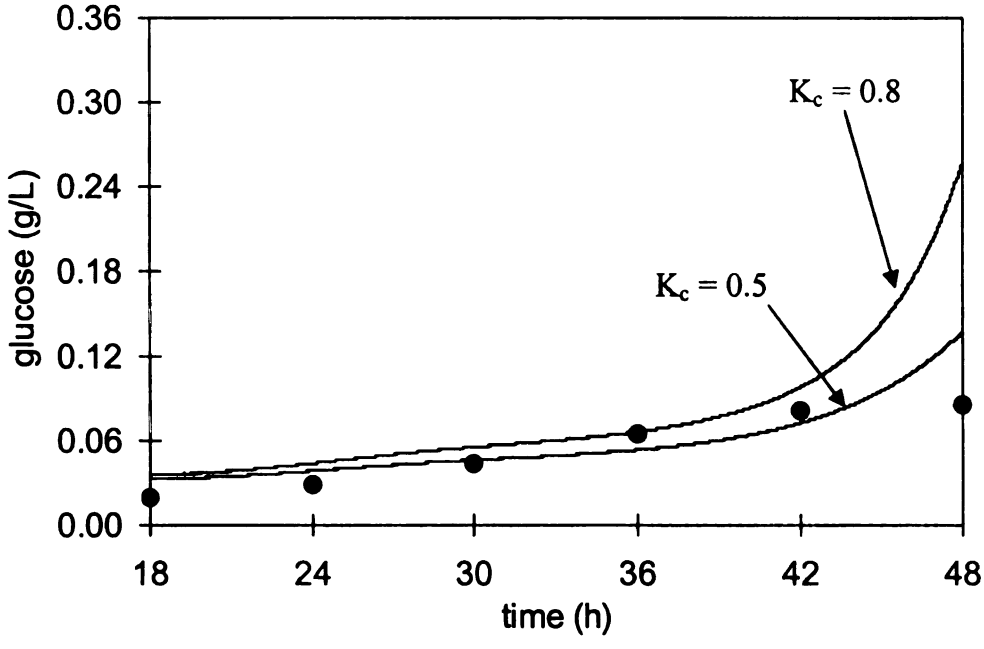

Figure 68. Predicted (——) and experimental (●) glucose concentrations for an estimated k_La of 500 h^{-1}.

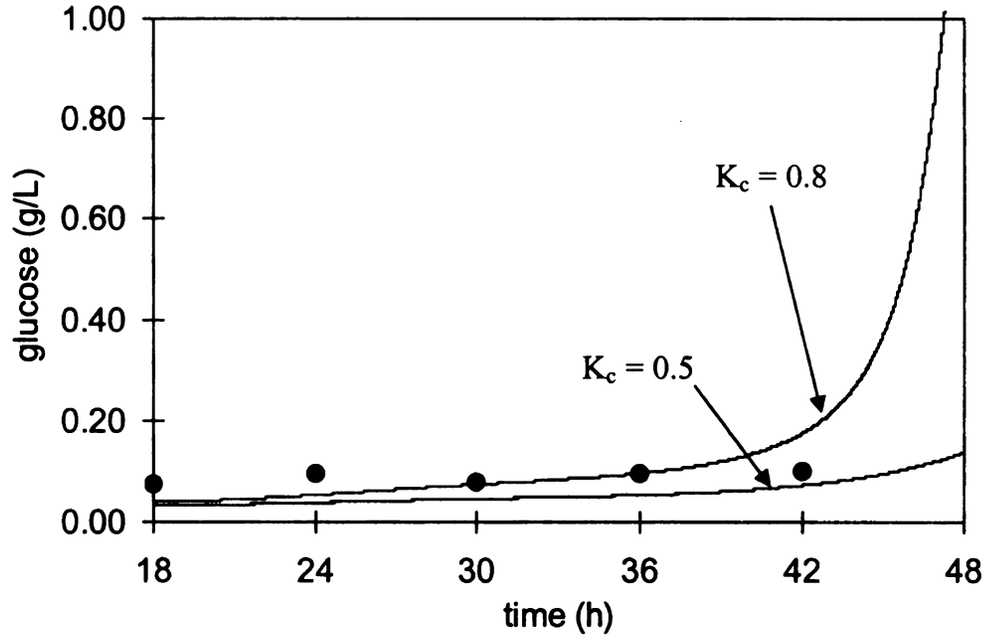

Figure 69. Predicted (——) and experimental (●) glucose concentrations for an estimated k_La of 650 h^{-1}.

Preparation for 8 L KB-controlled Fermentations: Microsparging Implementation.

The ability of microbubbles to enhance the mass transfer rate of sparingly soluble gases to liquid has previously been discussed (Chapter 1). Microbubble sparging was employed as an OTR enhancement technique in anticipation of 8 L KB-controlled fermentation OTR limitations. The in situ microbubble generation technique was chosen to augment conventional oxygen transfer methodologies in order to avoid inhibitory surfactant-biocatalyst interactions and volume increases associated with another liquid (surfactant) stream input to fed-batch fermentations. Additional volume increases would dilute product concentrations and could decrease the culturing time required to reach the reactor's capacity. Decreases in culturing duration would further exacerbate decreases in product titers attendant with unfavorable surfactant-biocatalyst interactions. The 10 L vessel was fit with a stainless steel, 0.5 μM pore size frit (3/8" OD x 6", Mott

Corporation). The microsparging and conventional sparging rates were independently modulated.

The impact of microsparging upon the impeller rate required to maintain a desired D.O. concentration set point was initially tested during standard glucose-limited fed-batch fermentations. The tests were performed in two ways. In the first test, the microbubble sparging was initiated after the maximum airflow rate was attained, but before the initial glucose charge was depleted. The impeller rate varied to maintain the D.O. concentration constant. The total airflow rate (conventional + microsparge) to the reactor was maintained at 1.0 vvm (8 L/min). Step changes (2 L/min) were utilized to vary the ratio of the two sparging rates. After a sparging rate step change, the controller adjusted the impeller rate until the D.O. concentration stabilized at the set point (10% of air saturation). The time required to attain pseudo-steady steady was between one and two minutes typically, before the next step change took place. This method had the advantage of glucose-rich culturing, which precluded substantial D.O. concentration oscillations. The drawback of this method was that it was done during a high culture growth period when the oxygen demand was highly dynamic.

The second microsparging test was performed late in fermentations (e.g., $t \geq 36$ h), when cellular metabolism transients were reduced. In this method, the GFR to the reactor was fixed at the average value from the preceding quarter hour, and the previously fixed impeller rate was manipulated to control the D.O. concentration at the set point (10% of air saturation). The ratio of the two spargers was once again varied while the overall airflow rate to the reactor was maintained at 8 L/min. The impeller rate achieved a new pseudo-steady-state value following each step change in about two or

three minutes. This method had the advantages of constant biomass concentration during step changes and minimal D.O. concentration oscillations during this portion of the fermentation.

The effect of microsparging on impeller rate was identical for both testing methodologies. Microsparging substantially decreased the impeller rate required to maintain a constant D.O. concentration (Figure 70). The decrease in impeller rate requirement when only microsparging was employed (8 L/min microsparging, 0 L/min conventional sparging) was transient. Initial microsparging-induced reductions in impeller rate gained when only microsparging was employed were lost after a few minutes. This is consistent with the notion that highly agitated vessels result in significant gas hold up when microsparging is employed.[67] Therefore, conventionally generated bubbles are required to sweep out spent microbubbles from the reactor via coalescence.[67] The lower limit of 3:1 for the sparging split (microsparging:conventional sparging) in the previously defined 8 L KB control system was based on the need for microbubble removal. Microsparging was employed in all KB-controlled 8 L fed-batch fermentations.

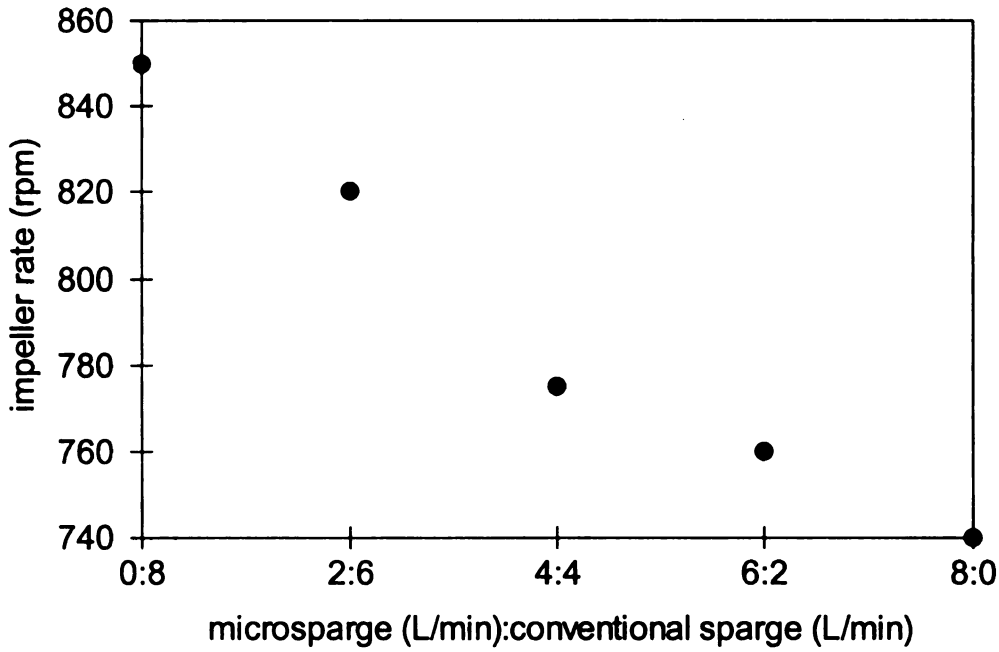

Figure 70. Effect of in situ microsparging on the impeller rate required to maintain a 10% D.O. concentration. Impeller rate (●).

8 L KB-controlled Fermentations.

The potential success of 8 L KB-controlled fermentations to amplify quinic acid titers in the absence of substantially enhanced DHQ concentrations was doubtful since 1 L fermentations failed to improve the QA:DHQ. The objective was to scale up the PS variable control methodology to 8 L under the supervision of the 8 L KB control system previously described. The Phase 1 and Phase 2 control methodologies of the KB control system were identical to those utilized in the standard glucose-limited culturing of QP1.1/pKD12.138A, with the addition of the rules listed in the KB control system definition. Phase 3 maintained the SOUR (Equation 16) constant by PID control of the impeller rate. PID control of the GFR maintained the D.O. concentration at the set point (10% of air saturation). As the SOUR declined due to increased biomass concentration,

the impeller rate increased to maintain SOUR constant. As the D.O. concentration increased due to increased impeller rate, the GFR increased to reduce the D.O. concentration back to the set point. Phase 4 maintained the CER constant by PID manipulation of the GFR, with D.O. controlled by PID manipulation of the impeller rate.

The application of KB control to 8 L fed-batch quinic acid fermentations progressed largely as expected, with DHQ formation still accounting for a significant carbon drain (Figure 71). The final quinic acid (44 g/L) and DHQ (19 g/L) titers were very similar to those of the modified 1 L KB-controlled fed-batch fermentation conditions (Figure 67). The QA:DHQ was 2.2 which was also similar to the 1 L modified KB control result of 2.4. OTR limitations were experienced on the 8 L scale, even in the presence of microsparging. Phase 3 of the KB control system consistently ramped the conventional airflow and microsparger rates to their maximum values during Phase 3, even when the default maximum for each rate was increased from 8 L/min to 10 L/min, providing a combined total sparger rate of 2.5 vvm. This combined sparger rate was still insufficient to meet the OTR demands of KB-controlled cultures and the Phase 3 SOUR set point was automatically decremented in order to maintain cultures aerobic during fermentations. The high total airflow rate was maintained throughout Phase 4 as well, and the control system decremented the CER set point in response to specific rule actions as required.

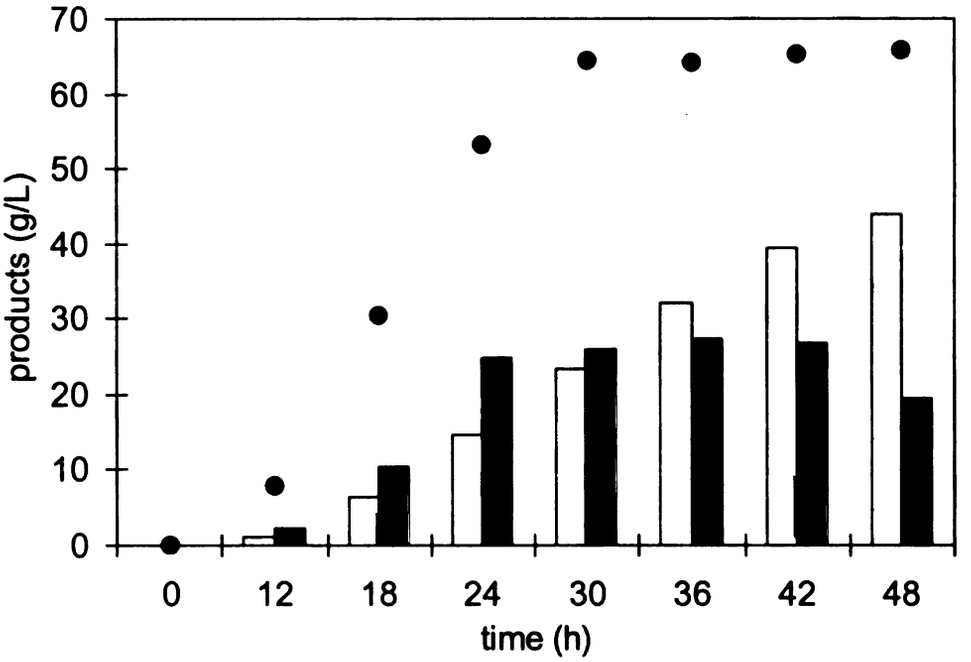

Figure 71. 8 L KB-controlled fed-batch fermentation product time course. Quinic acid □, DHQ ■, cell mass ●, in g/L.

Table 33. DAHP synthase and shikimate dehydrogenase enzyme activities (μmol/min/mg) for 8 L PS variable/KB-controlled QP1.1/pKD12.138A fermentations.

		specific activity (μmol/min/mg)			
Entry	Enzyme	12 h	24 h	36 h	48 h
1	DAHP synthase	0.32	0.11	0.18	0.14
2	shikimate dehydrogenase	12	16	33	38

The glucose concentration profiles of 8 L KB-controlled fed-batch fermentations were analyzed by coupling a Flownamics sampling probe with the YSI 2730 online monitoring and control accessory of the YSI 2700 to provide online glucose concentration sampling capability. The glucose concentration was analyzed every hour

automatically, and the resulting glucose concentration profile was similar to that of the modified 1 L KB-controlled fed-batch fermentation of QP1.1/pKD12.138A (**Figure 72**).

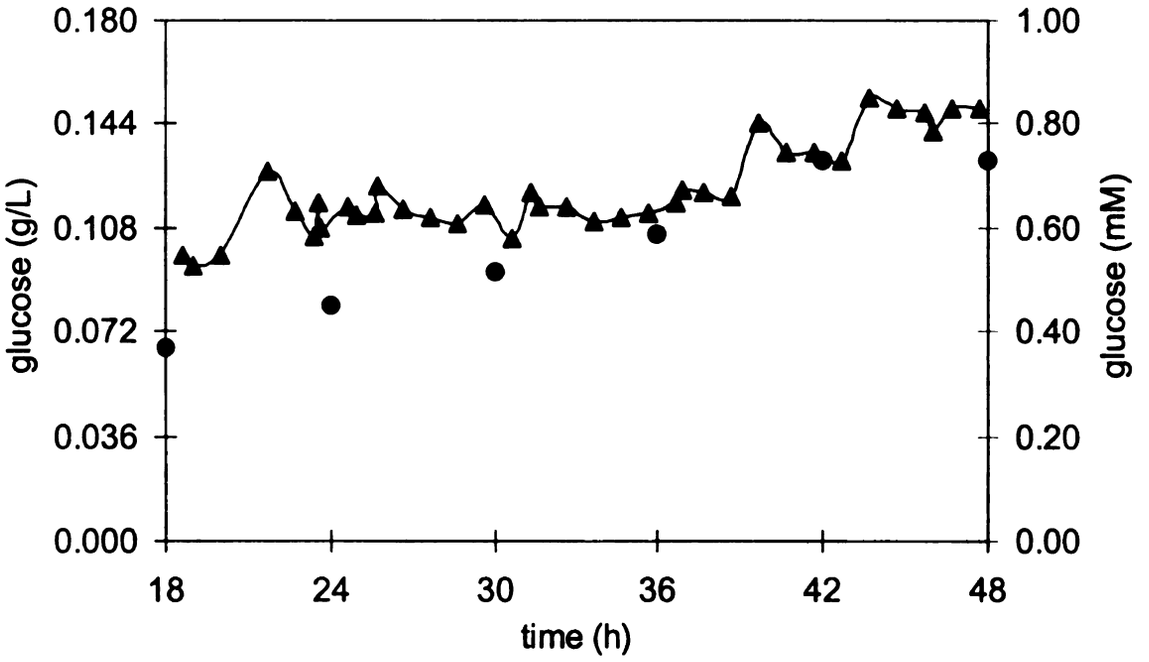

Figure 72. Glucose concentration profile comparison between 8 L KB-controlled and 1 L modified KB-controlled fed-batch fermentations of QP1.1/pKD12.138A. 8 L profile —▲—, 1 L profile ● .

Data acquired from a previous fermentation was used to train the ANN. Pseudo-online ANN predictions for quinic acid and DHQ that had previously shown excellent agreement with offline assays displayed significant deviations, especially at times subsequent to 30 h (Figure 73). This was not entirely surprising given the frequency and magnitude of control loop set point changes automatically initiated by the KB control system to compensate for the Phase 3 and Phase 4 OTR limitations and detected onsets of glucose accumulation experienced. The acetate excretion on 8 L KB-controlled fed-batch fermentations was rather high. Although the acetate concentration prediction profile was qualitatively correct, the magnitude was in substantial error relative to the experimental data subsequent to 24 h. Biomass concentration predictions closely approximate offline

assays. Accurate biomass prediction permitted accurate online calculation of the SOUR, the SCER, and the SGUR, resulting in correct KB control decisions based on PS variable calculations.

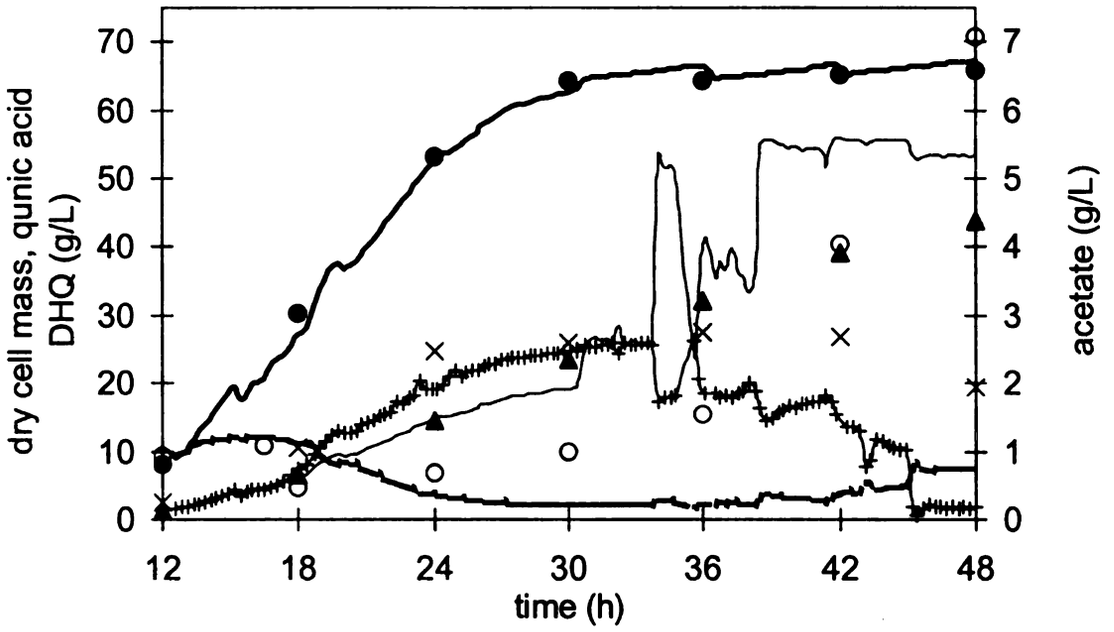

Figure 73. Actual (symbol) and ANN-predicted (line) concentration profiles for quinic acid (▲, ——), DHQ (× , ++++), cell mass (● , ——), and acetate (○ , ·····) in g/L for PS variable/KB-controlled 8 L fed-batch fermentation of QP1.1/pKD12.138A.

The high acetate accumulation during KB-controlled fed-batch fermentations was surprising, especially in light of glucose-rich fermentation results (Figure 47) where only 2.3 g/L of acetate was accumulated. Acetate accumulation was 7.1 g/L by 48 h. The acetate concentration neither constituted a significant drain on realizable hydroaromatic titers nor did it appear to inhibit the final biomass and hydroaromatic concentrations obtained.

Despite the acetate accumulation, KB-controlled 8 L fed-batch fermentations were capable of closely reproducing the 48 h 1 L modified KB-controlled fed-batch fermentation titers and QA:DHQ. The manual override of the MMI linked to the $SAER_{max}$ calculation was utilized to disable the rule responsible for control action based on the $SAER_{max}$ during 8 L KB-controlled fermentations. The MMI manual override capable of disabling control actions based on quinic acid productivity was also utilized due to the discrepancy between ANN-predicted and actual quinic acid formation (Figure 73).

PS Variable Scaling.

In addition to the fermentation metabolite concentration time courses, the success of the developed control systems was also quantified in terms of their ability to modify and scale the various PS variable profiles being monitored and controlled. The 1 L and 8 L profiles of SOUR, SGUR, and SCER as a function of time for standard glucose-limited fed-batch fermentations have been previously presented (Figure 58 and Figure 61, respectively). The 1 L (Figure 74), 1 L modified (Figure 75), and 8 L (Figure 76) KB-controlled time-dependent PS variable profiles were observed to shift relative to the standard glucose-limited culturing condition profiles for 1 L (Figure 58) and 8 L (Figure 62). The approximately constant SGUR in Phase 3 of the control strategies resulted from control of the SOUR. The SCER was observed to closely track the SOUR, which has previously been observed.[112b] Differences in the SGUR, SCER, and SOUR profiles relative to the standard glucose-limited conditions were expected given the application of control methods designed to directly manipulate a PS variable (SOUR) and increased

OTR during CER control of glucose feeding. The ability to accomplish similar SOUR, SCER, and SGUR profiles via KB control at both scales, especially in Phase 3, was hampered by the 8 L OTR limitations. As such, the SOUR could not be held constant due to the automatic decrements in the SOUR set point by the control system when the physical OTR limits of the system had been obtained. Further scale up of the SOUR control developed here may therefore be impeded by OTR limitations since the 2.5 vvm airflow rate typically employed is probably not industrially feasible.

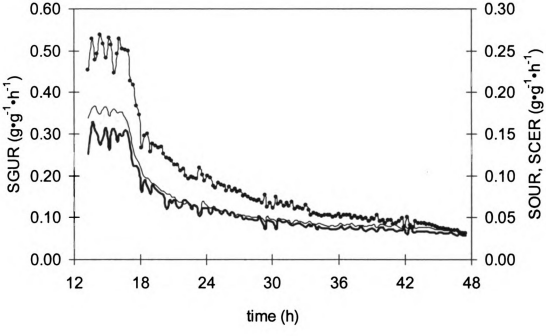

Figure 74. Online calculated 1 L KB-controlled, fed-batch fermentation PS variable profiles as a function of time. SOUR —, SCER —, SGUR —•—.

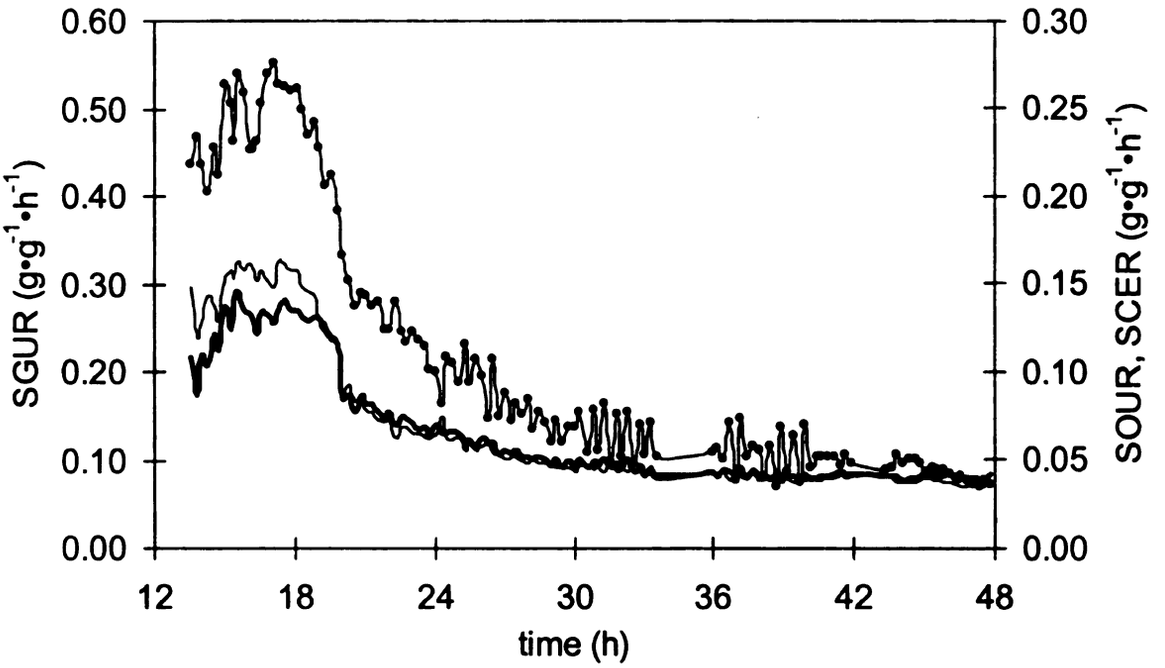

Figure 75. Online calculated 1 L modified KB-controlled, fed-batch fermentation PS variable profiles as a function of time. SOUR —— , SCER —— , SGUR —•— .

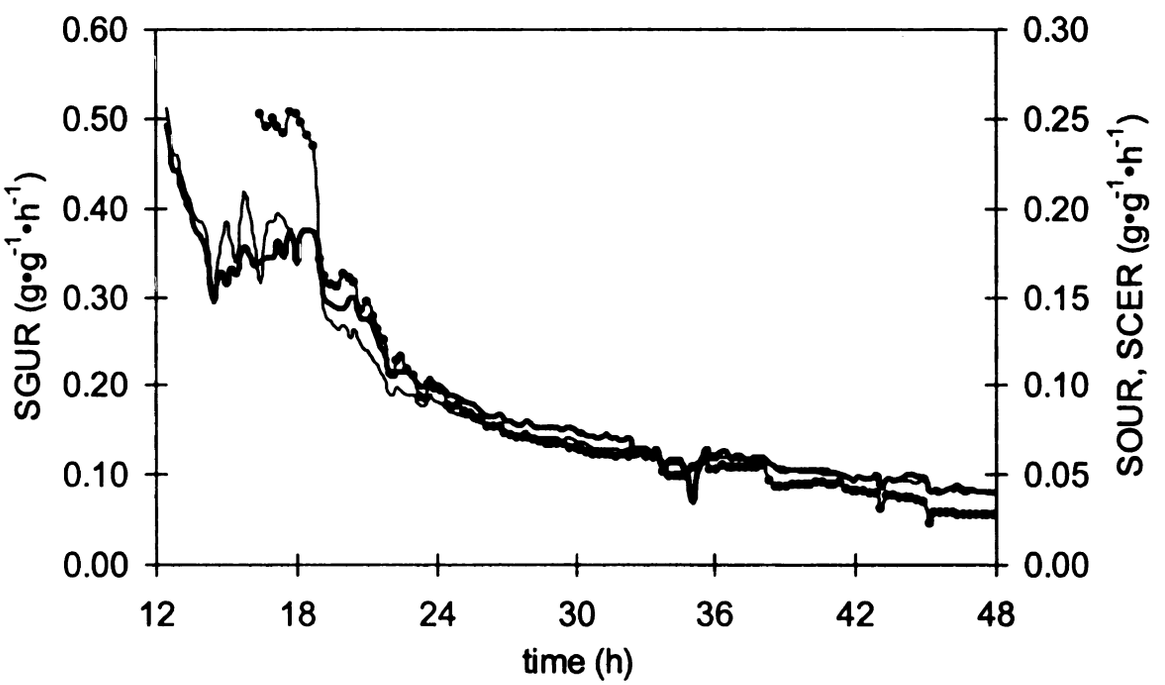

Figure 76. Online calculated 8 L KB-controlled, fed-batch fermentation PS variable profiles as a function of time. SOUR —— , SCER —— , SGUR —•— .

The 8 L KB-controlled SOUR and SCER profiles (Figure 76) were similar in magnitude and shape to the 1 L modified KB-controlled profiles (Figure 75). The direct comparison of these two conditions was more germane to PS variable control scaling than comparison of the 1 L and 8 L KB-controlled fermentations. The 1 L KB control scheme was modified to include a sliding Phase 4 CER set point to investigate the effect of pseudo-steady-state glucose profile on quinic acid-DHQ equilibrium. The comparison between the modified 1 L and 8 L KB control schemes becomes relevant since their glucose profiles (Figure 72) and metabolite concentration profiles (Figure 67 and Figure 71 respectively) were virtually identical. Comparing the SGUR profiles reveals a similar magnitude and shape at both scales, however the 8 L SGUR KB profile was slightly depressed relative to the 1 L modified KB profile past 19 h. The precipitous drop in the SGUR in Figure 76 at about 19 h corresponded to the onset of automatic SOUR set point decrements induced by OTR limitations. The 8 L SGUR dropped from about 0.50 $g \cdot g^{-1} \cdot h^{-1}$ to about 0.32 $g \cdot g^{-1} \cdot h^{-1}$. The 1 L KB-controlled SGUR also declined rapidly starting at about 17 h. This corresponded to a SOUR set point decrement due to glucose accumulation. The continued decline in the SGUR past 17.5 was induced by an automatic phase change initiated via glucose accumulation under Phase 3 control. The 8 L KB SGUR was further decreased to about 0.28 $g \cdot g^{-1} \cdot h^{-1}$ at about 21 h as a result of a second SOUR set point decrement, from whence it continued to decline via further KB control actions (e.g., phase change).

The time dependence of PS variables can be misleading in their interpretation. Due to the differences in scale and equipment, 8 L cultures generally grew slower than 1 L cultures. As such, direct comparison of PS variables in the time domain can cause the

variables compared to be out of phase. For example, the 8 L SOUR and SCER profiles depicted prior to about 16 h in Figure 76 were actually confined to Phase 2 of the control strategy (e.g., calculated but not controlled), while 1 L SOUR and SCER profiles of Figure 74 and Figure 75 were wholly contained within the KB control Phase 3 and Phase 4. PS variable evaluation can be facilitated by transforming to the biomass concentration domain as the comparison basis of 1 L and 8 L PS variable profiles. Figure 77 and Figure 78 illustrate the scale up-relevant, biomass concentration-dependent PS variable profiles of Phase 3 and Phase 4 for the modified 1 L and 8 L KB controlled fermentations respectively. The success of the control strategy to closely maintain the SGUR profile at or near 0.50 $g \cdot g^{-1} \cdot h^{-1}$ initially by controlling SOUR is evident in the biomass concentration domain. The inability to meet the OTR requirements of the 8 L cultures inevitably precluded the direct scaling of the profiles past about 32 g/L of biomass unfortunately.

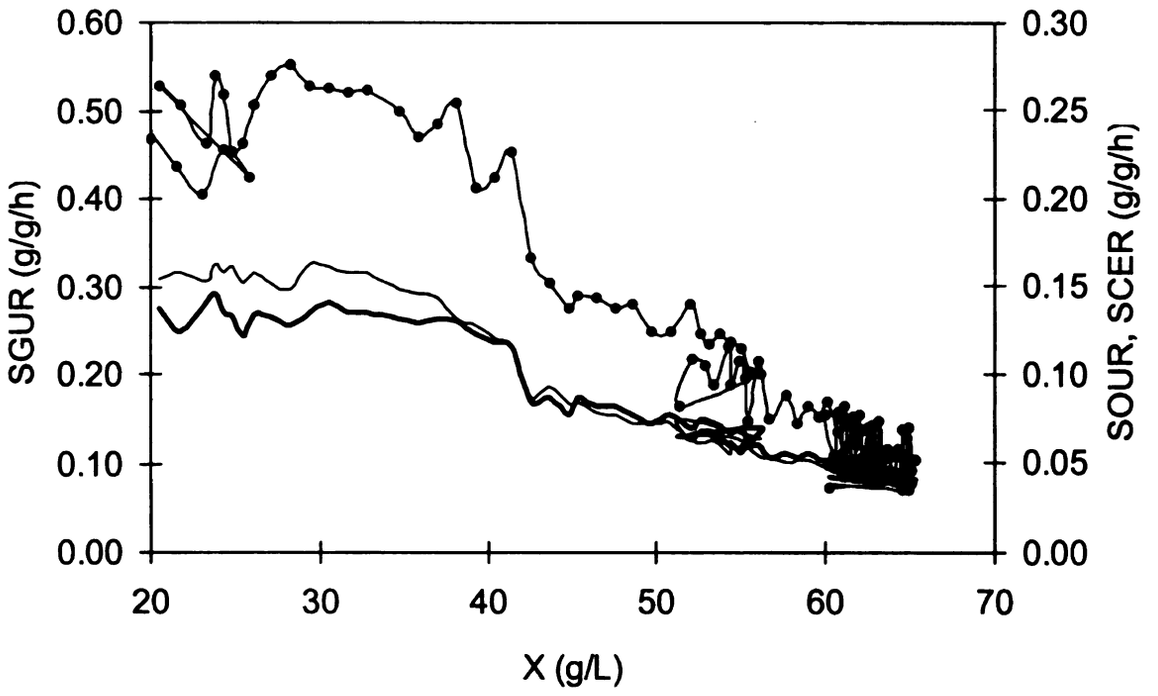

Figure 77. Online calculated 1 L modified KB-controlled, fed-batch fermentation PS variable profiles as a function of biomass concentration (X). SOUR —, SCER —, SGUR —•—.

Some transient drops recorded in SOUR, SCER, and SGUR resulted from the frequent MGA checks automatically initiated by the KB control systems, while sustained drops resulted from automatic set point attenuation or phase changes. Loop backs (e.g., Figure 78, about 38 g/L X) within the calculated PS variable profiles (e.g., Figure 77 at about 25 g/L and 58 g/L; Figure 78, at about 37 g/L) were artifacts of the online biomass concentration reinitialization process. The accumulation of values at the termini of the profiles (Figure 77 and Figure 78) reflected the effective absence of biomass concentration changes that typically occurred at concentrations around 60-65 g/L.

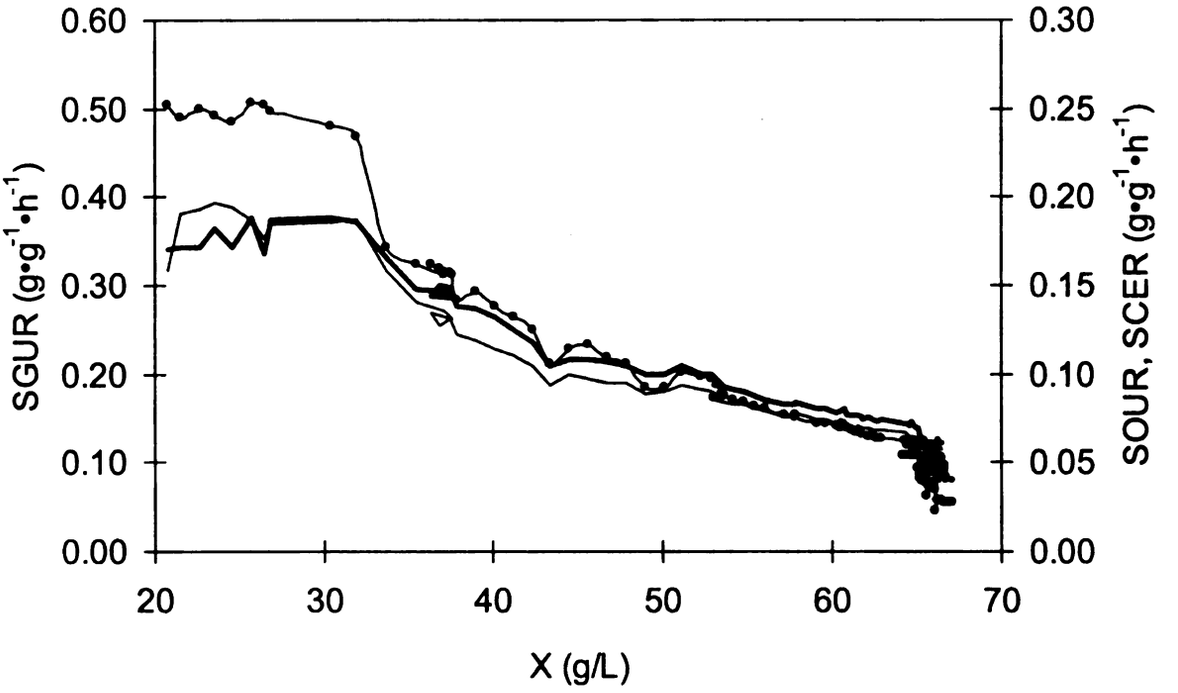

Figure 78. Online calculated 8 L KB-controlled, fed-batch fermentation PS variable profiles as a function of biomass concentration (X). SOUR —, SCER —, SGUR —•—.

Stoichiometric Modeling Considerations.

The development and implementation of a SM for prediction of biochemical pathway fluxes was described earlier in Chapter 4. The SM flux comparisons are confined to the 1 L scale between the standard glucose-limited and KB/PS variable controlled conditions due to the absence of accurate 8 L KB-controlled ANN fermentation predictions. Noise reduction in the flux data was accomplished via exponential smoothing (Appendix B).[154]

The transketolase-mediated flux to the pentose phosphate pathway (Figure 53, J4) was of interest due to the use of transketolase overexpression in the QP1.1/pKD12.138A construct. Transketolase is an enzyme in the pentose phosphate pathway that has been

overexpressed to enhance yield and titer of shikimate pathway metabolites from glucose via increased intracellular E4P availability as previously mentioned here (Chapter 1, 2, 3) and in literature.[49,51] The flux through transketolase increased between the standard glucose-limited and KB/PS variable-controlled fed-batch fermentation conditions (Figure 79), which is consistent with experimental observations of significantly increased total hydroaromatic production (Figure 56 and Figure 62) and glucose consumption (Figure 65). The flux profiles (Figure 79) tracked the GFR profiles for the respective conditions closely (Figure 65).

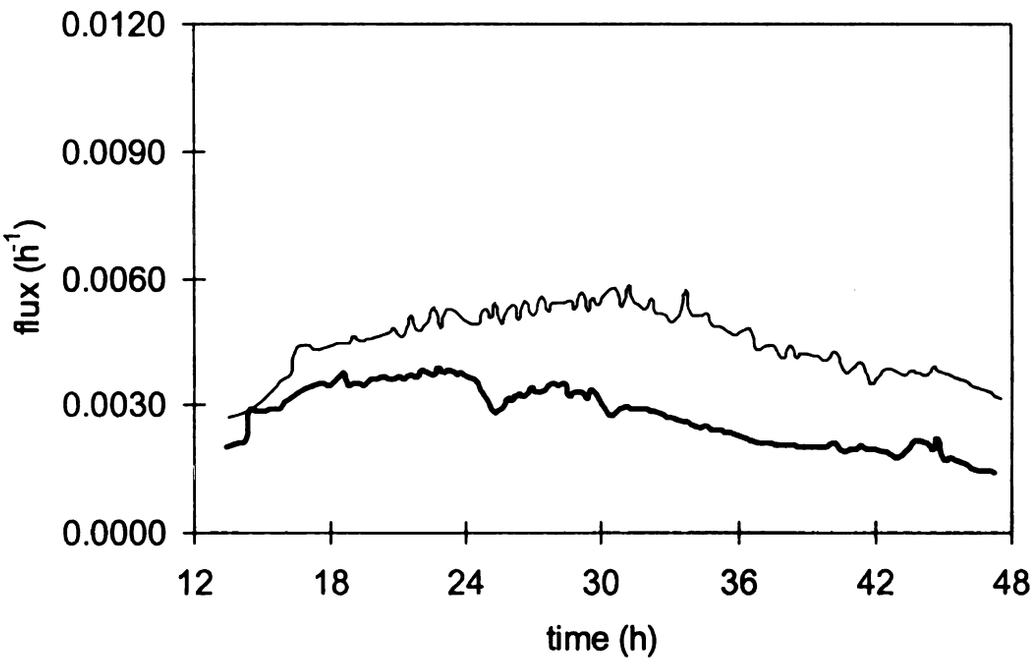

Figure 79. Predicted metabolic flux through transketolase for standard glucose-limited —, and KB/PS variable controlled —, 1 L fed-batch fermentations.

The first limiting factor in shikimate pathway metabolite overproduction in the presence of amplified DAHP synthase is E4P availability. Transketolase is known to alleviate intercellular limitations on E4P as previously discussed, at which time

intercellular PEP concentrations can become rate limiting in the absence of *pps*-mediated pyruvate recycling to PEP. The flux through pyruvate kinase (Figure 53, J13) was therefore of interest. The sign of flux predictions by a SM simply indicate the direction of the flux of interest. Therefore, if a flux is negative, the reaction predominates in the reverse of the written direction. In the case of J13, the flux was negative from the onset of glucose feeding until about 36 h (Figure 80). The cessation of biomass concentration increases at 36 h (Figure 56) alleviated the biosynthetic requirement for PEP. This coupled with the continued decline in PEP required for glucose uptake due to the declining GFR profile (Figure 65) permitted the J13 flux to become positive (e.g., PYR formed from PEP).

The formation of PYR from PEP via pyruvate kinase is an irreversible reaction. Pyruvate kinase cannot catalyze the formation of PEP from PYR as predicted by the model, and therefore requires some level of *pps*-encoded PEP synthase expression. Amplification of PEP synthase might therefore increase carbon flux directed into the shikimate pathway. Experimentally determined PEP synthase activity levels in QP1.1/pKD12.138A and QP1.1/pKD15.074A have previously been discussed (Table 22). Despite the inability of *pps* overexpression in QP1.1/pKD15.074A to significantly enhance carbon channeled into the shikimate pathway, overexpression of *pps* in QP1.1 with a titratable activity has been shown to substantially increase total hydroaromatic accumulation.[140]

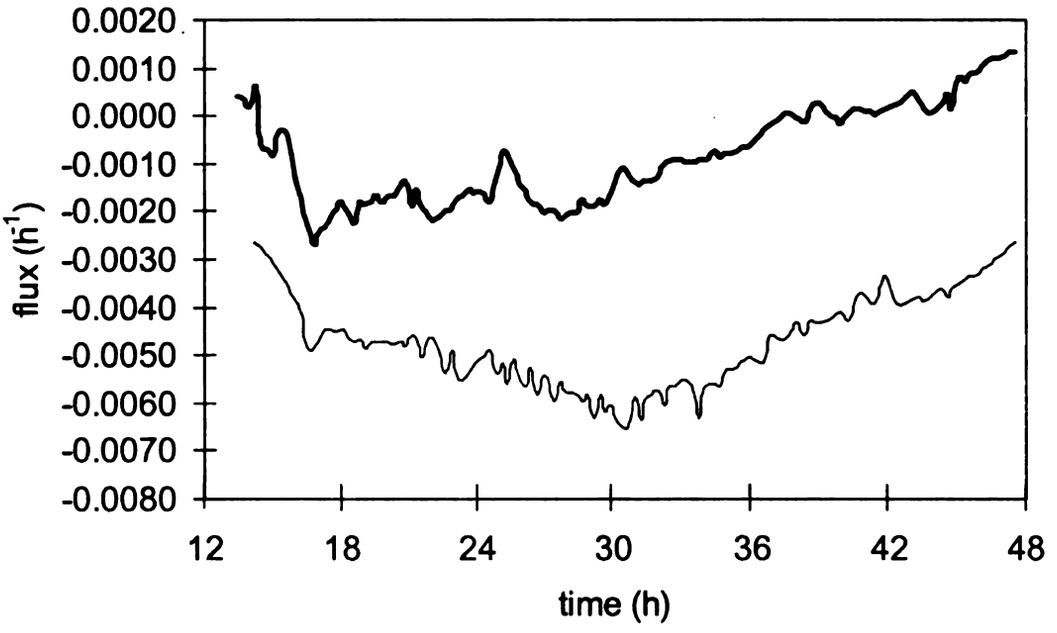

Figure 80. Predicted metabolic flux through pyruvate kinase for standard glucose-limited —— , and KB/PS variable controlled —— , 1 L fed-batch fermentations.

The apparent need for conversion of PYR to PEP to meet biosynthetic and DAHP synthase substrate requirements suggested other PEP utilizing reactions might be active. To this end, the fluxes to the TCA cycle through pyruvate dehydrogenase and citrate synthase (Figure 53, fluxes J14 and J16 respectively) and through PEP carboxylase (Figure 53, J20) were examined. The anapleurotic nature and of *ppc*-encoded PEP carboxylase has been well established,[53] and was observed to replenish TCA cycle intermediates here (Figure 81) at a modest level in comparison to the flux directed into the TCA cycle originating from PYR (J16), which constituted about 80-90% of the flux by 48 h.

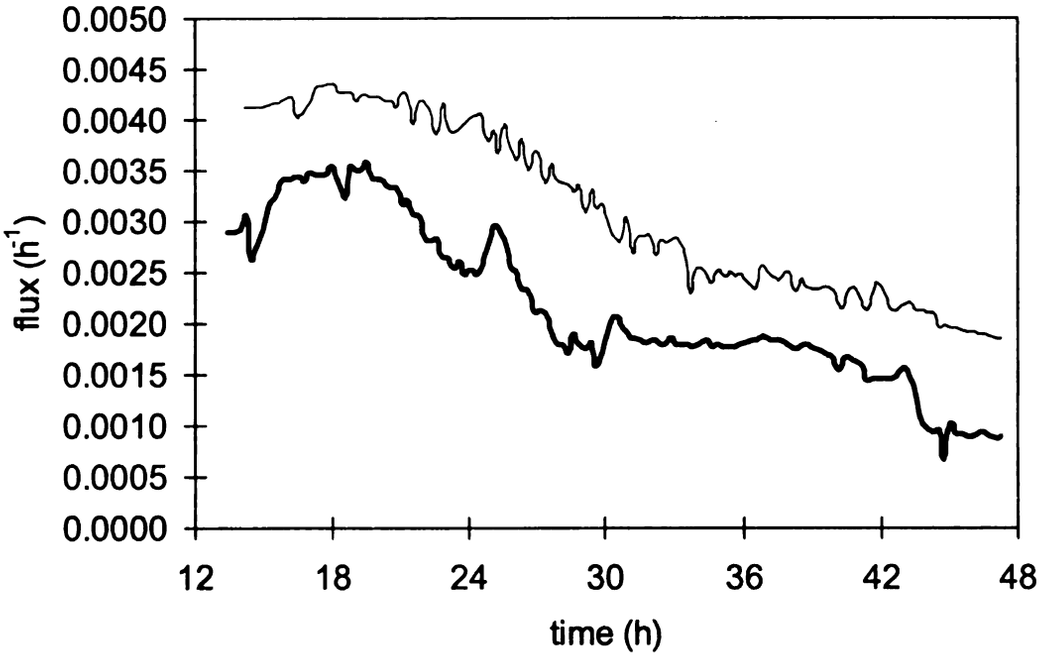

Figure 81. Predicted metabolic flux through PEP carboxylase for standard glucose-limited ——, and KB/PS variable controlled ——, 1 L fed-batch fermentations.

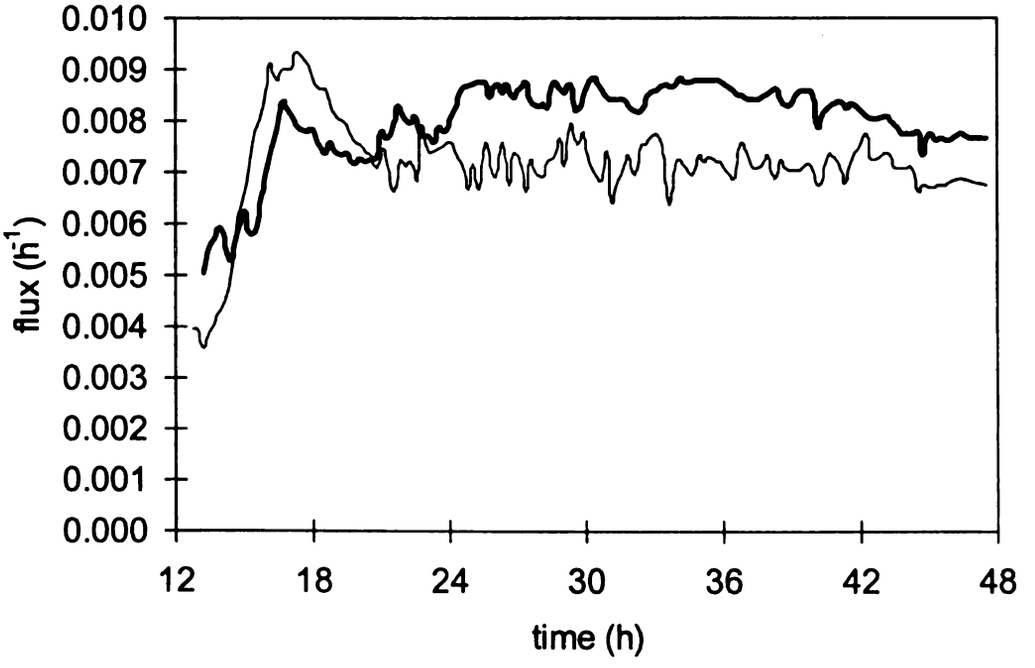

Figure 82. Predicted metabolic flux through citrate synthase for standard glucose-limited ——, and KB/PS variable controlled ——, 1 L fed-batch fermentations.

The flux of reducing equivalents to ATP through respiration was of interest from a product mixture standpoint. Excess reducing equivalents are assumed to proceed through respiration with ATP as the terminal biomolecule. The approximately equimolar accumulation of DHQ and quinic acid (Figure 44 and Figure 56) early in the growth phase (e.g., prior to 18 h) of fermentations raised the possibility that NADPH availability may have been a constraint on the conversion rate of DHQ to quinic acid due to the high NADPH requirement for protein biosynthesis.[155] The flux to ATP from NAD(P)H was directly proportional to the GFR (Figure 65) for both fermentation conditions prior to 18 h. Prior to 18 h, the flux through respiration for both culturing conditions was three to four times lower than its pseudo-steady-state value of about 0.035-0.040. The flux never reached zero however, suggesting excess reducing equivalents were available throughout the feeding portion of the fermentation. Therefore cofactor limitation most likely played a minimal role in determining the extent of DHQ conversion to quinic acid subsequent to 12 h when quantifiable flux through the shikimate pathway was developed. The flux magnitude was substantially higher relative to those previously discussed (Figure 83 relative to Figure 79-Figure 81), as multiple pathway branches fueled reducing equivalent availability.

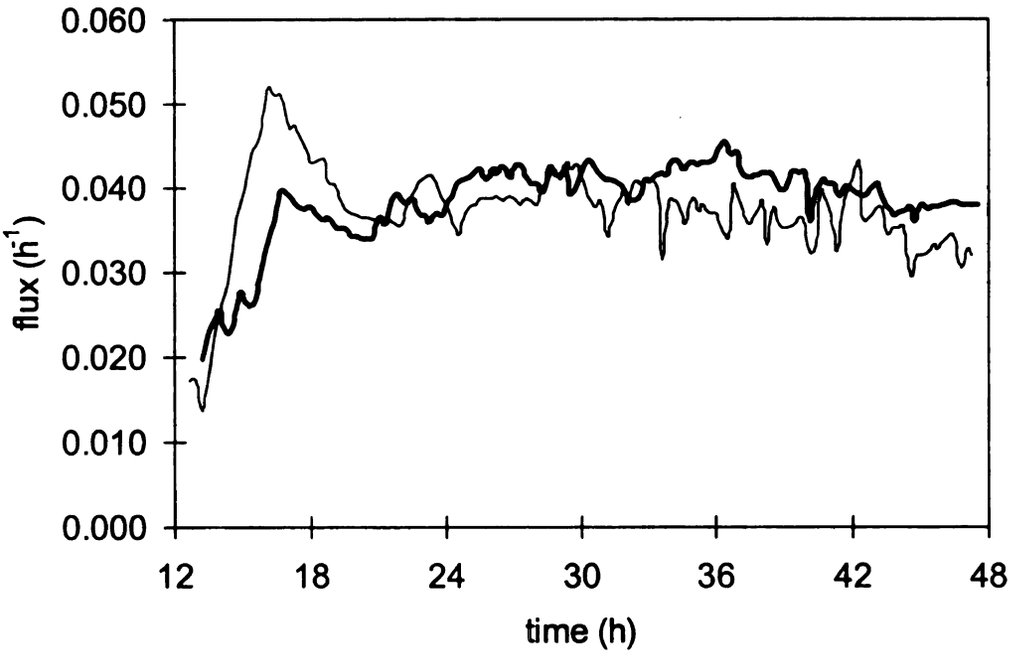

Figure 83. Predicted metabolic flux through respiratory conversion of NAD(P)H to ATP for standard glucose-limited —— , and KB/PS variable controlled —— , 1 L fed-batch fermentations.

As expected, the predicted flux through DAHP synthase (Figure 53, J6) reflected the accumulation rate of hydroaromatics (Figure 84). Both profiles increased until about 24 h as the rate of hydroaromatic production increased. Between 24 h and 30 h the standard glucose-limited fermentation flux through DAHP synthase was approximately constant while the flux through DAHP synthase for the KB-controlled fermentation continued to increase. The fluxes declined after 30 h as quinic acid and DHQ productivity and glucose flux into the system declined. The KB-controlled flux was higher than the standard glucose-limited flux throughout the fermentation and was commensurate with the enhanced hydroaromatic formation for the KB controlled fermentations (Figure 62) relative to the standard glucose-limited conditions (Figure 56).

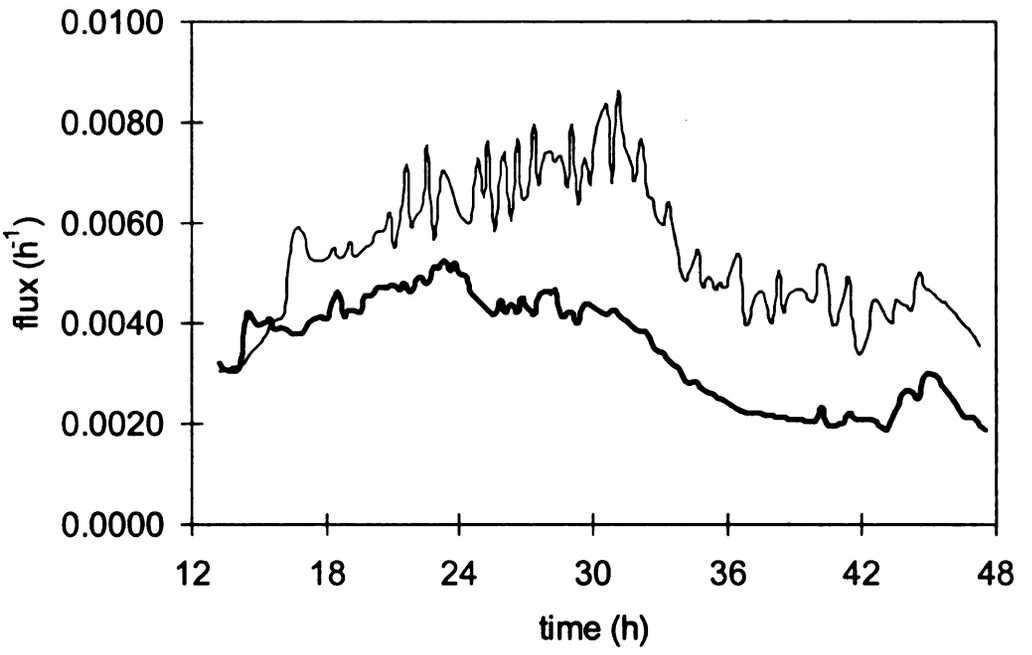

Figure 84. Predicted metabolic flux through DAHP synthase for standard glucose-limited —— , and KB/PS variable controlled —— , 1 L fed-batch fermentations.

Discussion

ANN Model.

The inability of the current data acquisition technique to communicate online glucose concentration measurements to the control systems or ANN precluded the use of this information in formulating control strategies. The use of the GFR as an input for metabolite concentration prediction was superior to offgas CO_2% after the first couple hours of feeding due to the static CO_2% profile assumed in the absence of airflow rate changes to the reactor (e.g., standard glucose-limited conditions). The use of the GFR as a predictor suffered from several drawbacks however. The GFR profile shape and magnitude varied from fermentation to fermentation, and the instantaneous GFR to the

reactor was often noisy. Online averaging of the GFR was accomplished by calculating the glucose fed to the reactor in each 0.25 h prediction interval and using it as the input to the ANN for prediction of metabolites. KB-induced set point attenuation sometimes resulted in the GFR violating the user-defined prediction limits of the ANN, and typically yielded very poor metabolite predictions (Figure 73). The strong dependence of metabolite concentration predictions upon the GFR late in fermentations (e.g., ≥30 h) was not surprising given the static nature of the second input to the ANN, namely the biomass concentration. As such, the online glucose concentration of fermentations might be better suited to metabolite prediction, or used in concert with the online GFR as inputs for the prediction of metabolite concentrations. The encoding of a custom data acquisition program or purchase of such a program capable of conveying glucose concentration data to control strategies might facilitate the culturing of *E. coli* QP1.1/pKD12.138A, or strains with similar glucose-dependent product mixtures such as SP1.1/pKD12.138A discussed in Chapter 2.

The ANN was used for online calculation and control of PS variables and SM flux calculations. The continued accuracy of ANN biomass concentration predictions, even when metabolite predictions became inaccurate, seemed to result from using the previous biomass concentration as a predictor for the next biomass concentration prediction. Attempts to capitalize upon this prediction method for quinic acid and DHQ predictions were unsuccessful. The modification of the ANN topology to accept GFR, CO_2%, and biomass concentrations as inputs for metabolite concentration predictions was also unsuccessful in achieving enhanced accuracy in pseudo-online predictions.

Rigidity of the Bioflo IIc System.

The reduction in the number of KB control rules and absence of KB equipment rules for the 1 L scale reflects the rigidity of the Bioflo IIc system. Impeller rate control of the D.O. concentration, temperature control, and pH control were relegated to the Bioflo IIc and could not be affected by the user in any fashion, including PID control loop parameter modification, other than manual set point attenuation. As such, the automatic adjustment of control loop set points, values, etc. was confined to external, computer-controlled values of airflow and GFR. Therefore, such variables as SGR could not be calculated and used to accomplish adjustments in the temperature set point. Furthermore, potentially useful information such as base or acid addition rate could not be calculated or used for control actions and/or intervention.

The Bioflo IIc system constraints necessitated creative solutions to achieving the desired control methodologies (e.g., SOUR). As such, the intended control methodology of utilizing impeller rate to maintain the SOUR set point constant in Phase 3 was altered to SOUR set point maintenance via the GFR to the reactor. This permitted implementation of the desired control action (SOUR set point maintenance) through an alternate control technique within the confines of the Bioflo IIc system.

KB and PS Variable Control.

ANN biomass predictions closely approximated the offline measurements in general. Accurate biomass predictions ensured accurate calculation of PS variables online and led to correct and timely decision making by the KB control system. The ability to recalibrate the biomass concentration from the control strategy MMI permitted

operator intervention if significant deviation (e.g., 5% or more) from offline-determined biomass concentration was encountered and increased the accuracy of PS variable calculation and control.

The KB/PS variable control strategies designed to maintain glucose-limited conditions under dynamic OTR conditions for 1 L and 8 L fed-batch fermentations accomplished this objective. The control of SOUR at a constant value required an increasing OTR commensurate with increasing biomass concentration during Phase 3, and resulted in an OTR profile similar to that observed under glucose-rich fermentation conditions (Figure 64). The novel capability to approximate the large OTR increase observed under glucose-rich conditions under substantially lower glucose concentrations was the control objective of the system. This objective was achieved and permitted further delineation between the pseudo-steady-state glucose concentration and enzyme activities upon product equilibrium. Reduction in the peak magnitude of the OTR profile (Figure 64) was not necessarily a drawback given the coupled nature of OTR and heat transfer rate (HTR) requirements. Final metabolite concentrations and biomass growth rates were not detrimentally affected by employing the KB control in place of glucose-rich culturing conditions. HTR limitations often become the rate-limiting step in the scale up of fed-batch fermentations.[59] The potential reduction in HTR resulting from the reduction in OTR could facilitate the implementation of this type of control scheme at an increased scale.

The 1 L NBS Bioflo IIc system was incapable of impeller manipulation for purposes other than D.O. concentration maintenance, precluding its direct use as a SOUR control actuator as previously mentioned (Table 25). The GFR was therefore chosen to

maintain the SOUR constant, resulting in different Phase 3 control loop algorithms for the 1 L and 8 L scale fermentations. The 8 L KB/PS variable control system utilized impeller rate control of SOUR with D.O. concentration maintenance via the GFR (Table 26). The ability of two different platforms and two different control methodologies to maintain PID control of the SOUR demonstrated the robustness of this control technique across different scales and equipment configurations.

Direct comparison of the 1 L (Figure 77) and 8 L (Figure 78) SGUR profiles as a function of biomass concentration was hampered by the OTR limitations experienced at the 8 L scale relative to the 1 L scale, as well as the dynamic nature of the control systems' set points. The 1 L SGUR was closely approximated by that of the 8 L SGUR initially, but OTR limitations on the 8 L scale initiated decrements in the SOUR set point to maintain the culture aerobic. As such, the decrease in SOUR translated into a depressed SGUR profile relative to the 1 L scale. In the absence of OTR limitations, the 1 L scale reduced the SOUR set point only in response to glucose accumulation despite maintaining glucose-limited conditions.

The use of CER as a control methodology for substrate feeding in fermentations has previously been explored.[156] Here it was substituted for GFR control of the D.O. concentration during Phase 4 of fed-batch fermentations. The decoupling of D.O. concentration control from the GFR permitted increased substrate accumulation relative to that observed under standard glucose-limited conditions (Figure 66). This is consistent with a prior literature report that maintained about 1 g/L of carbohydrate during the fed-batch fermentation production of cephalosporin C.[156] The increase in KB-controlled fed-batch fermentation pseudo-steady-state glucose concentrations relative to standard

glucose-limited conditions permitted substantial DHQ accumulation and is discussed in more detail below.

The 1 L KB-controlled conditions permitted a slight increase in the total hydroaromatic production relative to glucose-rich culturing conditions while decreasing the peak OTR by 25%. The control techniques elaborated here would be best suited towards bacterial systems that require catabolic repression to prevent unwanted gene expression but exhibit substrate inhibition in the presence of significant glucose concentrations.

Stoichiometric Modeling Considerations.

The co-consumption of acetate (Figure 57, Figure 60, and Figure 63) and glucose under glucose-limited feeding conditions was often observed, requiring an active glyoxylate shunt.[150] However, typical acetate accumulation of about 1 g/L in 1 L fermentations prior to its consumption did not constitute acetate utilization as a significant source of carbon. Therefore, the assumption of an inactive glyoxylate shunt was justified. The assumption of a true cycle for the TCA is often invoked when the TCA is part of a stoichiometric model and glucose is the carbon source.[84f,g,h,j,m]

The overexpression of transketolase by plasmid-localized *tktA* in construct QP1.1/pKD12.138A was the rationale for assuming negligible amounts of pentose phosphate pathway metabolites were derived from glucose-6-phosphate conversion to ribulose-5-phosphate. Furthermore, if both reactions were included in the model the coefficient matrix was singular due to the model's inability to distinguish between the

reactions from extracellular measuments.[84d,h,q] In such cases the reactions are "lumped" to achieve a non-singular linear system.[84d,h,q]

SM flux calculations involving PEP were of interest given the prominent role of PEP in central metabolism. The predicted *ppc* flux (J20) drain on PEP may have contributed to the lack of predicted or experimental acetate excretion on the 1 L scale since this link has previously been suggested.[84h] The predicted negative flux through pyruvate kinase (J13) was not surprising given the large flux of glucose to G6P as driven by the PTS, concomitantly converting PEP to PYR.

The pyruvate kinase flux was interesting for several reasons. The negative flux predicted for pyruvate kinase dictates the reaction was predicted to transpire in the direction opposite that of its written direction. Although conversion of PYR to PEP cannot be accomplished by pyruvate kinase, this conversion can be facilitated by PEP synthase. Intracellular PEP availability can be increased by *pps*-encoded PEP synthase overexpression as discussed in Chapters 1 and 3. The increased requirement for PEP synthase conversion of PYR to PEP to alleviate PEP substrate limitations during enhanced glucose uptake relative to standard glucose-limited conditions predicted here is consistent with the observations in Chapter 3 that overexpression of PEP synthase was unsuccessful at increasing quinic acid yields and titers during standard glucose-limited fermentation conditions. Under glucose-limited conditions the native expression level of PEP synthase by QP1.1/pKD12.138A (Table 22, entry 1) may be sufficient to alleviate intracellular PEP limitations. In Chapter 3, plasmid-localized *pps* was unsuccessful (Figure 46) in significantly increasing DHQ and quinic acid titers (e.g., alleviating DAHP synthase PEP substrate limitations). Subsequent experiments in the Frost laboratory with

an IPTG-titratable *pps* expression system have enhanced carbon flux through DAHP synthase[140] and suggest in vivo PEP limitation as predicted by the SM was indeed accurate for QP1.1/pKD12.138A under enhanced glucose uptake culturing conditions. Furthermore, the predicted intracellular PEP limitations were alleviated under the standard glucose-limited conditions by the cessation of biomass assembly (Figure 80). This suggests that reduction in the final biomass titers might also alleviate PEP constraints, permitting enhanced flux through DAHP synthase into the shikimate pathway. Efforts directed towards reduction in biomass concentration (Chapter 3) were therefore justified in so much as they might reduce yield losses due to PEP substrate incorporation into biomass and could prevent intercellular PEP limitations during peak metabolic activity based on SM calculations.

The model assumption that NADH and NADPH can be interconverted is justified by the presence of *pntA* and *pntB*-encoded transhydrogenases, however the model does not take into account the rate of interconversion of these species. *E. coli* is known to maintain an intracellular $NADP^+/NAD^+$ ratio of 0.33 by balancing de novo NAD^+ synthesis with the net production or consumption rate of $NADP^+$.[157] If the interconversion rate between the two molecules is not on par with that of NADH generation through central metabolism, NADPH availability might lag behind that of NADH during rapid growth. This might call into question the validity of the assumption that NADH and NADPH are equivalent for modeling purposes. The inability to quantify intracellular conversion between NADPH and NADH prevented their delineation in the SM. Therefore it is difficult to definitively assess the extent to which NADPH availability drives DHQ formation within the confines of a SM in lieu direct cofactor flux

or concentration measurement. However, if the rate of NADPH and NADH interconversion is sufficient to maintain a $NADP^+/NAD^+$ ratio of 0.33 then cofactor availability should not be problematic given the large excess flux of reducing equivalents to ATP (Figure 83).

8 L KB-controlled Fermentations and Acetate Excretion.

Acetate excretion on 8 L KB-controlled fermentations was in excess of acetate formation observed under any other culturing conditions, including the glucose-rich conditions employed in Chapter 3. QP1.1/pKD12.138A was observed to accumulate 7.1 g/L of acetate at the 8 L scale under KB control (Figure 73) while only 2.3 g/L of acetate were developed under glucose-rich conditions at the 1 L scale (Chapter 3, Figure 47). Acetate excretion could be caused by at least two different mechanisms. First, if the D.O. concentration of the fermentation was at or near 0% for an extended period of time, anaerobic conditions might have induced acetate excretion. Glucose might accumulate in this scenario since the OTR might be insufficient to oxidatively convert substrate to product. Neither D.O. concentrations approaching 0% (as monitored by the D.O. electrode) nor significant glucose accumulation (as monitored by both the MGA check and the YSI 2700) were observed to transpire during KB-controlled 8 L fermentations however.

Another possible cause of acetate formation is the decoupling of catabolism and anabolism, often referred to as "metabolic overflow". Metabolic overflow has been implicated as the source of acetate excretion under fully aerobic conditions and is characterized by a rate of substrate uptake that exceeds the cellular respiratory capacity to

transfer electrons to oxygen.[112b,h,i,m,n] Overflow of excess carbon flux into acetate results in net ATP generation, which has been hypothesized to be a cellular mechanism for increasing intracellular ATP availability, especially during rapid growth.[112m] If metabolic overflow constitutes a significant source of acetate biosynthesis during the fed-batch cultivation of QP1.1/pKD12.138A, then glucose-rich fermentation conditions should provide the upper limit for acetate excretion since the culture is restricted in neither glucose nor oxygen and could saturate the respiratory capacity of the culture. Therefore, acetate concentrations significantly in excess of the 2.3 g/L accumulated during glucose-limited results would suggest that insufficient oxygen was present to maintain aerobic conditions. The D.O. concentration readings were not observed to approach 0% as previously mentioned. Furthermore, 1 L KB-controlled fermentations accumulated 1.3 mM glucose in their medium by 48 h (Figure 66), while the acetate profile was stably maintained below 0.2 g/L (Figure 63). By contrast, the 8 L KB-controlled fermentations only achieved a glucose concentration of 0.83 mM by 48 h, yet 7.1 g/L of acetate was accumulated.

The lack of significant glucose accumulation, and apparently correct D.O. concentration set point maintenance as indicated by the D.O. probe readings suggests D.O. probe readings may have been inaccurate. Problematic D.O. probe grounding may have contributed to inaccurate D.O. probe readings and could have limited the culture in oxygen by preventing automatic control of relevant set points. Teflon compression sleeves, used in lieu of metal sleeves to prevent crimping of the D.O. probe bodies, may have partially insulated the D.O. probes, contributing to grounding problems. Depressed

D.O. concentrations relative to the readings could have led to the enhanced acetate excretion observed (Figure 73).

Glucose and Metabolite Equilibrium.

Despite achieving the desired control properties, the KB/PS variable control strategies were unable to enhance quinic acid titers in the absence of substantial DHQ accumulation. The inability of the KB/PS variable control strategies to overcome the quinic acid-DHQ equilibrium was not surprising in light of the apparent quinic acid-DHQ equilibrium dependence on pseudo-steady-state glucose concentrations. The glucose concentration maintained by KB/PS variable control conditions was increased relative to standard glucose-limited control conditions in general (Figure 66 and Figure 72). The glucose concentration (1.3 mM) developed by 48 h for the 1 L KB/PS variable control of QP1.1/pKD12.138A (Figure 66) led to a QA:DHQ of only 0.54. This was very similar to the 0.74 QA:DHQ developed under glucose-rich conditions (Figure 47), which typically employed a pseudo-steady state glucose concentration of 20-30 g/L (110-170 mM).

The ability of the control system to develop a final QA:DHQ that was nearly identical to that of the glucose-rich conditions helped to delineate the source of excess DHQ formation during quinic acid production. In Chapter 3, pseudo-steady state glucose concentrations, depressed shikimate dehydrogenase activity, and cofactor limitations were all cited as potential sources of unfavorable quinic acid-DHQ equilibrium. During KB-controlled fed-batch fermentation of QP1.1/pKD12.138A, shikimate dehydrogenase enzyme activities (Table 32, entry 2) were similar to activities measured under glucose-limited conditions (Table 29, entry 2). The lack of a substantial decrease in final DHQ

titer and/or commensurate increase in quinic acid concentration in the presence of nearly identical shikimate dehydrogenase activity levels observed under glucose-limited conditions suggests that shikimate dehydrogenase activity was not the determining factor of the QA:DHQ. The apparent ability of the glucose concentration to dictate metabolite equilibrium suggests that catabolic repression of DHQ transport is the most likely cause of DHQ accumulation. Repression of DHQ uptake could preclude shikimate dehydrogenase from multiple opportunities to convert DHQ to quinic acid. The low affinity of shikimate dehydrogenase for DHQ (K_m of 1.2 mM) could result in limited de novo conversion of DHQ to quinic acid and cause increased DHQ accumulation at the expense of quinic acid. Although cofactor availability may play a role in determining the final QA:DHQ ratio, it is likely a minor consideration as previously discussed.

In viewing glucose-limited, glucose-rich, KB and modified KB-controlled fermentation conditions for quinic acid production from glucose, a clearer picture emerges of the QA:DHQ dependence on glucose concentration. Transport of previously exported DHQ back into the cytoplasm of construct QP1.1/pKD12.138A is most likely subject to catabolite repression and would inhibit the extent to which DHQ can be converted to quinic acid. Repression of DHQ transport would be analogous to the use of glucose-rich fermentation conditions to catabolically repress shikimic acid transport and subsequent conversion to quinic acid employed to obtain pure shikimic acid from SP1.1 constructs in Chapter 2. The use of "glucose-limited" and "glucose-rich" to describe culturing conditions is then questionable, as a 100-fold decrease in glucose concentration from "glucose-rich" conditions still results in about the same QA:DHQ. The dependence of product ratios upon glucose concentration must therefore be viewed as a continuum.

In culturing QP1.1/pKD12.138A, the high shikimate pathway carbon throughput required to achieve industrially viable hydroaromatic titers must be tempered with the knowledge that metabolite selectivity is dependent upon the pseudo-steady-state glucose concentration. The pseudo-steady-state glucose concentration is in turn proportional to the GFR (Equation 32). The observation that both shikimic acid and quinic acid producing constructs appear sensitive to catabolic repression of excreted metabolite transport suggests other aromatic amino acid biosynthesis pathway intermediates might also possess this characteristic.

CHAPTER 5

Experimental

Culture Medium.

All solutions were prepared in distilled, deionized water. LB medium contained (1 L) Bacto tryptone (10 g), Bacto yeast extract (5 g), and NaCl (10 g). M9 salts (1 L) contained Na_2HPO_4 (6 g), KH_2PO_4 (3 g), NH_4Cl (1 g), and NaCl (0.5 g). M9 minimal medium contained D-glucose (10 g), $MgSO_4$ (0.12 g), and thiamine hydrochloride (0.001 g) in 1 L of M9 salts. M9 medium (1 L) was supplemented where appropriate with L-phenylalanine (0.040 g), L-tyrosine (0.040 g), L-tryptophan (0.040 g), *p*-hydroxybenzoic acid (0.010 g), potassium *p*-aminobenzoate (0.010 g), and 2,3-dihydroxybenzoic acid (0.010 g). Antibiotics were added where appropriate to the following final concentrations: ampicillin (Ap), 50 μg/mL; Cm, 20 μg/mL; kanamycin (Kan), 50 μg/mL; and tetracycline (Tc), 25 μg/mL. Solutions of M9 salts, $MgSO_4$, and glucose were autoclaved individually and then mixed. Amino acids, aromatic vitamins, shikimic acid, thiamine hydrochloride, and antibiotics were sterilized through 0.22-μm membranes. Solid medium was prepared by addition of Difco agar to a final concentration of 1.5% (w/v) to the liquid medium.

The basic fermentation medium (1 L) contained K_2HPO_4 (7.5 g), ammonium iron (III) citrate (0.3 g), citric acid monohydrate (2.1 g), L-phenylalanine (0.7 g), L-tyrosine (0.7 g), L-tryptophan (0.35 g), and concentrated H_2SO_4 (1.2 mL). Fermentation medium was adjusted to pH 7.0 by addition of concentrated NH_4OH before autoclaving. The

following supplements were added immediately prior to initiation of the fermentation: glucose, $MgSO_4$ (0.24 g), *p*-hydroxybenzoic acid (0.010 g), potassium *p*-aminobenzoate (0.010 g), 2,3-dihydroxybenzoic acid (0.010 g), trace minerals including $(NH_4)_6(Mo_7O_{24})\cdot 4H_2O$ (0.0037 g), $ZnSO_4\cdot 7H_2O$ (0.0029 g), H_3BO_3 (0.0247 g), $CuSO_4\cdot 5H_2O$ (0.0025 g), and $MnCl_2\cdot 4H_2O$ (0.0158 g). Methyl-α-D-glucopyranoside was added to a final concentration of 1 mM where indicated. Glucose, $MgSO_4$ (1 M), and methyl-α-D-glucopyranoside (100 mM) solutions were autoclaved separately while aromatic vitamins and trace minerals were sterilized through 0.22-μm membranes. Shikimic acid was added to the fermentation medium where indicated. A solution of shikimic acid (10 g) in water (50 mL) was adjusted to pH 7 by addition of KOH and sterilized through a 0.22-μm membrane prior to addition to the fermentation medium. Antifoam (Sigma 204) was added as needed.

Bacterial Strains and Plasmids.

E. coli K-12 strain RB791 was obtained from the American Type Culture Collection (ATCC strain 53622). *E. coli* ALO807[100] was provided by Professor M. G. Marinus (University of Massachusetts), *E. coli* JP11123[109c] was provided by Professor A. J. Pittard (University of Melbourne), and *E. coli* CL451[158] was provided by Professor B. A. D. Stocker (Stanford University). Plasmid constructions were carried out in *E. coli* DH5α, which is available from Gibco BRL Products. Homologous recombinations utilized plasmid pMAK705,[159] which contains a temperature-sensitive pSC101 replicon.

Storage of Bacterial Strains and Plasmids.

All bacterial strains were stored at -80 °C in glycerol. Cultures were grown in LB, with antibiotics where appropriate, for 12 h prior to preparation of the glycerol storage cultures. Storage cultures were prepared by adding 0.75 mL of the 12 h culture to a sterile vial containing 0.25 mL of 80% (v/v) glycerol. The solution was gently mixed by inversion, stored at room temperature for 2 h, and subsequently stored at -80 °C.

Genetic Manipulations.

Standard protocols were used for construction, purification, and analysis of plasmid DNA. T4 DNA ligase and Large Fragment of DNA polymerase I (Klenow fragment) were purchased from Gibco BRL Products. Calf intestinal alkaline phosphatase was purchased from Roche Molecular Biochemicals. PCR amplifications were performed according to Sambrook et al.[160] Each amplification reaction (0.1 mL) contained 10 mM KCl, 20 mM Tris-HCl (pH 8.8), 10 mM $(NH_4)_2SO_4$, 2 mM $MgSO_4$, 0.1% Triton X-100, dATP (0.2 mM), dCTP (0.2 mM), dGTP (0.2 mM), dTTP (0.2 mM), template DNA (0.02 μg-1 μg), 0.5 μM of each primer, and 2 units of Vent polymerase. Primers were synthesized by the Macromolecular Structure Facility at Michigan State University.

Preparation and Transformation of Competent Cells.

Competent cells were prepared according to a procedure modified from Sambrook et al.[160] LB medium (5 mL), containing antibiotics where appropriate, was inoculated with a single colony from a LB plate, containing antibiotics where appropriate, streaked

with the strain of interest. The culture was grown at 37 °C with shaking at 250 rpm in a model G76 New Brunswick Scientific (NBS) bench-top rotary shaker for 10-12 h. An aliquot (1 mL) from the culture (5 mL) was used to inoculate LB (100 mL) containing the appropriate antibiotics. The culture was grown at 37 °C with shaking at 250 rpm in a NBS series 25 incubator shaker until the optical density at 600 nm was between 0.4 and 0.6. The culture was transferred to a centrifuge bottle that had been sterilized with a 25 % (v/v) bleach solution and rinsed four times with sterile, deionized water. The cells were harvested by centrifugation (4000 *g*, 5 min, 4 °C) and the culture medium was decanted. All subsequent manipulations were carried out on ice. The harvested cells were washed by resuspending in ice cold 0.9 % NaCl (100 mL), and the cells were collected by centrifugation (4000 *g*, 5 min, 4 °C). The 0.9 % NaCl solution was decanted, the cells resuspended in ice cold 100 mM $CaCl_2$ (50 mL), and stored on ice for 30 min. After centrifugation (4000 *g*, 5 min, 4 °C), the cells were resuspended in 4 mL of ice cold 100 mM $CaCl_2$ containing 15% glycerol (v/v). Aliquots (0.25 mL) of competent cells were added to 1.5 mL microfuge tubes, frozen in liquid nitrogen, and stored at -78 °C.

Frozen competent cells were thawed on ice for 5 min before transformation. An aliquot (1 μL to 3 μL) of plasmid DNA (about 100 ng/μL in Tris-EDTA) was added to the thawed competent cells (0.1 mL). The solution was gently mixed by tapping and stored on ice (30 min). The cells were then heat shocked at 42 °C for 1.5 min and briefly returned to ice (5 min). LB (0.5 mL, no antibiotics) was added to the cells, and the sample was incubated at 37 °C (no agitation) for 1 h. Cells were collected by centrifugation in a Beckman microcentrifuge. If the transformation was to be plated onto

LB plates, 0.5 mL of the culture supernatant was removed, the cells resuspended in the remaining 0.1 mL of LB, and an aliquot (10 μL to 20 μL) spread onto plates containing the antibiotics where appropriate. If the transformation was to be plated onto M9 medium plates, the cells were washed twice with a solution of M9 inorganic salts (0.5 mL). After resuspension in a fresh aliquot (0.1 mL) of M9 inorganic salts solution, an aliquot of the cell suspension (0.04 mL) was spread onto a plate. An aliquot of competent cells with no DNA added was also carried through the transformation protocol and spread onto an additional plate of the same medium to verify the absence of growth on selective medium.

Large Scale Purification of Plasmid DNA.

Plasmid DNA was purified on a large scale using a modified alkaline lysis method described by Sambrook et al.[160] In a 2 L Erlenmeyer flask, 500 mL of LB medium containing the appropriate antibiotic was inoculated from a single colony, and the culture was incubated at 37 °C for approximately 15 h with agitation at 250 rpm. Cells were harvested by centrifugation (4000 *g*, 5 min, 4 °C) and resuspended in 10 mL of cold solution **1** (50 mM glucose, 20 M Tris-HCl, pH 8.0, 10 mM EDTA, pH 8.0) into which lysozyme (5 mg/mL) had been added immediately before use. The suspension was stored at room temperature for 5 min. Addition of 20 mL of solution **2** (1% SDS (w/v) in 0.2 N NaOH) was followed by gentle mixing and storage on ice for 15 min. Fifteen milliliters of ice cold solution **3** (3 M KOAc, prepared by combining 60 mL of 5 M potassium acetate, 11.5 mL of glacial acetic acid, and 28.5 mL of H_2O) was added. Vigorous shaking resulted in formation of a white precipitate. After the suspension was

stored on ice for 10 min, the cellular debris was removed by centrifugation (48,000 *g*, 20 min, 4 °C). The supernatant was transferred to two fresh centrifuge bottles and isopropanol (0.6 volumes) was added to precipitate the DNA. After the samples were left at room temperature for 15 min, the DNA was recovered by centrifugation (20000 *g*, 20 min, 4 °C). The DNA pellet was then rinsed with 70% ethanol and dried.

The isolated DNA was dissolved in TE (3 mL) and transferred to a Corex tube. Cold 5 M LiCl (3 mL) was added and the solution was gently mixed. The sample was then centrifuged (12000 *g*, 10 min, 4 °C) to remove high molecular weight RNA. The clear supernatant was transferred to a clean Corex tube and isopropanol (6 mL) was added followed by gentle mixing. The precipitated DNA was collected by centrifugation (12000*g*, 10 min, 4°C). The DNA was then rinsed with 70% ethanol and dried. After redissolving the DNA in 0.5 mL of TE containing 20 μg/mL of RNAase, the solution was transferred to a 1.5 mL microcentrifuge tube and stored at room temperature for 30 min. DNA was precipitated from solution upon addition of 500 μL of 1.6 M NaCl containing 13% polyethylene glycol (PEG-8000) (w/v) (Sigma). The solution was mixed and centrifuged (microcentrifuge, 10 min, 4 °C) to recover the precipitated DNA. The supernatant was removed and the DNA was then redissolved in 400 μL of TE. The sample was extracted sequentially with phenol (400 μL), phenol and SEVAG (400 μL each), and finally SEVAG (400 μL). Ammonium acetate (10 M, 100 μL) was added to the aqueous DNA solution. After mixing, 95% ethanol (1 mL) was added to precipitate the DNA. The sample was left at room temperature for 5 min and then centrifuged (microcentrifuge, 5 min, 4 °C). The DNA was rinsed with 70% ethanol, dried, and then redissolved in 250-500 μL of TE.

The concentration of DNA in the sample was determined as follows: an aliquot (10 μL) of the DNA solution was diluted to 1 mL in TE and the absorbance at 260 nm was measured relative to the absorbance of TE. The DNA concentration was calculated based on the fact that the absorbance at 260 nm of 50 μg/mL of double stranded DNA is 1.0.

Small Scale Purification of Plasmid DNA.

An overnight culture (5 mL) of the plasmid-containing strain was grown in LB medium containing the appropriate antibiotics. Cells from 3 mL of the culture were collected in a 1.5 mL microcentrifuge tube by centrifugation. The harvested cells were resuspended in 0.1 mL of cold solution **1** into which lysozyme (5 mg/mL) had been added immediately before use and the solution was stored on ice for 10 min. Addition of solution **2** (0.2 mL) was followed by gentle mixing and storage on ice for 5 to 10 min. Solution **3** (0.15 mL) was added to the sample and shaken vigorously. The sample was stored on ice for 5 min and the cellular debris was removed by centrifugation (microcentrifuge, 15 min, 4 °C). The supernatant was transferred to another microcentrifuge tube and extracted with equal volumes of phenol and SEVAG (0.2 mL each). The aqueous phase (approximately 0.5 mL) was transferred to a fresh microfuge tube and the DNA was precipitated by the addition of 95% ethanol (1 mL). The sample was left at room temperature for 5 min before centrifugation (15 min, rt) to isolate the DNA. The DNA pellet was rinsed with 70% ethanol, dried, and redissolved in 50 to 100 μL TE. DNA isolated from this method was used for restriction enzyme analysis and the concentration was not determined by spectroscopic methods.

Restriction Enzyme Digestion of DNA.

Restriction enzyme digests were performed using buffer solutions supplied by Gibco BRL or New England Biolabs. A typical digest (20 μL) contained approximately 0.8 μL of DNA (0.1 μg/μL in TE), 2 μL of restriction enzyme buffer (10X concentration), 1 μL of restriction enzyme, 1 μL of Bovine Serum Albumin (BSA) (2 mg/mL), and 8 μL of TE. Reactions were incubated at 37 °C for 1 h. Digests were terminated by addition of 2 μL of 10X Endostop solution and subsequently analyzed by agarose gel electrophoresis. 10X Endostop was stored at 4 °C and contained 50% glycerol (v/v), 0.1 M disodium EDTA (pH 7.5), 1% sodium dodecyl sulfate (SDS, w/v), 0.1% bromophenol blue (w/v), and 0.1% xylene cyanole FF (w/v). Prior to use, 0.12 mL DNAase-free RNAase was added to 1 mL of 10X Endostop solution. When DNA was required for subsequent cloning, restriction digests were terminated by addition of 1 μL of 0.5 M EDTA (pH 8.0) followed by extraction of the DNA with equal volumes of phenol and SEVAG and precipitation of the DNA. DNA was precipitated by addition of 0.1 volume of 3 M NaOAc (pH 5.2) followed by thorough mixing and the addition of 3 volumes of 95% ethanol. Samples were stored for at least 2 h at -78 °C. Precipitated DNA was recovered by centrifugation (15 min, 4 °C). DNA was dried with 70% ethanol and redissolved in TE.

Agarose Gel Electrophoresis.

Agarose gels were run in TAE buffer containing 40 mM Tris-acetate and 2 mM EDTA (pH 8.0). Gels typically contained 0.7% agarose (w/v) in TAE buffer. Lower concentrations of agarose (0.3%) were used to resolve genomic DNA (note:

electrophoresis was done at 4 °C). Ethidium bromide (0.5 μg/ml) was added to the agarose to allow visualization of DNA fragments under an UV lamp. The size of the DNA fragments were determined by using two sets of DNA standards: λ DNA digested with HindIII (23.1-kb, 9.4-kb, 6.6-kb, 4.4-kb, 2.3-kb, 2.0-kb, and 0.6-kb) and λ DNA digested with *Eco*RI and *Hind*III (21.2-kb, 5.1-kb, 5.0-kb, 4.3-kb, 3.5-kb, 2.0-kb, 1.9-kb, 1.6-kb, 1.4-kb, 0.9-kb, 0.8-kb, and 0.6-kb).

Isolation of DNA from Agarose.

The band of agarose containing the DNA of interest was excised from the gel and chopped thoroughly with a razor in a plastic weighing tray. The agarose was then transferred to a spin column consisting of a 500 μL microfuge tube packed tightly with glass wool and a tiny hole in its bottom. The spin column was then placed in a 1.5 mL microfuge tube and centrifuged for 5 min using a Beckman microfuge to separate the DNA solution from the agarose. The collected DNA was precipitated with 3 M NaOAc and 95% ethanol as previously described and redissolved in TE.

Treatment of Vector DNA with Calf Intestinal Alkaline Phosphatase.

Following restriction enzyme digestion, plasmid vectors were dephosphorylated to prevent self-ligation. Digested vector DNA was dissolved in TE (88 μL). To this sample was added 10 μL of dephosphorylation buffer (10X concentration) and 2 μL of calf intestinal alkaline phosphatase (2 units). The reaction was incubated at 37 °C for 1 h. The phosphatase was inactivated by the addition of 1 μL of 0.5 M EDTA (pH 8.0) followed by heat treatment (65 °C, 20 min). The sample was extracted with phenol and

SEVAG (100 μL each) to remove the protein, and the DNA was precipitated as previously described and redissolved in TE.

DNA Ligation.

DNA ligations were designed so that the molar ratio of insert DNA to vector DNA was 3 to 1. A typical ligation reaction contained 0.03 μg to 0.1 μg of vector DNA and 0.05 μg to 0.2 μg of insert DNA in a combined volume of 7 μL. To this sample, 2 μL of ligation buffer (5X concentration) and 1 μL of T4 DNA ligase (2 units) was added. The reaction was incubated at 16 °C for at least 4 h and then was used to transform competent DH5α cells.

Determination of Oxygen Transfer Conditions.

Standard fermentation oxygen transfer conditions were determined for the Frost Laboratory (Biostat MD) and Worden Laboratory (Bioflo IIc) using a steady-state dilution method with a constant reactor volume (1 L). Experimental buffer (1 L) contained K_2HPO_4 (1 g). Aspiration was employed to degas buffer agitated by a magnetic stirrer. Buffer (20 L) was degassed for a minimum of 15 h before use in oxygen transfer experiments. The centrifugal inlet pump (March Manufacturing, Inc. model AC-3C-MD) flow rate was restricted to either 7.0 L/min or 7.5 L/min by ¼" ID inlet and outlet tubing. The peristaltic outlet pump (Cole Parmer model 7529-20) was operated at its maximum flow rate (12 L/min). The outlet tube end was positioned at a height in the reactor corresponding to a liquid volume of 1 L when the impeller rate and airflow rate were at their process values (e.g., to account for vortex formation in non-

baffled systems). This ensured the liquid volume did not significantly deviate from 1 L. The D.O. was monitored using a Mettler-Toledo 12 mm sterilizable D.O. electrode fitted with an Ingold A-type oxygen-permeable membrane. Buffer was pumped into and out of the reactor until the system reached steady state, which was characterized by a constant DO concentration reading. The approximate k_La was then calculated and oxygen transfer conditions modified accordingly.

D.O. Electrode Calibration, Maintenance, and Storage.

Mettler-Toledo polarographic 12 mm D.O. electrodes (120 mm, 220 mm, and 420 mm insertion lengths) all employed A-type, oxygen-permeable membrane modules containing KCl/KOH (pH 13.0, Mettler-Toledo O_2 electrolyte) electrolyte. Subsequent to in-place steam sterilization, D.O. electrodes were connected to an appropriate voltage source (D.O. amplifier) and allowed to polarize for a minimum of 6 h prior to calibration. D.O. electrodes were calibrated in situ, just prior to the initiation of fermentations.

The electrode membranes were inspected prior to each sterilization, and the membrane module replaced as required. Electrolyte solution was replaced as required during membrane module replacements and as the first step in D.O. electrode troubleshooting. Electrolyte solution was never used longer than two months without being changed. D.O. probes were stored with the membrane submerged in deionized water when not in use.

pH Electrode Calibration, Maintenance, and Storage.

Mettler-Toledo gel-filled pH electrodes (200 mm and 225 mm insertion lengths) and Viscolyte B-filled pH electrodes (420 mm insertion length) were calibrated prior to in-place steam sterilization using a zero point buffer containing disodium hydrogen orthophosphate and potassium dihydrogen orthophosphate (pH 7.0) and a span (slope) buffer of potassium hydrogen phthalate (pH 4.0).

All pH electrodes were stored in potassium hydrogen phthalate buffer containing 3 M KCl (pH 4.0) such that the liquid level covered the electrodes' salt bridge. The reference junctions of gel-filled pH electrodes were unclogged by immersion in 3 M KCl, autoclaving, and allowing the electrodes to cool slowly while still immersed.

Fed-Batch Fermentations (General).

Details on the physical attributes of the specific fermentation systems employed are presented in Table 34.

Table 34. Fermentor platform-specific physical traits.

Platform	BBB Biostat MD	NBS Bioflo IIc	Dow
H_2SO_4 Tubing ID (in.)	1/16	1/32	1/8
NH_4OH Tubing ID (in.)	1/16	1/32	1/8
Antifoam Tubing ID (in.)	1/16	1/16	1/8
Vessel Working Volume (L)	2.0	1.25 (1.5)	10
Vessel Total Volume (L)	3.0	1.5 (1.7)	14
Vessel ID at Mouth (in.)	5 1/8	4 5/8	8 3/16
Vessel Depth at Center (in.)	9 7/16	7 1/2	17 7/8
Impeller Type	Disk (6 blade)	Disk (6 blade)	Disk (6 blade)
Impeller Diameter (in.)	2 1/16	2 1/4	2 7/8
Impeller Blade Length (in.)	9/16	9/16	3/4
Impeller Blade Depth (in.)	13/32	7/16	5/8
[a]Baffle Dimensions (4; in.)	3/8 x 5	5/8 x 4 3/4	7/8 x 15
Fermentor Type	Biostat MD	Bioflo IIc	Miniplant
Controller Hardware	DCU-1	G4LC32 or SNAP-LCSX	SNAP-LCSX
Controller Firmware	DCU-1	v. 81.19	v. 1.07

[a]BBB baffle dimensions were for custom baffle cages fabricated by the RCE machine shop.

The standard PID control equation varied between the various fermentation platforms. Default PID control loop parameters for fed-batch fermentations are provided in Table 35.

Table 35. Default PID control loop parameters for fed-batch fermentations.

Platform	Control Loop	K_c (X_p)	τ_I (s)	τ_D (s)
BBB Biostat MD	Impeller (pO_2)	0.57 (175.0%)	100.0	0.00
	Airflow (pO_2)	1.1 (90.0%)	50.0	0.00
	[a]Glucose (pO_2N)	0.11 (950.0%)	999.9	0.00
		0.30 (333.3%)	999.9	0.00
		0.50 (200.0%)	999.9	0.00
		0.60 (166.7%)	999.9	0.00
		0.80 (125.0%)	999.9	0.00
	Temperature	5.0 (20.0%)	300.0	0.00
	pH	3.3 (30.0%)	30.0	0.00
[b]NBS BiofloIIc/Opto22	Airflow	1.0	5.0	0.00
	Glucose	-1.0	1.0	0.00
	SOUR	0.80	1.0	0.00
	CER	0.10	0.20	0.00
[c]Miniplant/Opto22	Impeller	0.50	0.75	0.00
	Airflow	0.50	2.0	0.00
	Glucose	-0.50	1.0	0.00
	SOUR	150	200	0.00
	CER	5.0	10	0.00

[a]X_p of 200.0 % was for the adjusted glucose pump range (6 rpm), all others were for the unadjusted glucose pump range (32 rpm).
[b]The Bioflo IIc PID control parameters for D.O. (impeller only), temperature, and pH were burned into the controller firmware (unknown and unadjustable).
[c]Temperature and pH were digitally (e.g., on/off) controlled on the miniplant.

Equation 36 defines the standard BBB DCU-1 PID control loop position algorithm.[161] O(t) is the controller position output as a function of time, E(t) is the process error (variable set point minus current variable value), T_S is the sample time interval in seconds, τ_I is the integral time in seconds, τ_D is the derivative time in seconds, PV_i is the value of the variable being controlled at time=i, and PV_{i-1} is the previous value of the variable being controlled. Noting the nil value for all BBB Biostat control loop derivative terms in Table 35, Equation 36 reduces to Equation 37. The conversion between K_c, the proportional gain, and X_p, the proportional range, is given by Equation 38.

Equation 36. $$O(t) = K_c\left(E(t) + \frac{T_S}{\tau_I}\sum_{i\to\infty}^{i=n} E(t) + \frac{\tau_D}{T_S}\left(PV_i - PV_{i-1}\right)\right)$$

Equation 37. $$O(t) = K_c\left(E(t) + \frac{T_S}{\tau_I}\sum_{i\to\infty}^{i=n} E(t)\right)$$

Equation 38. $$X_p = \frac{100\%}{K_c}$$

Equation 39 gives the standard PID control loop equation for the Opto22 control systems, where $\Delta O(t)$ is the change in controller output, K_c is the proportional gain, τ_I is the integral time in minutes, τ_D is the derivative time in minutes, SR is the PID loop scan rate in seconds, CF is a conversion factor of 60 seconds/1 minute, $E(t)_i$ is the current error (set point-current value), $E(t)_{i-1}$ is the previous error from the last PID loop scan, and

$E(t)_0$ is the oldest error recorded by the control loop. The derivative time was zero for all control loops, which reduces Equation 39 to Equation 40.

Equation 39.

$$\Delta O(t) = K_c\left(\left(E(t)_i - E(t)_{i-1}\right) + \left(\tau_I\left(\frac{SR}{CF}\right)E(t)_i\right) + \tau_D\left(\frac{CF}{SR}\right)\left(E(t)_i - \left(2E(t)_{i-1}\right) + E(t)_o\right)\right)$$

Equation 40.

$$\Delta O(t) = K_c\left(\left(E(t)_i - E(t)_{i-1}\right) + \left(\tau_I\left(\frac{SR}{CF}\right)E(t)_i\right)\right)$$

Frost Laboratory fermentations employed a 2.0 L working capacity B. Braun Biotech (BBB) M2 culture vessel that was baffled as indicated. Utilities were supplied by a BBB Biostat MD controlled by a DCU-1. Data acquisition and process control utilized a Dell OptiPlex Gs^+ 5166M personal computer (PC) equipped with BBB MFCS/Win software (v1.1). Temperature and pH were controlled with PID control loops. Glucose feeding was controlled with a PID control loop unless otherwise indicated. Temperature was maintained at 33 °C (+/- 0.05 °C deadband) for all fermentations unless otherwise specified. The pH was maintained at 7.0 (+/- 0.05 pH unit deadband) by addition of concentrated NH_4OH or 2 N H_2SO_4. The D.O. was measured using a Mettler-Toledo 12 mm sterilizable O_2 sensor fitted with an Ingold A-type O_2 permeable membrane. The D.O. was maintained at 10% air saturation unless otherwise specified.

Small scale (1.0 L initial volume) Worden laboratory fermentations employed a baffled (316 stainless steel), modified 1.5 L working capacity NBS Bioflo IIc culture

vessel. The original vessel volume was increase from 1.25 L to 1.5 L by the fabrication of a custom glass sleeve by the Scientific Glass Blowing Shop. Utilities were supplied by a NBS Bioflo IIc independent of external control. Data acquisition and process control (airflow rate and glucose addition) utilized a 450 MHz Pentium II Computer Warehouse PC or a 1.3 GHz Pentium IV Dell OptiPlex GX400 PC equipped with an Opto22 Factory Floor (v3.1c) control package interfaced to an Opto22 32-bit G4LC32 controller or an Opto22 SNAP-LCSX controller via SNAP I/O modules. The Bioflo IIc automatically controlled temperature, pH, and D.O. concentration (via impeller rate only) via PID control loops. The Opto22 software controlled airflow and glucose feeding via PID control loops. The airflow rate was adjusted using a Varian 500 series model PFD-501 mass flow controller. The temperature was maintained at 33 °C. The pH was maintained at 7.0 by addition of concentrated NH_4OH or 6 N H_2SO_4. The D.O. was measured using a Mettler-Toledo 12 mm sterilizable O_2 sensor fitted with an Ingold A-type O_2 permeable membrane. The D.O. was maintained at 10% air saturation. Oxygen (O_2) and carbon dioxide (CO_2) exhaust gas concentrations were measured with a series 9500 O_2/CO_2 monitor from Alpha Omega Instruments Corporation. The 9500 monitor output signals were input to the G4LC32 or SNAP-LCSX controllers for use in process monitoring and control.

Larger scale (8.0 L initial volume) Worden laboratory fermentations employed a baffled (316 stainless steel) 10 L working capacity (14 L total capacity) NBS model MF-348 culture vessel. Utilities were supplied by a custom-built Dow Chemical Corporation miniplant. Data acquisition and process control utilized a 450 MHz Pentium II Computer Warehouse PC or a 1.3 GHz Pentium IV Dell OptiPlex GX400 PC equipped with an

Opto22 Factory Floor (v3.1c) control package interfaced to an Opto22 SNAP-LCSX controller with SNAP I/O modules. The temperature and pH were controlled digitally. Glucose addition was controlled by the indicated PID control loop. The temperature was maintained at 33 °C (+/- 0.05 °C deadband). The pH was maintained at 7.0 (+/- 0.05 pH unit deadband) by addition of concentrated NH_4OH or 18 N H_2SO_4. The D.O. concentration was measured using a Mettler-Toledo 12 mm sterilizable O_2 sensor fitted with an Ingold A-type O_2 permeable membrane and an Ingold model 4300 D.O. transmitter. The D.O. was maintained at 10% air saturation. O_2 and CO_2 exhaust gas concentrations were measured with a series 9500 O_2/CO_2 monitor from Alpha Omega Instruments Corporation. The 9500 monitor output signals were input to the SNAP-LCSX controller for use in process monitoring and control.

Inoculants were started by introduction of a single colony picked from an agar plate into 5 mL (Biostat MD and Bioflo IIc) or 10 mL (miniplant) of M9 medium. For strains possessing a plasmid that confers resistance to ampicillin, ampicillin was added to the medium at each step of the inoculum's preparation. Cultures were grown at 37 °C with agitation at 250 rpm until they were turbid (12-24 h) and subsequently transferred to 100 mL (Biostat MD and Bioflo IIc) or 800 mL (miniplant) of M9 medium. Cultures were grown at 37 °C and 250 rpm for an additional 8 to 12 h. After the culture reached an appropriate OD_{600} (2.5-3.5), the inoculum was transferred into the fermentation vessel and the batch fermentation was initiated (t = 0 h).

Standard Glucose-Limited Fed-Batch Fermentation Conditions (Frost Laboratory).

A three-staged algorithm was used to maintain the D.O. level at 10% air saturation during the fed-batch fermentations. In the first stage, the airflow was fixed at an initial setting of 0.06 L/(L·min) or 0.06 vvm, and the D.O. concentration was maintained by increasing the impeller rate from an initial set point of 50 rpm to a preset maximum of 940. In the second stage, the impeller rate was fixed at 940 rpm, and the D.O. concentration was maintained by increasing the airflow rate from 0.06 vvm to a preset maximum of 1.0 vvm. In the third stage, both the airflow rate and impeller rate were fixed at their maximum values, and the D.O. concentration was finally maintained at 10% air saturation for the remainder of the fermentation by oxygen sensor-controlled glucose feeding. At the beginning of the third stage, the D.O. concentration fell below 10% air saturation due to residual initial glucose in the medium. This state lasted for approximately 1/2 before glucose (65% w/v) feeding commenced. The glucose feed PID control parameters were set to 0.0 s (off) for the derivative control (τ_D) and 999.9 s (minimum control action) for integral control (τ_I). X_p was set to 950.0% to achieve a K_c of 0.1, 166.7% to achieve a K_c of 0.6, and 125.0% to achieve a K_c of 0.8, as required, when the glucose pump range maximum was 32 rpm. For subsequent fermentations, the glucose pump range maximum was decreased to 6 rpm to compensate for pump offset noise and required an X_p of 200.0% (K_c of 0.5) to achieve the identical control action as an X_p of 950.0% previously provided. Antifoam (Sigma 204) was added as needed.

Unlimited Glucose Fed-Batch Fermentation Conditions (Frost Laboratory).

For fermentations that employed glucose-rich conditions, a baffle cage (316 stainless steel) was introduced into the M2 culture vessel. A three-staged algorithm was used to maintain the D.O. concentration at 10% air saturation after addition of the inoculum to the M2 fermentor vessel. In the first stage, the airflow was fixed at an initial setting of 0.06 vvm, and the D.O. concentration was maintained by increasing the impeller rate from an initial set point of 50 rpm to a preset maximum of 750. In the second stage, the impeller rate was fixed at 750 rpm, and the D.O. concentration was maintained by increasing the airflow rate from 0.06 vvm to a preset maximum of 1.0 vvm. After the preset maxima of 750 rpm and 1.0 vvm were reached, the third stage of the fermentation was initiated in which glucose (65% w/v) was added to the vessel at a rate sufficient to maintain a glucose concentration of 10 to 20 g/L throughout the remainder of the run. The airflow rate was maintained at 1.0 vvm initially, and the impeller rate was allowed to vary in order to maintain the D.O. concentration at 10% air saturation. The airflow rate was manually adjusted to 1.5 vvm or 2.0 vvm to keep the impeller rate below 1600 rpm as required. The impeller rate typically varied from 750 rpm to 1600 rpm during the remainder of the run. Antifoam (Sigma 204) was added as needed.

Standard 1 L Glucose-Limited Fed-Batch Fermentation Conditions (Worden Laboratory).

A three-staged algorithm was used to maintain the D.O. level at 10% air saturation during the fed-batch fermentations. In the first stage, the airflow was fixed at

an initial setting of 0.10 vvm, and the D.O. concentration was maintained by increasing the impeller rate from an initial set point of 50 rpm to a preset maximum of 750. The Bioflo IIc D.O. set point was set to 12.5% in order to achieve control of the D.O. concentration at 10% due to the inefficient, unadjustable PID control parameters associated with the PID control of D.O. concentration by impeller rate. In the second stage, the impeller rate was fixed at 750 rpm, and the D.O. concentration was maintained by increasing the airflow rate from 0.10 vvm to a preset maximum of 1.0 vvm. In the third stage, both the airflow rate and impeller rate were fixed at their maximum values, and the D.O. concentration was maintained at 10% of air saturation for the remainder of the fermentation by oxygen sensor-controlled glucose feeding. At the beginning of the third stage, the D.O. concentration fell below 10% air saturation due to residual initial glucose in the medium. This state lasted for approximately 1/2 h before glucose (65% w/v) feeding commenced. Antifoam (Sigma 204) was added manually as needed.

1 L KB-Controlled, Glucose-Limited Worden Laboratory Fed-Batch Fermentation Conditions.

Phase 1 was identical to the first stage of the standard 1 L glucose-limited Worden laboratory fed-batch fermentation conditions in all respects. Phase 2 was identical to the second stage of the standard 1 L glucose-limited Worden laboratory fed-batch fermentation conditions in all respects. In Phase 3, the impeller rate varied from 700 rpm to 1000 rpm to maintain the D.O. concentration at the set point of 10% of air saturation, while the GFR maintained the SOUR at the set point, subject to automated intervention. PID control loop parameters were per Table 35. The initial Phase 3 SOUR set point was

0.13-0.15 $g \cdot g^{-1} \cdot h^{-1}$. Phase 4 was initiated when 40 g/L of biomass had been obtained as predicted by the ANN, but could also be initiated automatically by the control strategy prior to 40 g/L of biomass accumulation. The MGA check was suspended for the first hour of Phase 4 while the CER set point was automatically ramped from the terminal value from Phase 3 (5.0 to 5.3 g/h typically) to the user-defined initial Phase 4 value (4.0 g/h default). The CER was maintained at the set point by the GFR and was subject to automated intervention. The D.O. concentration was simultaneously maintained at the set point of 10% of air saturation by the impeller rate. For modified KB-controlled fermentations, a second CER set point was added to Phase 4 subsequent to the set point ramp previously mentioned. The initial set point of the added CER set point ramp started at the final CER set point value (4.0 g/h) of the first ramp and ended at 48 h (3.4 g/h)

Standard 8 L Glucose-Limited Worden Laboratory Fed-Batch Fermentation Conditions.

A three-staged algorithm was used to maintain the D.O. level at 10% air saturation during the fed-batch fermentations. In the first stage, the airflow was fixed at an initial setting of 0.10 vvm, and the D.O. concentration was maintained by increasing the impeller rate from an initial set point of 150 rpm to a preset maximum of 850. In the second stage, the impeller rate was fixed at 850 rpm, and the D.O. concentration was maintained by increasing the airflow rate from 0.10 vvm to a preset maximum of 1.0 vvm. In the third stage, both the airflow rate and impeller rate were fixed at their maximum values, and the D.O. concentration was maintained at 10% air saturation for the remainder of the fermentation by oxygen sensor-controlled glucose feeding. At the

beginning of the third stage, the D.O. concentration fell below 10% air saturation due to residual initial glucose in the medium. This state lasted for approximately ½ h before glucose (65% w/v) feeding commenced. Antifoam (Sigma 204) was added manually as needed. The glucose feed also contained a low concentration of antifoam (0.2%) to combat foaming problems experienced during 8.0 L fermentations.

8 L KB-Controlled, Glucose-Limited Worden Laboratory Fed-Batch Fermentation Conditions.

Phase 1 was identical to the first stage of the standard 8 L glucose-limited Worden laboratory fed-batch fermentation conditions in all respects. Phase 2 was identical to the second stage of the standard 8 L glucose-limited Worden laboratory fed-batch fermentation conditions in all respects. In Phase 3, the impeller rate varied from 800 rpm to 1020 rpm to maintain the SOUR at the set point, subject to automated intervention, while the GFR maintained the D.O. concentration at the set point of 10% of air saturation. The SOUR set point was automatically set by the control strategy to the value calculated when Phase 2 concluded, and was subject to automated and operator intervention. The PID control loop parameters were per Table 35. Phase 4 was initiated when 40 g/L of biomass had been obtained as predicted by the ANN, but could also be initiated automatically by the control strategy prior to 40 g/L of biomass accumulation per the KB control strategy explanation. The MGA check was suspended for the first hour of Phase 4 while the CER set point was automatically ramped from the terminal value from Phase 3 (45 to 50 g/h typically) to the user-defined initial Phase 4 value (42 g/h default). The CER was maintained at the set point by the GFR and was subject to

automatic and operator intervention. The D.O. concentration was simultaneously maintained at the set point of 10% of air saturation by the impeller rate during CER control.

Shake Flask Equilibration Experiments and Shikimic Acid Doping of Fermentation Broth.

Shikimic acid (purified in house by Dr. Draths) solutions were prepared by adding 1.14 g shikimic acid and 0.045 g K_2HPO_4 to 2 mL of water. The solution pH was adjusted to 6.0 by addition of 10 N KOH, and then to a pH of 7.0 by addition of 5 N KOH and 1 N KOH, and diluted to a volume of 6 mL by the addition of water. The solution was then sterile filtered through a 0.22 μm filter. An aliquot (150 mL) of fermentation broth was harvested at the specified time and split into three equal fractions. Fraction **1** was added to a sterile 250 mL Erlenmeyer flask, made 100 mM in shikimic acid by addition of the shikimic acid solution described above (t=0), and incubated at 37 °C with shaking at 250 rpm. The cells in the remaining two fractions were collected via centrifugation at 3,000 *g* for 5 min. at 4 °C. The supernatant of fraction **2** was retained, sterile filtered through a 0.22 μm filter, added to a sterile 250 mL Erlenmeyer flask, made 100 mM in shikimic acid by addition of the shikimic acid solution described above (t=0), and incubated at 37 °C with shaking at 250 rpm. The supernatant of fraction **3** was discarded and the cells resuspended in fully supplemented, fresh fermentation medium. The cells were collected by centrifugation at 3,000 *g* for 5 min. at 4 °C and the supernatant discarded again. The process was repeated once more, and the resuspension mixture was transferred to a sterile 250 mL Erlenmeyer flask, made 100 mM in shikimic

acid by addition of the shikimic acid solution described above (t=0), and incubated at 37 °C with shaking at 250 rpm. Aliquots (1.5 mL) were transferred from each flask to 1.5 mL microfuge tubes at the indicated intervals and centrifuged using a Beckman microfuge. Supernatant samples were retained for analysis by ^{1}H NMR.

Shikimic Acid Purification and Supplementation.

Fermentation broth (1100-1300 mL) was centrifuged at 14000 *g* for 20 minutes and the biomass discarded. The resulting supernatant was sterile filtered through a 0.22 μm membrane and used directly as a fermentation supplement if unpurified shikimic acid was required. Purification of shikimic acid was initiated by refluxing fermentation supernatant for 4 h, cooling to room temperature, and adjusting the pH to 2.5 by the addition of concentrated H_2SO_4. After centrifugation at 14000 *g* for 20 minutes, the clear yellow supernatant was poured away from the cellular debris and adjusted to pH 6.9 by addition of concentration NH_4OH. The solution was incubated for 1-2 h with 20 g/L Darco KB-B 100 activated carbon with swirling at 50 rpm and then filtered through Whatman 5 filter paper. The filtrate was washed with an additional 250 mL of water. The combined filtrates were then treated in the same manner a second time with activated carbon. This partially purified supernatant was sterilized by filtering through a 0.22 μm membrane and used as a fermentation supplement directly, or carried through the remainder of the purification process to obtain shikimic acid.

Addition of glacial acetic acid to the partially purified supernatant to a final concentration of 15% afforded a clear, yellow solution which was eluted through an AG1-x8 (acetate form, 5 cm x 20 cm) column at 4 °C. Following elution of the column

with an additional 400 mL of 15% aqueous acetic acid, the combined eluents were passed through a column of Dowex 50 (H^+ form, 5 cm x 20 cm) at 4 °C that was then washed with 400 mL of 15% aqueous acetic acid. The eluents off the cation exchange column were combined and concentrated to approximately 150 mL by boiling and then to dryness by rotary evaporation, leaving a hard white solid (83% recovery through this step). Recrystallization from a mixture of methanol and ethyl acetate afforded shikimic acid as a fine white powder (61% recovery based on shikimic acid quantified in crude fermentation broth). Purified shikimic acid (2.0 g) was dissolved in water to a final volume of 12 mL. A portion (10 mL) of this solution was filter sterilized through a 0.22 μm membrane and used as a fermentation supplement.

Fermentation Broth Analysis.

Aliquots (5 to 10 mL) of fermentation broths were harvested at the indicated timed intervals. Cell densities were determined by dilution of fermentation broth with water (1:10, 1:100, or 1:200) followed by measurement of absorption at 600 nm (OD_{600nm}). Dry cell weight (g/L) was calculated using a conversion coefficient of 0.43 $g/L/OD_{600nm}$.[162] The remaining fermentation broth was centrifuged to obtain cell-free supernatant.

Glucose concentrations in cell-free broth were measured using a Yellow Springs Instrument (YSI) Inc. model 2700 Biochemical Analyzer and model 2730 Monitoring and Control Accessory. Offline glucose assays were performed on crude fermentation supernatant. Samples withdrawn during the batch portion of fermentations utilized a sample size of 15 μL and a 7 g/L glucose calibration standard, while samples withdrawn

during the fed-batch portion of fermentations utilized a 65 μL sample size and a 0.5 g/L glucose calibration standard. Online glucose assays utilized the YSI 2730 Monitoring and Control Accessory in conjunction with a Flownamics 320 mm insertion depth cell separation probe (0.2 mL internal volume) fitted with a 0.22 μm ceramic frit. For the batch portion of fermentations, the sample size was 15 μL, the line purge volume was 1500 μL, and the glucose calibration standard was 7 g/L. For the fed-batch portion of fermentations, the sample size was 65 μL, the line purge volume was 1500 μL, and a 0.5 g/L glucose calibration standard was employed. The sampling interval was 1 h. Assay buffer and biochemical analyzer probe membranes were purchased from YSI.

Solute concentrations in the cell-free broth were quantified by ^{1}H NMR. Solutions were concentrated to dryness under reduced pressure, concentrated to dryness one additional time from D_2O, and then redissolved in D_2O containing a known concentration of the sodium salt of 3-(trimethylsilyl)propionic-*2,2,3,3-d*$_4$ acid (TSP, Lancaster Synthesis Inc). All ^{1}H NMR spectra were recorded on a Varian VXR-300 FT-NMR Spectrometer (300 MHz). Concentrations were determined by comparison of integrals corresponding to each compound with the integral corresponding to TSP (δ = 0.00 ppm). Standard concentration curves were determined for shikimic acid,[55b] quinic acid,[55b] and DHQ[163] solutions using authentic, purified metabolites. Compounds were quantified using the following resonances: shikimic acid (δ 4.57, d, 1 H); quinic acid (δ 4.16, m, 1 H); 3-dehydroshikimic acid (δ 4.28, d, 1 H); and 3-dehydroquinic acid (δ 4.35, d, 1 H).

Acetic acid was quantified, were indicated, on fermentations performed in the Worden laboratory by gas chromatography using a Perkin Elmer AutoSystem Gas

Chromatograph interfaced to a Microsys 486/50 MHz computer via a Perkin Elmer Nelson 600 Series LINK equipped with Perkin Elmer Nelson Turbochrom Chromatography Workstation v. 4.1. A glass, packed column (Alltech, HayeSep R 80/100 Mesh, 72" x ¼" OD x 2 mm ID) was used for analyte separation and a Flame Ionization Detector (FID) was used for quantification. The FID temperature was 250 °C. The injection temperature was 170 °C. The oven temperature was static at 230 °C, and held for ten minutes after sample injection. The airflow and hydrogen flow rates to the FID were 400 mL/min. and 45 mL/min. (30 psig), respectively. Helium was used as the carrier gas, with a flow rate of 40 mL/min. (40 psig). Fermentation supernatant was deproteinized by addition of concentration H_2SO_4 to a final concentration of 0.4% (v/v). The precipitated protein was removed via centrifugation in a Fisher Scientific Micro Centrifuge model 235C for 4 minutes. Propionic acid was used as an internal standard for acetic acid (RF of 1.4) concentration determination. Samples were prepared for quantification by adding an aliquot (80 µL) of an aqueous propionic acid solution (4% v/v) to an aliquot (320 µL) of deproteinized fermentation broth, vortexed, and injected onto the GC column. The standard injection volume was 1 µL.

General Enzyme Assay Methodology.

Cells were harvested and resuspended as indicated below. Cell suspensions were disrupted via two passes through a French pressure cell (SLM Aminco) at a pressure differential of 16,000 psi. Cellular debris was removed from the lysate by centrifugation at 48,000 *g* for 25 minutes at 4 °C. Protein concentrations were determined using the Bradford dye-binding procedure.[164] Protein assay solution was purchased from Bio-Rad.

Protein concentrations were determined by comparison to a standard curve prepared using bovine serum albumin.

DAHP Synthase Activity Determination.

DAHP synthase was assayed according to the procedure described by Schoner.[165] Aliquots (10 to 20 mL) of fermentation broth were removed at the indicated intervals. Cells were collected via centrifugation at 3,000 *g* for 5 min at 4 °C. Harvested cells were resuspended (5 to 10 mL) in 50 mM potassium phosphate (pH 6.5) containing PEP (10 mM) and $CoCl_2$ (0.05 mM) and stored at –80 °C until the completion of the fermentation. Cellular lysate was obtained and cellular debris removed, and protein concentrations determined as previously described. Cellular lysate was diluted in potassium phosphate (50mM), PEP (0.5 mM), and 1,3-propanediol (250 mM), pH 7.0. A solution of 12 mM E4P was prepared by concentrating a dilute (3 mM) E4P solution by rotary evaporation, and then neutralizing with 5 N KOH. Two solutions were individually prepared and incubated at 37 °C for five minutes. The first solution (1 mL) contained E4P (6 mM), PEP (12 mM), ovalbumin (1 mg), and potassium phosphate (25 mM), pH 7.0. The second solution (0.5 mL) consisted of the diluted lysate. The two solutions were mixed at time zero and aliquots (0.15 mL) were removed and quenched into 0.1 mL aliquots of 10% (w/v) trichloroacetic acid at timed intervals. Precipitated protein was removed by centrifugation, and the product DAH(P) in each sample was quantified using thiobarbituric acid as described below.

An aliquot (0.1 mL) of the deproteinized DAH(P) containing supernatant was incubated with an aliquot (0.1 mL) of 0.2 M $NaIO_4$ in the presence of 8.2 M H_3PO_4 at 37

°C for 5 min. The reaction was quenched by addition of 0.8 M $NaAsO_2$ in 0.5 M Na_2SO_4 and 0.1 M H_2SO_4 (0.5 mL) and vortexed until a dark brown color disappeared. Upon addition of 3 mL of 0.04 M thiobarbituric acid in 0.5 M Na_2SO_4 (pH 7.0), the sample was heated at 100 °C for 15 min. Samples were cooled (2 min), and the pink chromophore was then extracted into distilled cyclohexanone (4 mL). The aqueous and organic layers were separated by centrifugation (2000 *g*, 15 min). The organic layer absorbance was recorded at 549 nm (ε = 68,000 L/mol/cm). One unit of DAHP synthase activity was defined as the formation of 1 μmol of DAH(P) per minute at 37 °C.

Shikimate Dehydrogenase Activity Determination.

Shikimate dehydrogenase was assayed according to the procedure described by Chaudhuri et al.[166] Lysate was prepared and protein concentrations were determined as previously mentioned.

For reverse assays that employed shikimic acid as the substrate, cells were harvested and resuspended per the DAHP synthase protocol previously mentioned. Cellular lysate was diluted in 100 mM Tris-HCl (pH 9.0). Assays (1 mL) contained Tris-HCl (100 mM), shikimic acid (4 mM), and β-NADP (2 mM) sodium salt. Tris-HCL, shikimic acid, and diluted lysate solutions were mixed, and the spectrophotometer blanked. Addition of β-NADP initiated the assay. The formation of NADPH was monitored at 340 nm (ε = 6,220 L/mol/cm) for 60 seconds using a Hewlett Packard 8452A UV-Vis Diode Array Spectrophotometer. One unit of shikimate dehydrogenase activity was defined as the formation of 1 μmol of NADPH per minute.

For forward assays that employed DHS as the substrate, cells were harvested as previously mentioned and resuspended (5 to 10 mL) in 100 mM Tris-HCl (pH 9.0) containing EDTA (1.0 mM) and dithiothreitol (0.4 mM). Assays (1 mL) contained KH_2PO_4 (100 mM), DHS (2 mM), and NADPH (0.2 mM). KH_2PO_4, DHS, and lysate solutions diluted with assay buffer were mixed, and the spectrophotometer blanked. Addition of NADPH initiated the assay. The loss of NADPH was monitored at 340 nm (ε = 6,220 L/mol/cm) for 60 seconds using a Hewlett Packard 8452A UV-Vis Diode Array Spectrophotometer. One unit of shikimate dehydrogenase activity was defined as the loss of 1 μmol of NADPH per minute.

For forward assays that employed DHQ as the substrate, cells were harvested as previously mentioned and resuspended (5 to 10 mL) in 100 mM Tris-HCl (pH 9.0) containing EDTA (1.0 mM) and dithiothreitol (0.4 mM). Assays (1 mL) contained KH_2PO_4 (100 mM), DHQ (2 mM), and NADPH (0.2 mM). KH_2PO_4, DHQ, and lysate solutions diluted with assay buffer were mixed, and the spectrophotometer blanked. Addition of NADPH initiated the assay. The loss of NADPH was monitored at 340 nm (ε = 6,220 L/mol/cm) for 60 seconds using a Hewlett Packard 8452A UV-Vis Diode Array Spectrophotometer. One unit of shikimate dehydrogenase activity was defined as the loss of 1 μmol of NADPH per minute.

DHQ Dehydratase Activity Determination.

Cells were harvested as previously mentioned, and resuspended in 100 mM KH_2PO_4 (pH 7.0) containing dithiothreitol (DTT, 0.1 mM). Lysate was prepared and protein concentrations determined as previously mentioned. Cellular lysate was diluted

in 100 mM KH_2PO_4 (pH 7.0). Assays (1 mL) contained KH_2PO_4 (100 mM) and DHQ (0.33 mM). KH_2PO_4 and lysate solutions were mixed and the spectrophotometer was zeroed. Addition of DHQ initiated the assay. Formation of DHS was monitored at 234 nm (ε = 12,000 L/mol/cm) for 60 seconds using a Hewlett Packard 8452A UV-Vis Diode Array Spectrophotometer. One unit of DHQ dehydratase activity was defined as the formation of 1 μmol of DHS per minute.

Opto22 Software.

The Opto22 FactoryFloor® software control package was used for data acquisition and control of all fermentations performed in the Worden laboratory. FactoryFloor® version R2.1 was used for all fermentations that employed the Opto22 32-bit G4LC32 controller, while FactoryFloor® version 3.1 was utilized on all fermentations that employed the Opto22 SNAP-LCSX controller.

The com loop time of the strategy was minimized by the addition of 1 msec delay blocks in strategy charts containing blocks that looped back to themselves or control actions which could be executed with minimal computational time before returning to the top of a calculation loop. The OptoTerm com port timeout was set to 2500 msec. Lower com port timeouts led to com loop timeout errors because the com loop time would periodically exceed the timeout value due to the size of the control strategies relative to the speed of the SNAP-LCSX controllers, preventing communication between the controller and the control strategy. A timeout value of 2500 msec was sufficient to prevent timeout errors due to strategy size on both the 1 L and 8 L scales. A binary

communication protocol with a baud rate of 115200 was used for communication between the SNAP-LCSX controller and the PC.

OptoControl, OptoDisplay, and OptoServer were utilized as the ESDT for design of all KB control systems. The control system was entirely encoded in OptoControl, while the MMI for the control system was encoded exclusively in OptoDisplay. The OptoServer provided communication between all ANN/DDE C++ programs, Opto22 hardware, and other Opto22 software programs.

Artificial Neural Network Training.

Artificial Neural Network (ANN) training utilized a custom training program encoded by Mr. Kun Xu. Fermentation data (optical density at 600 nm, quinic acid, DHQ, and acetate concentrations in g/L) as a function of time obtained by offline assays from prior fermentation runs were fit with trend lines in Microsoft Excel. The trend line equations were then used to generate concentration data at 0.25 h intervals for all species to be predicted. The concentration data was then normalized to span the range 0.1 to 0.9. Training data consisting of input and output normalized data were copied to the Training.dat file located in the same root directory as the training program. The training program mode was set to training and the training parameters and topology were entered. The learning rate (β) default was 0.001 and momentum (α) default was 0.0065. The error limit default was 0.001 or 0.0001. The max cycles default was 20,000 when glucose feed rate was an input, and 25,000 when CO_2 % was an input. The noise factor was zero for all training operations. The default topology used was 2-5-1 for all training data sets. Training errors of 0.3 % or less were achieved whenever possible, while

training errors between 0.3 % and 0.4% were deemed acceptable for data sets where convergence was difficult (e.g., 1,000,000 or more cycles). Momentum values greater than 0.0068 often resulted in floating point errors, requiring that the value be reduced. The learning rate was always less than the momentum during ANN training. Once training was completed, a weight matrix was generated for the specified training data set by copying the input columns of the training data to the file Test.dat and operating the training program in the prediction mode. ANN prediction data was automatically generated and saved when operated in the prediction mode to the file Output.dat. The predicted data was compared to the original output data used in the training process. If the point-by-point error was too large (evaluated graphically), then the ANN was retrained to generate a different weight matrix for that data set and the output reexamined, otherwise weight matrix data was copied to the prediction program weight matrix file corresponding to the training data used. The procedure was repeated for each of the fermentation species' concentrations to be predicted online.

Appendix A – KB and Standard Control Strategies, C++ ANN, SM, and DDE Code for the NBS Bioflo IIc and the Dow Miniplant Platforms (Compact Disc Format)

Control Strategies.

The control strategies employed on the NBS Bioflo IIc and Dow Miniplant platforms were encoded in the Opto22 software in a top-down, flowchart format. As such, the control strategies were not conducive to the standard dissertation format and are provided in a compact disc format. The Opto22 Factory Floor® software package (v3.1d or higher) is required to access the control strategies. The file '1 L KB-PS control' contains the KB control system for the NBS Bioflo IIc. The file '1 L standard control' contains the standard glucose-limited control strategy for the NBS Bioflo IIc. The file '8 L KB-PS control' contains the KB control system for the Dow Miniplant system. The file '8 L standard control' contains the standard glucose-limited control strategy for the Dow Miniplant.

DDE, ANN, SM Code.

The file 'ANN training' contains the ANN training program (Project2.exe) and associated files used for offline ANN training. The 'ANN, SM, DDE' file contains individual files for the various platform and vessel-dependent programs used for online ANN predictions and SM calculations. Borland C++ Builder Professional v. 4.0 or higher is required to access the DDE/SM/ANN codes and DDE/ANN interface.

Appendix B – Stoichiometric Model: Reactions and Coefficient Matrix

Stoichiometric Model Reactions.

GLU + PEP + ADP ⟶ G6P + PYR + ATP

G6P ⟶ F6P

F6P + ATP ⟶ 2 GAP + ADP

F6P + GAP ⟶ X5P + E4P

GAP + ADP ⟶ PEP + ATP + NADH

PEP + E4P ⟶ DAHP

X5P ⟶ Ru5P

Ru5P ⟶ R5P

X5P + R5P ⟶ GAP + S7P

GAP + S7P ⟶ E4P + F6P

DAHP + NADPH ⟶ DHQ

DHQ + NADHP ⟶ QA

ADP + PEP ⟶ PYR + ATP

PYR + CoA + NAD ⟶ AcCoA + NADH + CO_2

AcCoA ⟶ ACE + ATP

AcCoA + OAA ⟶ ICT

ICT + NAD ⟶ KG + NADH + CO_2

KG + NAD + ATP ⟶ SUC + NADH + ATP + CO_2

SUC ⟶ OAA + NADH + $FADH_2$

PEP + CO_2 ⟶ OAA

NADH ⟶ NADPH

NADH ⟶ 2 ATP

$FADH_2 \longrightarrow ATP$

$ATP \longrightarrow *$

$0.0205\ G6P + 0.05191\ PEP + 0.28328\ PYR + 0.00709\ F6P + 0.1625\ GAP + 0.03610\ E4P + 0.08977\ R5P + 0.40288\ AcCoA + 0.17687\ OAA + 0.10789\ KG + 1.4678\ NADH + 1.8485\ ATP \longrightarrow 0.1793\ CO_2 + 0.0387\ ACE + 4.13245\ BM$

The intracellular utilization and hydrolysis of ATP is represented by the second to last reaction (flux J23). The coefficients for the formation of biomass from precursor molecules are taken from Neidhardt et al.[141] and Delgado and Liao.[84] The coefficient for biomass was determined from a carbon balance on the precursor metabolites that are incorporated into biomass. The formula for biomass (BM) was $CH_{1.8}O_{0.5}N_{0.2}$, with a formula weight of 24.6 g/Cmol.[138]

Offline exponential smoothing was utilized to reduce the noise associated with SM flux calculations. Noise in online SM flux determination[84a] and online mass balances[167] results from measurement error, system dynamics, etc. Recently a moving average technique has been applied to reduce noise in online balance calculations.[167] The exponential smoothing employed here is a moving average technique that weights all values relative to their proximity to the current value according to Equation 41 and Equation 42. Exponential smoothing is often applied in time series where the time step between measurements is equal.[154] In the case of fed-batch fermentation SM flux data

the time step was 0.25 h corresponding to the ANN prediction interval. The X values correspond to data points in the series of interest while α is the exponential smoothing parameter. The α parameter was automatically determined using the ISTM time series and forecasting program for each series of fluxes. ISTM determines α by minimizing the sum of the squares of the prediction errors when each smoothed value is used as the predictor of the next value in the series.[168]

Equation 41.

$$\hat{m}_t = \sum_{j=0}^{t-2} \alpha(1-\alpha)^j X_{t-j} + (1-\alpha)^{t-1} X_1 \qquad \text{for t } \geq 2.$$

Equation 42.

$$\hat{m}_1 = X_1 \qquad \text{for t = 1.}$$

Stoichiometric Model Coefficient Matrix.

	fluxes																							
species:	J1	J2	J3	J4	J5	J6	J7	J8	J9	J10	J11	J12	J13	J14	J15	J16	J17	J18	J19	J20	J21	J22	J23	J24
GLU	-1	0	0	0	0	0	0	0	0	0	0	0	0	0	0	0	0	0	0	0	0	0	0	0.00000
G6P	1	-1	0	0	0	0	0	0	0	0	0	0	0	0	0	0	0	0	0	0	0	0	0	-0.02050
PEP	-1	0	0	0	1	-1	0	0	0	0	0	0	-1	0	0	0	0	0	0	-1	0	0	0	-0.05191
PYR	1	0	0	0	0	0	0	0	0	0	0	0	1	-1	0	0	0	0	0	0	0	0	0	-0.28328
F6P	0	1	-1	-1	0	0	0	0	0	1	0	0	0	0	0	0	0	0	0	0	0	0	0	-0.00709
GAP	0	0	2	-1	-1	0	0	0	1	-1	0	0	0	0	0	0	0	0	0	0	0	0	0	-0.16250
X5P	0	0	0	1	0	0	1	0	-1	0	0	0	0	0	0	0	0	0	0	0	0	0	0	0.00000
E4P	0	0	0	1	0	-1	0	0	0	1	0	0	0	0	0	0	0	0	0	0	0	0	0	-0.03610
DAHP	0	0	0	0	0	1	0	0	0	0	-1	0	0	0	0	0	0	0	0	0	0	0	0	0.00000
Ru5P	0	0	0	0	0	0	-1	-1	0	0	0	0	0	0	0	0	0	0	0	0	0	0	0	0.00000
R5P	0	0	0	0	0	0	0	1	-1	0	0	0	0	0	0	0	0	0	0	0	0	0	0	-0.08977
S7P	0	0	0	0	0	0	0	0	1	-1	0	0	0	0	0	0	0	0	0	0	0	0	0	0.00000
DHQ	0	0	0	0	0	0	0	0	0	0	1	-1	0	0	0	0	0	0	0	0	0	0	0	0.00000
QA	0	0	0	0	0	0	0	0	0	0	0	1	0	0	0	0	0	0	0	0	0	0	0	0.00000
AcCoA	0	0	0	0	0	0	0	0	0	0	0	0	0	1	-1	-1	0	0	0	0	0	0	0	-0.40288
OAA	0	0	0	0	0	0	0	0	0	0	0	0	0	0	0	-1	0	0	1	1	0	0	0	-0.17687
ICT	0	0	0	0	0	0	0	0	0	0	0	0	0	0	0	1	-1	0	0	0	0	0	0	0.00000
KG	0	0	0	0	0	0	0	0	0	0	0	0	0	0	0	0	1	-1	0	0	0	0	0	-0.10789
SUC	0	0	0	0	0	0	0	0	0	0	0	0	0	0	0	0	0	1	-1	0	0	0	0	0.00000
NADH	0	0	0	0	1	0	0	0	0	0	0	-1	0	1	0	0	1	1	1	0	-1	0	0	-1.46780
$FADH_2$	0	0	0	0	0	0	0	0	0	0	0	0	0	0	0	0	0	0	1	0	0	-1	0	0.00000
ATP	1	0	-1	0	1	0	0	0	0	0	0	0	1	0	1	0	0	1	0	0	2	1	-1	-1.84850
CO2	0	0	0	0	0	0	0	0	0	0	0	0	0	1	0	0	1	1	0	-1	0	0	0	0.17930
ACE	0	0	0	0	0	0	0	0	0	0	0	0	0	0	1	0	0	0	0	0	0	0	0	0.03870
BM	0	0	0	0	0	0	0	0	0	0	0	0	0	0	0	0	0	0	0	0	0	0	0	4.13245

Appendix C – MATLAB Dynamic Fermentation Model

Dynamic Fed-Batch Fermentation Model MATLAB® Code.

```
global error
error=0;
y0=[0.3,0.00357376,3.0,1.2,1.0,0.0]';
%
% y0(1) is initial glucose condition/concentration
% y0(2) is initial oxygen condition/concentration
% y0(3) is initial volume condition
% y0(4) is initial accumulated error
tspan=[13.8,48.0]';
[t,y]=ode23('Bioreactor',tspan,y0);
figure(1)
plot(t,y(:,1)),title('Glucose Concentration(g/L)'),xlabel('Time(h)'),...ylabel('Glucose
Concentration(g/L)');
figure(2)
plot(t,y(:,2)),title('O2 Concentration (g/L)'),xlabel('Time(h)'),...ylabel('O2
concentration(g/L)');
figure(3)
plot(t,y(:,5)),title('Reactor Volume (L)'),xlabel('Time(h)'),...ylabel('Reactor Volume(L)');
figure(4)
plot(t,y(:,6)),title('Accumulated Error'),xlabel('Time(h)'),...ylabel('Accumulated Error');
end


function yp=bioreactor(t,y);
global error
t
Sf=650.0;
of=0.0;
Fs=0.0;
Co_setpoint=0.00357376;  % in g/L at 33C, not percent D.O.
SOUR_max=0.21; %
%SGUR_max=0.83;
kla=650.0;        % 425 or 650
Co_star=0.03573760; % in g/L at 33C
Ks=0.036;          % Km for PTS uptake of glucose in Neidhardt et al, range 0.036-0.072
g/L
Ko=0.00000071;     % Ko from Biochemical Engineering by Clark
Kc=-0.8;
Tau_i=75.0;
monod_glucose=y(1)/(Ks+y(1));
monod_oxygen=y(2)/(Ko+y(2));
monod=monod_glucose*monod_oxygen;
error=Co_setpoint-y(2);
V_l=y(5);
```

```
F=Fs+Kc*(error+(1/Tau_i)*y(6));
X=0.00207921810699596*t^3-0.26320436507935400*t^2+10.92854100529030000*t-
85.40414285713350000;
SGUR_max=(0.000001800625287504*t^4-0.00029196547779798*t^3+
0.01746945845913080*t^2 - 0.46396860397763600*t + 4.86780753591300000);
yp(1)=(F/V_l)*(Sf-y(1))-SGUR_max*monod*X; % glucose balance
yp(2)=(F/V_l)*(of-y(2))+kla*(Co_star-y(2))-SOUR_max*monod*X; % oxygen balance
yp(3)=0.8*F;        % volume
yp(4)=error;        % accumulated error
fid=fopen('concentration.dat','a');
fprintf(fid,'%f ',t,y);
fprintf(fid,'\n');
status=fclose(fid);
yp=yp';
```

Dynamic Fed-Batch Fermentation Model Parameters.

Table 36. Dynamic fed-batch fermentation model parameters.

Parameter	Source	Value	Description
S (g/L)	Calculated	f(t)	Glucose concentration
F_G (L/h)	Calculated	f(t)	Feed rate
V (L)	Calculated	f(t)	Reactor volume
C_o (g/L)	Calculated	f(t)	Liquid phase oxygen concentration
F_{SS} (L/h)	Empirical	0.0	Glucose flow rate steady-state bias
E(t)	Calculated	f(t)	Error
K_s (g/L)	Literature	0.036	*E. coli* Monod constant for glucose uptake
K_o (g/L)	Literature	7.1×10^{-7}	*E. coli* Monod constant for oxygen uptake
X (g/L)	Empirical	Curve fit	Cell mass concentration from fermentation data
S_f (g/L)	Empirical	650 g/L	Glucose feed concentration
$SGUR_{max}$ ($g \cdot g^{-1} \cdot h^{-1}$)	Empirical	Polynomial	Maximum SGUR, estimated from fermentation data
C_{of} (g/L)	Empirical	0.0	Oxygen concentration in the glucose feed
k_La (h^{-1})	Empirical	Per text	Mass transfer coefficient (m/h)* specific interfacial area (m^2/m^3)
C_L^* (g/L)	Literature	0.0357	Equilibrium oxygen concentration at saturation (g/L)
$SOUR_{max}$ ($g \cdot g^{-1} \cdot h^{-1}$)	Empirical	0.21	Maximum SOUR estimated from fermentation data
K_c (%/(L/h))	Fit	0.5 or 0.8	Controller proportional term ($\Delta C_o/\Delta F$)
τ_I (h)	Fit	75.0	Controller integral term

Literature Cited

[1] Campbell, C. J.; Laherrere, J. H. *Sci. Am.* **1998**, *278* (3), 78.

[2] Weissermel, K.; Arpe, H.-J. *Industrial Organic Chemistry, 3rd Ed.*; VCH: New York, 1997: p. 8.

[3] Weissermel, K.; Arpe, H.-J. *Industrial Organic Chemistry, 3rd Ed.*; VCH: New York, 1997: p. 316.

[4] Weissermel, K.; Arpe, H.-J. *Industrial Organic Chemistry, 3rd Ed.*; VCH: New York, 1997: p. 3-4.

[5] In *Kirk-Othmer Encyclopedia of Chemical Technology, 4th Ed.*; Kroschwitz, J. ed.; Wiley: New York, 1998; Suppl. Vol., p. 713.

[6] *World of Corn-2001*; National Corn Growers Association: (a) 2000 corn harvest: http://www.ncga.com/03world/main/US_corn_prod_2000.html. (b) starch content of corn: http://www.ncga.com/03world/main/kernel.html.

[7] Moniruzzaman, M.; Dien, B. S.; Ferrer, B.; Hespell, R. B.; Dale, B. E.; Ingram, L. O.; *Biotechnol. Lett.* **1996**, *18*, 985-990.

[8] Parekh, S.; Vinci, V.; Strobel, R. *Appl. Microb. Biotech.* **2000**, *54*, 287.

[9] Wilke, D. *Appl. Microb. Biotech.* **1999**, *52*, 135.

[10] Eggeling, L.; Sahm, H. *Appl. Microb. Biotech.* **1999**, *52*, 146.

[11] Datta, R.; Tsai, S.-P.; Bonsignore, P.; Moon, S.-H.; Frank, J. R. *FEMS Microbiol. Rev.* **1995**, *16*, 221.

[12] Haslam, E. *The Shikimate Pathway*; Halstead Press: New York, 1974.

[13] (a) Kishore, G. M.; Padgette, S. R.; Fraley, R. T. *Weed Technol.* **1992**, *6*, 626. (b) Edwards, J. W.; Kishore, G. M.; Stark, D. M. In *Kirk-Othmer Encycolpedia of Chemical Technology, 4th Ed.*; Wiley: New York, 1994; Vol. 12, p.493.

[14] Forlani, G.; Lejczak, B.; Kafarski, P. *J. Plant Growth Regul.* **1999**, *18*, 73.

[15] Ajioka, J. W.; Fitzpatrick, J. M.; Reitter, *Exp. Rev. Mol. Med.*, **2001**, (1), 1.

[16] Davis, D. D.; Kemp, D. R. In *Kirk-Othmer Encycolpedia of Chemical Technology, 4th Ed.*; Wiley: New York, 1998; Vol. 1, p. 466-493.

[17] Dickinson, R. E.; Cicerone, R. J. *Nature* **1986**, *319*, 109.

[18] Thiemens, M. H.; Trogler, W. C. *Science* **1991**, *252*, 932.

[19] Draths, K. M.; Frost, J. W. *J. Am. Chem. Soc.* **1994**, *116*, 399.

[20] Nu, W., Draths, K. M., Frost, J. W. *J. Am. Chem. Soc.*, **2001**, ASAP article.

[21] Krumenacker, L.; Costantini, M.; Pontal, P.; Sentenac, J. In *Kirk-Othmer Encyclopedia of Chemical Technology, 4th ed.*; Wiley: New York, 1995, Vol. 13, p. 997.

[22] (a) Franck, H.-G.; Stadelhofer, J. W. *Industrial Aromatic Chemistry*; Springer Verlag: New York, **1988**, p. 183-190. (b) Krumenacker, L.; Costantini, M.; Pontal, P.; Sentenac, J. In *Kirk-Othmer Encyclopedia of Chemical Technology, 4th ed.*; Wiley: New York, 1995, Vol. 13, p. 996-1014. (c) Szmant, H. H. In *Organic Building Blocks of the Chemical Industry*; New York: Wiley, **1989**, p. 512 – 519.

[23] (a) Draths, K. M.; Frost, J. W. *J. Am. Chem. Soc.* **1994**, *116*, 399. (b) Draths, K. M.; Frost, J. W. *J. Am. Chem. Soc.* **1995**, *117*, 2395.

[24] Dalton, D. R. In *Kirk-Othmer Encyclopedia of Chemical Technology, 4th ed.*; Wiley: New York, 1991 Vol. 1, p. 1071.

[25] Kambourakis, S. PhD. Dissertation. Michigan State University, 2000.

[26] Kambourakis, S.; Draths, K. M.; Frost, J. W. *J. Am. Chem. Soc.* **2000**, *122*, 9042.

[27] Leston, G. In *Kirk-Othmer Encyclopedia of Chemical Technology, 4th ed.*; Wiley: New York, Vol. 19, p. 780-787.

[28] Kambourakis, S.; Frost, J. W. *J. Org. Chem.* **2000**, *65*, 6904.

[29] (a) Entsch, B.; Palfey, B. A.; Ballou, D. P.; Massey, V. *J. Biol. Chem.* **1991**, *266*, 17341. (b) Eschrich, K.; van der Bolt, F. J. T.; de Kok, A.; van Berkel, W. J. H. *Eur. J. Biochem.* **1993**, *216*, 137.

[30] Priefert, H.; Rabenhorst, J.; Steinbuchel, A. Appl. Microbiol. Biotechnol. **2001**, *56*, 296.

[31] Esposito, L. J.; Formanek, K.; Kientz, G.; Mauger, F.; Maureaux, V.; Robert, G.; Truchet, F. In *Kirk-Othmer Encyclopedia of Chemical Technology, 4th ed.*; Wiley: New York, 1997, Vol. 24, p. 812-825.

[32] Li, K.; Frost, J. W. *J. Am. Chem. Soc.* **1998**, *120*, 10545.

[33] Li, K.; Mikola, M. R.; Draths, K. M.; Worden, R. M.; Frost, J. W. *Biotechnol. Bioeng.* **1999**, *64*, 61.

[34] Yi, J., Draths, K. M., Frost, J. W. unpublished results.

[35] (a) Gregory, P. In *Kirk-Othmer Encyclopedia of Chemical Technology, 4th ed.*; Wiley: New York, 1993, Vol. 8, p. 597. (b) Szmant, H. H. In *Organic Building Blocks of the Chemical Industry*; Wiley: New York, 1989: p 585.

[36] Murdock, D.; Ensley, B. D.; Serdar, C.; Thalen, M. *Bio/technology* **1993**, *11*, 381.

[37] Genencor, unpublished results.

[38] (a) Kirsch, M. A.; Williams, D. J. *Chemtech* **1994**, 24 (4), 40. (b) Russell, A. D.; J. *Appl. Bacteriol.* **1991**, *71*, 191.

[39] Barker, J. L. PhD. Dissertation. Michigan State University, 2001.

[40] Frank, H. G.; Stadelhofer, J. W. *Industrial Aromatic Chemistry*; Springer-Verlag: New York, 1988; p. 146-150. (b) Erickson, S. H. In *Kirk-Othmer Encyclopedia of Chemical Technology, 3rd ed.*; Wiley: New York, 1982, Vol. 20, p. 517-519.

[41] Arestra, M.; Quaranta, E.; Dileo, C.; Tommasi, I. *Tetrahedron* **1998**, *54*, 8841.

[42] Grelak, R. L.; Chen, K. K. Int. Pat. Appl. WO 9856920, 1998.

[43] Herrmann, K. In *Amino Acids Biosynthesis and Genetic Regulation*; Addison-Wesley Publishing Co.: London, 1983, p. 309-310.

[44] Im, S. W. K.; Davidson, H.; Pittard, J. *J. of Bacteriol.* **1971**, *108*, 400.

[45] Smith, L. C.; Ravel, J. M.; Lax, S. R.; Shive, W. *J. Biol. Chem.* **1962**, *237*, 3566.

[46] Ogino, T.; Garner, C.; Markley, J. L.; Herrmann, K. M. *Proc. Natl. Acad. Sci. USA,* **1982**, *79*, 5828.

[47] Herrmann, K. In *Amino Acids Biosynthesis and Genetic Regulation*; Addison-Wesley Publishing Co.: London, 1983, p. 308.

[48] Mikola, M. R.; Widman, M. T.; Worden, R. M. *Appl. Biochem. Biotechnol.* **1998**, *70*, 905.

[49] (a) Draths, K. M.; Frost, J. W. *J. Am. Chem. Soc.* **1990**, *112*, 1657. (b) Draths, K. M.; Pompliano, D. L.; Conley, D. L.; Frost, J. W.; Berry, A.; Disbrow, G. L.; Staversky, R. J.; Lievense, J. C. *J. Am. Chem. Soc.* **1992**, *114*, 3956.

[50] (a) Blackmore, P. F.; William, J. F.; Macleod, J. F. *FEBS Lett.* **1976**, *64*, 222. (b) Duke, C. C.; Macleod, J. F.; Williams, J. F. *Carbohydr. Res.* 1981, 95, 1.

[51] (a) Li, K.; Frost, J. W. *Biotechnol. Prog.* **1999**, *15*, 876. (b) Patnaik, R.; Spitzer, R. G.; Liao, J. C. *Biotechnol. Bioeng.* **1995**, 46, 361.

[52] Patnaik, R.; Liao, J. C. *Appl Environ. Microbiol.* **1994**, *60*, 3903.

[53] (a) Miller, J. E.; Backman, K. C.; O'Connor, J. J.; Hatch, T. T. *J. Ind. Microbiol.* **1987**, *2*, 143. (b) Flores, C.-L.; Gancedo, C. *FEBS Lett.* **1997**, *412*, 531. (c) Scrutton, M. C. *FEBS Lett.* **1978**, *89*, 1. (d) Ashworth, J. M.; Kornberg, H. L. *Proc. R. Soc. London B.* **1966**, *165*, 179. (e) Emmerling, M.; Dauner, M.; Ponti, A.; Fiaux, J.; Hochuli, M. Szyperski, T.; Wüthrich, K.; Bailey, J. E.; Sauer, U. **2002**, *184*, 152. (f) Terada, K.; Fujita, N.; Katsuki, H.; Izui, K. *Biosci. Biotech. Biochem.* **1995**, *59*, 735. (g) Fraenkel, D. G. In *Escherichia coli and Salmonella: Cellular and Molecular Biology*; Neidhardt, F. C., Ed.; ASM Press: Washington, DC, 1996, Chapter 14.

[54] (a)Voet, D.; Voet, J. G. In *Biochemistry, 2nd Ed.*; Wiley & Sons: New York, 1995. (b) Mori, M.; Yokota, A.; Sugitomo, S.; Kawamura, K. Patent JP 62,205,782, 1987.

[55] (a) Yi, J.; Li, K.; Draths, K. M.; Frost, J. W. unpublished results. (b) Chandran, S. S.; PhD Dissertation, Michigan State University, January 2001.

[56] Flores, N.; Xiao, J.; Berry, A.; Bolivar, F.; Fernando, V. *Nat. Biotechnol.* **1996**, *14*, 620.

[57] (a) Li, K.; Frost, J. W. *J. Am. Chem. Soc.* **1999**, *121*, 9461. (b) Hou, S.-Y.; Chao, Y.-P.; Liao, J. C. *J. Bacteriol.* **1995**, *177*, 1620.

[58] Meier, S. J.; Hatton, T. A.; Wang D. I. C. *Biotechnol. Bioeng.* **1999**, *62*, 468.

[59] Charles, M.; Wilson, J. In *Bioprocess Engineering: Systems, Equipment and Facilities*; Lydersen, B. K.; D'elia, N. A.; Nelson, K. L., Eds.; Wiley & Sons: New York, 1994: p. 9-10.

[60] Blanch, H. W.; Clark, D. S. In *Biochemical Engineering*; Marcel Dekker, Inc.: New York, 1996: p. 427.

[61] Charles, M.; Wilson, J. In *Bioprocess Engineering: Systems, Equipment and Facilities*; Lydersen, B. K.; D'elia, N. A.; Nelson, K. L., Eds.; Wiley & Sons: New York, 1994: p. 26-27.

[62] Bailey, J. E.; Ollis, D. F. *Biochemical Engineering Fundamentals*, 2^{nd} *ed.*, McGraw-Hill: New York, 1986: p. 393.

[63] Bailey, J. E.; Ollis, D. F. *Biochemical Engineering Fundamentals*, 2^{nd} *ed.*, McGraw-Hill: New York, 1986: p. 463.

[64] (a) Chen, J.-Y.; Wen, C.-M.; Chen, T.-L. *Biotechnol. Bioeng.* **1999**, *62*, 311. (b) Vasconcelos, J. M. T.; Alves, S. S.; Nienow, A. W.; Bujalski, W. *Can. J. Chem. Eng.* **1998**, *76*, 398. (b) Veglio, F.; Beolchini, F.; Ubaldini, S. *Proc. Biochem.* **1998**, *33*, 367. (d) Svihla, C. K.; Berson, R. E.; Hanley, T. R. In *Industrial Mixing Fundamentals with Applications, AIChE Symposium Series*; Tatterson, B. B., Ed., **1995**, *91*, 161-165. (e) Bredwell, M. D.; Worden, R. M. *Biotechnol. Prog.* **1998**, *14*, 31. (f) Bredwell, M. D.; Srivastava, P.; Worden, R. M. *Biotechnol. Prog.* **1999**, *15*, 834. (g) Ognean, T. *Biotechnol. Bioeng.* **1993**, *41*, 1014. (h) Kaster, J. A.; Michelsen, D. L.; Velander, W. H. *Appl. Biochem. Biotechnol.* **1990**, *24/25*, 469. (i) Hudcova, V.; Machon, V.; Nienow, A. W. *Biotechnol. Bioeng.* **1989**, *34*, 617. (j) Hubbard, D. W.; Harris, L. R.; Wierenga, M. K. *Chem. Eng. Prog.* **1988**, (8), 55. Mooyman, J. G. *Biotechnol. Bioeng.* **1987**, *29*, 180. (k) Vardar-Sukan, F. *Proc. Biochem.* **1986**, (4), 40. Lally, K. S.; Oldshue, J. Y.; Weetman, R. J. Mixing Equipment Co., Inc. Technical Report, November, 1985.; (l) Oosterhuis, N. M. G.; Kossen, N. W. F. *Biotechnol. Bioeng.* **1984**, *26*, 546. (m) Oosterhuis, N. M. G.; Kossen, N. W. F. *Chem. Eng. Res. Des.*, **1983**, *61*, 308. (n) Van't Riet, K. *Trends Biotechnol.* **1983**, *1*, 113. (o) Andrew, S. P. S. *Trans. IChemE.*, **1982**, *60*, 3. (p) Van't Riet, K. *Ind. Eng. Chem. Proc. Des. Dev.*, **1979**, *18*, 357. (q) Luong, H. T.; Volesky, B. *AIChE J.* **1979**, *25*, 893. (r) Ichii, T.; Takehara, S.; Konno, H.; Ishida, T.; Sato, H.; Suzuki, A.; Yamazumi, K. *J. Ferm. Bioeng.* **1993**, *75*, 375. (s) Bredwell, M. D.; Telgenhoff, M. D.; Worden, R. M. *Appl. Biochem. Biotechnol.* **1995**, *51/52*, 501.

[65] (a) Uhl, V. W.; Von Essen, J. *Biotechnol. Prog.* , 155. (b) Forschner, P.; Krebs, R.; Schneider, T. In *Process Mixing: Chemical and Biochemical Applications, AIChE Symposium Series*; Tatterson, B. B.; Calabrese, R. V., Eds., **1992**, *88*, 38. (c) Hubbard, D. W. *Biotechnol. Prog.;* **1987**, , 168. (d) Singh, V.; Fuchs, R.; Constantinides, A. *Biotechnol. Prog.* **1987**, ,200. (e) Hubbard, D. W. *Ann. New York Acad. Sci.* **1987**, *506*, 600.

[66] (a) Bredwell, M. D.; PhD. Dissertation, Michigan State University, 1998. (b) Srivastava, S.; PhD. Dissertation, Michigan State University, 2000. (c) Sebba, F. *Chem. Ind.* **1984**, *21*, 367. (d) Sebba, F. *Chem. Ind.* **1985**, (3), 91. (e) Sebba, F. *Foams and Biliquid Foams – Aphrons*; Wiley & Sons: New York, 1987.

[67] Konstantinov, K. Bayer Inc., personal communication.

[68] Belter, P. A.; Cussler, E. L.; Hu., W.-S. *Bioseparations: Downstream Processing for Biotechnology*; Wiley & Sons: New York, 1988: p. 2-3.

[69] Belter, P. A.; Cussler, E. L.; Hu., W.-S. *Bioseparations: Downstream Processing for Biotechnology*; Wiley & Sons: New York, 1988: p. 5.

[70] Belter, P. A.; Cussler, E. L.; Hu., W.-S. *Bioseparations: Downstream Processing for Biotechnology*; Wiley & Sons: New York, 1988: p. 17.

[71] Belter, P. A.; Cussler, E. L.; Hu., W.-S. *Bioseparations: Downstream Processing for Biotechnology*; Wiley & Sons: New York, 1988: p. 18-22.

[72] Belter, P. A.; Cussler, E. L.; Hu., W.-S. *Bioseparations: Downstream Processing for Biotechnology*; Wiley & Sons: New York, 1988: p. 273-274.

[73] Belter, P. A.; Cussler, E. L.; Hu., W.-S. *Bioseparations: Downstream Processing for Biotechnology*; Wiley & Sons: New York, 1988: p. 307.

[74] (a) Dale, B. E.; Leong, C. K.; Pham, T. K.; Esquivel, V. M.; Rios, I.; Latimer, V. M. *Biores. Technol.* **1996**, *56*, 111. (b) Moniruzzaman, M.; Dale, B. E.; Hespell, R. B.; Bothast, R. J. *Appl. Biochem. Biotechnol.* **1997**, *67*, 113. (c) Hespell, R. B.; O'Bryan, P. J.; Moniruzzaman, M.; Bothast, R. J. *Appl. Biochem. Biotechnol.* **1997**, *62*, 87.

[75] Dale, B. E.; Henk, L. L.; Shiang, M. *Dev. Ind. Microbiol.* **1985**, *26*, 223.

[76] Saha, B. C.; Dien, B. S.; Bothast, R. J. *Appl. Biochem. Biotechnol.* **1998**, *70-72*, 115.

[77] (a) Patnaik, P. R. *Lab. Robotics Automat.* **1997**, *9*, 297. (b) Warnes, M. R.; Glassey, J.; Montague, G. A.; Kara, B. *Neurocomputing* **1998**, *20*, 67. (c) Linko, P.; Zhu, Y.-H. *Proc. Biochem.* **1992**, *27*, 275. (d) Bachinger, Th.; Mårtensson, P.; Mandenius, C.-F. *J. Biotechnol.* **1998**, *60*, 55. (e) Mészáros, A.; Brdys', M. A.; Tatjewski, P.; Lednický, P. *Bioproc. Eng.* **1995**, *12*, 1. (f) Lednický, P.; Mészáros, A. *Bioproc. Eng.* **1998**, *18*, 427. (g) Syu, M. J.; Hou, C. L. *Bioproc. Eng.* **1999**, *21*, 141. (h) Simon, L.; Karim, M. N. *Biochem. Eng. J.* **2001**, *7*, 41. (i) Simon, L.; Karim, M. N; Schreiveis, A. *Biotechnol. Tech.* **1998**, *12*, 301. (j) Syu, M. J.; Hou, C. L. *Bioproc. Eng.* **1999**, *20*, 271. (k) Li, Y.; Brown, C. W.; Sun, F.-M.; McCrady, J. W.; Traxler, R. W.; Lo, S.-C. J. *Near Infrared Spectrosc.* **1999**, *7*, 101. (l) Montague, G.; Morris, J. *Trends Biotechnol.* **1994**, *12*, 312. (m) Soufian, M.; Soufian, M. *Lect. Notes Comput. Sc.* **1997**, *1226*, 577. (n) Glassey, J.; Montague, G. A.; Ward, A. C.; Kara, B. V. *Biotechnol. Bioeng.* **1994**, *44*, 397. (o) Patnaik, P. R. *Biochem. Eng. J.* **1999**, *3*, 113. (p) Albiol, J.; Campmajó, C.; Casas, C.; Poch, M. *Biotechnol. Prog.* **1995**, *11*, 88. (q) Massimo, C. D.; Willis, M. J.; Montague, G. A.; Tham, M. T.; Morris, A. J. *Bioproc. Eng.* **1991**, *7*, 77. (r) Muralikrishnan, G.; Chidambaram, M. *Bioproc. Eng.* **1995**, *12*, 35. (s) Petrova, M.; Knoprinkova, P.;

Patarinska, T.; Bliznakova, M. *Bioproc. Eng.* **1998**, *18*, 281. (t) Bhat, N.; McAvoy, T. J. *Comp. Chem. Eng.* **1990**, *14*, 573. (u) Zhu, Y. H.; Rajalahti, T.; Linko, S. *Chem. Eng. J.* **1996**, *62*, 207.

[78] (a) Kasprow, R. P.; Lange, A. J.; Kirwan, D. J. *Biotechnol. Prog.* **1998**, *14*, 318. (b) Kasprow, R. P.; Kirwan, D. J. **1998**, AIChE meeting session 15D07.

[79] (a) Hunt, K. J.; Sbarbaro, D.; Żbikowski, R.; Gawthrop, P. J. *Automatica* **1992**, *28*, 1083. (b) Tulunay, E. In *Neural Networks: Advances and Applications;* Gelenbe, E. ed.; Elsevier Sci. Pub.: London, 1991; p. 241-273. (c) Miller, W. T.; Sutton, R. S.; Werbos, P. J. *Neural Networks for Control*; MIT Press: Cambridge, 1990.

[80] Haykin, S., *Neural Networks. A Comprehensive Foundation;* Macmillan College Publishing Company: New York, 1994; p. 1-32.

[81] (a) Konstantinov, K.; Aarts, R.; Yoshida, T. In *Advances in Biochemical Engineering/Biotechnology*; *48*, Springer-Verlag: New York, 1992; 169-191. (b) Konstantinov, K.; Yoshida, T. *J. Ferm. Bioeng.* **1990**, *70*, 420. (c) Konstantinov, K.; Yoshida, T. *J. Ferm. Bioeng.* **1990**, *70*, 48. (d) Konstantinov, K.; Yoshida, T. *Biotechnol. Bioeng.* **1992**, *39*, 479. (e) Konstantinov, K.; Yoshida, T. *AIChE J.* **1992**, *38*, 1703. (f) Konstantinov, K. *Seibutsu-Kogaku Kais* **1993**, *71*, 253.

[82] Ignizio, J. P., In *Introduction to Expert Systems. The Development and Implementation of Rule-Based Expert Systems;* McGraw-Hill, Inc.: New York, 1991; p. 12.

[83] Ignizio, J. P., In *Introduction to Expert Systems. The Development and Implementation of Rule-Based Expert Systems;* McGraw-Hill, Inc.: New York, 1991; p. 202.

[84] (a) Takiguchi, N.; Shimizu, H.; Shioya, S. *Biotechnol. Bioeng.* **1997**, *55*, 170. (b) Schilling, C. H.; Edwards, J. S.; Palsson, B. O. *Biotechnol. Prog.* **1999**, *15*, 288. (c) Liao, J. C. *J. Biotechnol.* **1999**, *71*, 259. (d) Liao, J. C.; Delgado, J. *Biotechnol. Prog.* **1998**, *14*, 554. (e) Park, S. M.; Klapa, M. I.; Sinskey, A. J.; Stephanopoulos, G. *Biotechnol. Bioeng.* **1999**, *62*, 393. (f) Keasling, J. D.; Pramanik, J. *Biotechnol. Bioeng.* **1998**, *60*, 230. (g) Keasling, J. D.; Pramanik, J. *Biotechnol. Bioeng.* **1997**, *56*, 398. (h) Delgado, J.; Liao, J. C. *Biotechnol. Prog.* **1997**, *13*, 361. (i) Chen, R.; Hatzimanikatis, V.; Yap, W. M. G. J.; Postma, P. W.; Bailey, J. E. *Biotechnol. Prog.* **1997**, *13*, 768. (j) Varma, A.; Palsson, B. O. *J. Theor. Biol.* **1993**, *165*, 477. (k) Varma, A.; Palsson, B. O. *J. Theor. Biol.* **1993**, *165*, 503. (l) Savinell, J. M.; Palsson, B. O. *J. Theor. Biol.* **1992**, *155*, 201. (m) Savinell, J. M.; Palsson, B. O. *J. Theor. Biol.* **1992**, *155*, 215. (n) Savinell, J. M.; Palsson, B. O. *J. Theor. Biol.* **1992**, *154*, 421. (o) Savinell, J. M.; Palsson, B. O. *J. Theor. Biol.* **1992**, *154*, 455. (p) Vallino, J. J.; Stephanopoulos, G. *Biotechnol. Bioeng.* **1993**, *41*, 633. (q) Vallino, J. J.; Stephanopoulos, G. In *Frontiers in Bioprocessing*; CRC Press, Inc.: Boca Raton, 1990; Chapter 18. (r) Papoutsakis, E. T. *Biotechnol. Bioeng.* **1984**, *26*, 174.

[85] Haslam, E. *Shikimic Acid: Metabolism and Metabolites*; Wiley & Sons: New York, 1993.

[86] Herrmann, K. M.; Weaver, L. M. *Annu. Rev. Plant Physiol. Plant Mol. Biol.* **1999**, *50*, 473.

[87] Pittard, A. J. In *Escherichia coli and Salmonella: Cellular and Molecular Biology*; Neidhardt, F. C., Ed.; ASM Press: Washington, DC, 1996; Chapter 28.

[88] Roberts, F.; Roberts, C. W.; Johnson, J. J.; Kyle, D. E.; Krell, T.; Coggins, J. R.; Coombs, G. H.; Milhous, W. K.; Tzipori, S.; Ferguson, D. J. P.; Chakrabarti, D.; McLeod, R. *Nature* **1998**, *393*, 801.

[89] Tan, D. S.; Foley, M. A.; Shair, M. D.; Schreiber, S. L. *J. Am. Chem. Soc.* **1998**, *120*, 8565.

[90] Kim, C. U.; Lew, W.; Williams, M. A.; Liu, H.; Zhang, L.; Swaminathan, S.; Bischofberger, N.; Chen, M. S.; Mendel, D. B.; Tai, C. Y.; Laver, W. G.; Stevens, R. C. *J. Am. Chem. Soc.* **1997**, *119*, 681.

[91] Haslam, E. *Shikimic Acid: Metabolism and Metabolites*; Wiley & Sons: New York, 1993; p. 40-42.

[92] (a) Jiang, S.; McCullough, K. J.; Mekki, B.; Singh, G.; Wightman, R. H. *J. Chem. Soc. Perkin Trans. 1*, **1997**, *12*, 1805. (b) Adrio, J.; Carretero, J. C.; Ruano, J. L. G.; Cabrejas, L. M. M. *Tetrahedron Assymetry* **1997**, *8*, 1623. (c) Takeuchi, M.; Taniguchi, T.; Ogasawara, K. *Synthesis*, **2000**, *10*, 1375. (d) Yoshida, N.; Ogasawara, K. *Org. Lett.* **2000**, *2*, 1461. (e) Hiroya, K.; Ogasawara, K. *Chem. Commun.* **1998**, *18*, 2033.

[93] (a) Kambourakis, S.; Draths, K. M.; Frost, J. W. *J. Am. Chem. Soc.*, **2000**, *122*, 9042. (b) Hansen, C. A.; Dean, A. B.; Draths, K. M.; Frost, J. W. *J. Am. Chem. Soc.* **1999**, *121*, 3799.

[94] McCabe, W. L.; Smith, J. C.; Harriot, P. *Unit Operations of Chemical Engineering*, 5^{th} *ed.*; McGraw-Hill, Inc.: New York, 1993.

[95] Blanch, H. W.; Clark, D. S. *Biochemical Engineering*; Marcel Dekker, Inc.: New York, 1996: p. 397.

[96] Bailey, J. E.; Ollis, D. F. *Biochemical Engineering Fundamentals*, 2^{nd} *ed.*, McGraw-Hill: New York, 1986: p. 464.

[97] Draths, K. D.; Knop, D. R.; Frost, J. W. *J. Am. Chem. Soc.* **1999**, *121*, 1603.

[98] Dell, K. A.; Frost, J. W. *J. Am. Chem. Soc.* **1993**, *115*, 11581.

[99] Tobey, K. L.; Grant, G. A. *J. Biol. Chem.* **1986**, *261*, 12179.

[100] Løbner-Olesen, A.; Marinus, M. G. *J. Bacteriol.* **1992**, *174*, 525.

[101] Anton, I. A.; Coggins, J. R. *Biochem. J.* **1988**, *249*, 319.

[102] Bartolome, B.; Jubete, Y.; Martines, E.; de la Cruz, F. *Gene* **1991**, *102*, 75.

[103] Draths, K. M.; Ward, T. L.; Frost, J. W. *J. Am. Chem. Soc.* **1992**, *114*, 9725.

[104] (a) Mitsuhashi, S.; Davis, B. D. *Biochim. Biophys. Acta* **1954**, *15*, 268. (b) Davis, B. D.; Gilvarg, C.; Misuhashi, S. *Meth. Enzymol.* **1955**, *2*, 300.

[105] Gordon, M.; Haskins, F. A.; Mitchell, H. K. *Proc. Nat. Acad. Sci.* **1950**, *36*, 427.

[106] Lu, J.-L.; Liao, J. C. *Biotechnol. Bioeng.* **1997**, *53*, 132.

[107] Farabaugh, M. M. S. Thesis, Michigan State University, April 1996.

[108] Pittard, J.; Wallace, B. J. *J. Bacteriol.* **1966**, *91*, 1494.

[109] (a) Pittard, J.; Wallace, B. J. *J. Bacteriol.* **1966**, *92*, 1070. (b) Brown, K. D.; Doy, C. H. *Biochim. Biophys. Acta* **1976**, *428*, 550. (c) Whipp, M. J.; Camakaris, H.; Pittard, A. J. *Gene* **1998**, *209*, 185.

[110] (a) Davies, G. M.; Barrett-Bee, K. J.; Jude, D. A.; Lehan, M.; Nichols, W. W.; Rinder, P. E.; Thain, J. L.; Watkins, W. J.; Wilson, R. G. *Antimicrob. Agents Chemother.* **1994**, *38*, 403. (b) Ewart, C. D.; Jude, D. A.; Thain, J. L.; Nichols, W. W. *Antimicrob. Agents Chemother.* **1995**, *39*, 87.

[111] Lerner, G. C.; Inouye, M. *Nucleic Acids Research*, **1990**, *18*, 4631.

[112] (a) Konstantinov, K. B.; Nishio, N.; Seki, T.; Yoshida T. *J. Ferment. Bioeng.*, **1991**, *71*, 350. (b) Konstantinov, K. B.; Nishio, N.; Seki, T.; Yoshida T. *J. Ferment. Bioeng.*, **1990**, *70*, 253. (c) Konstantinov, K. B.; Kishimoto, M.; Seki, T.; Yoshida, T. *Biotechnol. Bioeng.*, **1990**, *36*, 750. (d) Kleman, G. L.; Strohl, W. R. *Appl. Environ. Microbiol.*, **1994**, *60*, 3952. (e) Noronha, S. B.; Yeh, H. J. C.; Spande, T. F.; Shiloach, J. *Biotechnol. Bioeng.*, **2000**, *68*, 316. (f) van de Walle, M.; Shiloach, J. *Biotechnol. Bioeng.*, **1998**, *57*, 71. (g) Shiloach, J.; Kaufman, J.; Guillard, A. S.; Fass, R. *Biotechnol. Bioeng.*, **1996**, *49*, 421. (h) Majewski, R. A.; Domach, M. M.; **1990**, *35*, 732. (i) Xu, B.; Jahic, M.; Enfors, S.-O. *Biotechnol. Prog.*, **1999**, *15*, 81. (j) Akesson, M.; Karlsson, E. N.; Hagander, P.;

Axelsson, J. P.; Tocaj, A. *Biotechnol. Bioeng.*, **1999**, *64*, 590. (k) Cockshott, A. R.; Bogle, I. D. L. *Bioproc. Eng.* **1999**, *20*, 83. (l) Pan, J. G.; Rhee, J. S.; Lebeault, J. M. *Biotechnol. Lett.* **1987**, *9*, 89. (m) Andersen, K. B.; von Meyenburg, K. *J. Bacteriol.* **1980**, *144*, 114. (n) Sonnleitner, B.; Käppeli, O. *Biotechnol. Bioeng.*, **1986**, *28*, 927. (o) Paalme, T.; Tiisma, K.; Kahru, A.; Vanatalu, K.; Vilu, R. *Biotechnol. Bioeng.* **1990**, *35*, 312.

[113] (a) Rogers,D.; Yu, S. *J. Bacteriol.*, **1962**, *84*, 877. (b) Hagihira, H.; Wilson, T. H.; Lin, E. C. C. *Biochim. Biophys. Acta*, **1963**, *78*, 505. (c) Gachelin, G. *Eur. J. Biochem.*, **1970**, *16*, 342. (d) Curtis, S. J.; Epstein, W. *J. Bacteriol.*, **1975**, *122*, 1189. (e) Stock, J. B.; Waygood, E. B.; Meadow, N. D.; Postma, P. W.; Roseman *J. Biol. Chem.*, **1982**, *257*, 14543. (f) Misset, O.; Blaauw, M.; Postma, P. W.; Robillard, G. T. *Biochemistry*, **1983**, *22*, 6163. (g) Liu, K. D.-F.; Roseman, S. *Proc. Natl. Acad. Sci. USA*, **1983**, *80*, 7142. (h) Buhr, A.; Daniels, G. A.; Erni, B. *J. Biol. Chem.*, **1992**, *267*, 3847. (i) Reizer, J.; Sutrina, S. L.; Wu, L.-F.; Deutscher, J.; Reddy, P.; Saier, M. H. *J. Biol. Chem.*, **1992**, *267*, 9158. (j)Van Der Vlag, J.; Van't Hof, R.; Van Dam, K.; Postma, P. W. *Eur. J. Biochem.*, **1995**, *230*, 170. (k) Rohwer, J. M.; Bader, R.; Westerhoff, H. V.; Postma, P. W. *Mol. Microbiol.*, **1998**, *29*, 641. (l) Lux, R.; Munasinghe, R. N.; Castellano, F.; Lengeler, J. W.; Corrie, J. E. T.; Khan, S. *Mol. Biol. Cell*, **1999**, *10*, 1133. (m) Grenier, F. C.; Waygood, E. B.; Saier, M. H. *J. Cell Biochem.* **1983**, *31*, 97. (n) Meadow, N. D.; Roseman, S. *J. Biol. Chem.*, **1982**, *257*, 14526. (o) Saier, M. H.; Feucht, B. U. *J. Biol. Chem.*, **1975**, *250*, 7078.

[114] Knop, D. R.; Draths, K. M.; Chandran, S. S.; Barker, J. L.; von Daeniken, R.; Weber, W.; Frost, J. W. *J. Am. Chem. Soc.*, **2001**, *123*, 10173.

[115] Giles, N. H.; Case, M. E.; Baum, J.; Geever, R.; Huiet, L.; Patel, V.; Tyler, B. *Microbiol. Rev.*, **1985**, *49*, 338.

[116] Jensen, R. A. *Mol. Biol. Evol.*, **1985**, *2*, 92.

[117] Saier, M. H., Jr.; Ramseier, T. M.; Reizer, J. In *Escherichia coli and Salmonella: Cellular and Molecular Biology*; Neidhardt, F. C., Ed.; ASM Press: Washington, DC, 1996, Chapter 85.

[118] Gottschalk, G. *Bacterial Metabolism*, 2nd ed.; Springer-Verlag: New York, **1985**, p. 185.

[119] El-Mansi, E. M. T.; Holms, W. H. *J. Gen. Microbiol.*, **1989**, *135*, 2875.

[120] Haslam, E. *Shikimic Acid: Metabolism and Metabolites*; Wiley & Sons: New York, 1993; p 56.

[121] Barco, A., Benetti, S., De Risi, C., Marchetti, P., Pollini, G. P., Zanirato, V. *Tetrahedron Asymmetry* **1997**, *8*, 3515.

[122] Phoon, C. W.; Abell, C. *J. Comb. Chem.* **1999**, *1*, 485.

[123] Su, Z.; Paquette, L. A. *J. Org. Chem.* **1995**, *60*, 764.

[124] The Taxol (paclitaxel) Story; Bristol-Myers Squibb Co.: http://www.taxol.com/timeli.html

[125] Shing, T. K. M.; Tam, E. K. *J. Org. Chem.* **1998**, *63*, 1547.

[126] Ulibarri, G., Nadler, W., Skrydstrup, T., Audrain, H., Chiaroni, A., Riche, C., and Grierison, D. S. *J. Org. Chem.* **1995**, *60*, 2753.

[127] Izuhara, T.; Katoh, T. *Tetrahedron Lett.* **2000**, *41*, 7651.

[128] Barros, M. T.; Maycock, C. D.; Ventura, M. R. *J. Org. Chem.* **1997**, *62*, 3984.

[129] White, J. D.; Toske, S. G.; Yakura, T. *SYNLETT* **1994**, *8*, 591.

[130] Haslam, E. *The Shikimate Pathway*; Halstead Press: New York, 1974: p. 12.

[131] Ran, N.; Knop, D. R.; Draths, K. M.; Frost, J. W. *J. Am. Chem. Soc.* **2001**, *123*, 10927.

[132] Woskresensky, A. *Justus Liebigs Ann. Chem.* **1838**, *27*, 257.

[133] Krumenacker, L.; Costantini, M.; Pontal, P.; Sentenac, J. In *Kirk-Othmer Encyclopedia of Chemical Technology, 4th ed.*; Wiley: New York, 1995, Vol. 13, p. 996-1014.

[134] University of Tasmania, Blackman, A. J.; (a) http://orbital.chem.utas.edu.au/teaching/KRA305/biosynthesis/ubsskfiles/ubsskall.html, (b) http://www.chem.utas.edu.au/staff/blackman/studstuf.htm

[135] Draths, K. D.; Knop, D. R.; Frost, J. W. *J. Am. Chem. Soc.* **1999**, *121*, 1603, supporting information, available at http://pubs.acs.org.

[136] Li, K.; Frost, J. W. unpublished result.

[137] Yi, J.; Li, K.; Draths, K. D.; Frost, J. W. unpublished results.

[138] Roels, J. A. *Energetics and Kinetics in Biotechnology*; Elsevier Biomedical Press: Amsterdam, 1983: p. 30.

[139] Gibson, J. M.; Thomas, P. S.; Thomas, J. D.; Barker, J. L.; Chandran, S. S.; Harrup, M. K.; Draths, K. M.; Frost, J. W. *Angew. Chem. Int. Ed.* **2001**, *40*, 1945, supporting information, available at http://www.angewandte.com.

[140] Ran, N.; Draths, K. D.; Frost, J. F. unpublished results.

[141] Neidhardt, F. C.; Ingraham, J. L.; Schaechter, M. *Physiology of the Bacterial Cell: A Molecular Approach*; Sinauer Associates, Inc.: Sunderland, MA., 1990: p. 155.

[142] Huisman, G. W.; Siegele, D. A.; Zambrano, M. M.; Kolter, R. In *Escherichia coli and Salmonella: Cellular and Molecular Biology*; Neidhardt, F. C., Ed.; ASM Press: Washington, DC, 1996, Chapter 106.

[143] Huisman, G. W.; Kolter, R. *Science* **1994**, *265*, 537.

[144] Pittard, A. J. In *Escherichia coli and Salmonella: Cellular and Molecular Biology*; Neidhardt, F. C., Ed.; ASM Press: Washington, DC, 1996, Chapter 28.

[145] (a) O'Connor, S. R.; Farmer, P. B.; Lauder, I. *J. Pathol.* **1999**, *189*, 448. (b) Farris, G. M.; Everitt, J. I.; Irons, R.; Popp, J. A. *Fundam. Appl. Toxicol.* **1993**, *20*, 503. (c) Huff, J. E.; Haseman, J. K.; DeMarini, D. M. *Environ. Health Perspect.* **1989**, *82*, 125.

[146] *Chem. Eng. News* **2000**, *78* (26), 51.

[147] *Trade Secrets, A Moyers Report*; http://www.pbs.org/tradesecrets/transcript.html.

[148] Konstantinov, K. B. *Biotechnol. Bioeng.* **1996**, *52*, 271.

[149] Konstantinov, K.; Yoshida, T. *Biotechnol. Bioeng.* **1989**, *33*, 1145.

[150] Cronan, JR., J. E.; LaPorte, D. In *Escherichia coli and Salmonella: Cellular and Molecular Biology*; Neidhardt, F. C., Ed.; ASM Press: Washington, DC, 1996, Chapter 16.

[151] McCabe, W. L.; Smith, J. C.; Harriot, P. *Unit Operations of Chemical Engineering, 5th ed.*; McGraw-Hill, Inc.: New York, 1993; p. 242-243.

[152] Bailey, J. E.; Ollis, D. F. *Biochemical Engineering Fundamentals, 2nd ed.*, McGraw-Hill: New York, 1986, Chapter 8.

[153] (a) Worden, R. M.; unpublished data. (b) Srivastava, P. *Analysis of DO-Stat Control Strategy in Fed Batch Fermentations*, a CHE882 course report, 1998.

[154] Brockwell, P. J.; Davis, R. A.; In *Introduction to Time Series and Forecasting*, Springer-Verlag: New York, 1996, p. 22-28.

[155] Voet, D.; Voet, J. G. In *Biochemistry, 2nd ed.*; Wiley & Sons: New York, 1995, Chapter 23.

[156] Takagi, M.; Ishimura, F.; Fujimatsu, I. *J. Ferm. Bioeng.* **1998**, *85*, 354.

[157] Penfound, T.; Foster, J. W. In *Escherichia coli and Salmonella: Cellular and Molecular Biology*; Neidhardt, F. C., Ed.; ASM Press: Washington, DC, 1996, Chapter 48.

[158] Berson, A. E.; Hudson, D. V.; Waleh, N. S. *Mol. Microbiol.* **1991**, *5*, 2261.

[159] Hamilton, C. M.; Aldea, M.; Washburn, B. K.; Babitzke, P., Kushner, S. P. *J. Bacteriol.* **1989**, *171*, 4617.

[160] Sambrook, J.; Fritsch, E. F.; Maniatis, T. *Molecular Cloning: A Laboratory Manual*; Cold Spring Harbor Laboratory Press: Plainview, NY., 1989.

[161] Braun, R.; Kell, P. proprietary B. Braun Biotech facsimile communication **2002**, 1.

[162] Li, K.; PhD Dissertation, Michigan State University, 1999.

[163] Ran, N.; Frost, J. W. 2001, unpublished results.

[164] Bradford, M. M. *Anal. Biochem.* **1976**, *72*, 248.

[165] Schoner, R.; Herrmann, K. M. *J. Biol. Chem.* **1976**, *251*, 5440.

[166] Chaudhuri, S.; Anton, I. A. ; Coggins, J. R. *Meth. Enzymol.* **1987**, *142*, 315.

[167] Herwig, C.; Marison, I.; von Stockar, U. *Biotechnol. Bioeng.* **2001**, *75*, 345.

[168] Brockwell, P. J.; Davis, R. A.; In *Introduction to Time Series and Forecasting*, Springer-Verlag: New York, 1996, p. 315-316.